

# **Radiological Assessment of Natural Radioactivity in Indian Building Materials**

*By*

**S. CHINNAESAKKI**

(PHYS01200704013)

**Bhabha Atomic Research Centre, Mumbai**

*A Thesis submitted to the  
Board of Studies in Physical Sciences  
In partial fulfillment of requirements  
For the Degree of*

**DOCTOR OF PHILOSOPHY**

*of*

**HOMI BHABHA NATIONAL INSTITUTE**



**December, 2014**



# HOMI BHABHA NATIONAL INSTITUTE

## Recommendations of the Viva Voce Board

As members of the Viva Voce Board, we certify that we have read the dissertation prepared by S. Chinnaesakki entitled "Radiological Assessment of Natural Radioactivity in Indian Building Materials" and recommend that it may be accepted as fulfilling the dissertation requirement for the Degree of Doctor of Philosophy.

*Shrapan Kumar Ghosh*

Date: 02-07-2015

**Chairman – Dr. S. K. Ghosh**

Bhabha Atomic Research Centre, Trombay, Mumbai-85.

*T. Palani*

Date: 02/07/2015

**Guide / Convener – Dr. T. Palani Selvam**

Bhabha Atomic Research Centre, Trombay, Mumbai-85.

*T. Palani Selvam*

Date: 02/07/2015

**Examiner: Dr. R. C. Ramola**

H. N. B. Garwal University, Srinagar, Uttarakhand - 246174

*R. C. Ramola*

Date: 02/07/2015

**Member: Dr. R. M. Tripathi**

Bhabha Atomic Research Centre, Trombay, Mumbai-85.

*R. M. Tripathi*

Date: 02/07/2015

**Member: Dr. M. P. Chougankar**

Ex. Bhabha Atomic Research Centre, Trombay, Mumbai-85.

*M. P. Chougankar*

Date: 02/07/2015

**Member: Dr. P. M. Ravi**

Bhabha Atomic Research Centre, Trombay, Mumbai-85.

Final approval and acceptance of this dissertation is contingent upon the candidate's submission of the final copies of the dissertation to HBNI.

I hereby certify that I have read this dissertation prepared under my direction and recommend that it may be accepted as fulfilling the dissertation requirement.

Date: July 02, 2015

Place: Mumbai

*T. Palani*

(T. Palani Selvam)

Guide / Convener



## STATEMENT BY AUTHOR

This dissertation has been submitted in partial fulfillment of requirements for an advanced degree at Homi Bhabha National Institute (HBNI) and is deposited in the Library to be made available to borrowers under rules of the HBNI.

Brief quotations from this dissertation are allowable without special permission, provided that accurate acknowledgement of source is made. Requests for permission for extended quotation from or reproduction of this manuscript in whole or in part may be granted by the Competent Authority of HBNI when in his or her judgment the proposed use of the material is in the interests of scholarship. In all other instances, however, permission must be obtained from the author.



(S. Chinnaesakki)

## DECLARATION

I, hereby declare that the investigation presented in the thesis has been carried out by me.  
The work is original and has not been submitted earlier as a whole or in part for a degree  
/ diploma at this or any other Institution / University.



(S. Chinnaesakki)



## List of publication arising from the thesis

### Publications in Refereed Journal:

#### a. Published

1. S. J. Sartandel, S. V. Bara, **S. Chinnaesakki**, S. K. Jha, R. M. Tripathi (2014). “Radiological measurement of phosphate rock and phosphogypsum from fertilizer industries in India”. *Journal of Radioanalytical and Nuclear Chemistry (Springer)*, Vol. 302, 1441 – 1447.
2. **S. Chinnaesakki**, S. V. Bara, S. J. Sartandel, R. M. Tripathi, V. D. Puranik (2012). “Performance of HPGe Gamma Spectrometry system for the measurement of Low Level Radioactivity”. *Journal of Radioanalytical and Nuclear Chemistry (Springer)*. Vol. 294, 143-147.
3. S. V. Bara, Vishal Arora, **S. Chinnaesakki**, S. J. Sartandel, , R. M. Tripathi, V. D. Puranik, B. S. Bajwa (2012), “Radiological Assessment of Natural and Fallout radioactivity in the soil of Chamba and Dharamshala areas of Himachal Pradesh, India”. *Journal of Radioanalytical and Nuclear Chemistry (Springer)*. Vol. 291, 769–776.
4. **S. Chinnaesakki**, Manish Chopra, Sanjeev Kumar, Vishal Arora, S. J. Sartandel, S. V. Bara, R. M. Tripathi, V. D. Puranik, B. S. Bajwa (2011). “Assessment of natural radioactivity in soil samples and comparison of direct and indirect measurement of environmental air kerma rate”. *Journal of Radioanalytical and Nuclear Chemistry (Springer)*, Vol. 289, 885–892.

5. **S. Chinnaesakki**, S. V. Bara, S. J. Sartandel, R. M. Tripathi and V. D. Puranik (2010). “Radiological Characterisation of Synthetic Rutile using HPGe Gamma Spectrometry” Radiation Protection Dosimetry (Oxford University Press), Vol. 140, No. 4, 378–382.
6. S. J. Sartandel, S. V. Bara, **S. Chinnaesakki**, R. M. Tripathi, and V. D. Puranik (2010). “Measurement of Naturally Occurring Radioactive Materials (NORM) in Beach Sand Minerals using HPGe Gamma Spectrometry”. Journal of Radioanalytical and Nuclear Chemistry (Springer). Vol. 294, 447-451.

#### **b. Communicated**

1. **S. Chinnaesakki**, T. Palani Selvam, S. V. Bara, P. M. Ravi, R. M. Tripathi, (2014). “Radiological Assessment of natural radioactivity in phosphogypsum as a building material.” Journal of Radioanalytical and Nuclear Chemistry (Springer).
2. **S. Chinnaesakki**, T. Palani Selvam, S. V. Bara, P. M. Ravi, R. M. Tripathi, (2014). “Radiological Assessment of natural radioactivity in fly ash brick as a building material.” Journal of Radioanalytical and Nuclear Chemistry (Springer).

#### **c. Other publications**

1. **S. Chinnaesakki**, S. V. Bara, S. J. Sartandel, R. M. Tripathi, V. D. Puranik (2012). "Natural Radioactivity in commercial cements and its radiological implication as Building materials" NSRP-19, December 12-14, 2012. Proc. Of the 19<sup>th</sup> National Symposium on radiation Physics.
2. T. V. Ramachandran, B. K. Sahoo, **S. Chinnaesakki** (2007). “Assessment of Natural Radioactivity content of the building materials in India”. Proc. Of the Nuclear and Radiochemistry Symposium (NUCAR, 2007), 587 – 588.

(S. Chinnaesakki)

**Dedicated to**

**My Beloved Parents**

**Smt. Pechiammal & Shri. Shunmugavelu**



## Acknowledgements

I am deeply indebted to **Prof. Y. S. Mayya** (presently Adjunct Professor, IIT Bombay, Mumbai), formerly Head, Radiological Physics and Advisory Division (RP&AD), BARC. He kindly accepted my registration for the Ph.D. under his guidance and provided invaluable support and motivation during the course of this work.

I am extremely grateful to **Prof. T. Palani Selvam**, Professor HBNI and Head, CRP & NM section, RP&AD, BARC, who accepted me wholeheartedly as his student, consequent on the retirement of Prof. Mayya. Without his deep involvement and invaluable guidance, this thesis would have never seen the light of day. He not only introduced me the subject of Monte Carlo technique but also encouraged me to solve some problems for this work.

I would like to thank my doctoral committee chairman Dr. S. K. Ghosh, Senior Professor, HBNI, & Raja Ramanna Fellow, BARC, (Ex. Dean Academic (Chemical Sciences, HBNI & Ex. Head, TCS, Chemistry Group), and the members Dr. R. M. Tripathi, Head, HPD, Dr. P. M. Ravi, Head, ESS, HPD, BARC, Dr. M. P. Chougankar Ex. Head, PM&PD Section, RP&AD, BARC, for their inspirational encouragement and critical review throughout this research work.

The encouragement and motivation by Dr. K. S. Pradeep Kumar, Associate Director, HS&EG, BARC, and Dr. D. N. Sharma, Member, NDMA, New Delhi (Ex. Director, HS&EG, BARC) is gratefully acknowledged.

It is my great pleasure to acknowledge the help and encouragement rendered by my friends Dr. S. Anand, HPD, BARC and Dr. B. K. Sahoo, RP&AD, BARC for all the help during the course of this work.

I wish to express my sincere thanks to Smt. Sheetal V. Bara and Smt. Sangeeta J. Sartandel, for their support during the course of this study. I also wish to thank all the friends and colleagues of HS&EG, BARC, for their encouragement and support.

I would like to thank my dear wife Priya for her love, affection and relentless support. I wish to express my sincere gratitude and indebtedness to my beloved parents, brothers and sister and other family members for their blessings, encouragement, and support. I also wish to acknowledge all the teachers, friends, relatives, and well-wishers for their kindness towards me.



# Contents

<b>Synopsis.....</b>	<b>i</b>
<b>List of Figures.....</b>	<b>ix</b>
<b>List of Tables .....</b>	<b>xi</b>
<b>Chapter 1 Introduction .....</b>	<b>1</b>
1.1 Overview and Motivation.....	1
1.2 Naturally Occurring Radioactive Material (NORM) .....	2
1.2.1 Cosmic Origin.....	3
1.2.2 Terrestrial Origin .....	5
1.2.2.1 Natural radioactive decay series.....	6
1.2.2.2 Singly occurring radionuclides.....	10
1.3 Enhanced Sources of Naturally Occurring Radioactive Material .....	12
1.4 Radiological significance of NORM.....	15
1.4.1 Dosimetric Quantities and units .....	15
1.4.2 External Radiation Exposure .....	29
1.4.3 Internal Radiation Exposure .....	32
1.4.4 Biological effects of low dose ionizing radiation .....	35
1.5 Analytical Technique for the measurement of NORM .....	38
1.5.1 Interaction of gamma radiation with matter .....	39
1.5.1.1 Photoelectric effect.....	40
1.5.1.2 Compton Scattering.....	42

1.5.1.3	Pair Production .....	45
1.5.2	NaI (TI) Scintillation Gamma spectrometry .....	50
1.5.3	HPGe Gamma Spectrometry .....	51
1.5.3.1	Principle of semiconductor radiation detector .....	51
1.5.3.2	HPGe Gamma spectrometer components .....	59
1.5.4	Gamma Spectrum Analysis .....	62
1.5.5	Radioanalytical Uncertainty .....	63
1.5.6	Minimum Detectable Activity (MDA) .....	68
1.5.7	Gamma Spectrometry of Natural Radionuclides .....	69
1.6	Scope of the present work .....	70
<b>Chapter 2 Literature Review .....</b>		<b>72</b>
2.1	Introduction .....	72
2.2	Computation of Indoor gamma dose .....	73
2.3	Indoor radon regulation – International trend .....	78
2.4	Regulatory aspects of NORM in building materials .....	78
2.5	Measurement of NORM in various building materials .....	92
2.5.1	Assessment of NORM in building materials by various countries .....	92
2.5.2	Study of natural radioactivity in building materials - Indian scenario .....	100
<b>Chapter 3 Standardisation of HPGe Gamma Ray Spectrometer .....</b>		<b>116</b>
3.1	Introduction .....	116
3.2	Specification of gamma spectrometry system used in the study .....	116

3.3	Formula used for the activity estimation.....	120
3.4	Reference materials for calibration .....	122
3.5	Energy calibration .....	124
3.6	Efficiency calibration .....	127
3.7	Corrections for self-attenuation in gamma-ray spectrometry .....	129
3.8	QA/QC of spectrometry system .....	130
3.8.1	IAEA-ALMERA Proficiency tests evaluation .....	133
<b>Chapter 4 Radioactivity Measurement Results and Discussion.....</b>		<b>135</b>
4.1	Introduction .....	135
4.2	Natural radioactivity in raw materials .....	135
4.3	Natural Radioactivity in conventional building materials.....	146
4.4	Natural Radioactivity in industrial by products, wastes etc. ....	149
4.4.1	Phosphogypsum.....	149
4.4.2	Fly ash.....	154
<b>Chapter 5 Computation of indoor gamma dose using Monte Carlo technique .....</b>		<b>157</b>
5.1	Introduction .....	157
5.2	History of Monte Carlo Technique .....	158
5.3	Monte Carlo vs. Deterministic Method.....	158
5.4	Random Variable and Random number .....	159
5.4.1	Discrete Random Variable.....	161

5.4.2	Continuous Random Variable .....	163
5.5	Random Sampling technique .....	164
5.5.1	Inversion technique.....	165
5.5.2	Rejection technique .....	167
5.6	Monte Carlo N-Particle Transport Code System (MCNP) .....	169
5.7	Estimation of Monte Carlo errors.....	170
5.8	Validation of MCNP for indoor dose computation.....	172
5.9	Indoor dose computation of Indian room models .....	173
5.9.1	Clay brick walls .....	174
5.9.2	Fly Ash Brick walls .....	189
5.9.3	Phosphogypsum wall panel .....	192
<b>Chapter 6 Radiological Assessment .....</b>		<b>196</b>
6.1	Introduction .....	196
6.2	Derivation of Activity Index for gamma dose .....	196
6.3	Activity index including radon contribution .....	198
6.4	Application of proposed Activity Index.....	200
<b>Chapter 7 Conclusions.....</b>		<b>204</b>
7.1	Summary and concluding remarks.....	204
7.2	Scope for future work.....	207
<b>Bibliography .....</b>		<b>208</b>

---

## Synopsis

---

Radiological assessment refers to the analysis of ionizing radiation sources and associated exposures, usually in the context of radiation protection of humans. Radiological assessment very often involves evaluating individual and societal benefits and detriments of a particular practice or circumstance involving radiation. Life on earth is continuously subjected to radiation of natural origin. There are two main contributors to natural radiation exposures: high-energy cosmic ray particles incident on the earth's atmosphere and radioactive nuclides that originated in the earth's crust and are present everywhere in the environment, including the human body itself. Both external and internal exposures to humans arise from these sources. Irradiation of the human body from external sources is mainly by gamma radiation from radionuclides in the  $^{238}\text{U}$  and  $^{232}\text{Th}$  series and from  $^{40}\text{K}$ . These radionuclides are also present in the body and irradiate various organs with alpha and beta particles, as well as gamma rays. The concern about radioactivity in general, and naturally occurring radioactive materials (NORM) in particular, has increased many fold throughout the world. This is due to the radiation arising from the primordial radionuclides present in conventional raw materials and solid industrial wastes and byproducts such as fly ash from thermal power stations and phosphogypsum from the fertilizer industries that are being used in the manufacture of building construction materials and other commodities extensively. These types of man-made alterations in the Natural Environment can increase radiation exposure of the public, sometimes in a substantial manner. Knowledge of the radioactivity levels of materials used in the manufacture of building materials is essential for the development of standards and guidelines so as to keep the natural radiation exposure level as low as reasonably achievable (ALARA). As people reside indoors almost 80 % of

the time, the radiological assessment of indoor exposure due to NORM in building construction materials is essential. Only some skeletal data is available on NORM in Indian building materials.

A natural radiation background exists everywhere and every natural substance contains some amount of radioactive material. Natural radiation and radioactivity are of importance to radiation physics for at least four reasons:

- i. They presaged and stimulated perhaps the greatest period of scientific discovery and thought in human history and the development of basic models of the atom, nuclear structure, and radioactive transformation.
- ii. The natural sources represent a continuous exposure of beings on the earth and thus are a benchmark for consideration of levels of radiation protection not only for enhanced sources of natural radiation and radioactivity, but other sources as well.
- iii. Human activities affect exposure to these sources, and understanding of such processes, including discovery and uses of uranium, thorium, and radon and their transformation products, is fundamental to assessing and controlling their radiological impacts.
- iv. Every measurement of a radiation level or the radioactivity in a sample or source must take into account the background associated with naturally occurring radioactive material and radiation sources.

Natural radioactivity measurement in building materials has been studied by many authors from across the globe. Each country has its own regulation on NORM in building materials. There are many radiological hazard indices have been used as a screening tool to control the radiation exposure of the public. The following are most cited:

(i) “Natural radioactivity of Australian building materials, industrial wastes and by-product (Beretka, 1985), in which the term radium equivalent activity ( $R_{aeq}$ ) coined and have been used extensively by the researchers all over the world. It is based on the fact that fact that  $10 \text{ Bq kg}^{-1}$  of  $^{226}\text{Ra}$ ,  $7 \text{ Bq kg}^{-1}$  of  $^{232}\text{Th}$  and  $130 \text{ Bq kg}^{-1}$  of  $^{40}\text{K}$  produce equal gamma-ray dose rate. The maximum value of  $R_{aeq}$  in building raw materials and products must be less than  $370 \text{ Bq kg}^{-1}$  for safe use, i.e., to keep the external dose below  $1.5 \text{ mGy a}^{-1}$ .

(ii) Radiological protection principles concerning the natural radioactivity of building materials. Radiation Protection No. 112, European commission regulation (EC, RP-112, 2000). In this guideline, the term activity concentration index (I) also called as gamma index have been defined is also used to control the gamma external exposure due to natural radionuclides in building materials.

$$I = [A_{\text{Ra}} / 300 + A_{\text{Th}} / 200 + A_{\text{K}} / 3000]$$

Where,  $A_{\text{Ra}}$ ,  $A_{\text{Th}}$  and  $A_{\text{K}}$  are the specific activities of  $^{226}\text{Ra}$ ,  $^{232}\text{Th}$  and  $^{40}\text{K}$ .

It is based on the excessive gamma dose rate of either  $0.3 \text{ mSv a}^{-1}$  or  $1 \text{ mSv a}^{-1}$  depends upon the usage of the materials. This index was derived for the typical room model adopted in Europe i.e.  $5 \text{ m} \times 4 \text{ m} \times 2.8 \text{ m}^3$  made up of concrete with density  $2.35 \text{ g/cc}$  and thickness  $50 \text{ cm}$ .

Similar individual guidelines are being into force in many countries. In India there is no such regulatory guidelines are available. All the Indian researchers have been using the above guidelines for assessing the NORM in Indian building materials. But, the room

model adopted in India is entirely different from Europe. Hence, it is inappropriate for Indian condition, here the room models are very much different from Europe. It is therefore necessary to compute the external gamma dose coefficients based on this the activity index is computed for the Indian standard room.

The present investigation is mainly focused on (i) measurement of natural radioactivity in various Indian building materials such as soil, sand, cement, fly ash, phosphogypsum etc. using HPGe gamma spectrometric technique. (ii) Monte Carlo computation of Indoor specific air kerma rate ( $\text{nGyh}^{-1}\text{Bqkg}^{-1}$ ) for India specific standard room models. External gamma dose coefficients for a general room model (3 m x 3m x 3m) as per the Indian Building Code have been evaluated using Monte Carlo numerical computation technique. The radioactivity data collected and published by various authors on NORM Indian building materials were analysed based on the new dose coefficients. The new activity Index, as a screening tool, in line the EC-RP112 is proposed.

The present study is divided into seven chapters described below.

## **Chapter-I Introduction**

This chapter is divided into three parts. The first part discusses about origin of radioactivity in general. The second part is about the sources of naturally occurring radioactive material (NORM) and its emission. The third part discusses the radiological significance of NORM.

## **Chapter-II Literature Review**

This chapter deals with the critical review of published work. Objective and scope of the present study is included this Chapter. In addition, discussions on gamma spectrometry as

an analytical tool, instrumentation of HPGe Gamma spectrometry and spectral analysis are included in this Chapter.

**Chapter-III Standardisation of HPGe Gamma Ray Spectrometer** This chapter is presented in three sections. The first section discusses the calibration of the gamma ray spectrometer for energy, and efficiency using the IAEA certified reference materials such as IAEA RGU-I, RGTh-I and IAEA-434 Phosphogypsum. The second section deals with the quality assurance and quality control aspects of the gamma spectrometer, including the performance evaluation of IAEA – ALMERA proficiency tests.

#### **Chapter-IV Radioactivity Measurement Results and Discussion**

##### **(i) Assessment of Natural Radioactivity Content of the Building Materials in India**

Building material samples such as brick, concrete, glazed tiles, lime, black sand, marble etc. were collected in Gujarat, India. The samples were analysed for their natural radioactivity content using the HPGe coupled gamma spectrometric system.  $^{238}\text{U}$  activity was varying from 8.3 Bq/kg in lime to 91.1 Bq/kg in fly ash brick, while the  $^{232}\text{Th}$  content varied from 4 Bq/kg in marble to 115.9 Bq/kg in fly ash bricks.  $^{40}\text{K}$  content varied from 10.1 Bq/kg in marble to 289.2 Bq/kg in fly ash bricks. The activity index (RP-112, EC, 1999) was estimated for all the samples. The study shows that the activity index varies from 0.07 to 1.02. This suggests that the natural radiation exposure from the building materials samples analysed will be well within the acceptable criteria.

##### **(ii) Radiological Characterization of Synthetic Rutile using HPGe Gamma Spectrometry**

Radiological characterization of synthetic rutile, which is the source material for the production of titanium, was carried out. The natural radioactivity due to uranium ( $^{238}\text{U}$ ), thorium ( $^{232}\text{Th}$ ) series radionuclides and potassium ( $^{40}\text{K}$ ) was measured in synthetic rutile samples of a production plant in Tamil Nadu, India. The n-type HPGe coupled gamma spectrometry was used for the analysis. From the concentration levels, the radiological parameters such as Radium equivalent activity ( $\text{Ra}_{\text{eq}}$ ), external hazard index ( $\text{H}_{\text{ex}}$ ) and activity index were evaluated. It is observed that thorium is more than any other radionuclides, which is due to the monazite present in the primary sand. The mean radium equivalent activity ( $\text{Ra}_{\text{eq}}$ ) is below the acceptable value of  $370 \text{ Bq kg}^{-1}$ . The external hazard index ( $\text{H}_{\text{ex}}$ ) and activity index are also well below the acceptable limit. The use of synthetic rutile for the manufacture of building materials will not pose any increased radiation exposure to the public.

### **(iii) Natural Radioactivity in commercial cements and its radiological implication as Building materials**

This study presents the HPGe Gamma spectrometric measurement of natural radioactivity mainly due to  $^{238}\text{U}$ ,  $^{226}\text{Ra}$ ,  $^{232}\text{Th}$  and  $^{40}\text{K}$  in commercially available cement samples, in India.  $^{238}\text{U}$  activity was found to be varying from  $45.3 \text{ Bq kg}^{-1}$  to  $300.8 \text{ Bq kg}^{-1}$  with the mean value of  $127.1 \text{ Bq kg}^{-1}$ .  $^{226}\text{Ra}$  activity was varying from  $20.3 - 79.3 \text{ Bq kg}^{-1}$  with the mean of  $40.3 \text{ Bq kg}^{-1}$ . The range and mean activity of  $^{232}\text{Th}$  was found to be  $18.8 - 63.5 \text{ Bq kg}^{-1}$  and  $36.8 \text{ Bq kg}^{-1}$  respectively.  $^{40}\text{K}$  activity was in the range of  $160.9 - 307.2 \text{ Bq kg}^{-1}$  with the mean of  $211.1 \text{ Bq kg}^{-1}$ . The Radiological parameters such as radium equivalent activity and activity index shows that the indoor external dose due to natural radioactivity in cement used for the construction will not exceed the dose criteria. It was

also found out that there is radioactive disequilibrium between  $^{238}\text{U}$  and  $^{226}\text{Ra}$ , which may be attributed to the partitioning of radionuclides during the production process of cement.

#### **(iv) Assessment of Natural radioactivity in Indian Phosphogypsum**

- Phosphogypsum is the by-product generated in large quantity, which is being used as a substitute for natural gypsum in building material industry.
- Phosphogypsum samples from various fertilizer industries were analysed for natural

Radioactivity. In addition, the wall panel made out of phosphogypsum was also analysed.

#### **(v) Assessment of Natural radioactivity in Fly ash and Fly ash brick**

Fly ash samples from various thermal power plants were analysed for natural radioactivity.

Fly ash brick samples were also analysed for natural radioactivity.

### **Chapter-V Computation of Indoor Gamma Radiation Dose**

Indoor gamma dose is mainly caused by the natural radionuclides of  $^{238}\text{U}$  series,  $^{232}\text{Th}$  series and  $^{40}\text{K}$  radionuclides present in the building materials. From the measured specific activity of these radionuclides, specific air-kerma rate ( $\text{nGyh}^{-1}\text{Bqkg}^{-1}$ ) has been computed using the Monte Carlo techniques. In the Monte Carlo calculations rooms of dimensions 3 m x 3 m x 3 m and 4.8 m x 3 m x 3 m with various combination of building construction materials (fly ash brick, phosphogypsum, concrete, clay brick and tiles) were carried out. Using the calculated specific air-kerma rate values activity index was estimated. The activity index serves as a regulatory tool to assess the NORM in the Indian building materials.

### **Chapter-VI Radiological Assessment**

This chapter is divided into four parts. The first part discusses about the estimated activity index for various building materials. Second part discusses the comparison of activity index estimated using the RP-112 basis with the newly computed dose coefficients. The fourth part of the thesis emphasizes on the proposal of a simple radiological regulatory screening tool for the Indian building materials.

## **Chapter-VII Conclusions**

In this Chapter, summary and important findings of the study are included. This Chapter also includes discussion on scope of future work.

---

## List of Figures

---

Figure 1.1 Uranium ( $^{238}\text{U}$ ) Natural Radioactive decay series. -----	8
Figure 1.2 Thorium ( $^{232}\text{Th}$ ) Natural Radioactive decay series. -----	9
Figure 1.3 $^{40}\text{K}$ Decay scheme -----	11
Figure 1.4 Photo electric effect -----	41
Figure 1.5 Compton scattering -----	43
Figure 1.6 Pair production -----	46
Figure 1.7 Annihilation due to pair production -----	47
Figure 1.8 Relative Importance of three interaction mechanisms -----	48
Figure 1.9 mass attenuation coefficient of Germanium -----	50
Figure 1.10 Band gap semiconductors: Silicon and Germanium -----	53
Figure 1.11 p-n junction and depletion region in semiconductors -----	57
Figure 1.12 p-n junction mechanism in semiconductors -----	58
Figure 1.13 Reverse bias in p-type germanium semiconductors -----	59
Figure 1.14 Block diagram of HPGe Gamma Spectrometry system -----	62
Figure 3.1 HPGe Gamma Spectrometry system in the Low Level Counting Lab -----	119
Figure 3.2 Background spectrum of a HPGe Gamma spectrometry system -----	120
Figure 3.3 HPGe gamma spectrum of IAEA RGU-I (Uranium ore) -----	123
Figure 3.4 HPGe Gamma spectrum of IAEA RGTh-I (Thorium Ore) -----	124
Figure 3.5 Energy calibration of HPGe Gamma spectrometry system -----	126
Figure 3.6 absolute efficiency (HPGe) - IAEA RGU-I & Th-I in -----	128
Figure 3.7 Quality Control chart of HPGe Gamma spectrometer using $^{210}\text{Pb}$ background -----	132
Figure 3.8 Quality Control chart of HPGe Gamma spectrometer using $^{40}\text{K}$ background -----	132
Figure 4.1 Secular equilibrium: $^{238}\text{U}$ series -----	138

Figure 4.2 Sampling locations of Ferozepur and Faridkot -----	140
Figure 4.3 HPGe Gamma spectrum of a soil samples of Punjab-----	141
Figure 4.4 HPGe Gamma spectrum of a Cement sample-----	147
Figure 4.5 HPGe Gamma spectrum of a phosphogypsum sample-----	152
Figure 4.6 HPGe (p-type, 50 %) Gamma Spectrum of a Fly ash brick sample -----	156
Figure 5.1 Probability density function of random numbers -----	160
Figure 5.2 Cumulative distribution function -----	161
Figure 5.3. Flow diagram of discrete random events-----	163
Figure 5.4 Random sampling - Inversion method -----	166
Figure 5.5 Random sampling using rejection method-----	168
Figure 5.6 Typical Indian Room model adopted for the computation of indoor gamma dose ---	174
Figure 5.7 Contribution of individual building materials on the total specific air kerma rate ----	178
Figure 5.8 Pie chart of individual building materials contribution to the total air kerma rate ----	179
Figure 5.9 Effect of clay brick density on the specific air kerma rate-----	181
Figure 5.10 Effect of brick wall thickness on the specific air kerma rate -----	184
Figure 5.11 Specific air kerma rate at 1 m and center of the room – various room models -----	187
Figure 5.12 Comparison of specific air kerma rate due to fly ash brick with clay brick -----	192
Figure 6.1 Comparison of activity index calculated using RP-112 and the proposed-----	202
Figure 6.2 Indoor occupancy effect on the Activity Index -----	203

---

## List of Tables

---

Table 1.1 Terrestrial radiation distribution in India -----	12
Table 1.2 Radiation weighting factor for different radiation-----	21
Table 1.3 Tissue weighting factor for different organs and tissues-----	23
Table 1.4 Annual average effective dose due to natural radiation -----	35
Table 2.1 Activity index (I) recommended by the European commission -----	83
Table 2.2 $A_x$ values for different specific areas in Israel -----	87
Table 2.3 NORM regulation - Recommendation by Shukla et al 1995 -----	89
Table 3.1 Main characteristics of HPGe Gamma Spectrometer-----	118
Table 3.2 Minimum Detectable Activity (MDA) of gamma spectrometry system -----	121
Table 3.3 IAEA Certified Reference Materials for calibration -----	122
Table 3.4 Prominent Gamma energies (keV) and emission probabilities -----	125
Table 3.5 IAEA Proficiency Test Evaluation results -----	134
Table 4.1 Radiological Parameters soil radioactivity – Ferozpur and Faridkot-----	140
Table 4.2 Descriptive statistics of Natural Radioactivity in Chamba soil samples -----	143
Table 4.3 Descriptive statistics of Natural Radioactivity in Dharamshala soil samples -----	143
Table 4.4 Descriptive statistics of Natural Radioactivity in Synthetic Rutile samples.-----	145
Table 4.5 Natural radioactivity in raw materials for cement -----	146
4.6 Activity concentration of Natural radionuclides in cement samples. -----	148
Table 4.7 Radioactivity concentration in phosphate rock and phosphogypsum-----	153
Table 4.8 Activity concentration in phosphogypsum from different countries-----	154
Table 4.9 Descriptive Statistics of Natural Radioactivity in Fly ash brick samples -----	155
Table 5.1 Specific air kerma rate - (Concrete structures)-----	173
Table 5.2 Chemical composition of clay brick -----	175
Table 5.3 Chemical composition of mortar-----	176

Table 5.4 Chemical composition of ordinary concrete-----	176
Table 5.5 Chemical composition of Floor tiles -----	176
Table 5.6 Chemical composition of dry air-----	177
Table 5.7 Specific air kerma rate - (Clay brick Walls ( $\rho = 1.6 \text{ g cm}^{-3}$ ) – bed room) -----	177
Table 5.8 Specific air kerma rate - (Clay brick Walls ( $\rho = 1.87 \text{ g cm}^{-3}$ ) – bed room) -----	180
Table 5.9 Indoor Gamma dose computation using Monte Carlo Method _ -----	182
Table 5.10 Indoor Gamma dose computation using Monte Carlo Method _ -----	183
Table 5.11 Specific air kerma rate - (Clay brick Walls – Living Room) -----	185
Table 5.12 Indoor Gamma dose computation using Monte Carlo Method _ -----	186
Table 5.13 Chemical composition of Marble -----	188
Table 5.14 Indoor Gamma dose computation using Monte Carlo Method _ -----	188
Table 5.15 Chemical composition of fly ash brick-----	189
Table 5.16 Specific air kerma rate (Fly ash brick Walls – Bed room) -----	190
Table 5.17 Specific air kerma rate (Fly ash brick Walls – Living Room)-----	191
Table 5.18 Chemical composition of Phosphogypsum-----	193
Table 5.19 Specific air kerma rate (Phosphogypsum wall panel – Bed room) -----	194
Table 5.20 Specific air kerma rate (Phosphogypsum wall panel – Living room)-----	194
Table 5.21 Summary of room models and corresponding Specific Air Kerma Rate-----	195
Table 6.1 Specific air kerma rate at 1 m height computed using Monte Carlo method-----	197
Table 6.2 Computed Activity Index and its comparison with $I_{RP112}$ -----	201

---

## Chapter 1 Introduction

---

### 1.1 Overview and Motivation

Radiological assessment refers to the analysis of ionizing radiation sources and associated exposures, usually in the context of radiation protection of humans. Radiological assessment very often involves evaluating individual and societal benefits and detriments of a particular practice or circumstance involving radiation [1]. Life on earth is continuously subjected to radiation of natural origin. There are two main contributors to natural radiation exposures: high-energy cosmic ray particles incident on the earth's atmosphere and radioactive nuclides that originated in the earth's crust and are present everywhere in the environment, including the human body itself. Both external and internal exposures to humans arise from these sources. Irradiation of the human body from external sources is mainly by gamma radiation from radionuclides of the  $^{238}\text{U}$  and  $^{232}\text{Th}$  series and from  $^{40}\text{K}$ . These radionuclides are also present in the body and irradiate various organs with alpha and beta particles, as well as gamma rays. The concern about radioactivity in general, and naturally occurring radioactive materials (NORM) in particular, has increased many fold throughout the world. This is due to the radiation arising from the primordial radionuclides present in conventional raw materials and solid industrial wastes and byproducts such as fly ash from thermal power stations and phosphogypsum from the fertilizer industries. These materials are being used in the manufacture of building construction materials and other commodities extensively. These types of man-made alterations in the Natural Environment can increase radiation exposure of the public, sometimes in a substantial manner.

Living in houses/work places built with materials containing NORM in excess, is of

radiological concern. Knowledge of the radioactivity levels of materials used in the manufacture of building materials is essential for the development of standards and guidelines so as to keep the natural radiation exposure level as low as reasonably achievable (ALARA). As people reside indoors almost 80 % of the time, the radiological assessment of indoor exposure due to NORM in building construction materials is essential. Only some skeletal data is available on NORM in Indian building materials.

A natural radiation background exists everywhere and every natural substance contains some amount of radioactive material. Natural radiation and radioactivity are of importance to radiation physics for the following reasons:

- i. The natural sources represent a continuous exposure of beings on the earth and thus are a benchmark for consideration of levels of radiation protection not only for enhanced sources of natural radiation and radioactivity, but other sources as well.
- ii. Human activities alter exposure to these sources, and understanding of such processes, including discovery and uses of uranium, thorium, and radon and their transformation products, is fundamental to assessing and controlling their radiological impacts.
- iii. Every measurement of a radiation level or the radioactivity in a sample or source must take into account the background associated with NORM [2].

## **1.2 Naturally Occurring Radioactive Material (NORM)**

Radioactive material containing no significant amounts of radionuclides other than naturally occurring radionuclides is known as NORM. The exact definition of significant amount would be a regulatory decision. Material in which the activity concentrations of the naturally occurring radionuclides have been changed by a process is included in a

naturally occurring radioactive material. Naturally occurring radioactive material or NORM should be used in the singular unless reference is made explicitly being made to various materials [3].

### 1.2.1 Cosmic Origin

During the first decade of the twentieth century, experiments suggested a hitherto unknown source of radiation that was thought to be entirely gamma radiation from terrestrial sources. An Austrian physicist, V. F. Hess, was investigating the attenuation of terrestrial gamma radiation by the atmosphere and conducted experiments with radiation detectors in balloons. The instruments registered increasing radiation levels with increasing altitude. He concluded, in 1912, that penetrating radiation was coming from extraterrestrial sources: cosmic radiation had been discovered [4].

Cosmic radiations are conventionally divided into two classes, namely primary and secondary cosmic radiation. The former is energetic charged particles of extra-terrestrial origin, while the latter are the products resulting from collisions of the primary cosmic rays with the atoms of the earth's atmosphere. After the inevitable interaction of a primary particle with some atom high in the atmosphere, the nuclear debris produced undergoes successive interactions with atoms further down in the atmosphere. In such collisions  $\pi$  – mesons are created and they decay into muons and gamma rays. Muons continue moving down to sea level before they decay. On the other hand, the gamma ray produce electron-positron pairs which in turn radiate more gamma rays. The huge number of electrons created in this way is called extensive air showers. The total number of primary cosmic rays striking the earth's atmosphere is roughly  $10^4 \text{ m}^{-2} \text{ s}^{-1}$ . The primary cosmic rays comprise about 90 % protons, 9 % He, 1 % heavier nuclei, and almost negligible anti nuclei.

The energy spectrum of a nuclear component extends smoothly from  $10^6$  eV to  $10^{20}$  eV. The mean particle energy of the galactic cosmic ray spectrum is about 1 GeV, and the number density of these particles in interstellar space is about  $10^{-3} \text{ m}^{-3}$ , almost equal to the energy density of the electromagnetic radiation and that of the magnetic fields. The energy spectrum falls off more gently than the thermal distribution; intensity at energy  $E$  is proportional to approximately  $E^{-2.6}$  [5].

The other origin of cosmic radiation is the sun. Particles of low energy are emitted continuously by the sun but more energetic ones are emitted during solar events such as magnetic disturbances or flares. Thus, emission of solar cosmic radiation tends to follow the 11 year solar cycle with a maximum during increased solar activity and a minimum in the 'quiet period'. Solar cosmic rays are usually of considerably lower energy than those of galactic origin and energies are typically between 1 and 100 MeV. They are of less significance at the earth's surface because most have insufficient energy to penetrate the earth's magnetic field.

On entering the earth's atmosphere, energetic particles, primarily photons, may interact with nuclei of atmospheric gases (nitrogen, oxygen and argon) in a variety of nuclear reactions. The products include neutrons, protons, muons, pions, and kaons, together with radioisotopes such as  $^3\text{H}$ ,  $^7\text{Be}$ ,  $^{14}\text{C}$ , and  $^{22}\text{Na}$  [4].

The magnetic field of the earth partly reduces the intensity of cosmic radiation reaching the top of the atmosphere, the form of the earth's field being such that only particles of higher energies can penetrate at lower geomagnetic latitudes. This produces the geomagnetic latitude effect, with minimum intensities and dose rates at the equator and

maximum near the geomagnetic poles. At ground level, the dominant component of the cosmic-ray field is muons with energies mostly between 1 and 20 GeV. These contribute about 80% of the absorbed dose rate in free air from the directly ionizing radiation; the remainder comes from electrons produced by the muons or present in the electromagnetic cascade. In the early literature, these two components of the charged particle flux were referred to as the “hard” and “soft” components, respectively, because the electrons are much more readily absorbed by any shielding. As altitude increases, the electrons become more important contributors to the dose rate. Many measurements have been made of the altitude profile of the charged-particle and photon ionization and the absorbed dose rate in free air at ground level. A review of this information in the UNSCEAR 1988 Report indicated that a representative value for this dose rate at sea level is  $32 \text{ nGy h}^{-1}$ . The geomagnetic latitude effect is about 10%, so that a value of  $30 \text{ nGy h}^{-1}$  is appropriate for latitudes below  $30^\circ$ . Considering that a large fraction of the world population lives at latitudes below  $30^\circ$  (50% in the northern hemisphere, 85% in the southern hemisphere, and 54% overall), the population-weighted average absorbed dose rate from the directly ionizing and photon components of cosmic radiation at sea level corresponds to  $31 \text{ nGy h}^{-1}$ , although it is not known to this precision. The dose rate values may be considered as averages over the 11-year solar activity cycle, with the total range of variation about 10%. Since mostly muons are involved, a radiation weighting factor of unity is appropriate, yielding the same values for the effective dose rate, i.e.  $31 \text{ nSv h}^{-1}$  or  $270 \text{ } \mu\text{Sv a}^{-1}$  [6].

### 1.2.2 Terrestrial Origin

Naturally occurring radionuclides of terrestrial origin (also called primordial radionuclides) are present in various degrees in all media in the environment, including the

human body itself. Only those radionuclides with half-lives comparable to the age of the earth, and their decay products, exist in significant quantities in these materials. These radionuclides are also present in the body and irradiate the various organs with alpha and beta particles, as well as gamma rays. Some other terrestrial radionuclides, including those of the  $^{235}\text{U}$  series,  $^{87}\text{Rb}$ ,  $^{138}\text{La}$ ,  $^{147}\text{Sm}$ , and  $^{176}\text{Lu}$ , exist in nature but at such low levels that their contributions to the dose in humans are small.

### 1.2.2.1 Natural radioactive decay series

Many of the naturally occurring radioactive elements are members of one of four long chains, or radioactive series, stretching through the last part of the chart of nuclides. The members of these series are genetically related by alpha and beta decay. In all the cases, their final product is a stable isotope of lead. Of the three series, namely the uranium series (starting with  $^{238}\text{U}$  and ending with  $^{206}\text{Pb}$ ), the thorium series (beginning with  $^{232}\text{Th}$  and ending with  $^{206}\text{Pb}$ ), and the actinium of  $^{235}\text{U}$  series (beginning with  $^{235}\text{U}$  and ending with  $^{207}\text{Pb}$ ), the first two contribute appreciably to population exposure. The fourth series is Neptunium (starting with  $^{237}\text{Np}$  and ending with  $^{209}\text{Bi}$ ). With the exception of Neptunium, each of the parent nuclide is primordial in origin because they are so long lived that they still exist some 4.5 billion years after the solar system was formed. Primordial sources of  $^{237}\text{Np}$  no longer exist because its half-life is only 2.1 million years. The radioactive transformations starting with  $^{241}\text{Pu}$  to  $^{241}\text{Am}$ , the two parent radionuclides produced in nuclear reactors that are now common sources of  $^{237}\text{Np}$ . The genealogical relationships of the uranium and thorium series are shown in fig 1.1 and 1.2 respectively.

The parent radionuclide  $^{238}\text{U}$  makes up 99.2739 % of natural uranium and is normally in equilibrium with its great granddaughter of  $^{234}\text{U}$ , whose content in natural uranium is about

0.0056 %. Whereas  $^{235}\text{U}$  in natural uranium is about 0.7205 %. Because uranium is present in soils and fertilisers, it is also present in food and water and so inevitably also in the human body. The uranium series contains several subseries in addition to  $^{238}\text{U}$  itself as shown in fig 1.1. The more important ones are  $^{230}\text{Th}$ ,  $^{226}\text{Ra}$ ,  $^{222}\text{Rn}$ , and  $^{210}\text{Pb}$  and their subsequent products. The radionuclides  $^{226}\text{Ra}$  and its decay products are responsible for radiation exposure of the public by both internally as well as externally. The half-life of  $^{226}\text{Ra}$  is 1622 years, and it decays by emitting alpha particle to  $^{222}\text{Rn}$ , having half-life of 3.8 days. The decay of  $^{222}\text{Rn}$  is followed by the consecutive transformation of a number of short lived alpha and beta decay products. After six decay stages  $^{210}\text{Pb}$  is produced, which has a relatively longer half-life of 22 years. Both  $^{210}\text{Pb}$  (a beta emitter), and  $^{210}\text{Po}$  (an alpha emitter), another long lived decay product of  $^{222}\text{Rn}$ , are present in atmosphere. They are also released during the combustion of coal.

The parent  $^{232}\text{Th}$  decays to stable  $^{208}\text{Pb}$  nine radioactive daughters as shown in fig. 1.2. With the exception of the parent  $^{232}\text{Th}$  (half-life  $1.4 \times 10^{10}$  y) the daughter half-lives are all less than seven years.  $^{228}\text{Th}$  and  $^{228}\text{Ac}$  have half-lives 1.9 y and 6.7 y respectively. The remaining radionuclides half-lives varying from nanoseconds to 10.64 h.

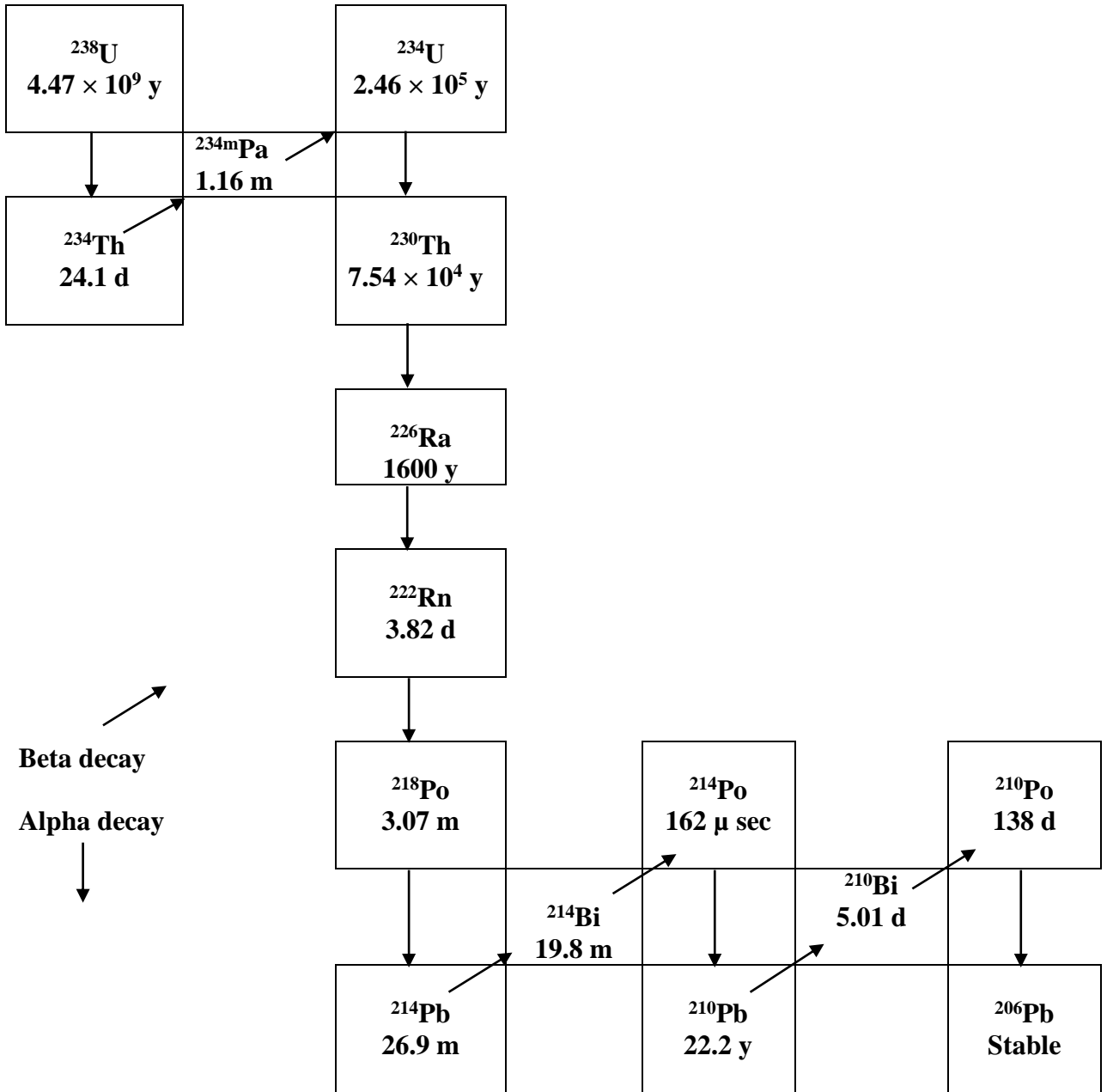


Figure 1.1 Uranium ( $^{238}\text{U}$ ) Natural Radioactive decay series.

[7]

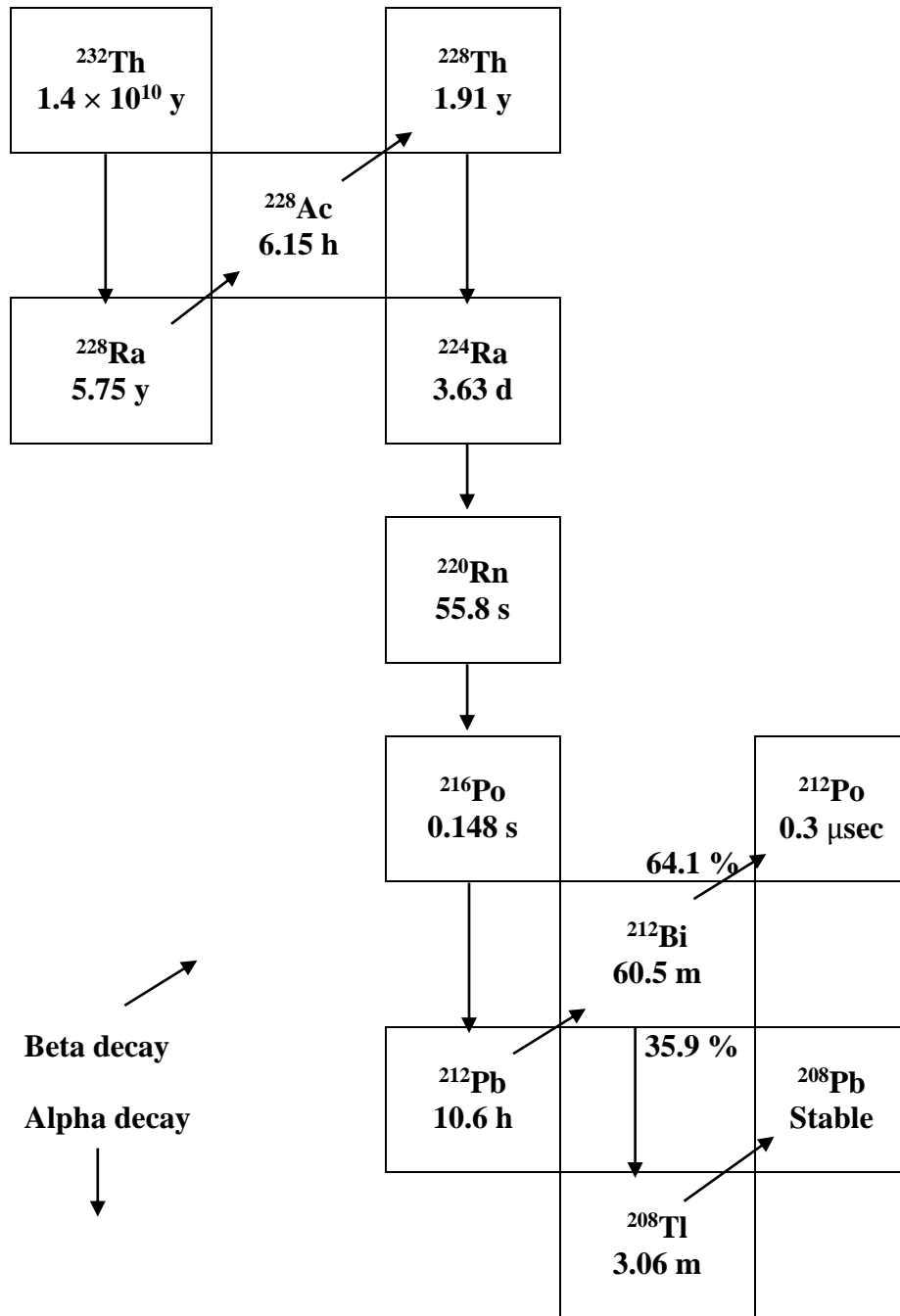


Figure 1.2 Thorium ( $^{232}\text{Th}$ ) Natural Radioactive decay series.

[7]

### 1.2.2.2 Singly occurring radionuclides

There are more than 20 very long-lived primordial radionuclides which were present when the earth was created and which still exist as singly occurring or isolated radionuclides not belonging to any of the decay series. In terms of doses, only two of these natural radionuclides, namely  $^{40}\text{K}$  and  $^{87}\text{Rb}$ , contribute significantly to population exposure.

The radionuclide  $^{40}\text{K}$  is present in natural potassium with an abundance of 0.018 % and has a half-life of  $1.27 \times 10^9$  years. Its decay scheme is shown in Fig. 1. 3. The principal transformation includes electron capture (about 10.67 %) and beta particle emission (about 89.23 %). The mean energy of beta particle is 0.5 MeV (Maximum energy of 1.312 MeV). Electron capture leads to an excited state of  $^{40}\text{Ar}$  which returns to ground state by the emission of an energetic gamma photon of energy 1460.83 keV. This occurs in 10.7 % of all the decays. The response to  $^{40}\text{K}$  characteristic photons is often used as reference energy for the calibration of detectors in the gamma spectrometry of environmental samples where natural potassium is practically always present. Potassium is widely distributed in nature, with concentrations ranging from about 0.1 % for limestone 1 % for sandstones to as much as 3.5 % for some granite. The mean activity of  $^{40}\text{K}$  in crustal rock can be more than 600  $\text{Bqkg}^{-1}$ , while in some granite it may reach values exceeding 2  $\text{kBq kg}^{-1}$ . The content of  $^{40}\text{K}$  in arable soils, however, has been increasing slightly due to the use of fertilizers rich in potassium. Applications of potassium bearing fertilizers for 20 years can increase the potassium content in soil by as much as ten times. Potassium is also an important biogenic element and is found in all living and formerly living organisms. A 70 kg man contains about 140 g of potassium, most of which is located in muscle. This corresponds to an activity of  $^{40}\text{K}$  in the body of about 4.4  $\text{kBq}$ . Since its location is in muscle, the amount of

potassium in the human body depends on age and also on sex. The concentration of  $^{40}\text{K}$  generally decreases with age and is usually greater in men than women [8]. The average elemental concentration of potassium in reference man is 2 % which produces annual doses of 140  $\mu\text{Sv}$  to bone surfaces, 170  $\mu\text{Sv}$  on average to soft tissue, and 27  $\mu\text{Sv}$  to red bone marrow.

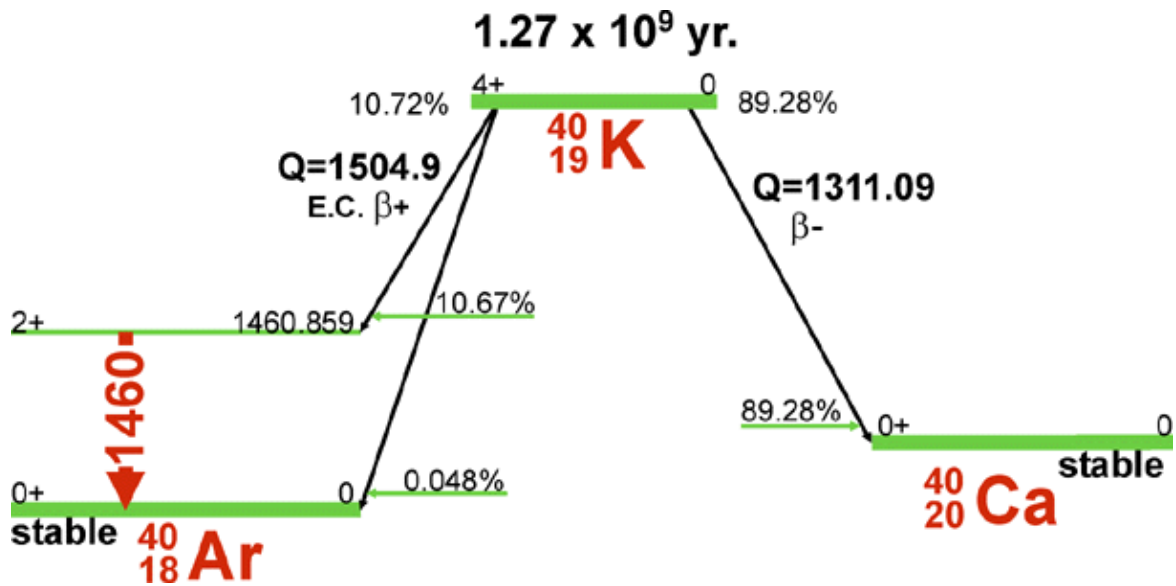


Figure 1.3  $^{40}\text{K}$  Decay scheme [9]

Rubidium-87 has a half-life of  $4.8 \times 10^{10}$  years and emits beta particles of maximum energy 292 keV (average energy  $\sim 79$  keV). Its natural isotopic abundance is 27.84 % and the mass concentrations in reference man range from 6 ppm in the thyroid to 20 ppm in the testes. It contributes an annual; dose to body tissues of 14  $\mu\text{Sv}$  to bone surface cells and an annual effective doses equivalent of about 6  $\mu\text{Sv}$  [2]. Table 1.1 shows the terrestrial radiation distribution of India.

**Table 1.1 Terrestrial radiation distribution in India. [10]**

S. No.	Location	Geological Formation	Range and mean of terrestrial radiation ( $\mu\text{Gy y}^{-1}$ )
1.	Ahmedabad (Gujarat)	U. Vindyan: Lime stone, quartzite	170 – 360 (327)
2.	Bhopal (M. P.)	Shale	178 – 886 (504)
3.	Mumbai (Maharashtra)	Deccan traps: Basalts	89 – 655
4.	Kolkata (W. Bengal)	Silt, Clay	400 – 724 (521)
5.	Dharmasala (H.P)	Clays, marl, sandstone, quartz	241 – 1068 (617)
6.	Guwahati (Assam)	Gneiss rocks	200 – 2397 (1079)
7.	Hyderabad (Andhra Pradesh)	Unclassified crystalline: granitic gneisses, granite	717 – 1461
8.	Jaipur (Rajasthan)	Alluvium: Blown sands, dunes	303 – 360 (327)
9.	Jhansi (U. P)	Bundelkhand granite	1191 – 1931 (1533)
10.	Kakinada (A. P.)	Alluvium: Sands silt	177 – 674 (408)
11.	Chennai (T. N.)	Laterite, Alluvium	217 – 703 (407)
12.	Minicoy (Lakshadweep)	Corals	20 – 205 (99)
13.	Panaji (Goa)	Schist, Amphibolite	97 – 1100 (455)
14.	Trivandrum (Kerala)	Quilon Warkala bed: Sandstone, clay, lime stone	178 – 1059 (569)
15.	Udaipur (Rajasthan)	Aravalli system: Schists, phyllite, conglomerates	112 – 1144 (371)

### 1.3 Enhanced Sources of Naturally Occurring Radioactive Material

Activities related to the extraction and processing of ores can lead to enhanced levels of NORM in products, by-products and wastes. Metal mining and smelting industry, phosphate industry, coal mining and power production from coal, oil and gas drilling

industry, rare earth and titanium oxide industry are the major non-nuclear industries of concern for NORM exposure of the public.

From radiological point of view, the use of fly ash generated during coal burning in the thermal power production, and phosphogypsum from phosphate fertiliser industry, in building materials, are more significant. Large quantities of coal ash (fly ash and bottom ash) are produced each year throughout the world. It is estimated that about 280 million tons of coal ash are produced annually in all coal-fired power plants. The use of coal ash is very wide; the largest in the manufacture of cement and concrete, then in road construction and it is also useful for the production of fertilisers. Although only about 5 % of the total ash production from coal burning power plants is used for the construction of dwellings, the impact in terms of population exposure cannot be neglected. It was assessed that the use of concrete containing fly ash for constructing houses would result in additional annual effective doses of 70  $\mu\text{Sv}$  and 30  $\mu\text{Sv}$  in concrete and wooden houses, respectively [8].

Phosphate rock is the basic material used in the production of all phosphate products and it is also the main source of phosphorous for many types of fertilisers. This rock is sedimentary, volcanic and biological origin. Total global phosphate deposits are estimated to be 163 billion ton. Most of these deposits are of sedimentary origin, with as little as 4% being of igneous origin [11]. Activity concentrations of  $^{232}\text{Th}$  and  $^{40}\text{K}$  in phosphate rocks of all types are similar to those found in normal soil, while concentrations of  $^{238}\text{U}$  and its decay products are usually elevated in phosphate deposits of sedimentary origin. A typical concentration of  $^{238}\text{U}$  in sedimentary phosphate deposits is about 1.5  $\text{kBq kg}^{-1}$ . The use of by-products of phosphate industrial activities seems to have the most significant

radiological impact attributable to phosphate rocks. The main products of these industrial operations are phosphogypsum in wet process fertiliser plants and calcium silicate in thermal process plants. It has been estimated that, by 2006, a total of 2.6–3.7 billion tons of phosphogypsum had been accumulated in stacks worldwide, representing 44–62 % of the total amount of phosphogypsum produced up to that time. Phosphogypsum is currently being added to stacks at an annual rate of about 40 million ton in the USA and 90 million ton elsewhere. At these rates, the total amount of phosphogypsum stored in stacks will more than double to 7–8 billion tons by 2040. Most of this growth will occur in countries with developing economies, where a three or fourfold increase can be predicted from current growth patterns. The actual growth is likely to be faster because of further reductions in discharges to water bodies and increased phosphogypsum production. Phosphogypsum has been used as a raw material for cement and as a source of plasterboard. Other construction uses include the production of bricks, blocks, tiles, artificial stone and even boats. Countries using phosphogypsum for building purposes, usually with certain restrictions, include Belgium, Brazil and India. Phosphogypsum is viewed as a potential building material in South Africa, where the construction of low cost housing is being encouraged. Almost all the uses of phosphogypsum for building products require the phosphogypsum to be well washed to remove the acidity from its residual water content and in some cases further processed to remove residual phosphate [11]. The concentration of  $^{226}\text{Ra}$  in phosphogypsum is typically about  $900 \text{ Bq kg}^{-1}$ . Assuming that 1 % of the world's population lives in houses that were constructed using building materials containing phosphogypsum, the annual effective dose would amount to about  $5 \times 10^4 \text{ man Sv}$ , which corresponds to a per caput annual effective dose of about  $10 \mu\text{Sv}$  [8].

Titanium pigment production, Oil and Gas extraction, Uranium mining, Zircon sand mining, metals ore processing are the other industries generate enhanced level of natural radioactivity.

#### **1.4 Radiological significance of NORM**

Unlike the anthropogenic radionuclides, which do not normally exist in appreciable concentrations for any length of time in the natural environment, NORM is widely distributed, and gives rise to a natural radiation background that varies by approximately two orders of magnitude over the Earth, and even more if localised mineral deposits are taken into account. This means every living species is exposed to this radiation, and in most situations this exposure is not amenable to control. There appears to be no scientific evidence relating general variations in this natural background to health effects. ICRP 103 recommendations [12] and The IAEA BSS GSR Part-3 [13] have classified the NORM related exposure to the public as existing exposure situation. Existing exposure situations are those that already exist when a decision on control has to be taken. There are many types of existing exposure situations that may cause exposures high enough to warrant radiological protective actions, or at least their consideration. Radon in dwellings or the workplace, and naturally occurring radioactive material (NORM) are well-known examples.

##### **1.4.1 Dosimetric Quantities and units**

Radiological protection has the general aim of protecting humans and the environment from harm caused by ionising radiation after external as well as internal exposures. This requires a quantitative description of the radiation fields external to and internal within the human body [12]. The physical theory of dosimetry for environmental radiation, including

radiation emitted from naturally occurring radioactive materials (NORM), is no different than that required in any other setting where doses are estimated. However, the application of such theory to environmental radiation and NORM may require considerations that differ from dose estimation elsewhere. This is especially true if the intent is to provide estimated doses for epidemiological analyses. It should be realised that the metrics of radiation dose for radiation protection purposes are generally not the same as for analytic epidemiological studies which require estimates of absorbed dose to specific organs of identified persons. In addition, exposure to environmental radiation and NORM typically involve radiation fields that vary considerably over space, and the patterns of an individual's movements, as well as the types of buildings in which they reside and work, can significantly affect the dose received from external radiation [14]. This section summarises the major dosimetric quantities and units used in radiation protection.

### **Activity**

The activity,  $A$ , of an amount of a radionuclide in a particular energy state at a given time, is the quotient of  $dN$  by  $dt$ , where  $dN$  is the number of spontaneous nuclear transformations from that energy state in time interval  $dt$ , thus  $A = dN/dt$ . Its unit is  $S^{-1}$ , the special name for the unit of activity is Becquerel (Bq). The mean number of spontaneous nuclear transitions per unit time interval.  $1 \text{ Bq} = 1 \text{ disintegration per second}$ .  $1 \text{ Ci (curie)} = 3.7 \times 10^{10} \text{ Bq}$ .  $1 \text{ g of } ^{226}\text{Ra}$  has an activity of  $3.7 \times 10^{10} \text{ Bq}$  [3] and [15].

### **Specific activity**

It is known as activity per unit mass,  $a$ , Becquerel per kilogram,  $\text{Bq/kg}$ , ( $\text{kg}^{-1}\text{s}^{-1}$ ). The number of atomic decays per unit time per unit mass. Used to describe the radionuclide content of rocks, building materials etc.

## Exposure

The ionizing power of electromagnetic radiation in air is known as exposure,  $X$ . It is the quotient of  $dQ$  by  $dm$ , where  $dQ$  is the absolute value of the total charge of the ions of one sign produced in air when all the electrons and positrons liberated or created by photons in air of mass  $dm$  are completely stopped in air, thus

$$X = \frac{dQ}{dm} \quad (1.1)$$

SI unit of exposure is  $C\ kg^{-1}$ .

The ionization produced by auger electron is included in the in  $dQ$ . The ionization due to photons emitted by radiative processes (i.e. Bremsstrahlung and fluorescence photons) is not to be included in  $dQ$ . The special name of the unit is Roentgen,  $R$ .  $1\ R = 2.58 \times 10^{-4}\ Ckg^{-1}$ .

## Exposure Rate

The exposure rate,  $X_r$ , is the quotient of  $dX$  by  $dt$ , where  $dX$  is the increment of exposure in the time interval  $dt$ , thus,

$$X_r = \frac{dX}{dt} \quad (1.2)$$

SI unit is  $C\ kg^{-1}\ s^{-1}$ . Exposure rate was used for the description of terrestrial gamma radiation in  $\mu Rh^{-1}$ .

## Fluence

Fluence,  $\Phi$ , is the quotient of  $dN$  by  $da$ , where  $da$  is the number of particles incident on a sphere of cross-sectional area  $da$ , thus,

$$\Phi = \frac{dN}{da} \quad (1.3)$$

The unit of Fluence is  $m^{-2}$ . Fluence is independent of the direction distribution of the particles entering the sphere. In radiation transport calculations, Fluence is frequently expressed in terms of the length of particle trajectories. Fluence,  $\Phi$  is then given by

$$\Phi = \frac{dl}{dV} \quad (1.4)$$

Where  $dl$  is the sum of the particle trajectories in the volume  $dV$ .

### **Kerma**

The kerma,  $K$ , is the quotient of  $dE_{tr}$  by  $dm$ , where  $dE_{tr}$  is the sum of initial kinetic energies of all charged the particles liberated by uncharged particles in a mass  $dm$  of material, thus

$$K = \frac{dE_{tr}}{dm} \quad (1.5)$$

SI unit of kerma is  $Jkg^{-1}$ . The special name of the unit is Gray (Gy). The quantity  $dE_{tr}$  includes the kinetic energy of the Auger electrons.

For a Fluence,  $\Phi$ , of uncharged particles of energy,  $E$ , the kerma,  $K$ , in a specific material is given by

$$K = \Phi E \frac{\mu_{tr}}{\rho} \quad (1.6)$$

$\frac{\mu_{tr}}{\rho}$  is the mass energy transfer coefficient of the material for these particles. Although kerma is a quantity which concerns initial transfer of energy to matter, it is sometimes used as an approximation to absorbed dose. Equality of absorbed dose and kerma is approached to the degree that charged particle equilibrium exists, that radiative losses are negligible, and that the energy of the uncharged particles large compared to the binding energy of the released charged particles. Charged particle equilibrium exists at a point if the distribution of the charged particle radiance with respect to energy is constant within distances equal to the maximum charged particle range.

### **Kerma rate**

The kerma rate,  $K_r$ , is the quotient of  $dK$  by  $dt$ , where  $dK$  is the increment of kerma in the time interval  $dt$ , thus

$$K_r = \frac{dK}{dt} \quad (1.7)$$

SI unit is  $\text{Jkg}^{-1}\text{s}^{-1}$ . Special name of the unit is Gray per second ( $\text{Gys}^{-1}$ ).

### **Absorbed Dose**

In radiation biology, clinical radiology, and radiological protection the absorbed dose,  $D$ , is the basic physical dose quantity, and it is used for all types of ionising radiation and any irradiation geometry. It is defined as the quotient of  $d\varepsilon$  by  $dm$ , where  $d\varepsilon$  is the mean energy imparted to matter of mass  $dm$  by ionizing radiation, that is

$$D = \frac{d\varepsilon}{dm} \quad (1.8)$$

The SI unit of absorbed dose is  $\text{Jkg}^{-1}$  and its special unit is gray (Gy).  $1 \text{ R} = 8.69 \times 10^{-3} \text{ Gy}$  (in air),  $1 \text{ R} = 9.57 \times 10^{-3} \text{ Gy}$  (in tissue).

### Absorbed Dose Rate

Absorbed dose rate,  $D_r$ , is the quotient of  $d\varepsilon$  by  $dt$ , where  $dD$  is the increment of absorbed dose in the time interval  $dt$ . Thus

$$D = \frac{d\varepsilon}{dm} \quad (1.9)$$

SI unit is  $\text{J kg}^{-1} \text{ s}^{-1}$ . Special name of the unit is Gray per second ( $\text{Gy s}^{-1}$ ). Gamma dose rate in air is used for the description of terrestrial radiation, and is usually expressed in  $\text{nGyh}^{-1}$ . For conversion of terrestrial exposure rate to terrestrial dose rate in air it holds:  $1 \mu\text{Rh}^{-1} = 8.69 \text{ nGyh}^{-1}$ .

### Equivalent Dose

The protection quantity equivalent dose in an organ or tissue,  $H_T$ , is defined as

$$H_T = \sum_R W_R D_{T,R} \quad (1.10)$$

$W_R$  is the radiation weighting factor for radiation R. The unit of equivalent dose is  $\text{J kg}^{-1}$  and has the special name Sievert (Sv). Table 1.2 shows the  $W_R$  values of various types of radiations recommended in ICRP 103 [12]. The radiation weighting factor ( $w_R$ ) for photons, electrons and muons is 1. For protons and charged pions it is 2, whereas for alpha particle and fission fragments it is 20. A continuous function of energy is used in case of neutron radiation weighting factors.

**Table 1.2 Radiation weighting factor for different radiation. [12]**

<b>Radiation type</b>	<b>Radiation weighting factor, <math>W_R</math></b>
Photons	1
Electrons and muons	1
Protons and charged pions	2
Alpha particle, fission fragments, heavy ions	20
Neutrons	A continuous curve as a function of neutron energy

### Effective Dose

The effective dose,  $E$ , is defined by a weighted sum of tissue equivalent doses as:

$$E = \sum_T W_T H_T = \sum_T W_T \sum_R W_R D_{T,R} \quad (1.11)$$

Where  $W_T$  is the tissue weighting factor for tissue  $T$  and  $\sum W_T = 1$ . The sum is performed over all organs and tissues of the human body considered to be sensitive to the induction of stochastic effects. These  $w_T$  values are chosen to represent the contributions of individual organs and tissues to overall radiation detriment from stochastic effects. The unit of effective dose is  $J kg^{-1}$  with the special name Sievert (Sv). The unit is the same for equivalent dose and effective dose as well as for some operational dose quantities. Table 1.3 shows the  $W_T$  values for various organ and tissues adopted ICRP 103 recommendation

[12]. For environmental gamma radiation the estimate is  $E = D'a \times t \times 0.7 \times 10^{-6}$ , where E is the effective dose (mSv),  $D'$ , is the dose rate in air ( $\text{nGyh}^{-1}$ ), t is the exposure time (h) and 0.7 is the conversion coefficient ( $\text{SvGy}^{-1}$ ) for human organs (UNSCEAR, 1988). For  $D'a = 100 \text{ nGyh}^{-1}$ ,  $t = 8760 \text{ h}$  (1 year),  $E = 0.613 \text{ mSv}$ .

The main and primary uses of effective dose in radiological protection for both occupational workers and the general public are:

- i. Prospective dose assessment for planning and optimisation of protection; and
- ii. Retrospective dose assessment for demonstrating compliance with dose limits, or for comparing with dose constraints or reference levels.

In this sense, effective dose is used for regulatory purposes worldwide. In practical radiological protection applications, effective dose is used for managing the risks of stochastic effects in workers and the public [12].

**Table 1.3 Tissue weighting factor for different organs and tissues. [12].**

<b>Tissue</b>	<b>weighting factor <math>W_T^*</math></b>	<b><math>\sum W_T</math></b>
Bone-marrow (red), Colon, Lung, Stomach, Breast, Remainder Tissues **(nominal weighting factor applied to the average dose to 14 tissues)	0.12	0.72
Gonads	0.08	0.08
Bladder, Esophagus, Liver, Thyroid	0.04	0.16
Bone surface, Brain, Salivary glands, Skin	0.01	0.04

\*ICRP 103

\*\*Remainder Tissues (14 in total): Adrenals, Extra thoracic (ET) region, Gall bladder, Heart, Kidneys, Lymphatic nodes, Muscle, Oral mucosa, Pancreas, Prostate, Small intestine, Spleen, Thymus, Uterus/cervix.

### **Annual Dose**

As prolonged exposures persist over time, the relevant dosimetric quantity for dealing with longed exposures is the committed effective dose in a specified period; for practical reasons, a period of one year is chosen. The annual effective dose is, unless otherwise indicated, simply termed annual dose in this report. The annual dose is thus defined as the sum of (i) the time integral, over a year, of the effective dose rate due to external irradiation caused by a prolonged exposure situation, and (ii) the committed effective dose due to internal contamination from any intakes, during the year, of the long-lived radionuclides (and their short-lived progeny) involved in the situation. The unit used in this report for the annual dose is a thousandth of a Sievert, i.e. millisievert (mSv), per annum [16].

**Reference Level**

For an emergency exposure situation or an existing exposure situation, the level of dose, risk or activity concentration above which it is not appropriate to plan to allow exposures to occur and below which optimization of protection and safety would continue to be implemented. The value chosen for a reference level will depend upon the prevailing circumstances for the exposure under consideration [13].

**Operational dose quantities**

The protection quantities ‘equivalent dose’ and ‘effective dose’ are not measurable, and therefore cannot be used directly as quantities in radiation monitoring. Operational quantities are, therefore, used for the assessment of effective dose or equivalent dose in tissues or organs for demonstration of compliance with regulations on occupational exposures and the application of the principle of as low as reasonably achievable, economic and societal factors being taken into account. The operational dose quantities, based on dose equivalent and defined by ICRU for measurements in external radiation fields, are the ambient dose equivalent, the directional dose equivalent, and the personal dose equivalent. The first two quantities are used for area monitoring, while the last quantity is for individual monitoring.

Operational quantities aim to provide a reasonable estimate, generally conservative, for the value of the protection quantities related to an exposure or potential exposure of persons under most irradiation conditions. They are often used in practical regulations or guidance. For monitoring of external radiation exposures, operational dose quantities as defined by ICRU were introduced into radiological protection practice in many countries. There are

situations in which personal dosimetry is not used but where area monitoring is applied to assess individual exposures. These situations include the assessment of doses to aircraft crew, prospective dose assessments, and assessment of doses in workplaces and in the natural environment.

i. **Dose equivalent**

The dose equivalent,  $H$ , is the product of  $Q$  and  $D$  at a point in tissue, where  $D$  is the absorbed dose and  $Q$  is the quality factor at that point, thus:

$$H = Q D \quad (1.12)$$

ii. **Operational quantities for area monitoring**

For all types of external radiation, the operational quantities for area monitoring are defined on the basis of a dose-equivalent quantity that would exist in the ICRU sphere as a theoretical construct of tissue-equivalent material (30 cm in diameter, ICRU 4-element tissue with a density of 1 g/cm<sup>3</sup>, and a mass composition of 76.2% oxygen, 11.1% carbon, 10.1% hydrogen, and 2.6% nitrogen). In most cases, this phantom adequately approximates the human body with regards to scattering and attenuation of radiation fields under consideration. The operational quantities for area monitoring defined in the ICRU sphere retain their character of a point quantity and the property of additivity. This is achieved by using a fixed depth in the definition of each quantity.

An expanded radiation field is defined as a hypothetical field in which the Fluence and its direction and energy distributions have the same value throughout the volume of interest as in the actual field at the point of reference. The expansion of the radiation field ensures that the whole ICRU sphere is exposed to a homogeneous radiation field with the same

Fluence, energy distribution, and direction distribution as in the point of interest of the real radiation field.

If all radiation is aligned in the expanded radiation field so that it is opposed to a radius vector  $X$  specified for the ICRU sphere, the aligned and expanded radiation field is obtained. In this hypothetical radiation field, the ICRU sphere is homogeneously irradiated from one direction, and the Fluence of the field is the integral of the direction distribution of Fluence at the point of interest in the real radiation field.

In the expanded and aligned radiation field, the value of the dose equivalent at any point in the ICRU sphere is independent of the direction distribution of the radiation that might exist in the real radiation field. Conversion coefficients relating radiation field quantities to the operational quantities for area monitoring are calculated for the particles at the point of interest in the real radiation field using the model of the expanded and aligned field and the ICRU sphere phantom, assuming a vacuum outside of the phantom.

**a) Ambient dose equivalent  $H^*(d)$**

The ambient dose equivalent,  $H^*(10)$ , at a point in a radiation field, is the dose equivalent that would be produced by the corresponding expanded and aligned field in the ICRU sphere at a depth of 10 mm on the radius opposing the direction of the aligned field.

**b) Directional dose equivalent  $H'(d, \Omega)$**

The directional dose equivalent,  $H'(d, \Omega)$ , at a point in a radiation field, is the dose equivalent that would be produced by the corresponding expanded field in the ICRU sphere at a depth,  $d$ , on a radius in a specified direction  $\Omega$ .

For assessing the dose to the skin and the extremities,  $d = 0.07$  mm is used and  $H'(d, \Omega)$  is then written as  $H'(0.07, \Omega)$ . In the case of monitoring the dose to the lens of the eye, the operational quantity  $H'(d, \Omega)$  with  $d = 3$  mm was recommended for use by ICRU. However, if the monitoring device is not designed to measure  $H'(3, \Omega)$ ,  $H'(0.07, \Omega)$  may be used as a surrogate.

### **iii. Operational quantities for individual monitoring**

Individual monitoring of external exposure is usually performed with personal dosimeters worn on the body, and the operational quantity defined for this application takes this situation into account. For individual monitoring, the operational quantity is the personal dose equivalent,  $H_p(d)$ .

The personal dose equivalent,  $H_p(d)$ , is the dose equivalent in ICRU soft tissue at an appropriate depth,  $d$ , below a specified point on the human body.

For assessment of the radiation protection quantity 'effective dose', a depth  $d = 10$  mm is selected, and for assessing the equivalent dose to the skin, hands, wrists, and feet, a depth  $d = 0.07$  mm is recommended. In special cases of monitoring the dose to the lens of the eye, a depth  $d = 3$  mm has been proposed to be most appropriate

Operational quantities that should be measured using portable instruments during dose rate surveys are therefore either:

- ambient dose equivalent at 10 mm depth,  $H^*(10)$  - SI unit: Sievert (Sv)
- ambient dose equivalent rate,  $H^*(10) \text{ h}^{-1}$  - SI unit: Sievert per hour ( $\text{Sv h}^{-1}$ )
- directional dose equivalent at 0.07 mm depth,  $H\phi(0.07)$  - SI unit: Sievert (Sv)
- directional dose equivalent rate,  $H\phi(0.07) \text{ h}^{-1}$  - SI unit: Sievert per hour ( $\text{Sv h}^{-1}$ )

Some instruments may use different quantities such as Fluence rate, air kerma rate, and absorbed dose rate in air. Estimation of dose is a specialist task when using instruments not scaled in dose equivalent or dose equivalent rate.

### Ground radioelement concentration units and conversion constants

In geology and nuclear geophysics, radioelement concentrations in rocks, air and water are expressed in the following units [17]:

- Mass concentration of K: % K (percent potassium)
- Mass concentration of U: ppm U (parts per million of uranium)
- Mass concentration of Th: ppm Th (parts per million of thorium)

$$1 \text{ ppm} = 10^{-6} \text{ g g}^{-1} = 1 \text{ g ton}^{-1}$$

The specific activity of K, U and Th is as follows:

- 1 ppm U in rock =  $12.35 \text{ Bq kg}^{-1} {}^{238}\text{U}$ , or  ${}^{226}\text{Ra}$
- 1 ppm Th in rock =  $4.06 \text{ Bq kg}^{-1} {}^{232}\text{Th}$
- 1% K in rock =  $313 \text{ Bq kg}^{-1} {}^{40}\text{K}$

Activity concentration of Rn in soil gas and air:  $\text{kBq m}^{-3}$ ,  $\text{Bq m}^{-3}$

Activity concentration of radioelements in groundwater:  $\text{Bq l}^{-1}$ ,  $\text{Bq m}^{-3}$

### 1.4.2 External Radiation Exposure

External exposures outdoors arise from terrestrial radionuclides present at trace levels in all soils. The specific levels are related to the types of rock from which the soils originate. Higher radiation levels are associated with igneous rocks, such as granite, and lower levels with sedimentary rocks. There are exceptions, however, as some shales and phosphate rocks have relatively high content of radionuclides. There have been many surveys to determine the background levels of radionuclides in soils, which can in turn be related to the absorbed dose rates in air. The latter can easily be measured directly, and these results provide an even more extensive evaluation of the background exposure levels in different countries. All of these spectrometric measurements indicate that the three components of the external radiation field, namely from the gamma-emitting radionuclides in the  $^{238}\text{U}$  and  $^{232}\text{Th}$  series and  $^{40}\text{K}$ , make approximately equal contributions to the externally incident gamma radiation dose to individuals in typical situations both outdoors and indoors. The absorbed dose rate from the terrestrial radionuclides in soil is usually reduced by the presence of water in the soil and snow cover. This reduction, however, in temperate zones with moderate precipitation, is not significant. It is only in extreme climates with heavy snow cover that the reduction may be sometimes as much as 20 %. On the other hand, in areas with intensive agricultural activities, the dose rate can be increased by the radionuclides present in phosphate fertilizers.

Since the indoor occupancy is 0.8 and there are generally higher radiation levels inside dwellings, one can expect that the population's indoor exposure will be much higher than its outdoor exposure. Indoor exposure to gamma rays, mainly determined by the materials of construction, is inherently greater than outdoor exposure if earth materials have been

used; the source geometry changes from half-space to a more surrounding configuration indoors. When the duration of occupancy is taken into account, indoor exposure becomes even more significant. Buildings constructed of wood add little to indoor exposures, which may then be comparable to outdoor exposures [6]. The ratio of indoor to outdoor exposure largely depends on the structural properties of houses, specially building materials, thickness and dispositions. In general, building materials can act not only as a source of radiation, but they can also provide shielding against outdoor radiation. In massive houses made of bricks, concrete or stones, the penetrating gamma radiation from outdoors may be considerably absorbed by the walls, resulting in a situation where the indoor dose rate depends only on the type and concentrations of natural radionuclides in the building materials. In this case, a crucial role is played by source geometry (the contribution from the floor and ceiling and the four walls) which enhances the exposure so that the indoor absorbed dose may be much higher than that in the open air.

Houses in various parts of the world and in different climatic regions differ considerably as to their design, construction and building materials used. Therefore it is very difficult to estimate indoor dose rates with reasonable accuracy and reliability. In order to improve the assessment of indoor radiation exposures it is necessary to have more data for representative housing stock around the world [8]. The population-weighted average is 84 nGy h<sup>-1</sup> with national averages ranging from 20 to 200 nGy h<sup>-1</sup>. The lowest values are in New Zealand, Iceland and the United States, all below 40 nGy h<sup>-1</sup>, which probably reflects the preponderance of wood-frame houses. The highest values (95 - 115 nGy h<sup>-1</sup>) are in Hungary, Malaysia, China, Albania, Portugal, Australia, Italy, Spain, Sweden, and Iran, which must reflect wide use of stone or masonry materials in buildings.

Effective dose (E) is the indicator of stochastic effect has been widely used in the assessment of environmental gamma radiation exposure. To estimate annual effective doses, account must be taken of (a) the conversion coefficient from absorbed dose in air to effective dose ( $\text{Sv Gy}^{-1}$ ) and (b) the indoor occupancy factor. Monte Carlo method has been used to study the indoor effective dose conversion factor from absorbed dose rate or air kerma rate, using anthropomorphic phantom. As causes of variation, posture of human bodies, biases of the environmental sources distributions, and body sizes were considered. The variation of effective dose in prone position is compared with that in a standing position was found to be 30 %. The bias of environmental gamma sources causes the effective dose per air kerma rate to vary by 20 % at maximum, but in some cases for low energy gamma rays the variation was found to be up to 40 % due to the change in the energy spectrum. The effective dose for the new born infant was estimated to be higher than that for an adult by a maximum of 80 – 90 % for low energy gamma rays from anthropogenic sources because of lower shielding effect of the smaller body. From this study it was found out that the conversion coefficient was  $0.7 \text{ Sv Gy}^{-1}$  for adult whereas for children it was  $0.8 \text{ Sv Gy}^{-1}$  [18]. This factor has been accepted by the United Nations Scientific Committee on Effect of Atomic Radiation (UNSCEAR) and used extensively to calculate the effective dose due to environmental gamma radiation. 0.8 for the indoor occupancy factor, i.e. the fraction of time spent indoors and outdoors is 0.8 and 0.2, respectively, have been adopted by the UNSCEAR.

$$\text{Indoors} = 84 \text{ nGy h}^{-1} \times 8,760 \text{ h} \times 0.8 \times 0.7 \text{ Sv Gy}^{-1} = 0.41 \text{ mSv} \quad (1.13)$$

$$\text{Outdoors} = 59 \text{ nGy h}^{-1} \times 8,760 \text{ h} \times 0.2 \times 0.7 \text{ Sv h}^{-1} = 0.07 \text{ mSv} \quad (1.14)$$

The resulting worldwide average of the annual effective dose is 0.48 mSv, with the results for individual countries being generally within the 0.3 - 0.6 mSv range. For children and infants, the values are about 10% and 30% higher, in direct proportion to an increase in the value of the conversion coefficient from absorbed dose in air to effective dose [6].

### 1.4.3 Internal Radiation Exposure

Internal exposure of the population is mainly due to the intake of terrestrial radionuclides through inhalation and ingestion. Maximum inhalation dose comes from  $^{238}\text{U}$  and  $^{232}\text{Th}$  natural radioactive series progeny radionuclides. Doses by ingestion are mainly due to  $^{40}\text{K}$  and to the  $^{238}\text{U}$  and  $^{232}\text{Th}$  series radionuclides present in foods and drinking water. Some information about the presence of  $^{40}\text{K}$  in the human body of  $55 \text{ Bq kg}^{-1}$  and a conversion coefficient of  $3 \mu\text{Sv y}^{-1}$  per  $\text{Bq kg}^{-1}$ , the annual effective dose from the presence of  $^{40}\text{K}$  in the body has been estimated to be about  $16 \mu\text{Sv}$  for adults and  $185 \mu\text{Sv}$  for children. It is worth noting that the most of the effective dose is delivered by beta particles. Since potassium is under homeostatic control in the human body internal exposure from  $^{40}\text{K}$  is relatively constant and does not depend on its concentrations in the environment. Another important source of internal exposure is inhalation of radon and its decay products.

Radon is a radioactive gas that emanates from rocks and soils and tends to concentrate in enclosed spaces like underground mines or houses. Soil gas infiltration is recognized as the most important source of residential radon. Radon is found in nature in three isotope formations:  $^{222}\text{Rn}$ ,  $^{220}\text{Rn}$  (sometimes called thoron) and  $^{219}\text{Rn}$ . The most important of them is  $^{222}\text{Rn}$ , the immediate decay product of  $^{226}\text{Ra}$ , a member of the uranium series. The half-

life of  $^{222}\text{Rn}$ , 3.8 days, is not enough so that after its formation in some depth in soil or building materials it can reach the outdoor and especially indoor air, where it can accumulate and under some conditions it may reach high concentrations. The second of the radon isotopes worthy of our attention,  $^{220}\text{Rn}$ , is formed in the thorium series from the decay of  $^{224}\text{Ra}$ . Its short half-life (56 s) limits the distance it can reach before decay. Finally,  $^{219}\text{Rn}$  can be found in air but its concentrations are very low, so that it does not present any radiological hazards. This radionuclide is a member of the actinium series (headed by  $^{235}\text{U}$ ) which has a natural abundance of about 100 times lower than radionuclides of the uranium or thorium series. Its sparse occurrence and very short half-life (4 s) are the main factors rendering it insignificant from the point of view of human exposure. After their production in soil or rock,  $^{222}\text{Rn}$  and  $^{220}\text{Rn}$  can leave the ground crust either by molecular diffusion or by convection and enter the atmosphere where their behavior and distribution is mainly governed by meteorological processes. Radon decay products are radioactive isotopes of Po, Bi, Pb, and Tl and they are easily attached to aerosol particles present in air [8]. The fraction of radon atoms released into rock or soil pore space from a radium-bearing grain is called the emanation coefficient, the emanation factor or the emanating power. Typical emanation coefficients for rocks and soils range from 0.05 to 0.7. Grain size and shape are two important factors that control the emanation of radon in soil. They determine how much radium is near enough the grain surface to allow radon to escape into pore spaces. Generally the radon emanation factor is inversely proportional to grain size. Soil moisture plays an important role in the emanation of radon and its diffusion in soil, for several reasons. Soil moisture, in the form of a thin film of water surrounding soil grains, directly affects radon emanation by capturing the radon recoils from the solid matrix. These

captures increase the likelihood that radon atoms will remain in the pore space instead of crossing the pores and imbedding themselves in adjacent soil grains.

The elimination of these radionuclides from the atmosphere occurs either by their decay or by such removal processes as dry deposition, rainout or washout. Similarly, in indoor air the decay products can be removed by radioactive decay, by ventilation, by air cleaning devices, and especially by plate out or deposition. Based on the results of epidemiological studies in Europe and North America, World Health Organization (WHO) has brought down the reference level from  $200 \text{ Bq m}^{-3}$  to  $100 \text{ Bq m}^{-3}$ . The annual effective dose incurred by the population from radon and its decay products is estimated to be 1.15 mSv. For thoron it is 0.1 mSv. Table 1.4 shows the annual average effective dose due to natural radiation sources.

**Table 1.4 Annual average effective dose due to natural radiation [19]**

Source of Exposure		Annual effective dose (mSv)	
Cosmic radiation	Directly ionizing and photon component	0.28	10
	Neutron component	0.1	
	Cosmogenic radionuclides	0.01	
	Total cosmic and cosmogenic	0.39	0.3 – 1.0
External terrestrial radiation	Outdoor	0.07	0.3 – 1.0
	Indoor	0.41	
	Total external terrestrial radiation	0.48	
Inhalation	Uranium and Thorium series	0.006	0.2 – 1.0
	Radon ( $^{222}\text{Rn}$ )	1.15	
	Thoron ( $^{220}\text{Rn}$ )	0.1	
	Total inhalation exposure	1.26	
Ingestion	$^{40}\text{K}$	0.17	0.2 – 1.0
	Uranium and Thorium series	0.12	
	Total ingestion exposure	0.29	
<b>Total</b>		<b>2.4</b>	<b>1.0 – 13.0</b>

#### 1.4.4 Biological effects of low dose ionizing radiation

Most adverse health effects of radiation exposure may be grouped in two general categories:

- i. Deterministic effects (harmful tissue reactions) due in large part to the killing/malfunction of cells following high doses; and
- ii. Stochastic effects, i.e., cancer and heritable effects involving either cancer development in exposed individuals owing to mutation of somatic cells or heritable disease in their offspring owing to mutation of reproductive (germ) cells [12]. For both radiation-induced cancer and heritable disease it is the probability of the occurrence of the effect, not its severity that depends upon the dose. The general assumption for radiological protection is that the risk of these stochastic effects increases in the low dose range linearly with dose, with no threshold (LNT model) [12].

For very low dose and dose rates of concern in public-health aspects of radiation exposure, both the BEIR and the UNSCEAR Committees base risk estimates on a linear, no threshold model (LNT) for dose response. One is the doubling dose method, sometimes called relative-risk method. The second is the direct method which is sometimes called the absolute – risk method. The third is the gene-number method which is sometimes identified as the second of two direct methods. The doubling dose method makes use of the natural frequency of hereditary illness and arrives at estimates of the degree to which the frequency ultimately would be increased as result of a sudden sustained increase in radiation exposure of the public.

A large body of evidence leaves no doubt that ionizing radiation, when delivered in high doses, is one of the main causes of cancer in the human. Excess cancer risk cannot be observed at doses less than about 0.2 Gy, and therefore, risks for lower doses cannot be determined directly (USCEAR 1988). Just how cancer is induced is not understood fully

but it is clear that (1) there are no unique cancer types created solely by ionizing radiation, and, (2) that induction is a multistep process involving initiation promotion, and progression. The initiating event is undoubtedly disruption of the genetic coding within a cell nucleus. The mutation must not be so severe that the cell is unable to reproduce and it must somehow confer a selective advantage in multiplication over sister cells in the host organ or tissue [1].

Because there is a risk of stochastic effects below the threshold for deterministic effects, the selection of a dose limit is only partially a scientific decision. It is mainly a value judgment based not only on scientific information but also on knowledge of the level of risk that is usually considered unacceptable under normal conditions. The annual dose from natural sources may not be harmless, but it can hardly be called unacceptable as it makes only small contribution to the health detriment that society experiences. The variation in the annual doses from radon in dwellings is of the order of  $10 \text{ mSv y}^{-1}$ , although much higher variations can be found. The worldwide average annual effective dose to adults from natural radiation sources is  $2.4 \text{ mSv y}^{-1}$ . The attributable lifetime probability of cancer death from an annual exposure of  $10 \text{ mSv}$  from birth over lifetime would be around 4 %, applying the relative risk model and a dose and dose rate correction factor (DDREF) OF 2. This probability corresponds to an average annual risk of about  $5 \times 10^{-4}$  with an age variation [20].

When radon gas is inhaled, densely ionizing alpha particles emitted by deposited short-lived decay products of radon ( $^{218}\text{Po}$  and  $^{214}\text{Po}$ ) can interact with biological tissue in the lungs leading to DNA damage. Cancer is generally thought to require the occurrence of at least one mutation, and proliferation of intermediate cells that have sustained some degree

of DNA damage can greatly increase the pool of cells available for the development of cancer. Since even a single alpha particle can cause major genetic damage to a cell, it is possible that radon-related DNA damage can occur at any level of exposure. Therefore, it is unlikely that there is a threshold concentration below which radon does not have the potential to cause lung cancer [21]. The International Commission on Radiological Protection (ICRP) has also issued a statement on radon in 2009 after the new ICRP recommendation in 2007. The ICRP reaffirms that radon exposure in dwellings due to unmodified concentrations of  $^{226}\text{Ra}$  in the earth's crust, or from the past practices not conducted within the ICRP's system of protection, is an existing exposure situation. Furthermore, the ICRP's protection policy for these situations continues to be based on setting a level of annual dose around 10 mSv from radon where action would almost certainly be warranted to reduce exposure. Taking account of the new findings, the ICRP has therefore revised the upper value for the reference level for radon gas in dwellings from the value in 2007 recommendation of  $600 \text{ Bq m}^{-3}$  to  $300 \text{ Bq m}^{-3}$  [22].

### **1.5 Analytical Technique for the measurement of NORM**

There are many radiometric and non-radiometric analytical techniques available for the assessment of NORM. Among them, gamma spectrometry method is widely. This is a nondestructive technique and involves simple sample processing. The outstanding advantage of gamma ray spectrometry is its ability to measure gamma emitters directly in the original sample without the need for chemical separations. Gamma ray spectrometry allows both qualitative identification and quantitative determination of the radionuclides in the sample [23]. Two most important detectors used in gamma spectrometric techniques are:

- i. NaI (Tl) scintillator
- ii. High Purity Germanium (HPGe) semiconductor

### **1.5.1 Interaction of gamma radiation with matter**

The instrumental detection of any particle or radiation depends upon the production of charged secondary particles which can be collected together to produce an electrical signal. Charged particles, for example, alpha and beta particles, produce a signal within a detector by ionization and excitation of the detector material directly. Gamma photons are uncharged and consequently cannot do this. Gamma-ray detection depends upon other types of interaction which transfer the gamma-ray energy to electrons within the detector material.

Among the different effects of interaction of electromagnetic radiation with matter the following three processes are important.

1. Photo electric Effect
2. Compton Effect and
3. Pair Production

The uncharged gamma photon causes transfer of its energy during its interaction with the absorber material. The secondary charged particle ( $\beta$  - rays) generated carries the entire energy of the incident photon. As the penetration distance of a 1 MeV electron through gases at STP conditions is a few meters, gas filled counters do not absorb the entire energy of the secondary charged particle, hence, gas filled counters are ruled out for use in gamma ray spectroscopy. Hence, solid / liquid media or scintillation techniques are used in gamma

ray spectroscopy. Semiconductor detection techniques are also widely used in gamma ray spectroscopy.

### 1.5.1.1 Photoelectric effect

Photoelectric absorption arises by interaction of the gamma-ray photon with one of the bound electrons in an atom as shown in figure 1.4. The electron is ejected from its shell as shown in figure with a kinetic energy  $E_e$ .

$$E_e = E_\gamma - E_b \quad (1.15)$$

$E_\gamma$  is the gamma-ray energy and  $E_b$  the energy binding the electron in its shell. The atom is left in an excited state with an excess energy of  $E_b$  and recovers its equilibrium in one of two ways. The atom may de-excite by redistribution of the excitation energy between the remaining electrons in the atom. This can result in the release of further electrons from the atom (an Auger cascade) which transfers a further fraction of the total gamma-ray energy to the detector. Alternatively, the vacancy left by the ejection of the photoelectron may be filled by a higher-energy electron falling into it with the emission of a characteristic X-ray which is called X-ray fluorescence. This X-ray may then in turn undergo photoelectric absorption, perhaps emitting further X-rays which are absorbed, in turn, until ultimately all of the energy of the gamma-ray is absorbed. In order to conserve momentum when an electron is ejected, a very small amount of energy must be retained by the recoiling atom. This is very small and can be ignored for all practical purposes. The energy level from which the electron is ejected depends upon the energy of the gamma-ray. The most likely to be ejected is a K electron. If sufficient energy is not available to eject a K electron, then L or M electrons will be ejected instead. This gives rise to the discontinuities in the

photoelectric absorption curves. These absorption edges occur at the binding energies corresponding to the electron shells. For Germanium, the K absorption edge occurs at 11.1 keV. For sodium iodide there are two K edges, one corresponding to the iodine K electron at 33.16 keV and the other to the cesium K electron at 35.96 keV. Below these energies, only L and higher order electrons can be photo electrically ejected. Since there is then one less way in which energy can be transferred to the interacting atom, the attenuation coefficient falls in a stepwise manner at the precise energy of the K electron. Similar edges corresponding to L and other less tightly bound electrons can be seen at lower energies in the curve for lead. The L electron shell has three sub-levels and this is reflected in the shape of the L edge.

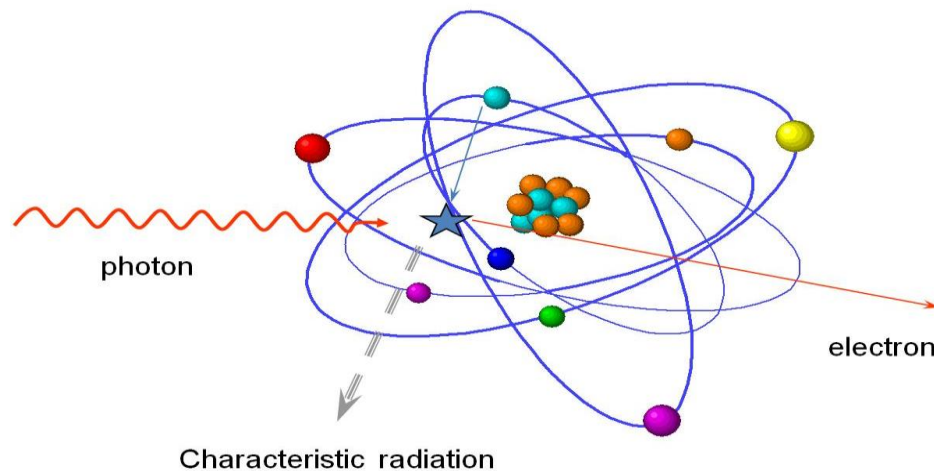


**Figure 1.4 Photo electric effect [24]**

The photoelectric process is the predominant mode of interaction of gamma rays of relatively low energy. The processes is also enhanced for absorber materials of high atomic number  $Z$ . No single analytical expression is valid for the probability of photoelectric absorption per atom over all ranges of photon energy and  $Z$ , but a rough approximation is

$$\tau \cong \text{Constatant} \times \frac{Z^n}{E_\gamma^{3.5}} \quad (1.16)$$

Where the exponent  $n$  varies between 4 and 5 over the gamma energy region of interest. This severe dependence of the photoelectric absorption probability on the atomic number of the absorber is a primary reason for the preponderance of high  $Z$  materials such as lead in gamma ray shielding [25].

### 1.5.1.2 Compton Scattering

In this case the gamma ray photon undergoes a billiard ball type of collision with an electron which is free or loosely bound. The photon is not only degraded in energy but also deflected from its original path, as shown in figure 1.5. As all angles of scattering are possible, the energy transferred to the electron can vary from zero to a large fraction of gamma ray energy. The relation between  $h\nu$  and  $h\nu'$  can be derived from the relativistic condition of conservation of momentum and energy.

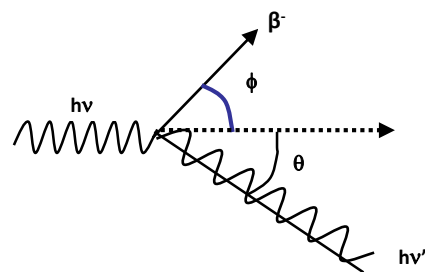
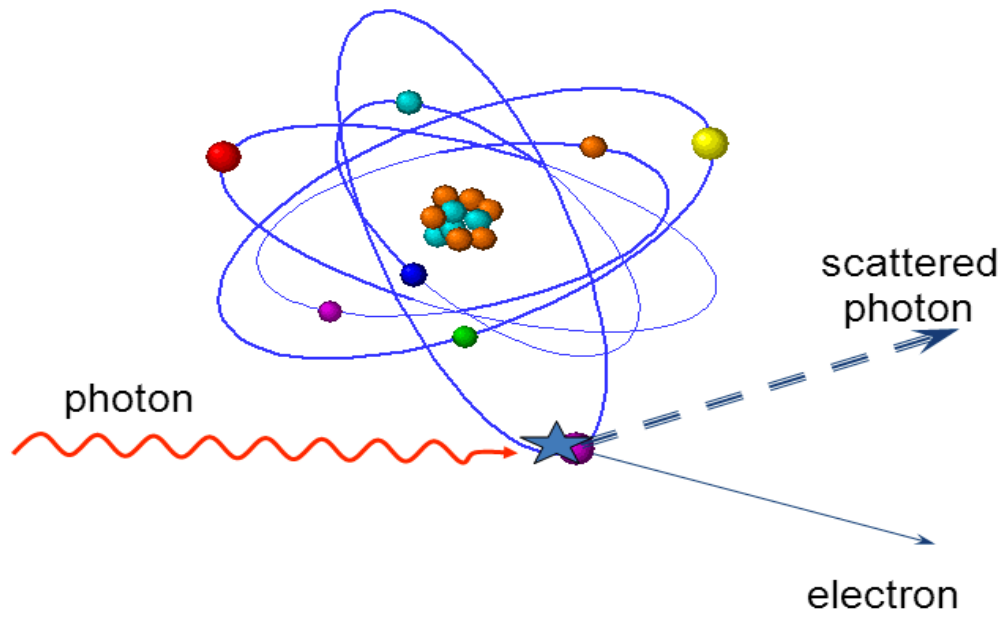


**Figure 1.5 Compton scattering** [24]

Electron energy is given by,

$$E = \sqrt{(E_0^2 + p^2 c^2)} \quad (1.17)$$

Where

$$E_0 = m_0 c^2 \quad (1.18)$$

$m_0$  = rest mass of electron and  $c$  = velocity of light

Energy conservation,

$$h\nu + E_0 = h\nu' + \sqrt{(E_0^2 + p^2 c^2)} \quad (1.19)$$

Momentum conservation parallel to the direction of incident photon,

$$\frac{h\nu}{c} = \frac{h\nu'}{c} \cos\theta + p \cos\Phi \quad (1.20)$$

Momentum conservation perpendicular to the direction of incident photon,

$$0 = \frac{h\nu'}{c} \sin\theta - p \sin\Phi \quad (1.21)$$

Solving above equations by eliminating  $\phi$  and  $E_0$ , we get the expression for the energy of scattered photon in terms of incident photon energy and scattering angle as,

$$hv' = \frac{hv}{1 + \frac{hv}{m_0c^2} (1 - \cos\theta)} \quad (1.22)$$

At  $\theta=0$ ,  $hv' = hv$  will be maximum and  $(E_e)_{\min} = 0$

At  $\theta = \pi$ , the value of  $hv'$  will be minimum,

$$hv' = \frac{hv}{1 + \frac{2hv}{m_0c^2}} \quad (1.23)$$

For  $hv \gg m_0c^2$ ,

$$(hv')_{\max} = \frac{m_0c^2}{2} = 256 \text{ keV} \quad (1.24)$$

$$(E_e)_{\max} = hv - m_0c^2 = hv - 256 \text{ keV} \quad (1.25)$$

Probability of Compton scattering,  $\sigma_{Cs} \propto Z/E$ . Compton scattering is the dominant process for gamma rays of intermediate energy (1-5 MeV) and for substances of medium Z. This is not a true absorption process since the scattered photon may not interact with the medium. In such a case the energy deposited by the gamma ray corresponds to the electron energy, which has a continuous distribution from zero to  $(hv-256)$  keV. This affects the response function of the detector.

### 1.5.1.3 Pair Production

This process is possible when  $E_\gamma$  exceeds 1.02 MeV. In the coulomb field of a nucleus (and less frequently that of an electron) the gamma ray photon disappears and is replaced by a pair of electron and positron. The presence of third body is needed to conserve energy and momentum. Figure 1.6 depicts the pair production mechanism.

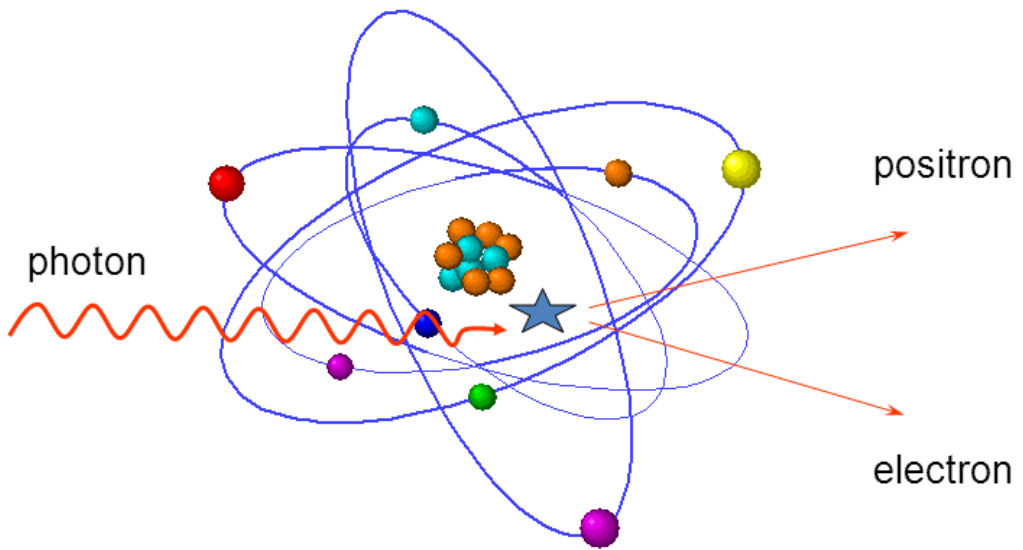


**Figure 1.6 Pair production [24]**

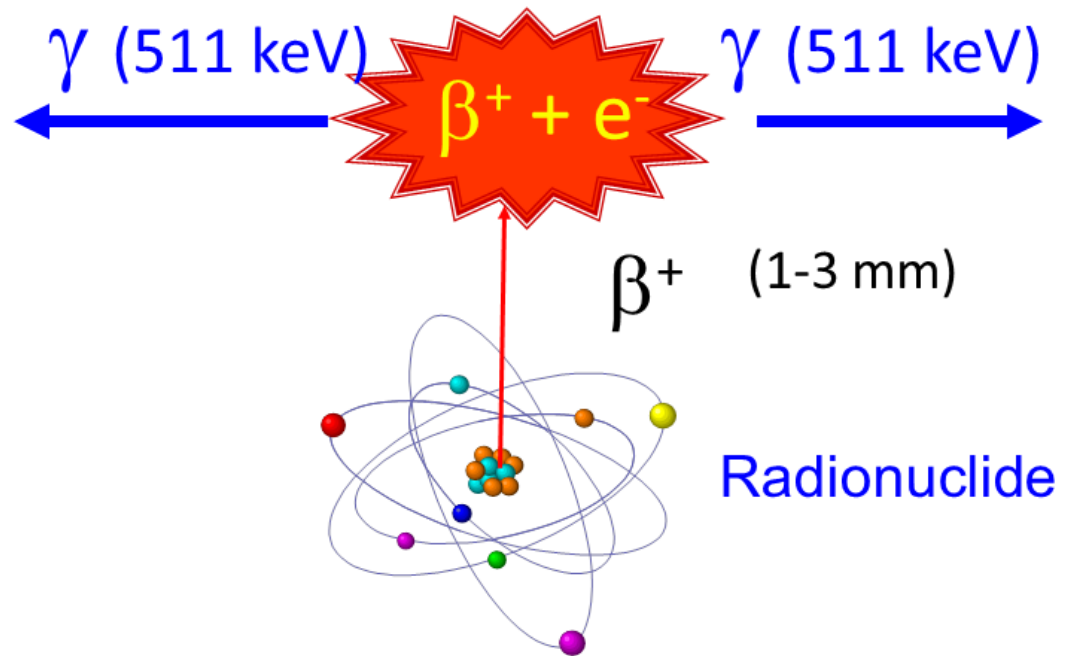


**Figure 1.7 Annihilation due to pair production [24]**

The energy of gamma ray photon in excess of 1.02 MeV goes to kinetic energy of the particles.

$$h\nu = E_{e^-} + E_{e^+} + 2m_0c^2 \quad (1.26)$$

Mechanism of pair production is similar to bremsstrahlung. After the pair is formed they lose their energy in the usual way. The positron, at the end of its track undergoes annihilation with an electron to produce two 0.511 MeV gamma ray photons, which is

shown in figure 1.7. Subsequent fate of these photons has important effect on the response of the detector. Probability of pair production is  $\sigma_{pp} \propto Z^2 \ln E$ . This process is important beyond 2 MeV.

The relative importance of the three interaction mechanisms discussed above for different absorber materials and gamma ray energies is shown in fig. 1.8. The line at the left represents the energy at which photoelectric absorption and Compton scattering are equally probable as a function of  $Z$ . The line at the right represents the energy at which Compton scattering and pair production are probable.

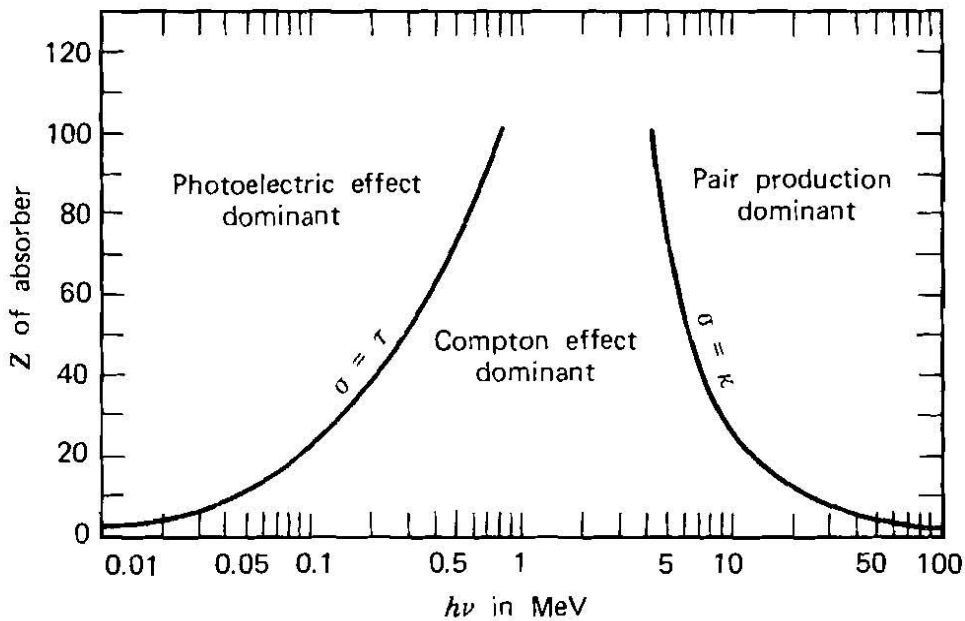


**Figure 1.8 Relative Importance of three interaction mechanisms [25]**

At any energy of the electromagnetic radiation any one or more processes of interaction assumes importance depending on the energy of the radiation and the Atomic number of the interacting material. The relative probability of each process is attributed by 'absorption

co-efficient' or 'cross section'. The cross section is the effective area which the target nucleus or atom presents to incident beam or radiation for the occurrence of the process. The intensity of the radiation as it passes through the medium decreases with the path length / thickness of the matter. The rate of decrease in the intensity is a function of the initial intensity and the thickness of the medium.

$$dI \propto -I \times dx$$

$$dI = -\mu I dx$$

$$\int \frac{dI}{I} = \int -\mu dx$$

$$(\log)_0^I = (-\log \mu x + C)_0^x$$

The intensity of radiation after traveling through a length / thickness 'x' in the medium is given as  $I_x = I_0 e^{-\mu x}$  where  $I_x$  is the transmitted intensity after passing through thickness of the medium and  $\mu$  is the linear attenuation co-efficient ( $\text{cm}^{-1}$ ). It is the sum of probabilities per unit length of gamma photon interaction such as

$$\mu = \tau \text{ (Photo electric absorption)} + \sigma \text{ (Compton scattering)} + \kappa \text{ (Pair production)}.$$

Relaxation length or Mean free path is the average distance traveled by the photons between two successive interactions and it is the reciprocal of the attenuation coefficient.

Use of linear attenuation coefficient is limited by the fact that it varies with the density of the absorber, even though the absorber material is same. Therefore mass attenuation coefficient is widely used. It is defined as  $\mu/\rho$ . Where  $\rho$  is the density of the medium. For a given energy, the mass attenuation coefficient of a compound does not change with the

physical state of the absorber. Fig. 2.6 shows the mass attenuation coefficient of germanium.

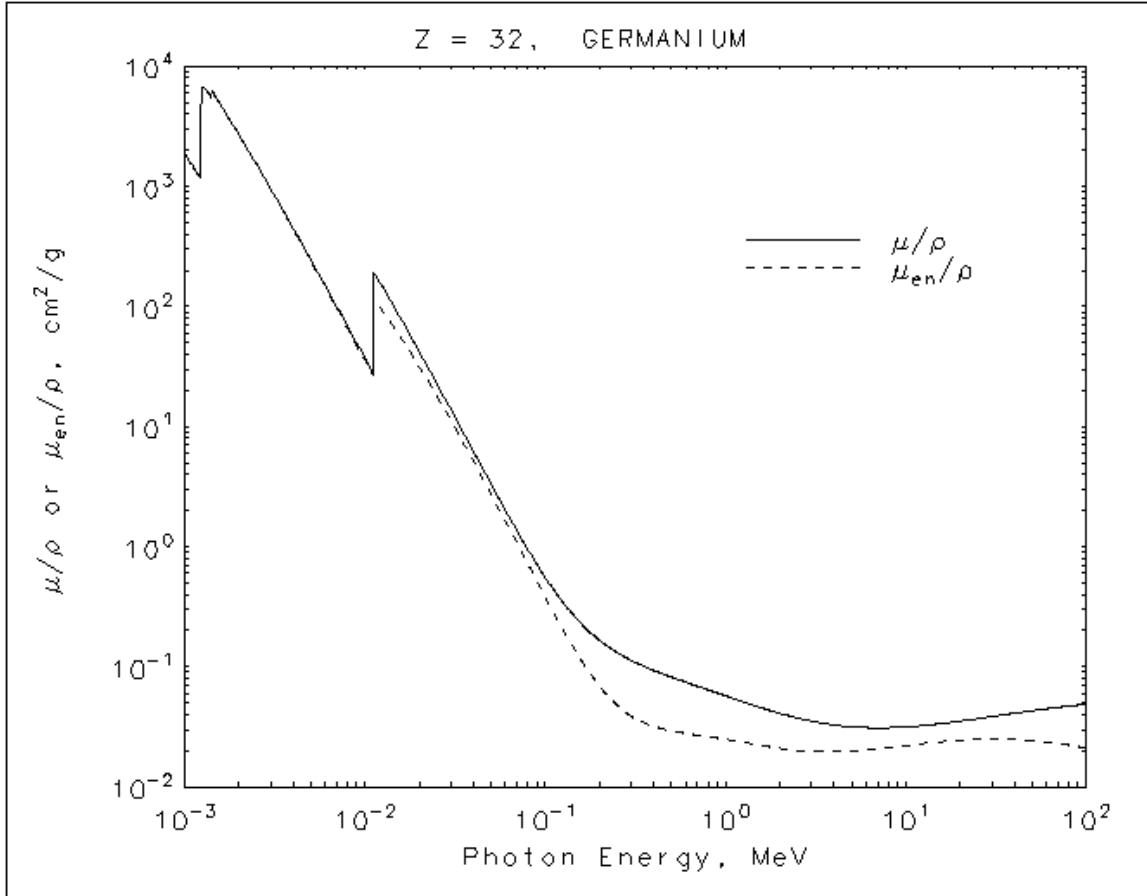


**Figure 1.9 mass attenuation coefficient of Germanium [26]**

### 1.5.2 NaI (Tl) Scintillation Gamma spectrometry

Scintillation detection has been used since the earliest days of radioactivity and is still today employed to measure the whole range of radioactive emissions – alpha and beta-particles, gamma-rays, neutrons and the more exotic leptons and mesons. The materials that have found particular application for gamma-ray measurements are all inorganic crystals: sodium iodides (NaI), cesium iodide (CsI), calcium fluoride (CaF<sub>2</sub>), bismuth germanate

(BGO) and, recently, lanthanum halides. Of these, the first is the most important and the last are materials rapidly gaining in importance.

NaI (Tl) is the most commonly used scintillation detector because of its extremely good light yield, excellent linearity and relatively high density and atomic number, which ensures high peak and full detection efficiency of gamma- and X-ray radiation. High transparency to the intrinsic radiation ensures good light absorption in large-sized single crystals. The decay time for the light output of a scintillator ranges from  $10^{-9}$  sec to  $10^{-6}$  sec. Scintillation detectors can be fabricated into various shapes and sizes for a particular purpose. But, one of their major limitations is its poor energy resolution. This is due to the fact that in a scintillation medium energy required to produce a photoelectron in a scintillation photo multiplier combination is in the range of 100 – 300 eV. It is brittle, sensitive to thermal gradients and thermal shock. It is hygroscopic and must be encapsulated at all times.

### **1.5.3 HPGe Gamma Spectrometry**

Gamma spectrometry with HPGe detector has almost replaced the conventional NaI (Tl) scintillation gamma spectrometry for the assessment of natural radioactivity. Gamma spectrum of terrestrial matrix is very complex due to multi gamma emission lines of  $^{238}\text{U}$  and  $^{232}\text{Th}$  natural radioactive decay series. Resolving these lines using NaI (Tl) spectrometry is very difficult due to its low resolution.

#### **1.5.3.1 Principle of semiconductor radiation detector**

In a free atom, the electrons are disposed in precisely determined energy levels. Combining a collection of atoms together into a solid structure broadens those energy levels into

energy bands, each of which can contain a fixed number of electrons. Between these bands are energy regions that are forbidden to electrons. The uppermost occupied energy band, the inhabitants of which are responsible for chemical reactions, is known as the valence band. In order for an electron to migrate within the material, it must be able to move out of its current energy state into another in order to move from atom to atom. (This is illustrated schematically in Figure 1.10.) If electrons can jump into suitable energy levels, then an external electric field applied to the material would cause a current to flow. There are three types of material: insulators, conductors and semiconductors. These differ in their electronic structures.

In an insulator, the valence band is full and the next available energy states are in a higher band, called the conduction band, separated by a forbidden region. For an electron to migrate through the material, it must gain sufficient energy to jump from the valence band across the band gap,  $E_g$ , into the conduction band. In an insulator, this gap is of the order of 10 eV, much greater than can be surmounted by thermal excitation. The electrons are immobile and the material is unable to pass an electrical current, however great the electric field (short of electrical breakdown).

In a metal, the valence bands are not full and in effect the conduction band is continuous with the valence band. Thermal excitation ensures that the conduction band is always populated to some extent and the imposition of an electric field, however small, will cause a current to flow. From the point of view of constructing a practical gamma ray detector, this is of little use because the extra current caused by the gamma-ray interaction would be insignificant compared to the normal background current. The band structure of semiconductors is not dissimilar to that of insulators. The valence bands are full but the

band gap is much smaller, of the order of 1 eV, similar to the energies achievable by thermal excitation. Under normal conditions there will always be a small population of electrons in the conduction band and the material will exhibit a limited degree of conductivity. The probability that an electron will be promoted to the conduction band is strongly influenced by temperature as shown in the equation given below. (T in Equation (1.42); k is the Boltzmann constant):

$$P(T) \propto T^{3/2} e^{(-E_g/2kT)} \quad (1.27)$$

Where T is the temperature in kelvin and k is the Boltzmann constant.  $E_g$  is the band gap of energy eV.

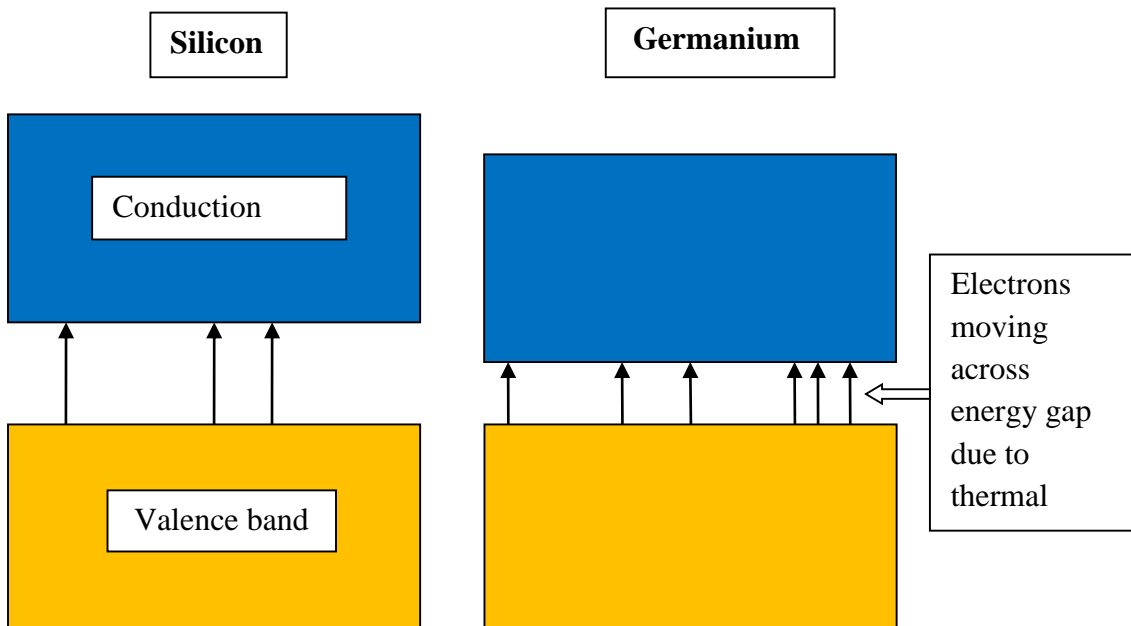


**Figure 1.10 Band gap semiconductors: Silicon and Germanium**

The interaction of a gamma-ray with the semiconductor material will produce primary electrons with energies considerably greater than thermal energies. Interaction of these can raise electrons from deep occupied bands well below the valence band into energy levels well above the base of the conduction band. These deeply embedded holes and the excited electrons will tend to redistribute themselves within the available energy bands until the holes lie at the top of the valence band and the electrons at the base of the conduction band indicated on the right hand side of Figure 1.12). In this process, further excitation can occur, giving a cascade of electron–hole pairs for each primary electron interaction. Under normal circumstances, the extra excited electrons in the conduction band might be expected to eventually de-excite and return to the valence band, restoring the conduction band population to that expected from thermal excitation alone. In the presence of an electric field, they will instead migrate up (electrons) or down (holes) the field gradient. The number of electron–hole pairs produced,  $n$ , will be related directly to the gamma-ray energy absorbed,  $E_{abs}$ , i.e. if  $\epsilon$  is the average energy needed to create an electron–hole pair

$$n = \frac{E_{abs}}{\epsilon} \quad (1.28)$$

Germanium is by far the most common gamma-ray detector material. Its higher atomic number than silicon makes it practicable to use it for the detection of higher energy gamma radiation. Over recent years, in response to the demand for this type of detector, the technology for the manufacture of high-purity germanium with a suitable degree of crystal perfection has improved considerably. This is emphasized by comparing the first germanium detectors commercially available (a few cubic centimeters in size, using lithium drifting to compensate for inadequate purity with a resolution of 4 to 5 keV at 1332 keV) with modern state-of-the-art detectors (hundreds of cubic centimeters of hyper-pure

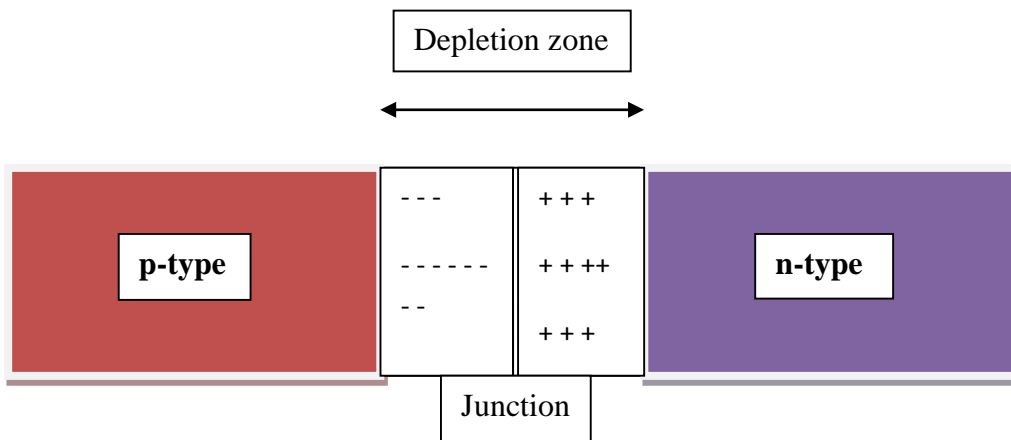
germanium offering better than 1.8 keV resolution). Detectors made from Germanium must be operated at low temperature in order to reduce the leakage current sufficiently [27].

The other potential semiconductor detector materials have a larger band gap than germanium and consequently would have the advantage of room temperature operation assuming that their other properties were satisfactory. Of these, only cadmium telluride, cadmium zinc telluride (CZT) and mercuric iodide have found their way into commercial production but only then for limited applications. The higher atomic numbers of these materials, and hence larger absorption coefficients, make them attractive detector materials. For example, 2mm of cadmium telluride is equivalent to 10mm of germanium in terms of gamma-ray absorption. However, in practice, a number of factors limit their use. In the first place is the availability of material with a satisfactory crystalline perfection, but restrictions that are more fundamental arise from the mobility of the charge carriers. The charge carrier mobility in these materials are considerably lower than those for germanium. This, compounded by the fact that the mobility of the holes, which are susceptible to trapping, is much lower than that for electrons, imposes severe charge collection problems on the detectors. In fact, trapping of the holes is enhanced to such an extent that complete charge collection is very difficult to achieve over distances of more than 1 mm. This means that only small detectors can be made from these materials. Because of their small size they are best used for measuring low-energy gamma rays.

In an absolutely pure semiconductor material, thermal excitation would promote a certain number of electrons from the valence band to the conduction band, leaving behind an equal number of positively charged holes. A material of this kind containing equal numbers of electrons and holes is described as an intrinsic semiconductor. It is, of course, not possible

to prepare any material completely free of impurities. In semiconductors, these can have a significant effect upon the conductivity. Consider germanium: it is tetravalent and in a crystal lattice will be surrounded by four other germanium atoms, each equally contributing electrons to the bonding between them. If one of these germanium atoms is replaced by an impurity atom of a different valency this will disturb the electronic balance of the lattice. For example, if the impurity is trivalent gallium or boron, then at the impurity lattice site there will be one electron too few to maintain the overall electronic configuration. In effect, we have a *hole*. Such impurities are referred to as acceptor impurities and when distributed throughout the semiconductor material give rise to extra energy states just above the valence band, called acceptor states. Germanium with this type of impurity would be called p-type germanium ('p' for positive acceptor impurities). On the other hand, pentavalent impurities, such as arsenic or phosphorus, will have one electron in excess of that required for electronic uniformity. The impurity atom will be a donor atom sitting in a donor site and will introduce donor states just below the conduction band. Germanium with such impurities is n-type germanium ('n' for negative donor impurities). It is, of course, possible that any particular piece of germanium will contain both types of impurity. Each of these impurities will effectively negate one of the opposite type and the net semiconductor character of the material will depend upon the type of impurity in excess. In the unlikely event of an exact cancellation, the material would be called compensated germanium. There is, of course, scope for adjusting the nature of the semiconductor by adding small amounts of impurity of an appropriate type; a process known as doping. The introduction of impurity atoms introduces extra states, either just above the valence band or just below the conduction band. The effect of this is to narrow the band gap and since the conductivity

depends upon the number of electrons in the conduction band, the conductivity of a doped material will be higher than the intrinsic conductivity. At very high dopant concentrations, and high conductivity, the semiconductor would be designated p<sup>+</sup> or n<sup>+</sup> as appropriate. Such a material is sometimes produced in situ by evaporation or ion bombardment of appropriate impurities to produce electrical contacts for detectors.



Figure

### 1.11 p-n junction and depletion region in semiconductors

The p-type material has an excess of holes and the n-type an excess of electrons. As these diffuse under thermal influence, holes may 'stray' from the p side to the n side of the junction and electrons from the n side to the p side. Excess holes meeting excess electrons will combine together, mutually annihilating. The result will be a region around the physical junction of the two types of material where the excess charge carriers have cancelled each other out. This is called a depletion region which is shown in figure 1.13.

The migration of the charge carriers gives rise to a space charge in this region and the generation of a voltage across the junction called the contact or diffusion voltage, about 0.4V high in germanium (Figure 1.14). The depletion region is the active element of the detector. This region is very thin, but if a positive voltage is connected to the n side of the junction the width of the depletion layer increases as the electrons are withdrawn from the material. The negative voltage applied to the p side of the junction will withdraw the holes. Because the positive voltage is connected to the negative type semiconductor, this is called a reverse biased junction, as shown in fig. 1.15.

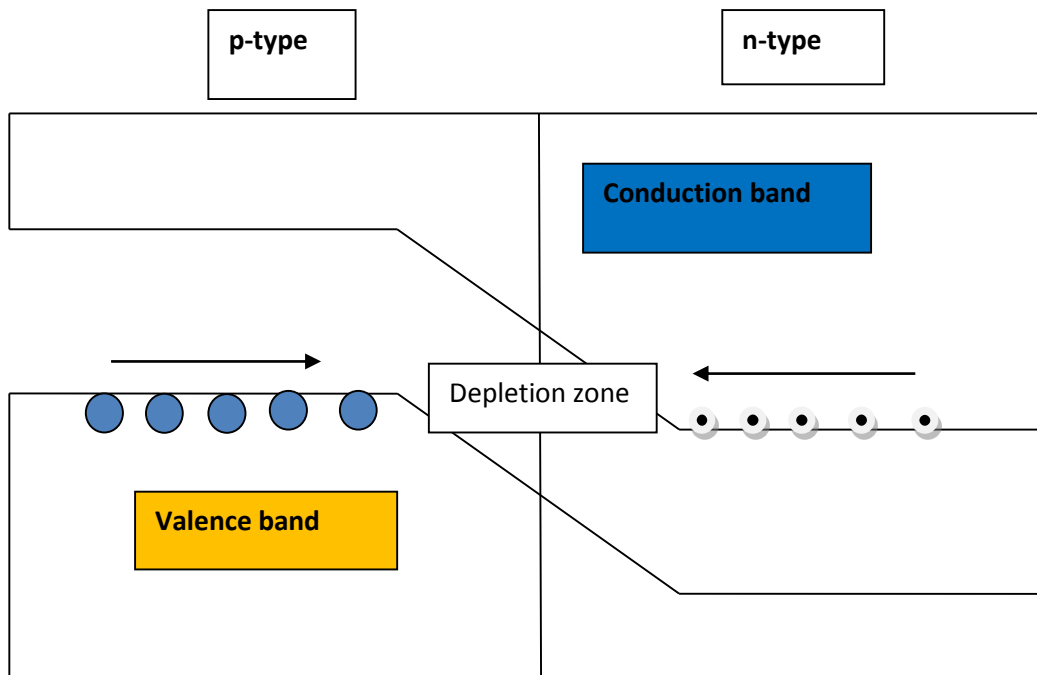


**Figure 1.12 p-n junction mechanism in semiconductors**

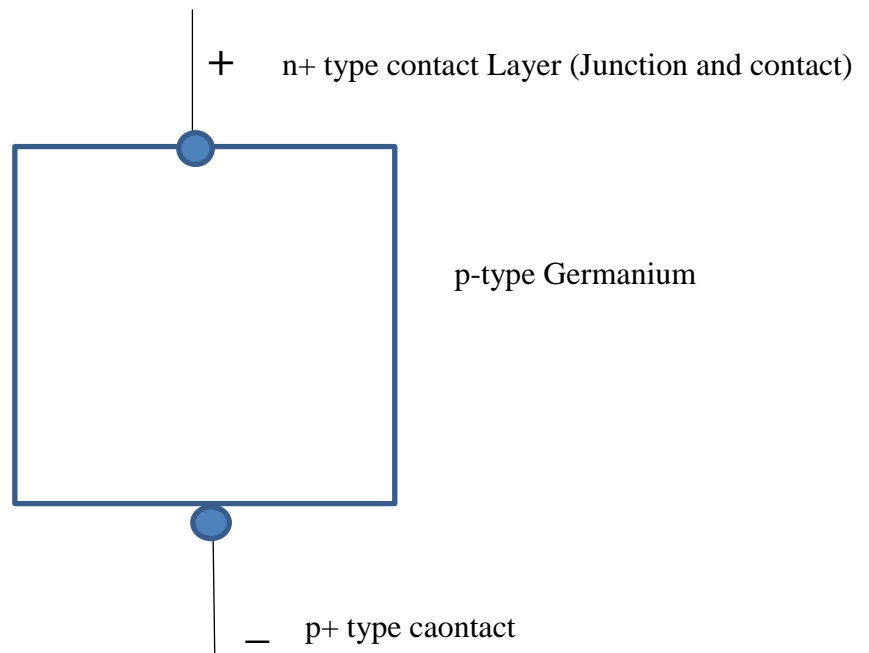


**Figure 1.13 Reverse bias in p-type germanium semiconductors**

### 1.5.3.2 HPGe Gamma spectrometer components

#### Detector Bias Supply

The detector bias supply for a semiconductor gamma ray detector is the least critical unit in the electronic system. Units would normally be able to supply up to 5000V with about 3000V being required by a typical high-purity germanium detector. As long as the bias is well above the depletion voltage, charge collection is not greatly affected by changes in bias, and the stability of the bias supply is not critical.

**Preamplifier**

The charge created within the detector by interaction with the gamma radiation is collected by the preamplifier. In spite of its name the function of the preamplifier is not to amplify the pulse – it merely goes before (i.e. pre-) the amplifier – but to interface the detector to the amplifier and collect the charge generated by absorption of the gamma-ray. It provides a high impedance load for the detector and a low impedance source for the amplifier. Preamplifiers, in general, can have various modes of operation: current-sensitive, voltage-sensitive and charge sensitive. Only the latter type is used in high-resolution gamma spectrometry using semiconductor detectors. In order to minimise the electronic noise the input stage of the preamplifier, usually a field effect transistor (FET) stage is cooled in the same manner as the preamplifier. The height or amplitude of the pulse from the preamplifier should be proportional to the amount of charge collected in the detector, and if all the photon energy was absorbed in the detector, it should be proportional to the incident photon energy [25].

**Spectroscopy Amplifier:**

The spectroscopy amplifier receives voltage pulses with sharp rise time and long tails from the preamplifier. It amplifies by almost 200 times and shapes them suitably for further analysis. To achieve the best resolution, these amplifiers have provisions like pole zero cancellation, base line restoration and variable shaping time constant. The important characteristics of the spectroscopy amplifier are the linearity, the output pulse shape, the gain stability and the noise level. Most amplifiers are provided with both a unipolar and bipolar output. Amplifiers generally provide several time constants for the pulse shaping

and will vary from 0.5  $\mu\text{sec}$  to 10  $\mu\text{sec}$ . For shaping pulses from the HPGe detectors the typical time constant may be in the range of 4  $\mu\text{sec}$  to 6  $\mu\text{sec}$ .

### **Multi-Channel Analyser (MCA)**

The voltage pulses obtained from the spectroscopy amplifier are converted into gamma ray spectrum using a multi-channel analyser (MCA). The MCA consists of an analog to digital convertor (ADC), an oscillator and memory. The basic function performed by an ADC in an MCA is to provide a digital number proportional to the amplitude of the pulse presented at its input. Wilkinson or Ramp type ADC is widely used for nuclear spectroscopy due to its good differential linearity (DNL), an important property for high resolution spectrometry. The principle employed in ramp type ADCs is voltage-to-time conversion and consists of following steps [25]:

- a) Charging of a precision capacitor (memory capacitor) to the peak value of the input pulse and detection of peak;
- b) Linear discharge of this capacitor till it reaches a reference voltage using a single constant current source.
- c) An 8K MCA card was used for this work. The MCA card is inserted in the personal computer with software for spectrum analysis and storage of the spectrum. The system is additionally equipped with software for analysis, printers and data storage units to edit and store the spectrum for further analysis. The block diagram of HPGe spectrometer is shown in fig. 1.16.

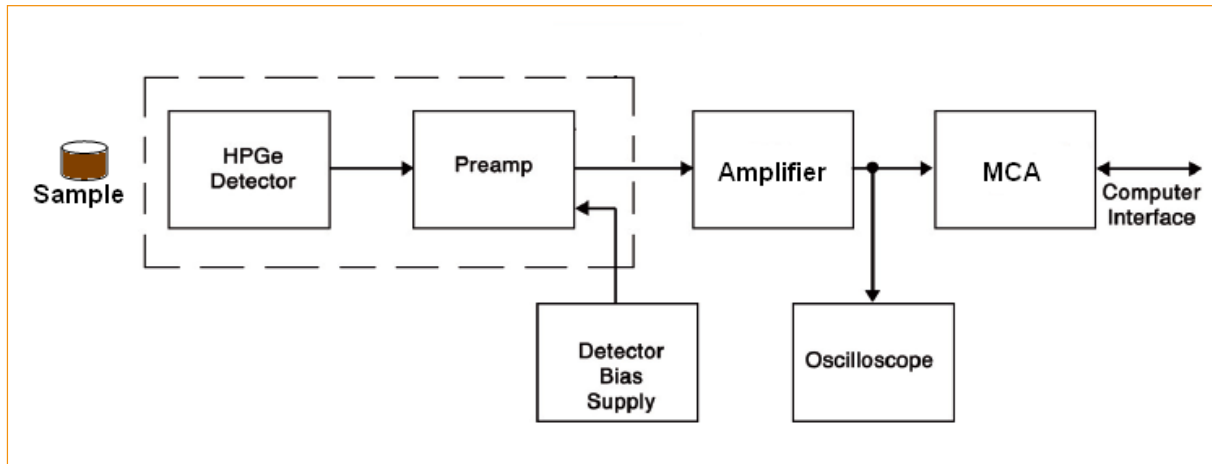


**Figure 1.14 Block diagram of HPGe Gamma Spectrometry system**

#### 1.5.4 Gamma Spectrum Analysis

The task in gamma and X-ray spectrometry is the analysis of the peaks in pulse height spectrum that corresponds to the full energy absorption events. The peak location is a measure of the photon energy and the peak area of the emission rate. The photon spectrum of a source usually consists of discrete lines of very small width, while the measured pulse height spectrum is a continuous distribution due to various interaction effects. The full energy peaks in this spectrum may only amount to a small fraction the total counts, but they provide the useful information. The rest has to be considered as spectral background, unwanted but unavoidable [27].

#### Manual peak area estimation

The background beneath the gamma-ray spectrum peaks can arise from many sources. In most cases, the background will represent the Compton continuum from other gamma ray interactions within the detector, within the sample itself and from general background

radiation interaction with the shielding and the detector. Both background radionuclides and other radionuclides in the sample will contribute to this peak background.

The linear Compton continuum under the total energy peak is obtained by interpolation of two extremes of the peak. If  $N_L$  and  $N_R$  are the number of channels taken for end point averaging on left and right of the peak extremes respectively, to reduce the error in Compton background and  $N_p$  is number of channels under the peak with  $C_L$ ,  $C_R$  and  $C_P$  being the integrated counts in these windows respectively, then Compton corrected counts under the peak i.e.,  $C$  is given by [28]:

$$C = C_P - \left\{ \frac{\left[ \left( \frac{C_L}{N_L} \right) \right] + \left( \frac{C_R}{N_R} \right)}{2} \right\} * N_P \quad (1.29)$$

### 1.5.5 Radioanalytical Uncertainty

The confidence that can be attached to a measurement result and the degree to which the result is expected to agree with other results is provided by the measurement uncertainty. Nuclear analytical techniques in general are to be considered as relative rather than absolute analytical techniques. The measurement procedures therefore require calibration by appropriate calibration standards and the results should always be validated to be reliable and comparable. The uncertainty component associated with the calibration will therefore in most cases include an uncertainty contribution from the reference materials and an uncertainty contribution from the calibration line fitting or the scaling factor. Data acquisition in nuclear analytical techniques frequently relies on the accumulation of counts

resulting from a decay process from a higher energy level to a lower energy level by the emission of particles and/or radiation. Those processes are characterised by a Poisson distribution and therefore the uncertainty associated with those processes can be readily derived from the standard deviation of the Poisson distribution, thereby avoiding the need for sometimes tedious and lengthy repetitions of the measurements. This is a typical feature of the quantification of uncertainty in nuclear analytical techniques. For a sufficiently large number of counts the normal distribution can be used as a good approximation of the Poisson distribution. Because of the radioactive decay, the measured quantities are not constant in time and useful information can only be extracted from the data when appropriate corrections for decay are applied. The correction factors for decay – and for build-up of the decay products, which sometimes are the measured quantities – are typically exponential functions of a single or several decay constants and time. The decay constant, governing the decay process, is a measured physical quantity and therefore subject to uncertainty and so is the measurement of time. The quantification of uncertainty in nuclear analytical techniques will therefore frequently involve non-linear components, whose contribution is not constant, but is a function of the time intervals between the different steps in the analytical procedure. This characteristic feature of nuclear analytical techniques might introduce a lot of complexity in the quantification of uncertainty, but on the other hand provides an opportunity for minimization of the uncertainty by an adequate scaling of the time intervals.

## **Sources of uncertainty**

### **a. Stability of the measuring system**

Stability of the measuring system must be ensured in order to obtain good results. The task is to control the stability of the measuring system rather than to correct the results of measurement. With present day electronics it is much easier to assure the stability of the system. Results obtained using an unstable measuring system must be rejected. The sample must be measured again in proper conditions.

**b. Energy calibration**

This is normally performed before measuring the sample. Whatever source is used it is wise to ensure that the calibration energies cover the entire range over which the spectrometer is to be used. Experience suggests that the linearity of modern ADCs is extremely good. The energy calibration is a simple but critical step. The measured energies are only used to identify the nuclides and, thus, the uncertainty in the energy is no longer used in the following calculations.

**c. Efficiency uncertainty**

Most algorithms used for efficiency calibration assume that the true efficiency function can be represented by a fitted analytical function. However, the correct allocation of uncertainties to an interpolated efficiency value is a complex problem. The uncertainty of the efficiency value calculated with the interpolation function cannot be only obtained from the uncertainties in the parameters. The possible correlations between the measured input efficiency data must be considered.

**d. Uncertainty of gamma emission probabilities**

Nuclear data of the for gamma emission probabilities, good data sources for a limited number of radionuclides are in IAEA-TECDOC-619 and in Firestone and Shirley. In a few cases this kind of uncertainty could be a major contributor to the combined uncertainty.

**e. Uncertainty in the half-life**

The published nuclear data [29] and [30] has the uncertainty in the half-life for all the radionuclides. Uncertainty in the half-life is still small compared with other uncertainty sources.

**f. Uncertainties to be quantified from the measurement results**

All other parameters are to be obtained from the measurement process unless some of the sample parameters (such as matrix etc.) are provided by the customer.

**g. Uncertainty due to differences in counting geometries of sample and standards**

The counting geometry of sample and standards should be the same. In order to minimise the uncertainties, the differences should be kept at a minimum. A proper mock up standard with the same physical and chemical properties as the sample should be used in non-destructive analysis.

**h. Uncertainty due to random coincidences**

Even with good pile-up rejection there could be some residual random coincidences. Any full energy photon which is summed with another pulse will not be recorded in the single photon peak and represents therefore a loss of counts or efficiency. This loss is count rate dependent, however, for low count rates this correction factor could be taken as 1 and the associated uncertainty can be neglected.

**i. Uncertainty due to true coincidences**

In the case of a nuclide decaying through a cascade of successive photon emissions located close to a detector, coincidence-summing effects could be important, especially in the case of high efficiency semiconductor detectors. Information on photons in cascade is more difficult to obtain. The main source is Nuclear Data Sheets. The best way to treat this problem is to use identical geometry for calibration and the measured sample, and also to have the same composition of radionuclides emitting photons in cascades (like  $^{60}\text{Co}$ ,  $^{152}\text{Eu}$ ,  $^{154}\text{Eu}$ ,  $^{133}\text{Ba}$ ,  $^{88}\text{Y}$ , etc.) in both samples. Usually, this will not be a realistic solution of the calibration problem. Radionuclides emitting photons in cascades are not appropriate for performing the fit necessary to obtain the efficiency curve. The solution is the use of the Monte-Carlo calculation of coincidence corrections or in the use of the same radionuclides for calibration and for measuring the sample.

**j. Uncertainty due to dead time effects**

We neglect the uncertainties associated with dead time effects, because counting rates in environmental samples are usually very low.

**k. Uncertainty due to decay time effects**

The decay time effects (measuring time, decay and counting time) usually can be neglected as exact timing is available.

Uncertainty due to self-attenuation correction

If the composition and the density of the sample to be measured differ from the calibration sample, self-attenuation corrections to the efficiency should be applied. These corrections depend on the sample geometry, composition and density, and on detector parameters. Of

course, the corrections are higher for large volume high Z and density samples and for low energy photons. If the major elements of the sample matrix are known, then the relative uncertainty of the self-attenuation correction factor is less than 1% (for energies higher than 60 keV) and less than 5% for energies less than 40 keV.

### **l. Uncertainty due to counting statistics**

Generally the uncertainty due to counting statistics is one of the most important sources of uncertainty. The mathematical procedure used to derive net peak areas and standard associated uncertainties is based, in many cases, on a simple background subtraction (including the background peak subtraction in the case of existence of such a peak at the given energy, both in the sample and the background spectra).

### **m. Uncertainty due to sample weighing**

It is assumed that the uncertainty due to sample weighing is estimated on the basis of information available on the precision of the balance used in the measurement process or from control charts of repetitive measurements.

## **1.5.6 Minimum Detectable Activity (MDA)**

The MDA is the minimum amount of radioactive nuclide that we can be confident that we can detect. First, this limit is, then, an activity rather than a count limit. It is often equated to the activity equivalent of the detection limit, LD. However, there is a problem. As we defined it above, the detection limit is that count which we can be 95% certain of detecting in the particular spectrum. However, as we saw, the detection limit is some way above the critical limit. We could, therefore, have the situation where a peak area measurement gave a net area which was significant (i.e. above the critical limit) but below the detection limit.

Our activity result would then be below the minimum detectable activity. A generally accepted expression for the estimate of the detection limits, which is frequently referred to as the lower limit of detection (LLD) and which contains a preselected risk of 5 % of concluding falsely that activity is present and a 95 % degree of confidence for detecting the presence of activity [23].

### 1.5.7 Gamma Spectrometry of Natural Radionuclides

Gamma spectrometry of NORM is difficult for a number of reasons. First, the activity levels are low and, if statistically significant results are to be obtained, need long count periods, ideally on a gamma spectrometer whose construction and location are optimized for low activity measurements. The second difficulty is the matter of spectrometer background. Uranium and thorium are not stable; they decay mainly by alpha-particle emission to nuclides that themselves are radioactive. Natural uranium is composed of three long-lived isotopes,  $^{238}\text{U}$ , a smaller proportion of  $^{235}\text{U}$  and an even smaller proportion of  $^{234}\text{U}$ , the decay-series daughter of  $^{238}\text{U}$ . Natural thorium has one single isotope,  $^{232}\text{Th}$ . Each of these nuclides decays to an unstable daughter leading, in turn, to a whole series of nuclides that terminate in one or other of the stable isotopes of lead. Under normal circumstances, in a natural material, the  $^{235}\text{U}/^{238}\text{U}$  ratio will be fixed and all nuclides in each of the series will be in equilibrium.

$^{238}\text{U}$  comprises 99.25% of natural uranium. That decays by alpha emission to  $^{234}\text{Th}$  which in turn decays to  $^{234\text{m}}\text{Pa}$  and so on until stable  $^{206}\text{Pb}$  is reached. If we look at the half-lives of the various nuclides they are all much less than the half-life of  $^{238}\text{U}$ . This means that, in a natural, undisturbed source of uranium, every daughter nuclide will be in secular equilibrium with the  $^{238}\text{U}$ . The activity of each daughter nuclide will be equal to the  $^{238}\text{U}$

activity. There are 14 radionuclides in the chain and so the total activity of such a source will be 14 times that of the parent, or of any individual nuclide.

$^{40}\text{K}$  is very evident in background spectra. It is present as 0.17% of natural potassium and is present in wood and building materials and even in the bodies of the gamma spectrometrists. The substantial presence of  $^{40}\text{K}$  in the detector background and in many samples, with its long Compton continuum, severely restricts the limit of detection of the many nuclides emitting gamma rays at lower energies. The gamma spectrometry of  $^{40}\text{K}$  is straightforward but peaked-background correction is always necessary. There is a spectral interference from the 1459.91 keV peak of  $^{228}\text{Ac}$ , which must be taken into account even when the activity of the  $^{232}\text{Th}$  daughters is low and the peak shape is not noticeably affected [31].

## **1.6 Scope of the present work**

The concern about radioactivity in general, and naturally occurring radioactive materials (NORM) in particular, has increased many fold throughout the world. This is due to the radiation arising from the primordial radionuclides present in conventional raw materials and solid industrial wastes and byproducts such as fly ash from thermal power stations and phosphogypsum from the fertilizer industries. These materials are being used in the manufacture of building construction materials and other commodities extensively. These types of man-made alterations in the Natural Environment can increase radiation exposure of the public, sometimes in a substantial manner. Living in houses/work places built with materials containing NORM in excess, is of radiological concern. To control public exposure from these, many countries have their own regulation in the form of some screening criteria.

In view of the above fact, this thesis include the following:

- Radioactivity measurement and analysis of most commonly used building materials and those made of fly ash and phosphogypsum for their radioactivity content. Hyper pure Germanium (HPGe) detector coupled high resolution gamma spectrometry system will be used for the purpose.
- Indoor gamma dose computation using Monte Carlo techniques, which will enable to derive a regulatory screening tool.
- Radiological assessment of natural radioactivity in building materials.



---

## Chapter 2 Literature Review

---

### 2.1 Introduction

Importance on the study of natural radioactivity in building materials has increased manifold since early 70s of this century. Recently all leading journals of radiological sciences have at least one paper on NORM in building materials in every issues of their publication. This is mainly attributed to the fact of increased awareness about radiation and natural radiation in particular. This chapter reviews the literature of such studies in order to identify the gaps that that exist in the literature.

This review covers literature pertaining to three broad areas of immediate relevance i.e.

- i. Computation of indoor gamma dose coefficient
- ii. Regulatory aspects of natural radioactivity in building materials.
- iii. Measurement of natural radioactivity in conventional and by-product building materials.

The literature on regulatory aspects would help to identify the existing work done and gaps in the area of regulation of NORM related public exposure. This will also help to arrive at India specific regulatory tools. The literature on the computation of indoor gamma dose coefficient would help to derive the same as per the room models representing typical Indian houses with various combination of building materials.

## 2.2 Computation of Indoor gamma dose

Stranden [32], Markkanan [33], Kiplinger [34], have calculated the radiation exposure from radioactivity in walls using analytical method. The exposure rate from a gamma source may be written as

$$\dot{X} = \frac{k}{\rho_a} \sum_i E_i \mu_a (E_i) \Phi(E_i) \quad (2.1)$$

$\dot{X}$  is the exposure rate,  $\rho_a$  is the density of air,  $E_i$  is the photon energy,  $\mu_a$  is the linear energy absorption coefficient in air,  $\Phi$  is the flux density of photons and  $k$  is a proportionality constant. The flux density from a point source in a medium may be written as

$$\Phi (E_i) = \frac{1}{4\pi l^2} B (E_{i,8}) R e^{(-\mu_m (E_i) s)} \quad (2.2)$$

$B (E_{i,8})$  is the build-up factor,  $R$  is the activity of source,  $l$  is the distance from the source,  $\mu_m$  is the attenuation coefficient in the medium and  $s$  is the distance the photon travels through the medium. For a uniform source distribution in the medium, the exposure rate at a point P is then

$$\dot{X} = \frac{k \cdot A}{4\pi \rho_a} \sum_i E_i N(E_i) \mu_a(E_i) \int_V B (E_{i,8}) \frac{e^{(-\mu_m (E_i) s)}}{l^2} dV \quad (2.3)$$

$N(E_i)$  is the number of photons with energy  $E_i$  emitted per primary disintegration and  $V$  is the volume of the medium. In this calculation, linear form of build-up factor was used.

$$B (E, s) = 1 + \alpha (E) \mu_m(E) s \quad (2.4)$$

The author used one-mean- free – path fit for  $\alpha(E)$  for concrete, and all the calculations in this work are related to concrete like materials with different densities. It was concluded that the differences in chemical composition of building materials are small, and the use of the composition of concrete will not give significant errors. Gamma lines of natural radioactive decay series  $^{232}\text{Th}$  and  $^{238}\text{U}$  were considered in the computation.

Markkanen [35] has also proposed the same approach. The geometry used in the calculation was 12 m x 7 m x 2.8 m. The absorbed dose rate in air D1 ( $\text{Gy h}^{-1}$ ) originating from the top layer at point P ( $X_p, Y_p, Z_p$ ) can be calculated by using the formula:

$$D1 = 5.77 \times 10^{-7} \frac{c_1 \rho_1}{4\pi} \sum \gamma_i \left(\frac{\mu_{en}}{\rho}\right)_i E_i \int B_i(1) \frac{e^{-\mu_i(1)S_1}}{l^2} dV \quad (2.5)$$

The build-up factor  $B_i(1)$  is written according to the Berger Model:

$$B_i(1) = 1 + C(E_i) \mu_i(1) S_1 e^{D(E_i) \mu_i(1) S_1} \quad (2.6)$$

$$S_1 = \left| \frac{z}{z_p - z} \right| \quad (2.7)$$

$c_1$  - Activity concentration of the top layer,  $\text{Bq kg}^{-1}$

$\rho_1$  - Bulk density of the top layer.  $\text{Kg m}^{-3}$

$\gamma_i$  - Gamma intensity of gamma line i

$E_i$  - Gamma energy of gamma line I, MeV

$\left(\frac{\mu_{en}}{\rho}\right)_i$  - Energy absorption coefficient in air for gamma energy,  $E_i$ ,  $\text{cm}^2 \text{g}^{-1}$

$\mu_i(1)$  - Attenuation coefficient in the top layer for gamma energy  $E_i$ ,  $\text{cm}^{-1}$

$C(E_i)$  - Coefficient in the Berger model

The constant  $5.77 \times 10^{-7}$  is derived from conversions of units:

$$3600 \text{ S h}^{-1} \times 1.6 \times 10^{-13} \text{ MeV h}^{-1} \times 1000 \text{ g kg}^{-1} = 5.77 \times 10^{-7} \quad (2.8)$$

The integration limits for x-, y- and z- directions are  $-a/2$ ,  $a/2$ ,  $-b/2$ ,  $b/2$ , and  $-h_1 \dots \dots 0$ , respectively.

The absorbed dose rate in air  $D_2$  at point P ( $X_p$ ,  $Y_p$ ,  $Z_p$ ) due to bottom layer can be calculated by using the formula:

$$D_2 = 5.77 \times 10^{-7} \frac{c_2 \rho_2}{4\pi} \sum \gamma_i \left( \frac{\mu_{en}}{\rho} \right)_i E_i \int B_i(z) \frac{e^{-(\mu_i(1)s_1 + \mu_i(2)s_2)}}{l^2} dV \quad (2.9)$$

$$S_2 = \left| \frac{h_1}{z_p - z} \right| l \quad (2.10)$$

$$S_2 = \left| \frac{z}{z_p - z} \right| l - S_1 \quad (2.11)$$

$S_2$  is the fraction of 1 within the bottom layer, cm

$\mu_i(2)$  Attenuation coefficient in the bottom layer for gamma energy,  $E_i \text{ cm}^{-1}$

The integration limits for x-, y- and z- directions are  $-a/2$ ,  $a/2$ ,  $-b/2$ ,  $b/2$ , and  $-(h_1+h_2) \dots \dots 0$ , respectively.

In this case, the estimate of the build-up factor is not as obvious as the attenuation term.

The approximation would be a product of the two build-up factors calculated separately

for both layers. This would, however overestimate the dose rate because the energy distribution of the flux has changed when the flux enters the upper layer. The following approximation is therefore is used:

$$B_i(2) = B_i(1) \left( 1 + \frac{\mu_i(2)s_2}{(\mu_i(1)s_1 + \mu_i(2)s_2)} \mu_i(2)s_2 e^{D(E_i)\mu_i(2)s_2} \right) \quad (2.12)$$

This is a product of the two build-up factors, but in the bottom layer only the fraction proportional to the mean free paths in the different layers is considered.

Maduar et.al [36] in 2004 studied the indoor gamma dose in dwellings. They also used the same photon transport model as above to compute the theoretical evaluation of the indoor gamma absorbed dose in the air in a hypothetical dwelling built with slabs containing defined concentrations of natural radionuclides and to determine the values of the dose conversion factors under different conditions of compartment geometry. In this work, the room was modelled as three pairs of rectangular slabs of finite thickness. Doses were evaluated, taking into account self-absorption and radiation build-up. Calculations were performed for  $^{40}\text{K}$ ,  $^{226}\text{Ra}$  and  $^{232}\text{Th}$ , considering concrete walls. The results obtained show good agreement with those reported in the literature. Dose conversion factors are presented in a practical manner, ready to use for radiological impact screening. Sensitivity analysis was also carried out in order to find out the variation of dose coefficient with respect to the variation of wall thickness and density of building materials used for the construction. By varying the wall thickness within 5 - 60 cm range, one can observe that the dose conversion factors initially increases up to a maximum equilibrium value. For a thickness of 40 cm,

the dose conversion factor already reaches a value only 4 % below the value for a 60 cm thickness. By varying material density, dose conversion factors increase with the building material density, tending also to a maximum equilibrium value. For a density  $> 3.5 \text{ g cm}^{-3}$ , the dose conversion factor practically remains constant.

Maduar et.al [37] also studied the indoor gamma dose due to the use of phosphogypsum plates in building construction. He also adopted the same analytical approach discussed as above to compute the indoor gamma dose in the experimental house made of phosphogypsum plates. The results show that the annual increment in the effective dose to an inhabitant of the house will remain below the 1 mSv limit for every reasonable scenario.

Al-Jundi et.al [38] has computed the indoor specific air kerma rate in a room model of 4 m x 4 m x 4 m using Monte Carlo method. Uniform chemical composition of the walls, floor and ceiling as well as uniform mass concentrations of the radionuclides in walls, floor and ceiling are assumed.

P. D. Jong et al. [39] has studied the indoor gamma dose in three room models representing the Dutch houses. The authors used the Monte Carlo method. He compared the obtained result with the Stranden geometry i.e. 4 m x 5 m x 2.8 m. Using the locally developed computer codes Marmer and Micro-Shield, correction factors are assessed that quantify the influence of several room and material related parameters on the specific absorbed dose rates. The investigated parameters are the position in the construction; the thickness, density, and dimensions of the construction parts; the contribution from the outer leave; the presence of doors and windows; the attenuation by internal partition walls; the

contribution from building materials present in adjacent rooms; and the effect of non-equilibrium due to  $^{222}\text{Rn}$  exhalation. To verify the precision, the proposed method is applied to three Dutch reference dwellings, i.e., a row house, a coupled house, and a gallery apartment. The averaged difference with MCNP calculations is found to be 4 %.

Risica et. al. [40] have carried out a sensitivity analysis concerning the effects changes in the parameters for the room on the dose in the room. The variation in the dose rate in air in relation to the position in the room was found to be approximately 10 % at a distance of up to 1 m from the walls. The authors also studied the variation of indoor gamma dose rate with respect to different width and length of the walls considering square and rectangular shapes of the room by keeping the height of 2.8 m constant. The maximum variation in the dose rate obtained was 6 % from the calculation for a room with a volume of  $60 \text{ m}^3$ . The effect of wall thickness on the indoor dose was also studied. Thickness up to 0.4 m, increasing the thickness increases the radiation dose rate, whereas when the thickness is greater than 0.4 m, self-absorption in the material in the material makes the effect of a further increase in dose rate is negligible.

### 2.3 Regulatory aspects of NORM in building materials

E. L. Hamilton [41] and OECD [42] defined a common index called the “radium equivalent activity ( $\text{Ra}_{\text{eq}}$ )” to obtain the sum of activities for the comparison of the specific activities of materials containing  $^{226}\text{Ra}$ ,  $^{232}\text{Th}$  and  $^{40}\text{K}$ . It was estimated that  $370 \text{ Bq kg}^{-1}$  ( $10 \text{ pCi g}^{-1}$ )  $^{226}\text{Ra}$ ,  $260 \text{ Bq kg}^{-1}$  ( $7 \text{ pCi g}^{-1}$ ) of  $^{232}\text{Th}$  and  $4810 \text{ Bq kg}^{-1}$  ( $130 \text{ pCi g}^{-1}$ ) of  $^{40}\text{K}$  produce same gamma dose rate. Thus the  $\text{Ra}_{\text{eq}}$  may be calculated using the formula:

$$\text{Ra}_{\text{eq}} = A_{\text{Ra}} + 1.43 A_{\text{Th}} + 0.077 A_{\text{K}} \quad (2.13)$$

$A_{Ra}$ ,  $A_{Th}$  and  $A_K$  are the specific activities of  $^{226}Ra$ ,  $^{232}Th$  and  $^{40}K$ , respectively. For limiting the radiation dose from building materials in Germany to  $1.5 \text{ mGy y}^{-1}$ , a conservative model was proposed based on infinitely thick walls without windows and doors to serve as a criterion:

$$\frac{A_{Ra}}{370} + \frac{A_{Th}}{259} + \frac{A_K}{4810} \leq 1 \quad (2.14)$$

This criterion considers only the extreme exposure risk due to gamma rays and corresponds to a maximum of  $370 \text{ Bq kg}^{-1}$  for the material. This model was accepted by many countries. Later on, these conservative assumptions were corrected after considering a finite thickness of walls, windows, and doors through the application of weighting factor of 0.7 in each case. Therefore, the maximum permissible concentrations were increased by a factor of 2. i.e.

$$\frac{A_{Ra}}{740} + \frac{A_{Th}}{520} + \frac{A_K}{9620} \leq 1 \quad (2.15)$$

### **i. Activity index – generic approach**

In general, an index is introduced and used as a screening tool to limit gamma exposure from building materials; it consists of the sum of the contributions of the natural radionuclides to the gamma dose. In order that the material complies with the screening, the index should not generally exceed the value of 1 as shown in equation 6.1.

$$I = \frac{C_{Ra-226}}{A_{Ra-226}} + \frac{C_{Th-232}}{A_{Th-232}} + \frac{C_{K-40}}{A_{K-40}} \leq 1 \quad (2.16)$$

Where  $C_x$  is the measured activity concentration ( $\text{Bq kg}^{-1}$ ) and  $A_x$  is the fixed parametric values ( $\text{Bq kg}^{-1}$ ).

The  $A_x$  parametric values are calculated after assuming a dose criterion to be complied with and a background to be subtracted. These values also depend on the geometric and structural characteristics of the indoor environment and the dose coefficients per unit activity concentration used, i.e. the chosen room model. For this reason,  $A_x$  values may significantly vary from country to country. Frequently, the assumptions account for the radionuclide concentrations of typical materials of each country, due to the socioeconomic consequences of banning the use and trade of these materials [43].

**ii. Radium equivalent activity [44]**

Radium equivalent concentration is the quantity representative of external gamma irradiation dose associated with a material. In order to compare the specific activity of materials containing different amounts of  $^{226}\text{Ra}$ ,  $^{232}\text{Th}$  and  $^{40}\text{K}$ , the radium equivalent activity  $R_{\text{eq}}$  is used as defined by the following expression.

$$R_{\text{eq}} = C_{\text{Ra}} + 1.43 C_{\text{Th}} + 0.077 C_{\text{K}} \quad (2.17)$$

Where  $C_{\text{Ra}}$ ,  $C_{\text{Th}}$  and  $C_{\text{K}}$ , are the activity concentrations of  $^{226}\text{Ra}$ ,  $^{232}\text{Th}$  and  $^{40}\text{K}$  respectively, expressed in  $\text{Bq kg}^{-1}$ . The maximum permissible value of  $R_{\text{eq}}$  in any building material is  $370 \text{ B kg}^{-1}$ , to limit the annual external dose within  $1.5 \text{ mGy}$ . The assumption used in the above equation is because  $10 \text{ Bq kg}^{-1}$  of  $^{226}\text{Ra}$ ,  $7 \text{ Bq kg}^{-1}$  of  $^{232}\text{Th}$ , and  $130 \text{ Bq kg}^{-1}$  of  $^{40}\text{K}$  produce an equal gamma ray dose.

**iii. External hazard index [44]**

External hazard index ( $H_{\text{ex}}$ ) The external hazard index  $H_{\text{ex}}$  can be calculated by the following equation:

$$H_{\text{ex}} = \frac{C_{\text{Ra}}}{370} + \frac{C_{\text{Th}}}{259} + \frac{C_{\text{K}}}{4810} \leq 1 \quad (2.18)$$

Where  $C_{\text{Ra}}$ ,  $C_{\text{Th}}$  and  $C_{\text{K}}$ , are the activity concentrations of  $^{226}\text{Ra}$ ,  $^{232}\text{Th}$  and  $^{40}\text{K}$  respectively, expressed in  $\text{Bq kg}^{-1}$ . The values of this index must be less than unity in order to keep the radiation hazard no significant. The radiation exposure due to the radioactivity from a construction material is limited to  $1.5 \text{ mGy y}^{-1}$ . The maximum value of  $H_{\text{ex}}$  equal to unity corresponds to the upper limit of  $R_{\text{a,eq}}$  ( $370 \text{ Bq kg}^{-1}$ ).

#### iv. Internal hazard Index [44]

The internal hazard index,  $H_{\text{in}}$ , gives the internal exposure to carcinogenic radon and its daughter products that are hazardous to the respiratory organs. It can be calculated by the following equation:

$$H_{\text{in}} = \frac{C_{\text{Ra}}}{185} + \frac{C_{\text{Th}}}{259} + \frac{C_{\text{K}}}{4810} \leq 1 \quad (2.19)$$

$C_{\text{Ra}}$ ,  $C_{\text{Th}}$  and  $C_{\text{K}}$ , are the activity concentrations of  $^{226}\text{Ra}$ ,  $^{232}\text{Th}$  and  $^{40}\text{K}$  respectively, expressed in  $\text{Bq kg}^{-1}$ . The value of this index should be less than unity to keep the radiation hazard insignificant.

#### v. Alpha Index [45]

In order to control indoor radon exposure, an index known as alpha index ( $I_{\alpha}$ ) has developed, as shown in equation 6.4.

$$I_{\alpha} = \frac{C_{\text{Ra}}}{200 \text{ Bq kg}^{-1}} \quad (2.20)$$

$C_{\text{Ra}}$  is the  $^{226}\text{Ra}$  activity concentration ( $\text{Bq kg}^{-1}$ ) in the building material. When the  $^{226}\text{Ra}$  activity concentration of a building material exceeds the value of  $200 \text{ Bq kg}^{-1}$ , it is possible

that the radon exhalation from this material could cause indoor radon concentrations exceeding  $200 \text{ Bq m}^{-3}$ . On the contrary, when the  $^{226}\text{Ra}$  activity concentration is below  $100 \text{ Bq kg}^{-1}$  it is unlikely that the radon exhalation from the building materials could cause indoor radon concentrations exceeding  $200 \text{ Bq m}^{-3}$ .

**vi. Activity Index, I of the European Commission [46]**

The activity concentration index (I) also called as gamma index defined in the recommendation No. RP-112, of European Union, is also used to control the gamma external exposure due to natural radionuclides in building materials. It is being used as a radiological screening tool for the building materials.

$$I = \frac{C_{\text{Ra}}}{300} + \frac{C_{\text{Th}}}{200} + \frac{C_{\text{K}}}{3000} \quad (2.21)$$

Where,  $C_{\text{Ra}}$ ,  $C_{\text{Th}}$  and  $C_{\text{K}}$ , are the activity concentrations of  $^{226}\text{Ra}$ ,  $^{232}\text{Th}$  and  $^{40}\text{K}$  respectively.

. It is based on the excessive gamma dose rate of either  $0.3 \text{ mSv a}^{-1}$  or  $1 \text{ mSv a}^{-1}$  depends upon the usage of the materials, as shown in table 2.1.

**Table 2.1 Activity index (I) recommended by the European commission**

Dose criterion	0.3 mSv y <sup>-1</sup>	1 mSv y <sup>-1</sup>
Materials used in bulk quantities, e.g. concrete	$I \leq 0.5$	$I \leq 1$
Superficial and other materials with restricted use: tiles, boards, etc.	$I \leq 2$	$I \leq 6$

A modified  $I_{RP112}$  index is here proposed to also account for radon contribution to the effective dose indoors. This index follows the same approach of the Austrian index, however different hypotheses and dose criterion were applied. The modified  $I_{RP112}$  index ( $I_{RP112 Rn}$ ) is

$$I = \frac{(1 + \alpha)C_{Ra}}{300} + \frac{C_{Th}}{200} + \frac{C_K}{3000} \quad (2.22)$$

where  $\alpha$  is a factor calculated accounting for the Rn exhalation rate (E) from building materials, the subtracted outdoor  $^{222}\text{Rn}$  background and the dose criterion chosen for the indoor  $^{222}\text{Rn}$ . The outdoor radon background is assumed to be equal to the typical outdoor radon concentration of  $10 \text{ Bq m}^{-3}$  which it corresponds to an effective dose indoors at home of about  $0.3 \text{ mSv year}^{-1}$ .

In order to estimate  $\alpha$  value, the following expression was used:

$$\alpha = \frac{300 \lambda \varepsilon \rho d \text{ SV}^{-1}}{2 v C_{Rn}^0} \quad (2.23)$$

Where  $C_{Rn}^0$  is the sum of Rn activity concentration corresponding to the dose criterion chosen and the outdoor background of  $10 \text{ Bq m}^{-3}$ ;  $m$  the ventilation rate ( $\text{h}^{-1}$ );  $\text{SV}^{-1}$  the

surface to volume ratio of the room ( $m^{-1}$ );  $k$  the  $^{222}\text{Rn}$  decay constant ( $h^{-1}$ );  $\varepsilon$  the emanation power;  $\rho$  the density of building materials ( $kg\ m^{-3}$ ) and  $d$  is the building material thickness (m).

This equation comes from the classical expression of the radon activity concentration produced by building materials:

$$C_{Rn} = E\ SV^{-1}\nu^{-1} \quad (2.24)$$

Where  $E$  = Exhalation rate ( $Bq\ m^{-2}\ h^{-1}$ )

$$E = C_{Ra}\lambda\ \varepsilon\ \rho\ d/2 \quad (2.25)$$

$C_{Ra} = ^{226}\text{Ra}$  activity concentration in building materials ( $Bq\ kg^{-1}$ ). The dose criterion chosen for indoor  $^{222}\text{Rn}$  is  $3\ mSv\ year^{-1}$ , the lowest dose reference level in the range recommended by ICRP for exposure to radon in dwellings. It now corresponds to about  $100\ Bq\ m^{-3}$  indoors at home. Assuming the same geometry and size as for the RP 112 room,  $\varepsilon = 0.1$  and  $m = 0.7\ h^{-1}$ ,  $\alpha$  is equal to 1.09.

### vii. Austrian index

In 1995 Austrian legislation established an index  $I$  that accounts for exposure from both gamma radiation and radon exhalation from building materials which is shown in equation 6.6.

$$I = \frac{(1 + 0.15 K)C_{Ra-226}}{1000\ Bq\ kg^{-1}} + \frac{C_{Th-232}}{600\ Bq\ kg^{-1}} + \frac{C_{K-40}}{10,000\ Bq\ kg^{-1}} \quad (2.26)$$

Where  $k$  is a constant which depends on some characteristics of the materials, i.e. density, thickness and radon emanation power. The dose criterion used to calculate the  $A_x$  is 2.5 mSv year<sup>-1</sup>.

A new regulation including radon contribution to indoor dose was developed in 2009. The revised index is shown in equation 6.8.

$$I = \frac{(1 + 0.07 \varepsilon \rho d)C_{\text{Ra-226}}}{880 \text{ Bq kg}^{-1}} + \frac{C_{\text{Th-232}}}{530 \text{ Bq kg}^{-1}} + \frac{C_{\text{K-40}}}{8800 \text{ Bq kg}^{-1}} \quad (2.27)$$

where  $e$  is the radon emanation power,  $q$  the wall density,  $d$  the wall thickness and 0.07 is a constant, expressed in (m<sup>2</sup> kg<sup>-1</sup>), resulting from the exposure model applied. Where specific information is not available,  $\varepsilon$  can be set at 10%,  $d$  at 0.3 m and  $\rho$  at 2000 kg m<sup>-3</sup>. These parameters affect only the contribution of the radon term, and the estimation of the excess gamma dose remains independent of the density of the material and geometry of the room. The dose criterion used to calculate the  $A_x$  is 1 mSv year<sup>-1</sup>, and the assumed outdoor background dose is 1.2 mSv year<sup>-1</sup>.

### viii. Israel index

In 2009, Israel also adopted a similar approach and issued the standard SI 5098 for building materials radioactivity. It should be pointed out, however, that this is not a screening tool, but a standard, actually the third version of it: the first SI 5098 Standard was issued in 2002 and a revised Standard in 2007. The 2009 standard accounts for both gamma radiation and radon exhalation from building material, and introduces a total activity concentration index  $I$ :

$$I = \frac{C_{\text{Ra-226}}}{A_1(1 - \varepsilon)} + \frac{C_{\text{Ra-226}}}{A_2 \varepsilon} + \frac{C_{\text{Th-232}}}{A_3} + \frac{C_{\text{K-40}}}{A_4} \quad (2.28)$$

The gamma activity index:  $I_\gamma$ :

$$I_\gamma = \frac{C_{\text{Ra-226}}}{A_1} + \frac{C_{\text{Th-232}}}{A_3} + \frac{C_{\text{K-40}}}{A_4} \quad (2.29)$$

As for the total index  $I$  in Eq. (2.28) the first, third and fourth terms account for the excess indoor gamma dose; the second term, for the radon inhalation dose. The first term takes into account the gamma dose reduction from the  $^{226}\text{Ra}$  chain due to emanation and exhalation of  $^{222}\text{Rn}$ . Indeed, radioactive equilibrium disturbance in the material, due to radon emanation, results to activity contents of  $^{214}\text{Pb}$  and  $^{214}\text{Bi}$  in the material lower than that of  $^{226}\text{Ra}$ .

The  $A_x$  (table 2.2) parameters are calculated assuming an excess dose of  $0.3 \text{ mSv year}^{-1}$  (dose criterion) above background, i.e., the typical levels of indoor exposure which would be received in a room built from materials with typical activities. This dose criterion refers to the sum of gamma and radon exposure. Indeed, the building product must comply with both the total activity concentration index  $I$  and the gamma activity concentration index  $I_\gamma$ , which have two different series of reference values, e.g., in the case of concrete,  $I \leq 1$  and  $I_\gamma \leq 0.4$ .

**Table 2.2  $A_x$  values for different specific areas in Israel**

Building material	Typical specific area (kg m <sup>-2</sup> )	Activity (Bq kg <sup>-1</sup> )			
		A <sub>1</sub>	A <sub>2</sub>	A <sub>3</sub>	A <sub>4</sub>
Concrete	470	414	11	293	4070
Brick	225	605	235	433	6210

### ix. Dutch Radiation performance index

The Netherlands proposed a new so-called Radiation Performance Index, a model which estimates the annual effective dose from the indoor gamma radiation and radon concentration in the following way:

$$E = C_h c_{dc} + E_\gamma \leq 1 \quad (2.30)$$

where  $E$  is the annual effective dose rate (mSv year<sup>-1</sup>);  $C_h$  the annual average indoor concentration of radon exceeding the value outdoors (Bq m<sup>-3</sup>), released from building materials and, for ground floor rooms only, from the crawl space;  $c_{dc}$  the dose conversion factor (mSv year<sup>-1</sup> per Bq m<sup>-3</sup>) and  $E_\gamma$  is the effective dose rate due to gamma radiation (mSv year<sup>-1</sup>) is calculated using the following relation:

### x. Index of former Yugoslavia

The former Yugoslavia introduced an index  $I$  which also accounted for artificial radionuclide concentrations. This index is expressed by the following equation:

$$I = \frac{C_{\text{Ra-226}}}{400} + \frac{C_{\text{Th-232}}}{300} + \frac{C_{\text{K-40}}}{5000} + \frac{C_a}{4000} \quad (2.31)$$

Where,  $C_a$  is the sum of activity concentrations (in Bq kg<sup>-1</sup>) of all artificial radionuclides in the sample. The regulation was designed and drafted several months after the Chernobyl

accident in 1986 and adopted early in 1987. The reason for introducing limits for artificial radionuclides in building materials resided on the fact that the former Yugoslavia imported at this period several products from the former Soviet Union, including building materials, timber, etc., potentially contaminated with long-lived artificial radionuclides from the Chernobyl accident. It should be noted however that no contamination was ever reported in Yugoslavia.

#### **xi. The indexes in the Czech Republic**

Starting from 1970, the Czech Republic had to face a serious situation with several thousand houses built with material rich in radium or contaminated with residues from uranium paint and radium factories (with  $^{226}\text{Ra}$  activity concentration up to  $1 \text{ MBq kg}^{-1}$ ). The Czech Republic is also one of the countries with the highest indoor radon concentration in the world (mean radon concentration =  $140 \text{ Bq m}^{-3}$ ).

In 1987 the Czech Republic had to introduce an ad hoc legislation stating interventional levels for already existing houses, which is the only example found in literature of the use of an index to identify existing dwellings of concern. For this purpose, the following index  $S$  was introduced, in order to limit both gamma and indoor radon exposures in dwellings:

$$S = \frac{D}{2} \mu \text{ Gy h}^{-1} + \frac{C_{\text{Rn}}}{400 \text{ Bq m}^3} \quad (2.32)$$

Where  $D$  is the gamma dose rate ( $1 \text{ Gy h}^{-1}$ ) and  $C_{\text{Rn}}$  the annual average radon concentration ( $\text{Bq m}^{-3}$ ). This index results from the choice of a recommended value of  $400 \text{ Bq m}^{-3}$  for radon activity concentration, and  $2 \mu\text{Gy h}^{-1}$  for indoor gamma dose rate, to remediate

existing buildings. This sum rule (used only if  $D > 0.5 \mu\text{Gy h}^{-1}$ ) and value  $S = 1$  were used for decision making on remedial measures with governmental support.

Czech legislation concerning radioactivity in building materials is now based on a two-step procedure to account for both gamma and radon exposure: firstly, the index I, as defined by the RP 112 document, is used as a screening tool. Producers and importers should ensure systematic measurements of natural radionuclides in building materials and submit the results to the State Office for Nuclear Safety. If the index I is higher than 0.5 – a value corresponding to the exemption level of  $0.3 \text{ mSv year}^{-1}$  – a cost-benefit analysis should be done by the producer with a criterion aimed at reducing the public doses to a level as low as reasonably achievable.

## xii. India

Shukla et al [47] proposed a regulation to control radiation exposure due to building materials.

**Table 2.3 NORM regulation - Recommendation by Shukla et al 1995**

Criteria	Proposal
<b>External exposure</b> Indoor exposure exceeds the outdoor exposure of $x \mu\text{Gy y}^{-1}$ or Indoor does not exceed $1 \text{ mSv y}^{-1}$ with 0.8 occupancy factor	$250 x (\text{Bq kg}^{-1})$ of radium equivalent  $370 \text{ Bq kg}^{-1}$ of radium equivalent.
<b>Inhalation exposure</b> Indoor equilibrium equivalent $^{222}\text{Rn}$ concentration not to exceed $100 \text{ Bq m}^{-3}$ .	$85 \text{ Bq kg}^{-1}$ of $^{226}\text{Ra}$

Table 2.3 shows the recommendation of Shukla et al 1995, which has the following assumption:

- a. Equilibrium factor = 0.5
- b. Radium equivalent activity of  $370 \text{ Bqkg}^{-1}$ , which was derived from the outdoor specific air kerma rate.
- c. Room model was  $5\text{m} \times 4\text{m} \times 2.8 \text{ m}$

Atomic Energy Regulatory Board (AERB) has also introduced a safety directive on the use of phosphogypsum in building materials and in agriculture. As per this directive, all the phosphate fertilizer industries in India has to submit a quarterly report on radioactivity level in both imported rock phosphate and phosphogypsum. It has also recommended that the exempted level  $^{226}\text{Ra}$  in phosphogypsum is  $1 \text{ Bq g}^{-1}$ , same as that of the IAEA value. However, it cannot exceed  $40 \text{ kBq m}^{-2}$  when used for making panels and boards [48]. This has been derived from the activity index of the European Commission. This is the only regulation put in place in India as far as NORM in building material is concerned. This directive has not covered about use of fly ash and other industrial wastes and by products being used in the building material industry. Therefore, a single screening criteria is required which can take care of both excess internal as well as external radiation exposures and must be applicable to all the building materials.

#### **2.4 Indoor radon regulation – International trend**

F. Bochicchio [49] has reviewed the current trend on the regulation of indoor radon. The International Commission on Radiological Protection (ICRP) recommended in 1993 to select the action levels (AL) in the range of  $200 - 600 \text{ Bq m}^{-3}$  for dwellings and in the range of  $500 - 1500 \text{ Bq m}^{-3}$  for work places. These ranges were based on risk evaluations derived from the miner epidemiological studies available at that time. The upper value of these ranges remained unchanged in the 2007 recommendations, whereas the lower range was

removed and the AL concept was replaced with the concept of reference level (RL). World Health Organisation (WHO) dealt with radon exposure control within the framework of indoor air quality. In 2001, WHO proposed to consider simple remedial measures for buildings with radon progeny concentration  $> 100 \text{ Bq m}^{-3}$  (equivalent to  $250 \text{ Bq m}^{-3}$  of radon concentration).

Many epidemiological studies on lung cancer risk from radon were carried out in dwellings and mines. Three main pooled analyses of case - control epidemiological studies have been published recently. These analyses involved two studies carried out in China, 13 in Europe, and 7 in North America. The results were consistent among and within these three analyses, showing a linear increase of lung cancer relative risk in the range of 8 – 16 % for prolonged exposure (30 y) per each  $100 \text{ Bq m}^{-3}$  increase of average concentration. Whereas epidemiological studies on miners were generally characterized by the high exposure levels, more recent studies carried out in Czech and France allowed to better evaluate the effect of low exposures. The lung cancer risk evaluated with these studies was about the double of that estimated with previous studies on miners, which were used as the basis for the international regulations.

Taking into account the above findings, many international organisations started a process to update and revise their recommendations. WHO hand book on radon published on 2009 [50] recommends that radon concentration should be  $< 100 \text{ Bq m}^{-3}$ , or, if this RL is not considered feasible for some countries, the chosen RL should be not  $> 300 \text{ Bq m}^{-3}$ . The ICRP published in November 2009 a statement on Radon, anticipating some elements that will be included in a forthcoming ICRP recommendations on radon. As regards radon in

dwellings, ICRP reduced the upper value for RL from 600 to 300 Bq m<sup>-3</sup> and lower RLs should be considered according to local circumstances.

IAEA Specific Safety Guide No. SSG – 32, 2015 [51] Provides the recommendations and guidance on meeting the requirements of GSR Part 3 [13] for protection of the public against exposure indoors due to natural sources of ionising radiation. It provides recommendations and guidance to be followed by the regulatory body and all other authorities and organisations with responsibilities in relation to exposure to radiation from natural sources.

## **2.5 Measurement of NORM in various building materials**

The building materials analysed in most of the literatures include Soil, Sand, Cement, Concrete, Brick, Fly ash, Phosphogypsum, etc.

### **2.5.1 Assessment of NORM in building materials by various countries**

Hamilton et.al [41] reported the natural radioactivity in building materials used in the United Kingdom (UK) such as clay bricks, calcium silicate bricks, granite, gypsum, Portland cement blocks, rock wool, silica wool were analysed for natural radioactivity due to <sup>226</sup>Ra, <sup>232</sup>Th and <sup>40</sup>K using conventional NaI (Tl) gamma spectrometry. In order to compare the relative radioactivity of materials that contain <sup>226</sup>Ra, <sup>232</sup>Th and <sup>40</sup>K, a common index is required to in order that the sum of the activities of the various radionuclides may be added in similar units. For this purpose, activities have been expressed as radium equivalents in which the concentrations of the various radioelements are given in terms of the concentration of radium which gives the same gamma ray emission per gram. The number of gamma ray photon per disintegration of <sup>226</sup>Ra, <sup>232</sup>Th and <sup>40</sup>K are 2.17, 2.81 and

0.1 so that the following relations are calculated: 1 g of K is equivalent to 42 pCi of  $^{226}\text{Ra}$ , and 1 pCi of  $^{232}\text{Th}$  is equivalent to 1.29 pCi of  $^{226}\text{Ra}$ . The justification for use of the radium equivalent calculated in this way is that the radiation dose will bear a simple relationship to the radium equivalent, since the mean energies of  $^{226}\text{Ra}$ ,  $^{232}\text{Th}$  and  $^{40}\text{K}$  are all about 1 MeV; furthermore, the absorption coefficient for photon in materials of low atomic number, such as are used in building materials, changes very little with photon energy at energies around 1 MeV; for example, the mass energy absorption coefficient is about  $0.03 \text{ cm}^2 \text{ g}^{-1}$  for granite, clays, cement, sandstone, and gypsum. The mean radium equivalent expressed in pCi  $\text{g}^{-1}$  for conventional building materials was varying by a factor of 12. The highest value was found for the most common building materials, clay bricks.

Stranden's paper "Radioactivity of building materials and gamma radiation in dwellings" [32] has been one of the highly cited articles among the researchers carrying out natural radioactivity analysis of building materials. In his work, he studied NORM in concrete, bricks and Light weight clay aggregate (leca) samples collected all over Norway. For the radioactivity measurement  $7.62 \text{ cm} \times 7.62 \text{ cm}$  NaI (TI) scintillation gamma spectrometry was used. In concrete, the mean activity (pCi  $\text{g}^{-1}$ ) due to  $^{226}\text{Ra}$ ,  $^{232}\text{Th}$  and  $^{40}\text{K}$  was 0.75, 0.96, and 17.57 respectively, whereas in bricks it was 1.7, 2.0, and 30.7 respectively. In Leca samples the mean activity due to  $^{226}\text{Ra}$ ,  $^{232}\text{Th}$  and  $^{40}\text{K}$  was 1.4, 1.5, and 21.9 respectively. Specific exposure rate ( $\mu\text{R h}^{-1} / \text{Bq kg}^{-1}$ ) was computed for a standard room model  $4 \times 5 \times 2.8 \text{ m}^3$  using standard numerical integration method. The measurements were performed by a Reuter Stokes Environmental Monitor, and a value of  $3.6 \mu\text{R h}^{-1}$  was subtracted for cosmic radiation. The calculated values found were all within 16% of the experimental results and, taking the uncertainties into consideration, the calculations seem

to be fairly correct, as a function of wall thickness for different densities of building materials. The calculations are carried out for a distance of 3 m along the axis of a 6 m x 2.5 m wall. It can be seen that the exposure from an internal wall of gypsum of density 0.8 g and thickness 7.5 cm will be only about 20 % of the exposure from a 20 cm thick concrete wall of density  $2.35 \text{ g cm}^{-3}$  considered to have the same concentration of radioactivity. In Norway internal gypsum walls have been often constructed of two sheets about 1 cm thick with insulating materials in between. The exposure from such walls will only be a few per cent of that from a solid concrete wall. To be able to calculate the exposure inside Norwegian dwellings with walls of traditional materials the following model was adopted. For concrete walls (a) the room is  $9 \times 5 \times 2.5 \text{ m}^3$ ; (b) three walls, the floor and the ceiling are made of concrete, one short wall is neglected to allow for windows; and (c) the floor and ceiling are 25 cm thick and the walls are 20 cm thick. This will give values representative for a dwelling in a modern block of flats. Brick and light-weight expanded clay aggregate (LECA) are only used in walls.

In Australia, J. Beretka et. al [44] carried out extensive survey on natural radioactivity in building materials both conventional and industrial wastes and by products. The samples analysed include sand, lime, Portland cement, gypsum, clay bricks, mud bricks, concrete blocks, tiles, wood, fly ash, phosphogypsum, slag, zircon sand, rutile / ilmenite, red sand. For the radioactivity measurement,  $150 \text{ mm} \times 100 \text{ mm}$  NaI (Tl) scintillation detector based gamma spectrometer was used. To compare the specific activities of materials which contain  $^{226}\text{Ra}$ ,  $^{232}\text{Th}$  and  $^{40}\text{K}$ , a common index radium equivalent activity was defined.

In Italy, Bruzzi et.al [52] discussed a method of calculation developed for evaluating the contributions of external (gamma) and internal (alpha) doses due to the natural

radioactivity of building materials. The radionuclides examined are  $^{40}\text{K}$  and members of the  $^{235}\text{U}$ ,  $^{238}\text{U}$ , and  $^{232}\text{Th}$  radioactive decay chains. The method makes it possible to correlate the specific activities of these radionuclides in material used for constructing the walls of a room with the alpha and gamma dose absorbed by an individual at the center of the room. Monte Carlo N- Particle code, MCNP was used to study the variation of indoor gamma dose due to the variation of the room model parameters of typical room having the dimension of  $4 \times 4 \times 2.8 \text{ m}^3$ . The fact that the dose due to radon, for high levels of specific activity of the materials was found to be considerably lower than the gamma dose and showed that it is necessary to take account of both contributions in characterizing building materials from the point of view of radiological protection.

### **France**

Samir Dziri et al. [53] studied various construction materials used in France. In this study, they have used the Monte Carlo code MCNPX for the simulation of effective dose. The specific radioactivity of several building materials used in France, which is considered a direct exposure to radiation, has been assessed by  $\gamma$ -ray spectrometry. Corrected for coincidence summing and self-absorption effects, the values for  $^{226}\text{Ra}$ ,  $^{232}\text{Th}$  and  $^{40}\text{K}$  were in the ranges 4 - 56, 3 - 72 and 9 - 1136  $\text{Bq}\cdot\text{kg}^{-1}$ , respectively. The samples were found to have radium-equivalent activities between 5 and 245  $\text{Bq}\cdot\text{kg}^{-1}$ . Values of 0.02 - 0.67 for the external and 0.03 - 0.82 for the internal hazard indexes were estimated. The calculated absorbed dose in air agrees closely with MCNPX simulations. The conversion of absorbed dose to annual effective dose gave values between 0.03 - 1.09  $\text{mSv}\cdot\text{y}^{-1}$ . All these values are below action limits recommended by the International Commission on Radiological Protection. The materials examined would not contribute a significant radiation exposure

for an occupant and thus are acceptable for construction. Here the authors used the radiological indices such as external hazard index, internal hazard index and radium equivalent activity.

### **China**

Xinwei et al [54] has studied the NORM in building material samples such as cement, sand, clay bricks ceramic tile, roof tile glazed tile, used for construction in Wein region of Republic of China. NaI (Tl) gamma spectrometer was used for radioactivity analysis. They concluded that the measurement results show that the natural radionuclides contents of the studied building materials are in the range of Chinese soil values. The radium equivalent activity and external hazard index values of glazed tile are close to or higher than the recommended limit. The internal hazard index values and the annual effective dose rate values of roof tile, glazed tile and some cement samples made from fly ash are close to or higher than unity and  $1 \text{ mSv y}^{-1}$ , respectively. The study shows that roof tile and glazed tile should be limited to use in the construction of building and the monitoring on the natural radioactivity level of cement made from fly ash should be intensified for avoiding unnecessary radiation exposure to residents.

### **Brazil**

N. C. Silva et.al. [55] studied the NORM level in Brazilian phosphogypsum. Partitioning of natural radionuclides in the uranium and thorium decay chains was also reviewed. Alpha spectrometry with semiconductor surface barrier detectors was used for the analysis of uranium isotopes ( $^{238}\text{U}$  and  $^{234}\text{U}$ ). Gamma Spectrometry for the determination of  $^{226}\text{Ra}$ ,  $^{228}\text{Ra}$ ,  $^{210}\text{Pb}$ .

Uranium: Three naturally occurring isotopes of uranium exist:  $^{235}\text{U}$ ,  $^{238}\text{U}$  and its daughter  $^{234}\text{U}$ . Due to their isotopic abundances, half-lives and similar chemical behavior, the radionuclides  $^{238}\text{U}$  and daughters  $^{234}\text{U}$  are normally found in secular radioactive equilibrium in environmental samples. In these samples,  $^{235}\text{U}$ , due to its reduced isotopic abundance and long half-life, presents a specific activity in the order of  $10^{-3}$  of the specific activity of  $^{238}\text{U}$ , allowing its activity to be ignored.

During the acidulation of phosphatic rock, the major part of uranium (85 - 90 %) is incorporated into the phosphoric acid. The result of the alpha spectrometry showed that the isotopes of  $^{238}\text{U}$  and  $^{234}\text{U}$  are found in secular equilibrium in the phosphogypsum and the sum of their activities gives a good correlation with the values obtained by spectrophotometry. During the chemical processing of the phosphate rock, thorium is distributed in a form similar to that of uranium, hence up to 94 % of the thorium present in the phosphatic rock was incorporated in the phosphoric acid, and thus the phosphogypsum presents a low level of  $^{232}\text{Th}$ .

## Israel

Samples of typical raw materials, industrial by-products and building products and their components were collected from different productive quarries and building factories in Israel. Concentrations of natural radionuclides ( $^{226}\text{Ra}$ ,  $^{232}\text{Th}$ , and  $^{40}\text{K}$ ) in these samples were determined using a gamma-ray spectrometer based on Ge-detector. It was observed that isotope  $^{40}\text{K}$  contributes the most specific activity, compared with other isotopes. However, it was demonstrated that recalculation of radioactivity in terms of effective specific activity, which is determined taking into account the biologic action of each isotope on a human

being, leads to the conclusion that the most contribution comes from  $^{226}\text{Ra}$ , and to a lesser extent from  $^{232}\text{Th}$ . The isotope of  $^{226}\text{Ra}$  is only responsible for the effective radioactivity of phosphogypsum. The results indicated that a radium equivalent varies within the range of  $158.8 - 18.8 \text{ Bq kg}^{-1}$  in the samples of building products,  $74.3 - 17.5 \text{ Bq kg}^{-1}$  in the samples of building binders,  $164.5 - 17.7 \text{ Bq kg}^{-1}$  in the samples of aggregates, and  $761.4 - 241.6 \text{ Bq kg}^{-1}$  in the samples of industrial by-products used in construction.

K. Kovler et. al. [56] made an attempt to check whether the scintillation NaI (Tl) detectors, in spite of their poor resolution, can determine accurately the content of NORM in building materials. The activity concentrations of natural radionuclides were measured using two types of detectors:

- i. NaI (Tl) spectrometer equipped with the special software based on matrix method of least squares, and
- ii. HPGe spectrometer.

Synthetic compositions with activity concentrations varying in a wide range, from 1/5 to 5 times median activity concentrations of the natural radionuclides available in the earth crust and the samples of popular building materials, such as concrete, pumice and gypsum, were tested, while the density of the tested samples changed in a wide range ( $860$  up to  $2410 \text{ kg m}^{-3}$ ). The result obtained in the NaI (Tl) system were similar to those obtained with the HPGe spectrometer, mostly within the uncertainty range. This study showed that scintillation spectrometers equipped with a special software aimed to compensate for the lower spectral resolution of NaI (Tl) detectors can be successfully used for the radiation control of mass building materials.

## European Union

R.Travesi et.al [57] carried out the review on the database of activity concentration measurements of natural radionuclides ( $^{226}\text{Ra}$ ,  $^{232}\text{Th}$  and  $^{40}\text{K}$ ) in building material. It contains about 10,000 samples of both bulk material (bricks, concrete, cement, natural- and phosphogypsum, sedimentary and igneous bulk stones) and superficial material (igneous and metamorphic stones) used in the construction industry in most European Union Member States. The database allowed the authors to calculate the activity concentration index I suggested by a European technical guidance document and recently used as a basis for elaborating the draft Euratom Basic Safety Standards Directive e for bricks, concrete and phosphogypsum used in the European Union. The analysis of these materials, made on averaged and probably overestimated I Values, showed that the adoption of the dose criterion of  $0.3 \text{ mSv y}^{-1}$  of the European technical guidance document RP112 (European Commission, 1999) as exemption level is probably too ambitious a health goal. Indeed, too many materials would exceed the value of index I relevant to this dose criterion. Probably a health goal of  $1 \text{ mSv y}^{-1}$  would be more realistic. In the authors' opinion a cost/effective goal would be a dose criterion between 0.3 and 1, as recommended by RP112.

## Hungary - NORM in coal slag in building construction

J. Somlai [58] et.al studied the dose to the school children in the school constructed with the coal as one of the building materials. Their study was primarily related to the assessment of radiation impact due to the used coal slag from the Transdanubian Middle Mountains and elevated in  $^{226}\text{Ra}$  concentration. Altogether nine schools were examined in the cities of Ajka, Tatabanya and Vezprem. Primary exploratory measurements were

carried out using the portable survey meters. In addition, indoor radon concentration was measured using the air sampling method for 24 hrs. In all the classroom survey, the average external dose rate was at 1 m height was found to be less than  $120 \text{ nGy h}^{-1}$  and did not exceed 120 at any other sites. Radon concentration was found to be  $125 \text{ Bq m}^{-3}$  and not exceeded  $200 \text{ Bq m}^{-3}$  in any of the cases.

## **2.5.2 Study of natural radioactivity in building materials - Indian scenario**

### **NORM in Indian Soil**

S. Sadasivan et.al [59] has carried out the measurement of natural radioactivity in Indian soil from the samples collected across India in 24 locations. The sampling was done at undisturbed open plain areas and away from any slopy terrain. In Himalayan and sub Himalayan regions, it was not always possible to choose locations which are away from slopy terrains. At such places, samples were collected from the available open areas not close to the slopy terrains and also which were least disturbed due to the land slides in the regions. Samples of depth soils were collected with a post-hole auger of 15 cm dia. at an interval of 15 cm depth, mostly. The sample collections were done from the soil layers of 0 - 15 cm and 15 - 30 cm thickness. In some cases, samples were also collected from the depth of 30 - 45 cm. In addition, top layer soil in Mumbai was collected from 0 - 5 cm depth and analyzed on a regular basis.  $^{137}\text{Cs}$ ,  $^{40}\text{K}$ ,  $^{232}\text{Th}$  and  $^{238}\text{U}$  in soil samples were measured by using a high resolution gamma-ray spectrometer consisting of an HPGe detector of 30% relative efficiency housed in a 7.5 cm thick lead shield, PC coupled 8K MCA card and associated electronics. The activity profile for natural radionuclides ( $^{40}\text{K}$ ,  $^{232}\text{Th}$  and  $^{238}\text{U}$ ) exhibits a uniform distribution, within  $\pm 15\%$  of variation with respect to depth. This is to be expected as primordial radionuclides form the part of rock and

soil and are therefore generally uniformly distributed. The variation of natural radioactivity levels at different sampling sites is due to the variation of concentrations of these elements in the geological formations. Natural radioactivity measurements show that Tehri Garhwal, located in Himalayas, has higher levels of  $^{238}\text{U}$ . Also, levels of  $^{238}\text{U}$  in Shillong situated at the foothill of the Himalayas were comparatively higher. The geological formation of Tehri Garhwal and Shillong is alluvium type.<sup>7</sup> It was observed that Aligarh as well as Kolkatta located in the Indo-Gangetic plane shows similar levels of  $^{238}\text{U}$  and  $^{232}\text{Th}$ . Also, the geological formation of both these places is alluvium, which exhibits higher  $^{238}\text{U}$  compared to other formations in India. This could be one of the reasons for similarity in levels of  $^{238}\text{U}$  and  $^{232}\text{Th}$ . Some places in peninsular India like Hyderabad and Visakhapatnam and Chingleput located at east coast exhibit higher concentrations of  $^{232}\text{Th}$  compared to other normal areas of India. Hyderabad and Visakhapatnam have granite gneisses formation and Chingleput has charnockites formation. These geological formations are reported to contain higher thorium than the other formations in India. However, the levels of  $^{238}\text{U}$  and  $^{232}\text{Th}$  in the soils of the places studied are low compared to the levels measured in soils from higher background areas of Southwest India. External dose rates from soil radioactivity. Geometric mean of the activity levels due to  $^{226}\text{Ra}$ ,  $^{232}\text{Th}$ ,  $^{40}\text{K}$  was found to be  $26 \text{ Bq kg}^{-1}$ ,  $41 \text{ Bq kg}^{-1}$  and  $321 \text{ Bq kg}^{-1}$ . The terrestrial dose rates are ranging from  $18 \text{ nGy h}^{-1}$  in Mumbai to  $144 \text{ nGy h}^{-1}$  in Hyderabad.

#### **Kannan et al., [60], Kalpakkam, Tamil nadu**

The authors studied the distribution of natural and anthropogenic radionuclides in soil and beach sand samples of Kalpakkam where the concentration of  $^{238}\text{U}$ ,  $^{232}\text{Th}$  and  $^{40}\text{K}$  were 5

to 71, 15 to 776 and 200 to 854 Bq kg<sup>-1</sup> of dry soil samples respectively. In beach sands the concentration of <sup>238</sup>U, <sup>232</sup>Th and <sup>40</sup>K contents varied in the range of 36 to 258, 352 to 3872 and 324 to 405 Bq kg<sup>-1</sup> respectively. The total absorbed gamma dose rate in air due to the presence of <sup>238</sup>U, <sup>232</sup>Th and <sup>40</sup>K in Kalpakkam soil samples varied between 24 and 556 nGy h<sup>-1</sup> with a mean value of 103 nGy h<sup>-1</sup>. The presence of <sup>232</sup>Th in beach sand contributed maximum (94.0%) to the total absorbed gamma dose rate in air followed by <sup>238</sup>U (4.7%) and minimum contribution was by <sup>40</sup>K (1.3%).

### **Indoor Radon, Kalpakkam**

B. Danalakshmi et al. [61] carried out the Radon measurements in the residential colony of Nuclear Power Station at Kalpakkam using track detectors was carried out to generate baseline data of Radon levels in the dwellings. Solid State Nuclear Track Detector LR-115 films were exposed for one year covering the four seasons and processed using Spark Counter. The radon concentration level is even below the threshold action level of 200 Bqm<sup>-3</sup> as stipulated by ICRP (200 - 600 Bqm<sup>-3</sup>).

### **M. Sowmya et.al [62] Kalpakkam, Tamilnadu**

The activity concentration of naturally occurring radioactive elements such as <sup>226</sup>Ra, <sup>232</sup>Th and <sup>40</sup>K were measured for 46 soil samples collected in the vicinity of the Madras atomic power station, Kalpakkam, South India using gamma-ray spectroscopy. The average activity concentration of <sup>226</sup>Ra, <sup>232</sup>Th and <sup>40</sup>K in soil samples were found to be 22.6 ±12.6, 92.8±44.3 and 434.1±131.1 Bq kg<sup>-1</sup>, respectively.

### **Ravisankar et al. [63], Tamil Nadu**

Building materials such as various flooring materials viz. plain tile, color tile, vitrified tile, green granite, black granite, orange marble, used in Thiruvannamalai district of Tamilnadu, India,. For the measurement of radioactivity due to  $^{226}\text{Ra}$ ,  $^{232}\text{Th}$ , and  $^{40}\text{K}$ ,  $3'' \times 3''$  NaI (TI) scintillation gamma spectrometer was used. The highest value of the specific activities of  $^{226}\text{Ra}$ ,  $^{232}\text{Th}$  and  $^{40}\text{K}$  are 66.11 (coloured tile), 63.15 (vitrified tile) and 1366.85 Bq kg<sup>-1</sup> (orange marble) respectively while the lowest value of the specific activities of the same radionuclides are 6.17, 4.62 & 139.17 Bq kg<sup>-1</sup> (black granite). Radium equivalent activity of these samples were calculated. These values ranging from 23.49 Bq kg<sup>-1</sup> (black granite) to 202.63 Bq kg<sup>-1</sup> (orange marble) are less than the maximum admissible value of 370 Bq kg<sup>-1</sup>, which is equivalent to an external dose of 1.5 mSv yr<sup>-1</sup>. Thus, all the materials selected for this study would not pose a significant radiological hazard when used in building constructions.

### **G. Senthilkumar et al [64]**

The activity of  $^{226}\text{Ra}$  varies from 11.2 to 54.09 Bq kg<sup>-1</sup> and the arithmetic mean is 35.73 Bq kg<sup>-1</sup>. The activity concentration of  $^{232}\text{Th}$  varies from 23.47 to 49.62 Bq kg<sup>-1</sup> and the arithmetic mean is 37.75 Bq kg<sup>-1</sup>. The activity concentration of  $^{40}\text{K}$  varies from 113.43 to 233.92 Bq kg<sup>-1</sup> and the arithmetic mean is 159.83 Bq kg<sup>-1</sup>. Radium equivalent activity was also found to be 161.9 Bq kg<sup>-1</sup> well below the allowable value of 370 Bq kg<sup>-1</sup>. The authors used Austrian standard to screen the building materials which include radon dose contribution also. The Austrian index is given below.

$$\frac{C_{\text{Ra}}}{740} (1 + 0.1\epsilon\text{pd}) + \frac{C_{\text{Th}}}{520} + \frac{C_{\text{K}}}{9620} \leq 1 \quad (2.33)$$

where  $\epsilon$  denotes the fraction for radon from walls,  $\rho$  is the mass density ( $\text{kg m}^{-3}$ ) and  $d$  the thickness (m) of the walls. The Austrian NORM S5200 has adopted the values 0.1, 2000  $\text{kg m}^{-3}$  and 0.3 m to be used for  $\epsilon$ ,  $\rho$  and  $d$ , respectively. For Indian condition, actual values of these parameters would be different.

#### **M.P. Chougaonkar et al [65] HBRA, Kerala**

Study of the profiles of radiation exposures to the populations living in the high background radiation areas (HBRAs) of the monazite-bearing region in Kerala, India, has been conducted by monitoring 200 dwellings selected from two villages in this region. Each of these dwellings was monitored for 1 year and the study lasted for a period of 2 years. The indoor gamma ray dose measurements were carried out using thermo luminescent dosimeters (TLDs) and the inhalation doses due to radon, thoron and their progenies were monitored using solid-state nuclear track detector (SSNTD) based twin-cup dosimeters. Outdoor gamma ray dose measurements were carried out using Geiger Muller (GM) tube based survey meters. Annual effective doses were computed, using occupancy factors of 0.8 and 0.2, respectively, for indoor and outdoor, by adding the three components. Occupants of 41.6% of the houses surveyed were observed to receive the annual effective doses ranging between 0.5 and 5 mSv/a, 41.6% between 5 and 10 mSv/a, 10.2% between 10 and 15 mSv/a, and 6.6% greater than 15 mSv/a. The inhalation component was generally smaller than the external gamma ray component and on an average it was found to constitute about 30% of the total dose.

#### **Khandaker et al [66], HBRA, Kerala**

Concentrations of primordial radionuclides in common construction materials collected from the south-west coastal region of India were determined using a high-purity

germanium gamma-ray spectrometer. Average specific activities ( $\text{Bq kg}^{-1}$ ) for  $^{238}\text{U}$  ( $^{226}\text{Ra}$ ) in cement, brick, soil and stone samples were obtained as  $54\pm 13$ ,  $21\pm 4$ ,  $50\pm 12$  and  $46\pm 8$ , respectively. Respective values of  $^{232}\text{Th}$  were obtained as  $65\pm 10$ ,  $21\pm 3$ ,  $58\pm 10$  and  $57\pm 12$ . Concentrations of  $^{40}\text{K}$  radionuclide in cement, brick, soil and stone samples were found to be  $440\pm 91$ ,  $290\pm 20$ ,  $380\pm 61$  and  $432\pm 64$ , respectively. The activity level reported here is similar to the global and Indian average level, though the study area is one of the high natural background areas of the world.

### **Gudalore, Tamil Nadu [67]**

Each soil sample is obtained from five subsamples collected in an area of approximately  $2500 \text{ m}^2$ .

Gamma spectra from the samples are recorded using a  $3'' \times 3''$  NaI (Tl) detector coupled to a 4 K multi-channel analyser. The spectrometer is calibrated using standard samples supplied by International Atomic Energy Agency, Vienna (IAEA). The minimum detectable activity for  $^{232}\text{Th}$ ,  $^{238}\text{U}$  and  $^{40}\text{K}$  are 1.0, 8.5 and  $13.25 \text{ Bq kg}^{-1}$  at a background shielding factor of 95%. The analysis of the gamma spectra obtained is performed with dedicated software, and the choice of the reference peak is made in such a way that they are sufficiently discriminated. Of the peaks that could be identified via the software, reference is made to that at 1.764 MeV for  $^{214}\text{Bi}$ , in the  $^{238}\text{U}$  decay chain, that at 2.614 MeV for  $^{208}\text{Tl}$  in the  $^{232}\text{Th}$  decay chain, and one at 1.460 MeV of  $^{40}\text{K}$ . Each measurement is performed with a counting time of 20,000 s.

The activity concentration of primordial radionuclides in soil samples of Gudalore Taluk in the Udhagamandalam district has been measured from the gamma ray spectrum of the soil. The mean activities of  $^{232}\text{Th}$ ,  $^{238}\text{U}$  and  $^{40}\text{K}$  are 75.3244.1, 37.7210.1 and 195.2285.1

Bq kg<sup>-1</sup> dry weight, respectively. The average outdoor absorbed dose rate in air at a height of 1 m above ground is 74.3227.8 nGy h<sup>-1</sup>, corresponding to an annual effective dose equivalent of 455.6 mSv. The dose equivalent ranges from 168.3 to 1250.5 mSv. The results have been compared with other global radioactivity measurements and evaluations.

### **Garhwal, Himalaya**

Ramola et. al. [68] carried out the survey of natural radioactivity in soil samples of Garhwal Himalayan region. In this study, soil samples up to a depth of 10 cm were collected from different lithological units of the Thauldhar and Budhakedar regions of Garhwal Himalaya, India. The radionuclides <sup>226</sup>Ra, <sup>232</sup>Th and <sup>40</sup>K, were measured in soil samples using NaI (Tl) (63 mm x 63 mm) gamma spectrometry system. The activity concentrations of the naturally occurring radionuclides <sup>226</sup>Ra, <sup>232</sup>Th and <sup>40</sup>K in the analysed samples were found to vary from below detection level (BDL) to 131 ± 18 Bq kg<sup>-1</sup>, 9 ± 6 Bq kg<sup>-1</sup>, 384 ± 53 Bq kg<sup>-1</sup>, 471 ± 96 Bq kg<sup>-1</sup> to 1406 ± 175 Bq kg<sup>-1</sup>, respectively. The external absorbed gamma dose rates due to <sup>226</sup>Ra, <sup>232</sup>Th and <sup>40</sup>K were found to vary from 49 to 306 nGy h<sup>-1</sup>. The average radium equivalent activity from these soil samples was 300 Bq kg<sup>-1</sup>.

M. Yadav et.al [69] reported the natural radioactivity levels in the same region. The study area belongs to the main central thrust (MCT), which is the area with unique property having single largest structure within the collision of Indian plate with Asian Plate. Boundaries of these plates are known as the seismic belts of the world. In this study, top surface soil samples were collected from different geological formations of Ukhimath area in Garhwal Himalaya. Samples were analysed using the NaI (Tl) (63 mm x 63 mm) based gamma spectrometry system. The natural radionuclides <sup>226</sup>Ra, <sup>232</sup>Th and <sup>40</sup>K activity

concentrations were found to be in the range of  $8 \pm 1$  to  $50 \pm 10$  Bq kg<sup>-1</sup> with an average of 20 Bq kg<sup>-1</sup>,  $7 \pm 1$  to  $88 \pm 16$  Bq kg<sup>-1</sup> with an average of 26 Bq kg<sup>-1</sup> and  $115 \pm 18$  to  $885 \pm 132$  Bq kg<sup>-1</sup> with an average of 329 Bq kg<sup>-1</sup>, respectively. From the activity concentrations, radiological parameters such as absorbed dose rate at 1 m height, radium equivalent activity ( $R_{eq}$ ), and external hazard index ( $H_{ex}$ ) were calculated. The mean absorbed dose rate varied from 13 to 113 nGy h<sup>-1</sup> with an average of 39 nGy h<sup>-1</sup>. The annual outdoor effective dose rate was found to vary from 0.02 to 0.14 mSv with an average of 0.05 mSv. The calculated  $H_{ex}$  was in the range of 0.07 – 0.66 with an average of 0.23.

### **Kumaun, Himalaya**

Ramola et.al [70] carried out the detailed radionuclide analysis of Kumaun, Himalaya, India. The study area falls in the subtropical Lesser Himalayan belt in the eastern part of Kumaun Himalaya. In this study, soil samples were collected from a depth of 60 cm in 1000 ml plastic beakers, keeping in view that the top layer soil is removed by leaching process. HPGe detectors (with relative efficiency of 45 % and 43 % having energy resolution of 1.8 keV and 1.87 keV respectively) based gamma spectrometry systems were used for the analysis of natural radionuclides <sup>226</sup>Ra, <sup>232</sup>Th and <sup>40</sup>K. The mean concentration of <sup>238</sup>U and <sup>232</sup>Th in the soil samples varied from 0.5 to 5 ppm (6 to 60 Bq kg<sup>-1</sup>) and 2 to 20 ppm (8 to 80 Bq kg<sup>-1</sup>) respectively. The reported activity concentration for the different rock formations varied from 32.6 to 1305.5 Bq kg<sup>-1</sup> for <sup>238</sup>U, 16.3 to 136.3 Bq kg<sup>-1</sup> for <sup>232</sup>Th and 124.6 to 1758.0 Bq kg<sup>-1</sup> for <sup>40</sup>K. <sup>226</sup>Ra / <sup>238</sup>U concentration were recorded with respect to different geological formation. It was observed that the ratio decreased slightly from Berinag to Deoban and Saryu Formations. Whereas the <sup>238</sup>U / <sup>232</sup>Th ratio did not show any definite pattern. The activity ratio indicated that there is extreme disequilibrium in the

$^{238}\text{U}$  natural radioactivity decay series from  $^{238}\text{U}$  to  $^{226}\text{Ra}$ , which is due to the granitic rocks of the concordant Champawat body. These are magmatic in origin as indicated by complexly twined and zoned plagioclases. The rocks of this regions are comagmatic and are bound to systematic progressive changes in the proportion of  $\text{N}_2\text{O}$ ,  $\text{K}_2\text{O}$ ,  $\text{CaO}$ ,  $\text{Fe}_2\text{O}_7$ , and  $\text{FeO}$ . These complex chemical reactions may have resulted in the disequilibrium of the radionuclides. Correlation between various measured radionuclides in the samples collected from the study area showed that the strong correlation between  $^{40}\text{K}$  and  $^{238}\text{U}$  (0.6),  $^{40}\text{K}$  and  $^{232}\text{Th}$  (0.7),  $^{235}\text{U}$  and  $^{226}\text{Ra}$  (0.8) as well as  $^{226}\text{Ra}$  and  $^{232}\text{Th}$  (0.7). A weak negative correlation was observed between  $^{40}\text{K}$  and  $^{230}\text{Th}$  (-0.2),  $^{238}\text{U}$  and  $^{230}\text{Th}$  (-0.3),  $^{226}\text{Ra}$  and  $^{230}\text{Th}$  (-0.4) as well as  $^{232}\text{Th}$  and  $^{230}\text{Th}$  (-0.5). The negative correlation shows that the radionuclide concentrations are associated with different chemical and geological properties of the elements. The different contents of clay and sand in the soil samples also contribute to the correlation coefficient, with micro-cracks, fractures and mobility characteristic of the radionuclides in the geological medium. Uranium chemistry changes with reducing and oxidizing environment, but radium chemistry is relatively simple as it behaves like the other alkaline earth metals. The distribution of the radionuclides varied with rock type due to different chemical properties of the measured radionuclides and the rocks. It was found out from this study that high activity levels were found in Saryu Formation consisting of augn-gnesis, granite interbedded with schists and flaggy quartzite. Presence of uranium mineralization in the shear zone associated with different thrusts and faults may be responsible for high radioactivity in the study area. The total air absorbed dose rate in air above 1m height was calculated from the activity concentrations of three radionuclides  $^{226}\text{Ra}$ ,  $^{232}\text{Th}$  and  $^{40}\text{K}$ , which varied from 39.1 to 226.8 nGy h<sup>-1</sup> with the mean

value of  $118.7 \text{ nGy h}^{-1}$ . In order to control the indoor dose in the dwellings due to natural radioactivity in the studied rock and soil if used for construction, the internal ( $H_{\text{in}}$ ) and external ( $H_{\text{ex}}$ ) hazard indices were calculated.  $H_{\text{in}}$  has been used to control the internal exposure by radon and its progeny, which should be less than so that materials can be used for construction. For the soil samples collected from igneous rocks of the Saryu Formation, the estimated  $H_{\text{in}}$  was 1.8, which indicates high radium activity in the rock formation.

The authors reported  $^{230}\text{Th}$  value as part of evaluating disequilibrium between uranium decay series radionuclides. However, there is no mention about the analytical technique used. Since this radionuclide cannot be measured using gamma spectrometry due to very weak gamma emission at low energy. The formula used in calculating the activity hazard indices was based on the external gamma dose rate at 1m height per unit specific activity on the open ground uniformly distributed. This may not adequately reflect the indoor exposure in the dwellings. Hence it is necessary to derive a new activity index for indoor dose restriction assuming various room models.

### **Radon and Thoron in homes of Indian Himalaya**

R. C. Ramola [71] carried out the indoor radon and thoron survey in Indian Himalaya. The study covered both Garhwal and Kumaun region of the Himalaya. LR-115 based plastic track detector was used for the measurement. The survey was made in various residential houses of the area at a height of 2.5 m above the floor using a twin chamber radon dosimeter, which can record the values of radon, thoron, and their progeny separately. The concentrations of radon and thoron in these homes were found to vary from 11 to 191 and 1 to 156  $\text{Bq m}^{-3}$ , respectively. The equilibrium factor between radon and progeny varies from 0.02 to 0.9 with an average of 0.26 for the region. The resulting dose rate due to radon,

thoron and their decay products was found to vary from 0.02 to 0.84  $\mu\text{Sv h}^{-1}$  with an arithmetic mean of 0.27  $\mu\text{Sv h}^{-1}$ . The surveyed houses are located in the hilly region of Garhwal Himalayas, which consists of the rock type phylites, quartzite and gneisses with slightly higher uranium content. Most of the houses in the cities and towns of the studied area are constructed with cement and bricks whereas in surrounding villages the houses are made of mud. These houses are constructed with local stones and rocks with thin paste of mud. In general, the radon concentration was found higher in mud houses than in concrete houses. The ground floor of such houses is directly constructed on the soil top with a coating of mud, which allows more radon to diffuse inside the house because of higher porosity of materials used. The emanation of radon is also higher from rocks and local stones. In addition, the mud houses, have small doors and a small window (some without window), which remains closed for most of the time to conserve energy in this hilly region. Due to poor ventilation conditions, the radon accumulated inside the house and thus results in higher radon concentration. Radon and progeny concentrations in the house of the study area were found to be highest in winter and lowest in summer. However, no systematic seasonal variation was observed.

### **New Delhi**

R. G. Sonkawade et al [72] carried out the assessment of natural radioactivity in common building materials and radiation shielding materials. The studied samples include radiation shielding bricks, granite, soil, hematite, bricks, and sand. High resolution gamma spectrometry system n-type (HPGe with 20 % relative efficiency and 2 keV energy resolution at 1332 keV  $^{60}\text{Co}$  gamma line) was used for the measurement of natural radioactivity due to  $^{238}\text{U}$ ,  $^{232}\text{Th}$  and  $^{40}\text{K}$  in the above samples. For the measurement of radon

concentration and hence the exhalation rate, “Can technique” was used. In this technique, LR-115 based plastic track detector was used. The activity concentrations  $^{238}\text{U}$ ,  $^{232}\text{Th}$  and  $^{40}\text{K}$  radionuclides varied from  $29 \pm 1$  to  $98 \pm 4$  Bq kg<sup>-1</sup>,  $20 \pm 2$  to  $112 \pm 2.8$  Bq kg<sup>-1</sup>  $200 \pm 8$  to  $1908 \pm 15.6$  Bq kg<sup>-1</sup>, respectively, in various materials studied in this work. The study showed that the average  $^{232}\text{Th}$  activity in marble samples were below the detection limit. Radon activity varied from  $190 \pm 11$  to  $313 \pm 14$  Bq m<sup>-3</sup>, the mass exhalation rate for radon varied from  $1.05 \pm 0.07$  to  $1.92 \pm 0.09$  mBq kg<sup>-1</sup>h<sup>-1</sup> and surface exhalation rate varied from  $9.0 \pm 0.3$  to  $19.8 \pm 22$  mBq m<sup>2</sup> h<sup>-1</sup>. The authors also estimated the external gamma dose rate at 1m height from the measured specific activity levels using the dose conversion factors of the UNSEAR 2000 [6]. From the absorbed dose rate, the annual effective dose was calculated by assuming that the people stay 80 % of the time stay indoors and the conversion coefficient from absorbed dose in air to effective dose  $0.7$  Sv Gy<sup>-1</sup>. The minimum and maximum values of annual effective dose was found to be in the range of  $0.11$  to  $0.91$  mSv.

### **Aligarh, Uttar Pradesh**

Viresh Kumar et. al [73] carried out the assessment of natural radioactivity in conventional building materials (sand, clay brick, Portland cement) and by-products (slag, fly ash) from Uttar Pradesh. NaI (Tl) 12.5 cm x 10 cm based gamma spectrometer was used for the measurement of natural radioactivity due to  $^{226}\text{Ra}$ ,  $^{232}\text{Th}$  and  $^{40}\text{K}$ . The authors reviewed the genesis most common radiological parameter, the radium equivalent activity ( $R_{\text{eq}}$ ) and calculated the  $R_{\text{eq}}$  using the new formula for the analysed building material samples. Based on the above new criterion as shown in equation 2.2., the radiological assessment of

measured radioactivity levels indicated that the building materials examined in this work could be used for constructions.

### **Sirsa, Haryana**

R. Mehra et.al [74] studied the natural radioactivity levels in the soil of Sirsa district of Haryana. HPGe (20 % relative efficiency) based gamma spectrometry was used for the measurement. The range of activity concentrations of  $^{226}\text{Ra}$ ,  $^{232}\text{Th}$ , and  $^{40}\text{K}$  in the soil samples from the studied areas varies from 19.18 Bq kg<sup>-1</sup> to 40.31 Bq kg<sup>-1</sup>, 59.43 Bq kg<sup>-1</sup> to 89.54 Bq kg<sup>-1</sup> and 223.22 Bq kg<sup>-1</sup> to 313.32 Bq kg<sup>-1</sup> respectively.

### **Kaiga, Karnataka**

Patra et.al [75] studied the natural radioactivity due to  $^{238}\text{U}$ ,  $^{232}\text{Th}$  and  $^{40}\text{K}$  in geological matrices rock and soil in and around Kaiga region of Karnataka state. The activity of  $^{238}\text{U}$  in the soil samples ranged from 12.8 – 42.2 Bq kg<sup>-1</sup> with a mean of 31.7 Bq kg<sup>-1</sup>;  $^{232}\text{Th}$  ranged from 19.8 – 45.3 Bq kg<sup>-1</sup> with the mean of 31.7 Bq kg<sup>-1</sup> and  $^{40}\text{K}$  ranged from 135.8 – 344.6 Bq kg<sup>-1</sup> with a mean of 201.4 Bq kg<sup>-1</sup>. The study revealed that the mean concentration levels measured in Kaiga region from naturally occurring isotopes such as  $^{232}\text{Th}$  is comparable with worldwide soil,  $^{238}\text{U}$  and  $^{232}\text{Th}$  concentrations are lower than the corresponding values obtained worldwide. In the rock samples  $^{238}\text{U}$  was in the range of 0.5 – 11.5 Bq kg<sup>-1</sup> with the mean of 4.3 Bq kg<sup>-1</sup>;  $^{232}\text{Th}$  was in the range of 1.2 – 14.2 Bq kg<sup>-1</sup> with the mean of 8.1 Bq kg<sup>-1</sup> and  $^{40}\text{K}$  was in the range of 14.8 – 866.2 Bq kg<sup>-1</sup>. Comparison of the natural radioactivity levels in the soil and rock was made. The observed activity ratios Soil/rock due to  $^{238}\text{U}$ ,  $^{232}\text{Th}$  and  $^{40}\text{K}$  were found to be 5.6, 3.9, and 0.58, respectively. The absorbed dose rate in outdoor air were found to be in the range of 20 – 58 nGy h<sup>-1</sup> with

a mean of  $33.3 \text{ nGy h}^{-1}$  which is below the corresponding population weighted value of  $60 \text{ nGy h}^{-1}$ .

T. V. Ramachandran et.al. [76] carried out a countrywide survey on indoor  $^{222}\text{Rn}$  and  $^{220}\text{Rn}$  levels for India was carried out in dwellings using Solid State Nuclear Track Detector (SSNTD) based passive detector techniques. Calibration factors for the measurements were derived experimentally as well as theoretically. More than 5000 measurements have been carried out in 1500 dwellings across the country comprising urban and rural locations. The results showed that the  $^{222}\text{Rn}$  gas concentrations at different locations varied between 4.6 and  $147.3 \text{ Bq m}^{-3}$  with an overall geometric mean of  $23 \text{ Bq m}^{-3}$ . The  $^{220}\text{Rn}$  gas concentrations were less than the  $^{222}\text{Rn}$  gas concentrations at these locations ( $3.5 - 42.8 \text{ Bq m}^{-3}$ ) with an overall geometric mean of  $12 \text{ Bq m}^{-3}$ . The inhalation dose rates due to  $^{222}\text{Rn}$ ,  $^{220}\text{Rn}$  and their progeny ranged from  $0.2 \text{ mSv y}^{-1}$  at Hyderabad to  $5.1 \text{ mSv y}^{-1}$  at Namrup with a geometric mean of  $0.94 \text{ mSv y}^{-1}$ .

### **South Konkan, Maharashtra**

S. J. Dhawal et. al. [77] assessed the level of natural radioactivity due to radionuclides,  $^{238}\text{U}$ ,  $^{232}\text{Th}$ , and  $^{40}\text{K}$  in 50 soil samples collected from South Konkan, Maharashtra, India. The mean activity concentrations of  $^{238}\text{U}$ ,  $^{232}\text{Th}$ , and  $^{40}\text{K}$  were found to be  $44.97 \text{ Bq kg}^{-1}$ ,  $59.7 \text{ Bq kg}^{-1}$  and  $217.5 \text{ Bq kg}^{-1}$ , respectively.

### **Radon in Indian granite – Tamil Nadu**

S. R. Menon et.al [78] has carried out the measurement of natural radioactivity levels, radon and thoron levels in granite samples of India. Radon and thoron exhalation rates were measured from 9 different samples of building materials collected from the state of Tamil Nadu, India. Eight of the samples were Indian granite while one sample was

phosphogypsum sample. These samples were in the form of cuboidal blocks and hence, the radon exhalation from these samples were expressed in terms of radon activity released per unit surface area per unit time i.e., surface exhalation rate of radon. The exhalation rates were measured by two independent methods, viz., (i) active, dynamic method utilizing a continuous radon monitor and (ii) passive, ‘can’ technique based on Solid State Nuclear Track Detectors (SSNTDs).  $^{222}\text{Rn}$  and  $^{220}\text{Rn}$  exhalation rate (ER) were  $0.017 \text{ Bqm}^{-2} \text{ h}^{-1}$  per  $\text{Bqkg}^{-1}$ , respectively. Radioactivity measurement was carried out using HPGe gamma spectrometry system.  $^{226}\text{Ra}$  was in the range of (Sentine Red Granite) 25 – (Chocolate Brown Granite)  $184 \text{ Bq kg}^{-1}$ , whereas  $^{232}\text{Th}$  was in the range of (Imperial white granite) 96 – (Bone red Granite)  $196 \text{ Bq kg}^{-1}$ .

D. D. Jyanthi et.al. [79] carried out the study on indoor radon thoron levels and the corresponding effective dose of the population of high background areas of Kanyakumari district, Tamilnadu, India. SSNTD technique was used for the measurement of indoor radon and thoron. To measure the external gamma dose rate indoor, thermo luminescence dosimetric (TLD) technique was used. The effective dose equivalent of radon varies from 7.28 to 29.4 nSv per  $\text{Bq h m}^{-3}$  and for thoron 93.5 to 614.4 nSv per  $\text{Bq h}^{-1} \text{ m}^{-3}$ . The equilibrium equivalent concentration (EEC) of radon varies from 13.0 to 52.5  $\text{Bq m}^{-3}$  and that of thoron varies from 0.7 to 4.9  $\text{Bq m}^{-3}$ . Across the village in this study, the radon level varies from 13 – 52  $\text{Bq m}^{-3}$ . The annual effective dose equivalent was found to be varied from 2.6 – 8.7  $\text{mSv y}^{-1}$  with the arithmetic mean of 4.72  $\text{mSv y}^{-1}$ . The contribution of  $^{232}\text{Th}$  for the inhalation exposure is much lower than that due to radon progeny. From the study it is evident that the annual effective dose in all the villages of the study is found to be below the remedial action limit of  $10 \text{ mSv y}^{-1}$ .

**NORM in Indian Fly ash**

K. Kant et.al. [80] carried out the measurement of radon exhalation rates and natural radioactivity in Indian fly ash samples using SSNTD technique. In the study, fly ash samples from the thermal power plants in North India. Gamma spectrometry system having HPGe (20 % relative efficiency) coupled with 4 K MCA was used for the radioactivity measurement. The activity concentrations of  $^{238}\text{U}$ ,  $^{232}\text{Th}$ , and  $^{40}\text{K}$  was found to be varied from 99 – 203 Bq kg<sup>-1</sup>, 145 – 288 Bq kg<sup>-1</sup> and 355 – 516 Bq kg<sup>-1</sup>, respectively in various fly ash samples. Radon activity varied from 214 – 590 Bq m<sup>-3</sup>, radon mass exhalation rate was in the range of 7.8 – 21.6 mBq kg<sup>-1</sup> h<sup>-1</sup> and radon surface exhalation rate ranged from 138 – 381 mBq m<sup>-2</sup> h<sup>-1</sup>.

**Gogi, Karnataka**

N. Karunakara et. al [81] has carried out the detailed assessment of soil natural radioactivity levels in and around a proposed uranium mining site, Gogi, in Karnataka, India. The concentration of  $^{226}\text{Ra}$ ,  $^{232}\text{Th}$ , and  $^{40}\text{K}$  in the soil varied in the range of 5.8 – 154.8 Bq kg<sup>-1</sup>, 10.2 – 576.9 Bq kg<sup>-1</sup>, and 56.2 – 1371.1 Bq kg<sup>-1</sup>, respectively, with the corresponding geometric mean values of 34.3 Bq kg<sup>-1</sup>, 78.4 Bq kg<sup>-1</sup>, and 609.9 Bq kg<sup>-1</sup>, considering all the 39 locations in the 0 – 30 km region. The study revealed that highly nonuniform distribution of these radionuclides in the region with activity concentration in the soil varying significantly within a small area, which is due to the highly localised mineralisation of elements.

---

## Chapter 3 Standardisation of HPGe Gamma Ray Spectrometer

---

### 3.1 Introduction

For any measurement standardization of the instrument is a must before deploying into routine measurement for the specific application. Standardisation is nothing but calibration of the instrument with respect to the measurand. The term Calibration is defined as the relating the instrument output to the quantity to be measured.

### 3.2 Specification of gamma spectrometry system used in the study

The Low Level Counting Laboratory (LLCL) at BARC Hospital is equipped with both high and low resolution gamma spectrometry systems. For the analysis of NORM in building materials, p-type HPGe with 50 % relative efficiency based gamma spectrometer has been used. Table 3.1 shows the important specification of the spectrometry system. Fig. 3.1 shows the photo of the system installed in the LLCL. This system has the advantage of measuring the low energy up to 30 keV due to its thin carbon fiber entrance window. Size of the detector is (dia. 80.8 mm and depth 41.3 mm) with carbon fiber end window (thickness is 0.75 mm). It is shielded with 100 mm thick lead and new combination of graded z- inner linings (10 mm copper (Cu) with 0.3mm Nickel (Ni) electrochemical coating). Relative efficiency of the detector is 50 % with respect to 7.62cm x7.62cm NaI (Tl) scintillation detector at 1332 keV of  $^{60}\text{Co}$  gamma line. Background spectrum of the system is shown in 3.2. It shows the significant reduction in the background at low energy part of the spectrum due to the graded shielding arrangement. This will help in the accurate analysis of low energy natural gamma emitters such as  $^{210}\text{Pb}$  (46.5 keV) and  $^{238}\text{U}$  through its progeny  $^{234}\text{Th}$  [63 2 keV (3.7%)].

For routine measurement of low-level radioactivity, HPGe coupled high-resolution gamma spectrometry system has been used. The system consisting of a coaxial n-type HPGe detector with 50% relative efficiency (with respect to 7.62 cm x 7.62 cm NaI (Tl)), Nuclear Instrument Module (NIM) compatible pulse processing electronic accessories and spectrum stabilised 8 K MCA (PHAST, Electronics Division, BARC). The energy resolution of the detector measured as full width at half maximum (FWHM) is 1.85 keV for 1332.5 keV of  $^{60}\text{Co}$  gamma energy at a source to detector distance of 25 cm. To reduce the background contribution, the detector is enveloped with by 7.5 cm thick lead. For routine radioactivity analysis of the environmental samples, IAEA protocol TRS-295 [4] has been followed in the laboratory. The certified reference materials IAEA RGU-I, RGTh-I, RGK-I and samples of previous inter-comparison exercises have been used for the energy and efficiency calibration of the system covering the energy range of 46.53 - 2614.53 keV. The spectrum acquisition time is 100000 seconds for the samples analysis and weekly background observation. Table 3.2 shows the minimum detectable activity (MDA) of the spectrometry system for a 300 g soil sample and counting time of 100,000 sec.

**Table 3.1 Main characteristics of HPGe Gamma Spectrometer**

<b>Specifications</b>	<b>Specified</b>	<b>Measured</b>
Rel. efficiency, %	50	54
Energy resolution (FWHM), keV @ 1332 keV and 122 keV	1.85	1.88
	0.705	0.85
Peak to Compton ratio	65:1	64:1
FWTM/FWHM	1.83	1.86
FWFM/FWHM	2.3	2.49



**Figure 3.1 HPGe Gamma Spectrometry system in the Low Level Counting Lab**

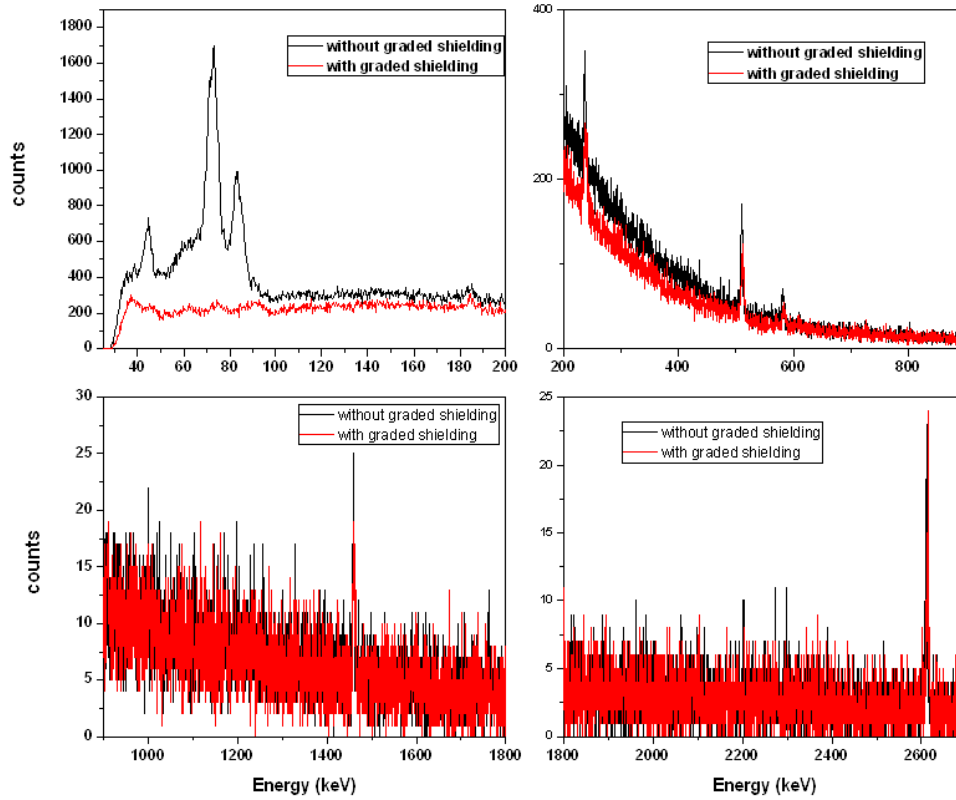


**Figure 3.2 Background spectrum of a Gamma spectrometry system with p-type HPGe (50 % Relative Efficiency)**

### 3.3 Formula used for the activity estimation

Radioactivity concentration in a sample is calculated using the following formula

$$\text{Activity (Bqkg}^{-1}\text{)} = \frac{(N - B)}{(T \times \gamma \times \varepsilon \times w)} \quad (3.1)$$

Minimum Detectable activity (MDA) in a sample is calculated using the following formula

$$\text{MDA (Bq kg}^{-1}\text{)} = \frac{4.66 \sqrt{B}}{(T \times \gamma \times \varepsilon \times w)} \quad (3.2)$$

Combined standard uncertainty is calculated using the following formula [82]

$$\sigma(A) = A \sqrt{\left[\left(\frac{\sigma_c}{c}\right)^2 + \left(\frac{\sigma_\varepsilon}{\varepsilon}\right)^2 + \left(\frac{\sigma_\gamma}{\gamma}\right)^2\right]} \quad (3.3)$$

N – Gross counts (sample + background)

B – Background counts

T – Counting time (sec)

$\gamma$  – Gamma emission probability

$\varepsilon$  – Absolute efficiency of the detector at particular gamma energy

w – Sample weight (kg)

A - Measured Activity Concentration (Bq/kg)

$\sigma_c$  - Counting uncertainty

$\sigma_\varepsilon$  - Uncertainty in the absolute efficiency of the detector

$\sigma_\gamma$  - Uncertainty in Gamma emission probability of particular gamma energy used for activity calculation.

**Table 3.2 Minimum Detectable Activity (MDA) of gamma spectrometry system**

Radionuclides		E $\gamma$ (keV)	(Bq kg <sup>-1</sup> ) <sup>a</sup>
Uranium series	<sup>210</sup> Pb	46.53	2.0
	<sup>238</sup> U ( <sup>234</sup> Th)	63.25	2.0
	<sup>226</sup> Ra( <sup>214</sup> Bi)	1764.5	1.0
Thorium series	<sup>232</sup> Th ( <sup>208</sup> Tl)	2614.53	3.0
Potassium	<sup>40</sup> K	1460.83	2.5
Cesium	<sup>137</sup> Cs	661.6	0.1

### 3.4 Reference materials for calibration

A material or substance, one or more properties of which are sufficiently well established to be used for the calibration of an apparatus, the assessment of a measurement method, or for assigning values to materials. The Low Level Counting Lab (LLCL) of HPD, BARC, has been using the IAEA reference materials for the calibration of the HPGe spectrometry system as shown in table 3.3. Gamma spectrum obtained using the uranium ore, IAEA RGU-I and thorium ore reference material are shown in fig. 3.3 and fig 3.4 respectively.

**Table 3.3 IAEA Certified Reference Materials for calibration**

S. No.	Standard code	Name	Prominent radionuclides
1.	IAEA RGU-I	Uranium Ore	$^{238}\text{U}$ in radioactive equilibrium with progenies
2.	IAEA RGU-I	Thorium Ore	$^{232}\text{Th}$ in radioactive equilibrium with progenies
3.	IAEA RGK-I	Potassium Sulphate	$^{40}\text{K}$
4.	IAEA - 434	Phosphogypsum	$^{238}\text{U}$ , $^{226}\text{Ra}$ , and $^{210}\text{Pb}$
5.	IAEA-152	Milk Powder	$^{137}\text{Cs}$ , $^{40}\text{K}$
6.	BRIT, India	Point sources	$^{241}\text{Am}$ , $^{137}\text{Cs}$ , $^{133}\text{Ba}$ , $^{57}\text{Co}$ , $^{60}\text{Co}$ etc.
7.	BRIT, India	Liquid source	$^{137}\text{Cs}$ , $^{133}\text{Ba}$ , $^{152}\text{Eu}$

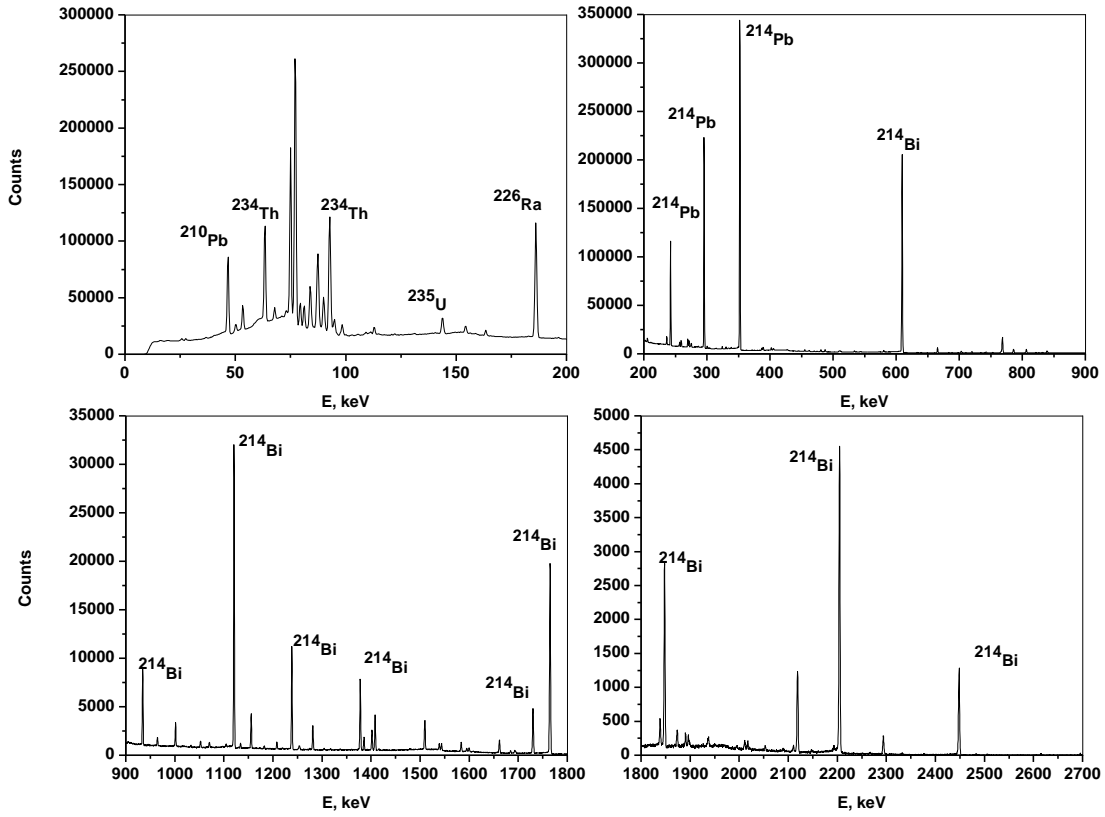
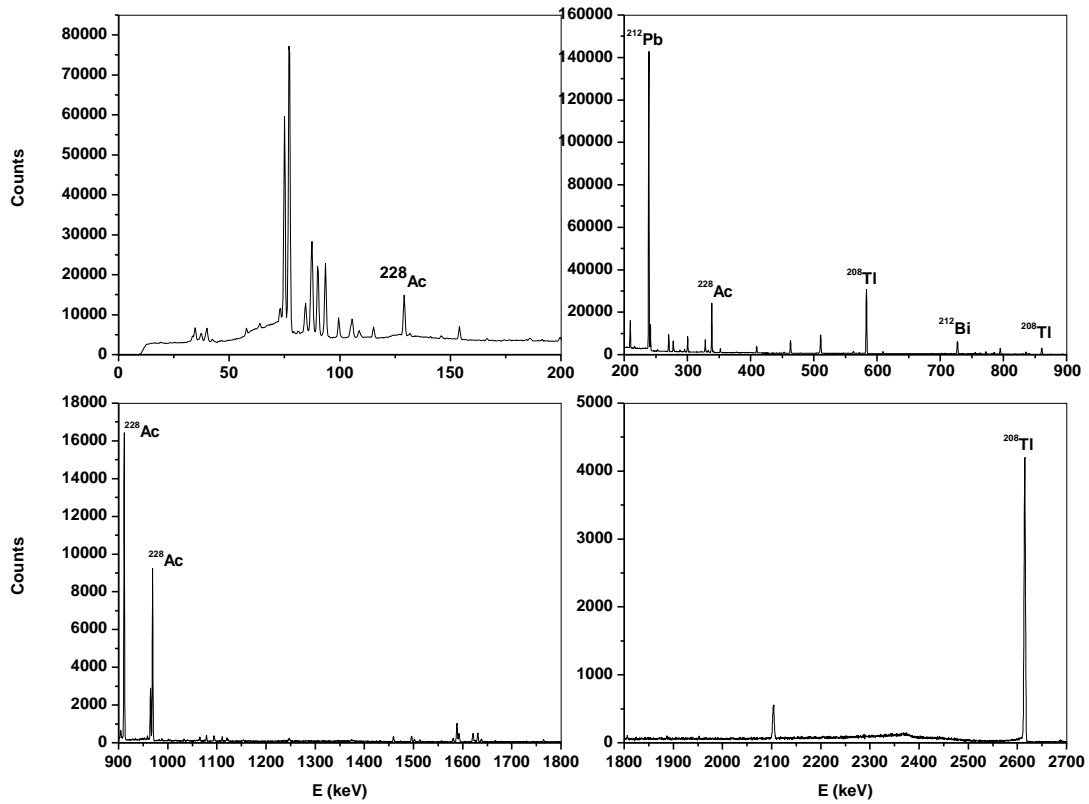


Figure 3.3 HPGe (p-type, 50 %) gamma spectrum of IAEA RGU-I (Uranium ore)



**Figure 3.4 HPGe (p-type HPGe, 50%) Gamma spectrum of IAEA RGTh-I (Thorium Ore)**

### 3.5 Energy calibration

The object of energy calibration is to derive a relationship between peak position in the spectrum and the corresponding gamma-ray energy. The energy calibration includes the calculation of two sets of parameters: the energy versus the channel number, and the peak shape or FWHM (Full Width at Half Maximum) versus the energy.

For the gamma spectrometric assay of NORM, the system has been calibrated covering the energy range of 46 – 2614 keV which includes all the gamma energies of the  $^{238}\text{U}$  and  $^{232}\text{Th}$

natural radioactive decay series. Table 3.4 shows the prominent gamma energies of these series and some important man-made radionuclides used for calibration.

**Table 3.4 Prominent Gamma energies (keV) and emission probabilities. [29], [30]**

Radionuclide		$E_{\gamma}$ (keV) <sup>a</sup>	$P_{\gamma}$ %
Uranium series	<sup>234</sup> Th	63.29	$4.8 \pm 0.04$
		92.59	$5.58 \pm 0.01$
	<sup>234m</sup> Pa	1001.025	$0.832 \pm 0.01$
	<sup>226</sup> Ra	186.211	$3.533 \pm 0.028$
	<sup>214</sup> Bi	1764.539	$15.17 \pm 0.12$
		1120.287	$14.78 \pm 0.11$
		609.316	$45.16 \pm 0.33$
	<sup>214</sup> Pb	351.932	$35.34 \pm 0.27$
		295.224	$18.28 \pm 0.14$
	<sup>210</sup> Pb	46.53	$4.25 \pm 0.1$
Thorium series	<sup>228</sup> Ac	911.204	$25.8 \pm 0.4$
		338.32	$11.27 \pm 0.5$
	<sup>212</sup> Pb	238.632	$43.6 \pm 0.3$
		300.09	$3.18 \pm 0.13$
	<sup>212</sup> Bi	727.33	$6.58 \pm 0.5$
	<sup>208</sup> Tl	2614.511	$35.85 \pm 0.07$
		583.187	$30.55 \pm 0.17$
		860.56	$4.48 \pm 0.04$
Potassium	<sup>40</sup> K	1460.822	$10.66 \pm 0.13$
Manganese	<sup>54</sup> Mn	834.838	$99.97 \pm 0.0011$
Cobalt	<sup>57</sup> Co	122.060	$85.51 \pm 0.06$
	<sup>60</sup> Co	1173.22	$99.85 \pm 0.03$
		1332.492	$99.98 \pm 0.0006$
Zinc	<sup>65</sup> Zn	1115.539	$50.6 \pm 0.22$
Cesium	<sup>137</sup> Cs	661.6	$84.99 \pm 0.2$

	$^{134}\text{Cs}$	604.72	$97.65 \pm 0.18$
Europium	$^{152}\text{Eu}$	121.78	$28.41 \pm 0.13$
Americium	$^{241}\text{Am}$	59.54	$35.78 \pm 0.09$

Energy calibration is carried out by using sources of known distinct gamma energies. The spectrum is acquired for a reasonable time so that photo peaks have sufficient counts for the analysis. The region of interest and the centroid channel numbers are identified. Then the slope of the straight line plot of channel no~ energy represents the energy calibration factor. Energy (keV) of any channel can be determined with the straight-line equation

$$E (\text{keV}) = (m \times c) + c \quad (3.4)$$

Where  $c$  = intercept and  $m$ = slope of the straight line

Energy calibration for HPGe is  $\sim 0.4$  keV/ch and for NaI (Tl) it is  $\sim 10$  keV/ch.

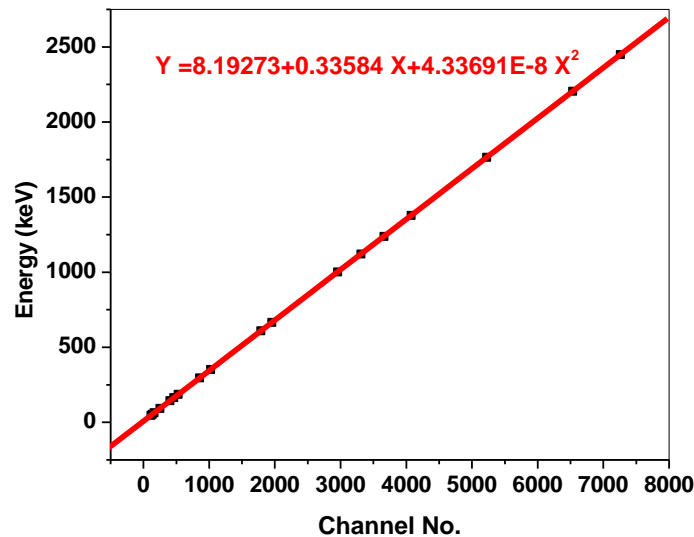


**Figure 3.5 Energy calibration of HPGe Gamma spectrometry system**

### **3.6 Efficiency calibration**

Relative efficiency is a general performance measure relating the efficiency of detection of the  $^{60}\text{Co}$  gamma ray at 1332 keV of the detector to that of a standard sodium iodide scintillation detector.

#### **Absolute full energy peak efficiency**

In gamma spectrometry, our intention is to relate the peak area in our spectrum to the amount of radioactivity it represents. For this, we need the absolute full energy peak efficiency. This relates the peak area, at a particular energy, to the number of gamma-rays emitted by the source and must depend upon the geometrical arrangement of source and detector.

#### **Absolute total efficiency**

It relates the number of gamma rays emitted by the source to the number of counts detected anywhere in the spectrum. This takes into account the full energy peak and all incomplete absorptions represented by the Compton continuum.

#### **Intrinsic efficiency**

It relates the counts in the spectrum to the number of gamma rays incident on the detector. This efficiency is a basic parameter of the detector and is independent of the source/detector geometry.

The efficiency calibration includes the calculation of the efficiency of the semiconductor detector system as a function of energy. This includes effects from the intrinsic detector crystal, the detector-source geometry, the materials surrounding the detector and absorption in the source matrix. The efficiency calibration is needed for each source-

detector combination. The generally accepted analytical expression used for fitting the absolute efficiency data is as follows:

$$\ln \epsilon = a_1 + a_2 \ln E$$

$\epsilon$  = Full energy peak efficiency%

E = Energy (keV)

This expression is adequate independently for 200 – 2000 keV and 50 – 100 keV and 100 – 200 keV. A single 4<sup>th</sup> or 5<sup>th</sup> order logarithmic polynomial can also be used for the entire energy range of 50 – 2000 keV. Fig. 3.6 shows the absolute efficiency least fitting of the IAEA RGU-I and RGTh-I in 250 ml geometry.

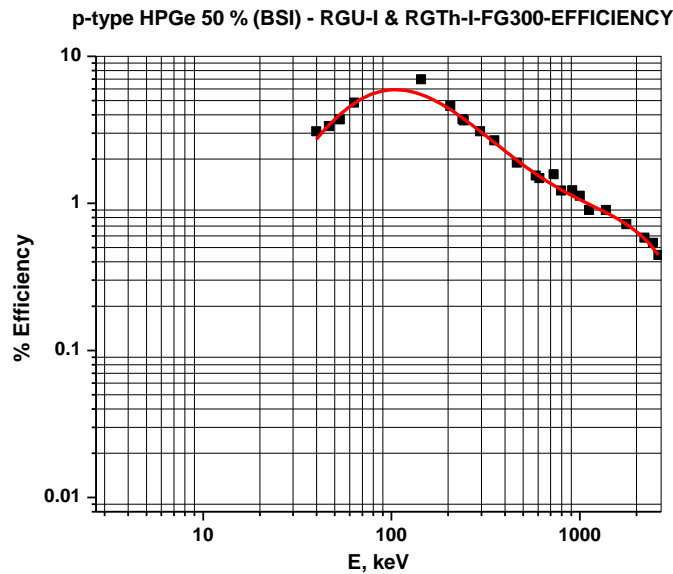


**Figure 3.6 absolute efficiency (HPGe (p-type 50 %) - IAEA RGU-I & Th-I in 250 cm<sup>3</sup> plastic container at contact**

### 3.7 Corrections for self-attenuation in gamma-ray spectrometry

Any gamma ray that is emitted by the decay of a radioisotope in a material has a distinct probability of undergoing various interactions with the material and being attenuated prior to being counted on a detection system. These interactions with the material result in scattering of the gamma ray, absorption, or loss of energy to the material (e.g. Compton scattering). The attenuation of these gamma rays by the emitting material results in an underestimation of the intensity of photo peaks in the spectrum for these materials, particularly at low energies of less than 100 keV

In order to obtain correct results, the samples should be counted under exactly the same measuring conditions as those under which system has been calibrated, but differences can always occur and corrections are needed to account the variation in counting parameter. The density of soil samples varied from 1.4 to 1.9 g cm<sup>-3</sup> and density of standard used for estimation was 1.4 g cm<sup>-3</sup>, hence density correction factors were applied to get correct estimation of concentration.

The extent of this gamma ray self-attenuation is dependent on both the geometry of the measured sample as well as the linear attenuation coefficient,  $\mu$ , for the material in the sample. The linear attenuation coefficient is itself reliant on the properties of the material, such as density and composition, and the energy of the gamma rays in question. The intensity of a gamma ray source passing through an attenuating material is given as the following:

$$I(E) = I_0(E)e^{-\mu(E)x} \quad (3.5)$$

$I(E)$  is the attenuated intensity of the gamma rays emitted,  $I_0(E)$  is the initial intensity of the gamma rays at energy  $E$  and  $\mu(E)$  linear attenuation coefficient of the attenuating material at energy  $E$ , and  $x$  is the linear thickness of the material.

$$I = \int_0^t N_0 e^{-\mu x} \frac{dx}{1} = N_0 \frac{1 - e^{-\mu t}}{\mu t} \quad (3.6)$$

For the self-attenuation fraction, [27]

$$a = 1 - \frac{N}{N_0} = 1 - \frac{1 - e^{-\mu t}}{\mu t} \quad (3.7)$$

This expression assumes that all the gamma-rays leave the sample perpendicular to the surface. The correction factor due to differences between the density of the sample and the standard source is  $C = F_{(\text{sample})} / F_{(\text{standard})}$

The mass attenuation coefficients used for sample and standard nearest to their densities were taken from table [26].

### 3.8 QA/QC of spectrometry system

Quality Control (QC) in gamma-ray spectrometry, as an assemblage of operational techniques and activities that are used to fulfill the requirements of a quality system based on ISO/IEC DIS 17025, 1999, requires monitoring of the performance of the spectrometer, the analysis procedure and the consistency of the results. To comply with these requirements the system of QC includes execution of procedures designed to check whether the measurements and the spectral analyses were correctly performed. Besides control of the routine measurement and analysis procedure, monitoring includes duplicate measurements and analyses, analyses of reference materials, and participation in the proficiency tests.

The stability of the system is ensured by observing the variation of detector background. Quality Control (QC) charts are used to study the fluctuation of data in a continuous process. Here, 25 observations of the HPGe detector background were used for plotting the QC chart. The upper layer of the QC chart is the X bar graph. This layer displays the mean value for each of the subgroups as a scatter graph with drop lines to the average of the mean for each group (X bar). This layer also displays two limit lines that are positioned at 3 times the standard deviations (99 % confidence level) away from the X bar. The lower layer of the QC chart is the R chart. This layer displays the range for each of the subgroups as a column graph. The range for each of the subgroups is plotted from the average line (or R bar). This line represents the group's average range, or the average of the mean range within each subgroup. This layer also displays two limit lines - the UCL and LCL lines. The upper part of the chart reveals the background fluctuation with respect to the subgroup mean and the lower part describes the background variation in terms of range. The subgroup mean is marked as the control limit (CL). The LCL and UCL denote lower and upper control limit respectively. The LCL and UCL is given by the following by the equation

$$LCL = \mu - 3 \left( \frac{\sigma}{\sqrt{n}} \right) \quad (3.8)$$

$$UCL = \mu + 3 \left( \frac{\sigma}{\sqrt{n}} \right) \quad (3.9)$$

Where  $\frac{\sigma}{\sqrt{n}}$  is the standard deviation of the sample mean and  $\mu$  is the sample mean [10].

Fig.3.7 and 3.8 show the quality control (X bar R) chart of the  $^{210}\text{Pb}$  and  $^{40}\text{K}$  background variation.

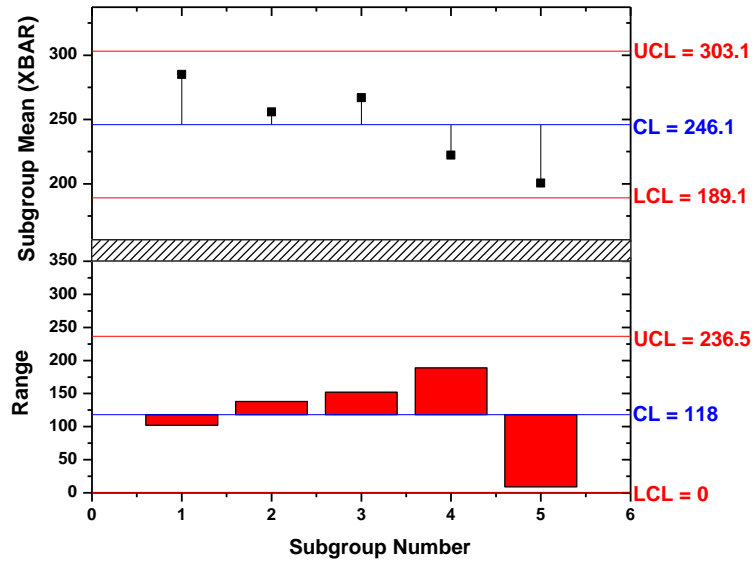


Figure 3.7 Quality Control chart of HPGe Gamma spectrometer using  $^{210}\text{Pb}$  background

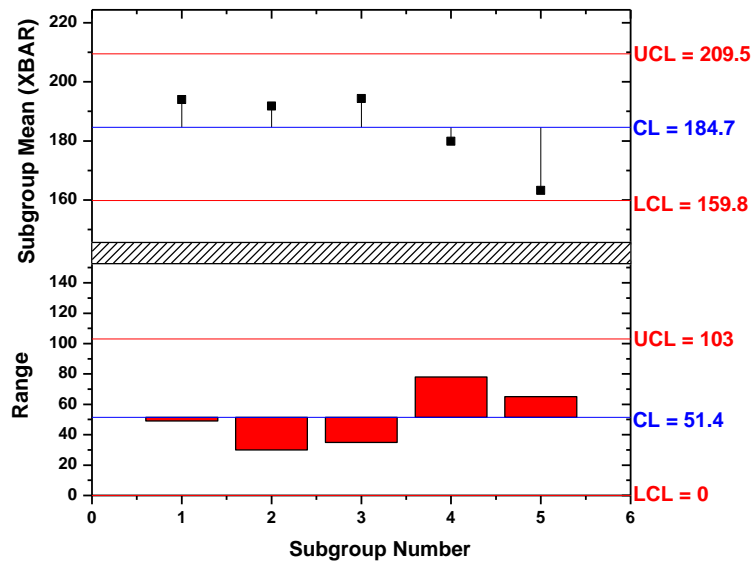


Figure 3.8 Quality Control chart of HPGe Gamma spectrometer using  $^{40}\text{K}$  background

### 3.8.1 IAEA-ALMERA Proficiency tests evaluation

The Low Level Counting Laboratory (LLCL) of HPD, BARC, has been participating in the IAEA PTs since the beginning. The participant's results were evaluated for accuracy and precision using the acceptance criteria [83]. The participant result is assigned 'Acceptable' status for trueness if  $A1 \leq A2$

Where 
$$A1 = |Value_{IAEA} - Value_{Lab}| \quad (3.10)$$

$$A2 = 2.58 \times \sqrt{(Unc_{IAEA}^2 + Unc_{Lab}^2)} \quad (3.11)$$

For the evaluation of precision, an estimator 'P' is calculated.

$$P = \sqrt{\left[ \left( \frac{Unc_{IAEA}}{Value_{IAEA}} \right)^2 + \left( \frac{Unc_{Lab}}{Value_{Lab}} \right)^2 \right]} \times 100 \quad (3.12)$$

where Unc. – Measurement uncertainty.

The limit of acceptable Precision (LAP) for each analyte was predefined by the IAEA. Participants' results are scored as 'Acceptable' for precision when  $P \leq LAP$ . Table 3.5 shows the analytical performance evaluation of the IAEA – ALMERA PTs in various matrices. The laboratory results are in good agreement with the target value.

Table 3.5 IAEA Proficiency Test Evaluation results

Matrix	Analyte	Activity (Bq kg <sup>-1</sup> )	
		Target	Measured
Soil (IAEA-1806)	<sup>54</sup> Mn	26.8 ± 0.7	28 ± 0.4
	<sup>60</sup> Co	21.3 ± 0.5	20.5 ± 0.4
	<sup>65</sup> Zn	56.6 ± 1.8	59.5 ± 1.1
	<sup>137</sup> Cs	110.9 ± 2.1	111.2 ± 1.1
Spiked Std. Solution (IAEA-CU-2007-04)	<sup>241</sup> Am	7.11 ± 0.05	6.51 ± 0.2
	<sup>60</sup> Co	7.52 ± 0.06	7.10 ± 0.2
	<sup>134</sup> Cs	7.65 ± 0.1	7.21 ± 0.24
	<sup>137</sup> Cs	8.12 ± 0.06	7.37 ± 0.25
	<sup>54</sup> Mn	4.74 ± 0.02	4.48 ± 0.2
	<sup>210</sup> Pb	29.34 ± 0.5	23.91 ± 2.3
	<sup>65</sup> Zn	13.06 ± 0.15	12.69 ± 0.61
Spinach (IAEA-CU-2007-04)	<sup>137</sup> Cs	1235 ± 35	1415.96 ± 89.5
	<sup>40</sup> K	1188 ± 30	1335.36 ± 104.3
Phosphogypsum [IAEA-434 - (IAEA-CU-2008-04r)]	<sup>210</sup> Pb	680 ± 29	764.7 ± 69.9
	<sup>226</sup> Ra	780 ± 31	773.4 ± 41.2
	<sup>238</sup> U	120 ± 5.5	163.9 ± 36.2
Filter paper (IAEA-CU-2009-02)	<sup>57</sup> Co	1.61 ± 0.06	1.38 ± 0.08
	<sup>134</sup> Cs	0.50 ± 0.02	0.41 ± 0.04
	<sup>137</sup> Cs	0.50 ± 0.02	0.37 ± 0.03
	<sup>152</sup> Eu	1.06 ± 0.04	0.9 ± 0.06
	<sup>241</sup> Am	1.58 ± 0.06	2.09 ± 0.09



---

## Chapter 4 Radioactivity Measurement Results and Discussion

---

### 4.1 Introduction

Natural radioactivity levels in various building materials were carried out using HPGe coupled gamma spectrometer. The samples include raw materials (soil, beneficiated ilmenite, and limestone), conventional building materials (cement, clay brick, natural gypsum, sand) and industrial by products (fly ash, phosphogypsum, fly ash brick, phosphogypsum wall panel). The IAEA protocol [23] on measurement of radionuclides in food and environment has been used for the collection, processing and gamma spectrometric analysis of building material samples.

### 4.2 Natural radioactivity in raw materials

The soil samples were collected by removing top-soil from undisturbed areas at the center of a large, flat open area and away from roads, buildings and big trees. After site selection, an area of 1m x 1m was marked on the flat ground. Vegetation covering the surface was removed using 5 cm depth topsoil cutter. Soil samples were gently removed and put in plastic bags with a coring tool. About 10 cores of such soil sample was removed for making a representative sample. The plastic bag of sample was sealed with stapler and then placed in another bag labeled with sample number, date, location and depth. These samples were brought to the laboratory for processing. The processed sample was filled in plastic container of 6.5cm diameter and 7.5cm height. The containers (volume 250 cm<sup>3</sup>) were filled full, for uniformity and sealed to make it air-tight. This typically amounted to 250-300 g depending on the density of the sample.

For measurement of radioactivity, HPGe high resolution gamma ray spectrometric technique was used, as discussed in detail in the previous chapter.

In order to ascertain the establishment of secular equilibrium between  $^{226}\text{Ra}$  &  $^{228}\text{Th}$  and their respective daughter products, the samples were kept sealed for one month. This is because  $^{220}\text{Rn}$  and  $^{222}\text{Rn}$  in  $^{232}\text{Th}$  and  $^{238}\text{U}$  series respectively, are the gaseous daughter products and they decay to particulate radionuclide with half-life of 3.82 days and 55 seconds respectively. The gaseous daughters would thus be lost and the measurements will have error if the container is not air-tight. Due to this reason, the sample containers are kept sealed so that no  $^{220}\text{Rn}$  and  $^{222}\text{Rn}$  leaks out of it. In secular equilibrium the half-life of the parent is very much longer than the half-life of the daughter and after seven half-lives of daughter, the secular equilibrium is achieved i.e. the activity of daughter becomes equal to that of the parent.

The important secular equilibrium derivation used in natural radioactivity measurement is shown in below [84].

$$A_D = A_P(1 - e^{-\lambda_D t}) \quad 4.1)$$

Where  $t$  = number of days elapsed

$\lambda_D$  = Decay constant of the daughter

$A_D$  = Activity of daughter radionuclide

$A_P$  = Activity of parent radionuclide,

$$A_D = A_P \left(1 - \frac{1}{e^{\frac{\ln 2}{T_D} t}}\right) \quad (4.2)$$

For  $^{222}\text{Rn}$ , after 7 half-lives ( $T_D$ )

$$A_D = A_P \left(1 - \frac{1}{128}\right) \quad (4.3)$$

$$A_D \approx A_P$$

Therefore the activity of the daughter is equal to the activity of the parent. As per the above derivation of secular equilibrium shown in equation 4.2 and 4.3 for estimation of  $^{226}\text{Ra}$  activity through its daughter product  $^{214}\text{Bi}$  the storage time is 28 days (fig 4.1) because, the longest lived daughter product of  $^{226}\text{Ra}$  is  $^{222}\text{Rn}$  ( $T_{1/2} = 3.82$  days), up to  $^{214}\text{Bi}$ . Likewise, for estimation of  $^{228}\text{Th}$  through its daughter product  $^{208}\text{Tl}$ , the longest lived daughter product is  $^{224}\text{Ra}$  ( $T_{1/2} = 3.6$  days). This gives the required period of 28 days to attain secular equilibrium among  $^{238}\text{U}$  and  $^{232}\text{Th}$  series radionuclides. In case of  $^{238}\text{U}$  analysis using gamma spectrometry, one has to use the gamma lines of 63 keV and 92.5 keV of its daughter nuclide  $^{234}\text{Th}$  (half-life, 24.1 days). Here also one has to assume secular equilibrium between them. It will take approximately 150 days to reach secular equilibrium, as shown in fig. 4.1.

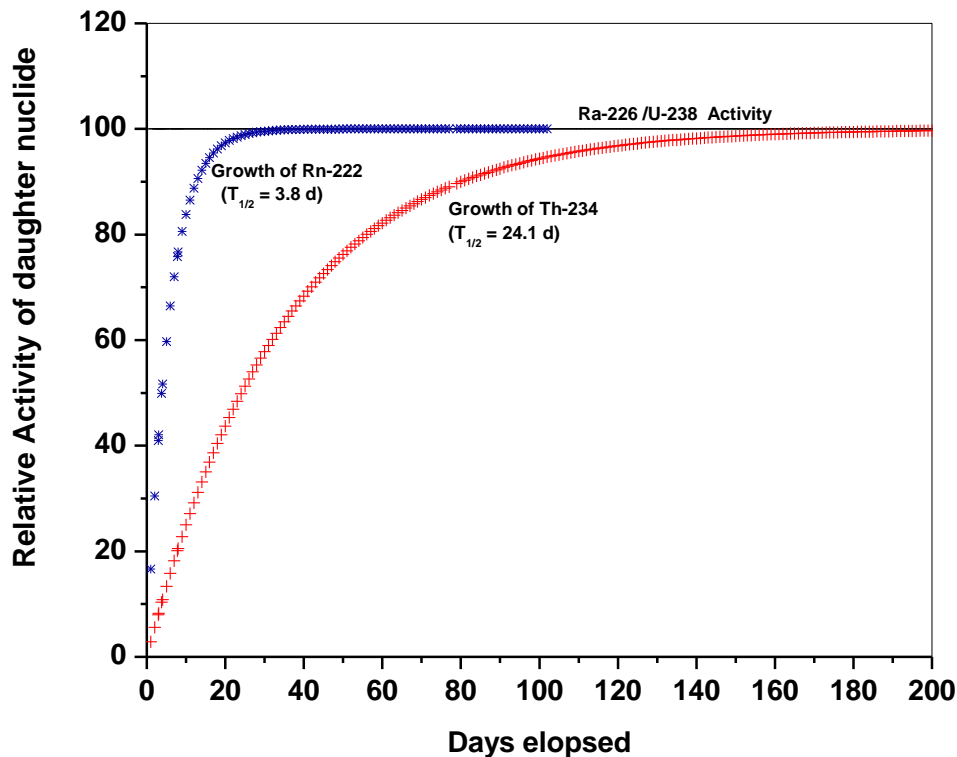


**Figure 4.1 Secular equilibrium:  $^{238}\text{U}$  series**

**i. Natural radioactivity in soil samples – Ferozepur and Faridkot**

This study presents the HPGe Gamma spectrometric measurement of natural radioactivity mainly due to  $^{226}\text{Ra}$ ,  $^{232}\text{Th}$  and  $^{40}\text{K}$  in soil samples collected in Ferozepur and Faridkot district of Punjab, India. The surface soil samples were collected and processed as per the procedure described in IAEA TRS-295 [23]. The sampling locations with latitude, longitude and altitude are shown in fig. 4.1. The environmental air kerma rate also measured in all the sampling locations using the gamma survey meter. The processed samples were filled in the cylindrical plastic containers ( $\text{Ø}7 \text{ cm} \times 6.5 \text{ cm}$ ), sealed completely air tight and kept for about one month so as to ensure secular equilibrium between radium and radon progenies of both uranium and thorium series. The samples

were analysed by using high resolution gamma spectrometry system consists of coaxial p-type High Purity Germanium (HPGe) detector having 50% relative efficiency with respect to 7.62 cm x 7.62 cm NaI (Tl), its energy resolution measured in terms of full width at half maximum (FWHM) is 2.1 keV at 1332.5 keV of  $^{60}\text{Co}$  gamma energy at 25 cm from the top of the detector. Spectrum stabilised 8 K MCA (PHAST, Electronics Division, BARC) along with other electronic accessories were coupled with the HPGe detector. The detector is shielded with 7.5 cm lead to reduce the background contribution of the surrounding.  $^{226}\text{Ra}$  activity varied from 28.6 to 51.1 Bq kg<sup>-1</sup> with the mean of 39.7 Bq kg<sup>-1</sup>. The range and mean activity of  $^{232}\text{Th}$  was 42.9 – 73.2 Bq kg<sup>-1</sup> and 58.2 Bq kg<sup>-1</sup> respectively.  $^{40}\text{K}$  activity was in the range of 470.9 – 754.9 Bq kg<sup>-1</sup> with the mean of 586.4 Bq kg<sup>-1</sup> as shown in table 4.1. Gamma spectrum obtained using HPGe gamma spectrometer is shown in Figure 4.1 for a soil sample of the study area. Radiological hazard indices such as activity index (I) and radium equivalent activity were also estimated.

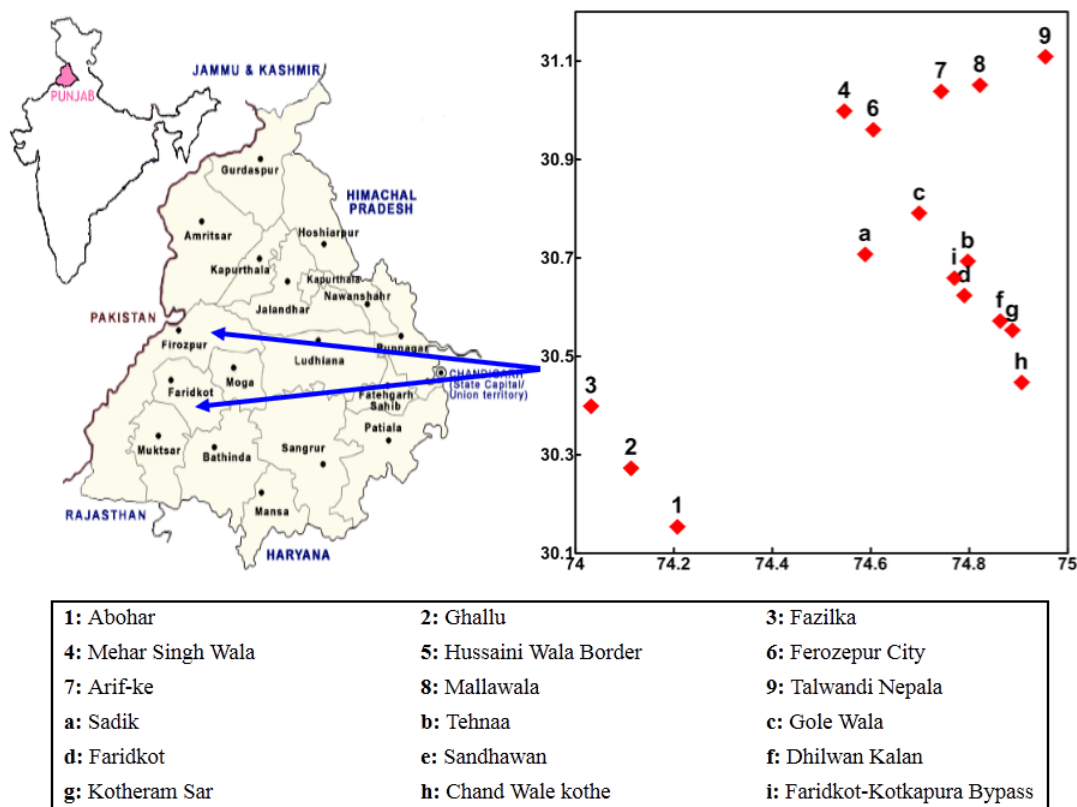
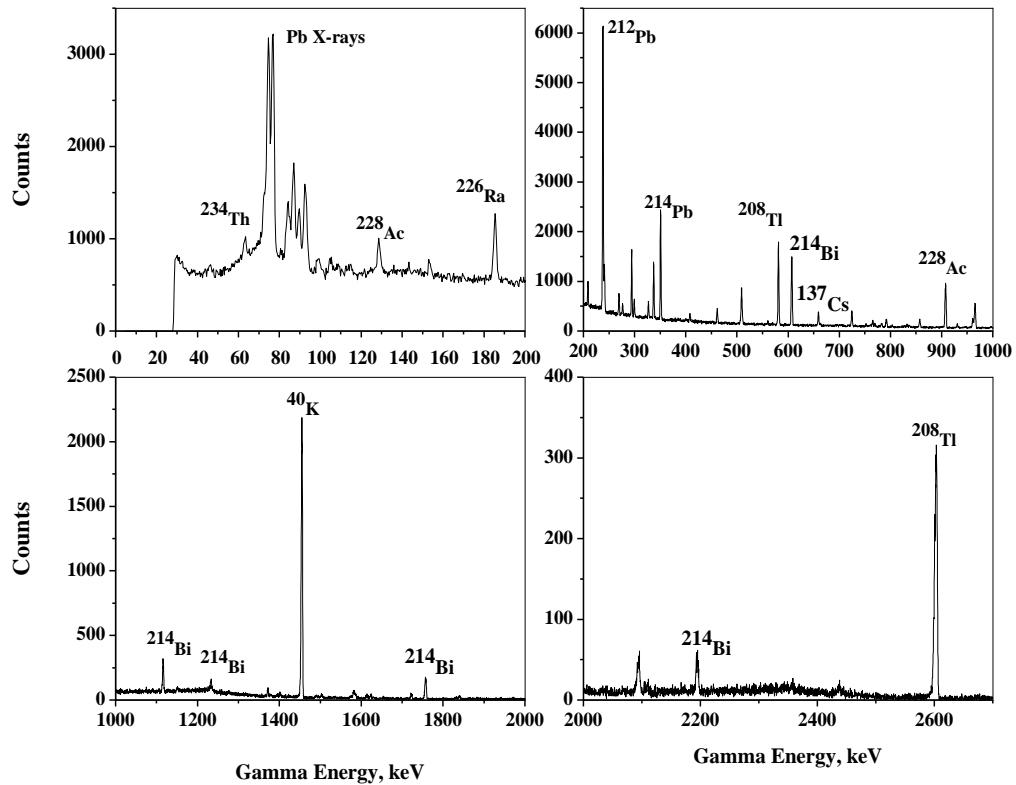


Figure 4.2 Sampling locations of Ferozpur and Faridkot

Table 4.1 Radiological Parameters soil radioactivity – Ferozpur and Faridkot

Parameter	Activity (Bq kg <sup>-1</sup> )			Radium Equivalent Activity, Bqkg <sup>-1</sup>	Activity Index, I	Measured Gamma dose rate, nGy h <sup>-1</sup>
	<sup>226</sup> Ra	<sup>232</sup> Th	<sup>40</sup> K			
Mean	39.46	58.2	595.2	168.7	0.62	110.6
Standard Error	1.4	1.7	17.8	4.8	0.02	1.9
Standard Deviation	5.8	7.2	75.5	20.7	0.07	8.3
Kurtosis	0.6	0.7	-0.2	0.4	0.3	0.1
Skewness	0.1	0.02	0.4	0.3	0.3	-0.67
Range	22.5	30.30	284	77.4	0.3	30.6
Minimum	28.6	42.90	470.90	132.9	0.5	92.1
Maximum	51.1	73.20	754.9	210.4	0.8	122.8
Count (n)	18	18	18	18	18	18



**Figure 4.3 HPGe Gamma spectrum of a soil samples of Punjab**

**ii. Natural radioactivity in soil samples – Chamba and Dharamshala**

**Geology of the area**

Dharamshala is a pilgrim for the Buddhist in the district of Kangra. Kangra district is situated in Western Himalayas, between  $31^{\circ}2$  to  $32^{\circ}5$  N and  $75^{\circ}$  to  $77^{\circ}45$  E. The district has a geographical area of 5,739 km. which constitutes 10.31 % of geographical area of the State. The district has varying altitude ranging from 427 to 6401m above mean sea level, with some plain areas touching Gurdaspur district of Punjab in the West and Una district of Himachal Pradesh in the South. In the East it touches Mandi district, in North with Kullu and Chamba. The district has considerable diversity in its soils, physiography, land use

pattern and cropping system. Chamba is the headquarters of the Chamba district a well-known hill station in India, situated between  $32^{\circ} 11$  to  $33^{\circ} 13$  N and  $75^{\circ}49$  to  $77^{\circ} 33$ E with an estimated area of 6528 square Kilometers. Chamba is bordered by Jammu and Kashmir to the north-west and west, the Ladakh area of Jammu and Kashmir and Lahaul and Bara Banghal to the north-east and east, Kangra to the south-east. Temperature in chamba rages between  $38.0^{\circ}\text{c}$  to  $-1.0^{\circ}\text{c}$ . It has an average elevation of 1,006 meters above sea level.

Forty-two soil samples from Chamba and Dharamshala areas of western Himalaya were analysed for natural and manmade radioactivity contents using high resolution gamma spectrometry. The mean activity concentration at Chamba as shown in table 4.2 for  $^{238}\text{U}$ ,  $^{232}\text{Th}$  and  $^{40}\text{K}$  and  $^{137}\text{Cs}$  was  $32.3 \text{ Bq kg}^{-1}$ ,  $58.4 \text{ Bq kg}^{-1}$ ,  $588.3 \text{ Bq kg}^{-1}$ ,  $10.9 \text{ Bq kg}^{-1}$ . The mean activity concentration at Dharamshala area for  $^{238}\text{U}$ ,  $^{232}\text{Th}$  and  $^{40}\text{K}$  and  $^{137}\text{Cs}$  was  $35.7 \text{ Bq kg}^{-1}$ ,  $61.3 \text{ Bq kg}^{-1}$ ,  $594.9 \text{ Bq kg}^{-1}$ ,  $10.0 \text{ Bq kg}^{-1}$  respectively, as shown in table 4.3. The estimated activity was almost similar to the Indian average value of 29, 64 and  $400 \text{ Bq kg}^{-1}$ , of  $^{238}\text{U}$ ,  $^{232}\text{Th}$  and  $^{40}\text{K}$ , respectively, [85].

**Table 4.2 Descriptive statistics of Natural Radioactivity in Chamba soil samples**

Parameter	Activity (Bq kg <sup>-1</sup> )		
	<sup>226</sup> Ra	<sup>232</sup> Th	<sup>40</sup> K
Mean	38.8	58.4	588.3
Standard Error	2.0	2.1	21.8
Median	37.4	57.3	628.2
Mode	#N/A	52	#N/A
Standard Deviation	9.6	10.1	104.6
Sample Variance	92.4	101.7	10937.7
Range	45.2	47.1	404.9
Minimum	26.9	45.0	399.0
Maximum	72.1	92.1	803.9

**Table 4.3 Descriptive statistics of Natural Radioactivity in Dharamshala soil samples**

Parameter	Activity (Bq kg <sup>-1</sup> )		
	<sup>226</sup> Ra	<sup>232</sup> Th	<sup>40</sup> K
Mean	41.8	61.3	594.9
Standard Error	1.4	2.1	27.2
Median	40.9	62.8	624.9
Mode	39.7	64.3	#N/A
Standard Deviation	6.3	9.0	118.4
Sample Variance	39.5	80.5	14010.7
Range	25.1	44.1	585.5
Minimum	32.8	28.9	226.3
Maximum	57.9	73.0	811.8

**iii. Natural Radioactivity in soil samples of Vizag**

Thirty-three soil samples from Vishakhapatnam, were analysed for natural and manmade radioactivity contents using high resolution gamma spectrometry. Radioactivity concentration of  $^{238}\text{U}$ ,  $^{226}\text{Ra}$ ,  $^{232}\text{Th}$ ,  $^{40}\text{K}$ , and  $^{137}\text{Cs}$  in soil samples ranged from 17.7-62.8, 19.9-65.9, 61-366, 99-1474, and  $\leq 0.2$ -5.1 Bq/kg respectively [86].

**iv. Natural Radioactivity in beach sand minerals**

In India, the beach sand minerals of economic interest from coastal Kerala, Tamil Nadu and Orissa are enriched with NORM due to the occurrence of monazite deposits and heavy minerals such as zircon, ilmenite, magnetite, garnet, rutile etc. Since many of these ores are rich in  $^{232}\text{Th}$  and other radio elements, certification of radioactivity levels has become mandatory in recent years. The average activity concentrations of  $^{226}\text{Ra}$  in zircon, rutile and garnet were  $3795 \pm 28$ ,  $1170 \pm 9$  and  $16.7 \pm 1.6$  Bqkg<sup>-1</sup> respectively. The average activity concentrations of  $^{232}\text{Th}$  observed in zircon, rutile and garnet were  $635 \pm 8$ ,  $45.2 \pm 4.4$  and  $63.6 \pm 2.7$  Bqkg<sup>-1</sup> respectively.  $^{226}\text{Ra}$  concentration in ilmenite ore was found to be ranging from  $17.6 \pm 0.7$  to  $443 \pm 4$  Bqkg<sup>-1</sup>.  $^{232}\text{Th}$  ranged from  $80.4 \pm 1.1$  to  $1971 \pm 6$  Bq kg<sup>-1</sup> and  $^{40}\text{K}$  ranged from  $\leq 5.5$  to  $25.0 \pm 0.5$  Bqkg<sup>-1</sup> [87].

**v. Radiological characterization of synthetic rutile**

Titanium dioxide (TiO<sub>2</sub>) industry is one of non-nuclear industries dealing with NORM. The main uses of TiO<sub>2</sub> are in coatings such as paints (57%), followed by plastics (24%), then high grade papers (10%) and printing inks (3%). There is also a wide range of minor uses in total volume terms many of which are still important and include uses such as pharmaceuticals, foodstuffs, and cosmetics<sup>(1)</sup>. The main raw materials used for the production of this material are rutile (TiO<sub>2</sub>) and ilmenite (FeO·TiO<sub>2</sub>) which are found in

the black monazite sand of coastal Tamil Nadu and Kerala, India. Titanium content in the ilmenite (50 – 60%) is upgraded to about 94% by chemical processes [88]. This beneficiated ilmenite is also known as synthetic rutile. Natural radioactivity due to  $^{238}\text{U}$  (uranium, half-life =  $4.49 \times 10^9$  y) and  $^{232}\text{Th}$  (thorium half-life =  $1.4 \times 10^{10}$  y) series radionuclides and  $^{40}\text{K}$  (potassium, half-life =  $1.28 \times 10^9$  y) are present in synthetic rutile. Samples of synthetic rutile were collected from a production plant in Tamil Nadu, India. The n-type HPGe coupled gamma spectrometry was used for the analysis. The activity concentrations of  $^{226}\text{Ra}$ ,  $^{232}\text{Th}$ , and  $^{40}\text{K}$  were presented in table 4.4. It is observed that  $^{232}\text{Th}$  activity was in the range of 92 – 560 Bq kg<sup>-1</sup> with mean value of 195.6 Bq kg<sup>-1</sup>.  $^{226}\text{Ra}$  activity level was varying between 18.7 – 199.3 Bq kg<sup>-1</sup> with the mean value of 61.4 Bq/kg.  $^{40}\text{K}$  activity was in the range of 7 – 117 Bq kg<sup>-1</sup>. It is observed that  $^{40}\text{K}$  level is very low. This may be attributed to the fact that the source rock for the minerals in beach sand contains very low concentration of potassium [89].

**Table 4.4 Descriptive statistics of Natural Radioactivity in Synthetic Rutile samples.**

Parameter	Activity (Bqkg <sup>-1</sup> )			Activity Index, I
	$^{226}\text{Ra}$	$^{232}\text{Th}$	$^{40}\text{K}$	
Mean	61.4	195.6	18.1	1.2
Standard Error	4.6	10.8	1.7	0.1
Median	44.5	170.6	14.4	1.0
Mode	45.1	130.2	8.0	#N/A
Standard Deviation	39.9	93.2	14.9	0.6
Minimum	18.7	92.3	7.0	0.6
Maximum	199.3	560.0	117.0	3.5
Count (N)	75	75	75	75

### Natural Radioactivity in raw materials for cement

Raw materials for the manufacture of cement such as limestone, soil-clay, gypsum, iron ore, and bauxite samples were analysed for natural radioactivity. The results of the analysis are shown in table 4.5 below.  $^{226}\text{Ra}$  was found to be high in Iron ore, gypsum, and bauxite as compared to coal and limestone.  $^{232}\text{Th}$  activity in bauxite was higher than all other materials. The activity due to  $^{40}\text{K}$  was very close to the normal soil activity.

**Table 4.5 Natural radioactivity in raw materials for cement**

S. No.	Sample name	Activity (Bq/kg)		
		$^{226}\text{Ra}$	$^{232}\text{Th}$	$^{40}\text{K}$
i.	Limestone	$9.3 \pm 0.7$	$4.3 \pm 0.6$	$71.7 \pm 2.0$
ii.	Soil-Clay	$19.3 \pm 0.9$	$26.7 \pm 1.0$	$135.8 \pm 2.5$
iii.	Gypsum	$111.1 \pm 2.2$	$78.0 \pm 1.5$	$150.0 \pm 2.6$
iv.	Iron Ore	$124.8 \pm 2.2$	$37.9 \pm 1.4$	$74.7 \pm 4.7$
v.	Bauxite	$98.5 \pm 2.2$	$96.8 \pm 2.1$	$27.6 \pm 5.6$
vi.	Coal	$64.4 \pm 5.9$	$55.3 \pm 1.9$	$56.9 \pm 6.4$

### 4.3 Natural Radioactivity in conventional building materials

Samples of conventional building materials such as cement, clay brick, marble, rock, concrete samples were analysed for natural radioactivity.

#### i. Natural Radioactivity in commercial cements

Natural radioactivity mainly due to  $^{238}\text{U}$ ,  $^{226}\text{Ra}$ ,  $^{232}\text{Th}$  and  $^{40}\text{K}$  in commercially available cement samples, in India were measured using HPGe gamma spectrometry. Fig. 4. 3 shows the gamma spectrum of a cement sample, which indicates that all the prominent gamma lines of the natural gamma emitters.  $^{238}\text{U}$  activity was found to be varying from 45.3 Bq

kg<sup>-1</sup> to 300.8 Bq kg<sup>-1</sup> with the mean value of 127.1 Bq kg<sup>-1</sup>. <sup>226</sup>Ra activity was varying from 20.3 – 79.3 Bq kg<sup>-1</sup> with the mean of 40.3 Bq kg<sup>-1</sup>. The range and mean activity of <sup>232</sup>Th was found to be 18.8 – 63.5 Bq kg<sup>-1</sup> and 36.8 Bq kg<sup>-1</sup> respectively. <sup>40</sup>K activity was in the range of 160.9 – 307.2 Bq kg<sup>-1</sup> with the mean of 211.1 Bq kg<sup>-1</sup>, as shown in table 4.6. The Radiological parameters such as radium equivalent activity and activity index shows that the indoor external dose due to natural radioactivity in cement used for the construction will not exceed the dose criteria. It was also found out that there is radioactive disequilibrium between <sup>238</sup>U and <sup>226</sup>Ra, which may be attributed to the partitioning of radionuclides during the production process of cement.

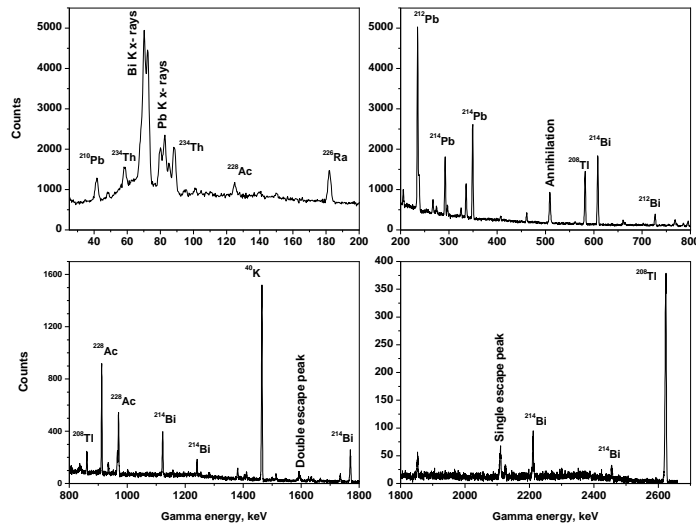


**Figure 4.4 HPGe Gamma spectrum of a Cement sample**

#### 4.6 Activity concentration of Natural radionuclides in cement samples.

Parameter	Activity (Bq kg <sup>-1</sup> )		
	<sup>226</sup> Ra	<sup>232</sup> Th	<sup>40</sup> K
Mean	40.3	36.8	211.1
Standard Error	3.8	3.6	9.4
Median	37.5	35.7	210.1
Mode	#N/A	#N/A	#N/A
Standard Deviation	16.2	15.1	39.9
Sample Variance	264.0	228.2	1595.9
Range	59.0	44.7	146.3
Minimum	20.3	18.8	160.9
Maximum	79.3	63.5	307.2

#### ii. Assessment of Natural Radioactivity Content of the Building Materials in India

Building material samples such as brick, concrete, glazed tiles, lime, black sand, marble etc. were collected in Gujarat, India. The samples were analysed for their natural radioactivity content using the HPGe coupled gamma spectrometric system. <sup>238</sup>U activity was varying from 8.3 Bq/kg in lime to 91.1 Bq/kg in fly ash brick, while the <sup>232</sup>Th content varied from 4 Bq/kg in marble to 115.9 Bq/kg in fly ash bricks. <sup>40</sup>K content varied from 10.1 Bq/kg in marble to 289.2 Bq kg<sup>-1</sup> in fly ash bricks. The activity index (RP-112, EC, 1999) was estimated for all the samples. The study shows that the activity index varies from 0.07 to 1.02. This suggests that the natural radiation exposure from the building materials samples analysed will be well within the acceptable criteria [90].

#### 4.4 Natural Radioactivity in industrial by products, wastes etc.

Building materials made of industrial by products and wastes such as phosphogypsum and fly ash from fertiliser industries and thermal power plants, respectively, were analysed for natural radioactivity.

##### 4.4.1 Phosphogypsum

Phosphate rock (PR) is a general term which refers to rock with high concentration of phosphate minerals, most commonly of the apatite group  $\{Ca_5(PO_4)_3[F, OH \text{ or } Cl]\}$ . It can be of sedimentary, volcanic or biological origin. There are phosphate deposits all over the world, with United States producing most phosphate in the world, while Morocco and China rank second and third, respectively. Active mining also occurs in a number of locations including Russia, Tunisia, Jordan, Brazil, Israel, South Africa, Syria, Togo, and Senegal. Investigators have reported a wide variation in the concentrations of uranium and radium in PR from various parts of the world. For  $^{238}U$  a range of 37–4900 Bq kg<sup>-1</sup> and for  $^{226}Ra$  a range of 100 - 10000 Bq kg<sup>-1</sup> are reported [86].

PR is the starting raw material for phosphate products such as phosphoric acid, phosphate fertilizers and industrial products. Given that the Indian economy is predominantly based on agriculture, fertilizer production plays a pivotal role. Only, about 35 % to 40 % of the raw material requirements for phosphate fertilizer production are currently met through indigenous sources and the rest is met through import. In fertilizer plants, powdered rock is digested with hot sulphuric acid to produce phosphoric acid needed in fertilizer production. During this reaction phosphogypsum (PG) is produced as a by-product. There are approximately five tons of PG produced for every ton of phosphoric acid produced. Current worldwide production of phosphoric acid yields over 100 million tons of PG per

year. The acid is then used for the production of various fertilizers. The by-product PG in India is generally disposed of as land fill in low-lying areas apart from the limited usage in cement industry and soil conditioning. The radium that is found naturally associated with PR becomes associated with the PG after the rock is reacted with sulphuric acid. Depending on radioactivity levels in PG it may be used as a raw material in building products. It has only been in recent years that the question of radioactivity has been raised and this question now influences every decision relative to potential use in building products.

Radiological assessment of PG would be important if it is used as either land-filling or building material. The knowledge will also help in predicting the occupational exposures that may occur during processing of PR and its corresponding by-products. The Atomic Energy Regulatory Board (AERB), India has been examining the radiological safety implications of adding PG in building and construction materials and use in agriculture. In compliance with these draft regulations, representative samples of PR ore drawn from the consignment used for processing in fertilizer plants and its corresponding by-product PG were assessed for concentration of natural radionuclides. The present study was carried to find range of natural radioactivity concentrations in PR and PG samples of various fertilizer industries in India using imported and Indian PR.

Natural radionuclides from the uranium and thorium series were measured, using high-resolution gamma-spectrometry in phosphate rock and phosphogypsum samples from the phosphate fertilizer industry in India. Table 4.7 shows the mean activity concentrations of  $^{238}\text{U}$ ,  $^{226}\text{Ra}$ ,  $^{210}\text{Pb}$ ,  $^{232}\text{Th}$ , and  $^{40}\text{K}$  in phosphate rock were found to range from 53-1490 Bq  $\text{kg}^{-1}$ , 51-1449 Bq  $\text{kg}^{-1}$ , 52-1306 Bq  $\text{kg}^{-1}$ , 7-85 Bq  $\text{kg}^{-1}$  and 18-392 Bq  $\text{kg}^{-1}$ , respectively, while the concentration of  $^{238}\text{U}$ ,  $^{226}\text{Ra}$ ,  $^{210}\text{Pb}$ ,  $^{228}\text{Ra}$ , and  $^{40}\text{K}$  in phosphogypsum samples

ranged from 10-76 Bq kg<sup>-1</sup>, 35-695 Bq kg<sup>-1</sup>, 37-681 Bq kg<sup>-1</sup>, 5-24 Bq kg<sup>-1</sup> and 12-205 Bq kg<sup>-1</sup>, respectively. Fig. 4.5 also showed that the thorium series gamma lines were found to be very low and hence <sup>232</sup>Th activity is low in phosphogypsum samples. Equilibrium was found to be disrupted during the chemical processing of phosphate rock with 83 % of the <sup>226</sup>Ra and only 5 % of <sup>238</sup>U fractionating to phosphogypsum. Activity concentrations of <sup>238</sup>U and <sup>226</sup>Ra in phosphogypsum produced from various fertilizer industries of India showed levels < 1000 Bq kg<sup>-1</sup> and pose no restriction for use in building / construction material [86]. Table 4.8 shows the reported level of natural radioactivity in phosphogypsum in various countries, which indicates that the levels measured in this study also was found to be of the same order.

#### **Phosphogypsum rapid wall panel (PGRWAP)**

It is one of the alternates of conventional building materials to replace brick, sand. Samples of PGRWP were received for the analysis of natural radioactivity. The mean activity level due to <sup>226</sup>Ra, <sup>232</sup>Th and <sup>40</sup>K was 534.3 Bq kg<sup>-1</sup>, 42.9 Bq kg<sup>-1</sup>, 66.3 Bq kg<sup>-1</sup> respectively.

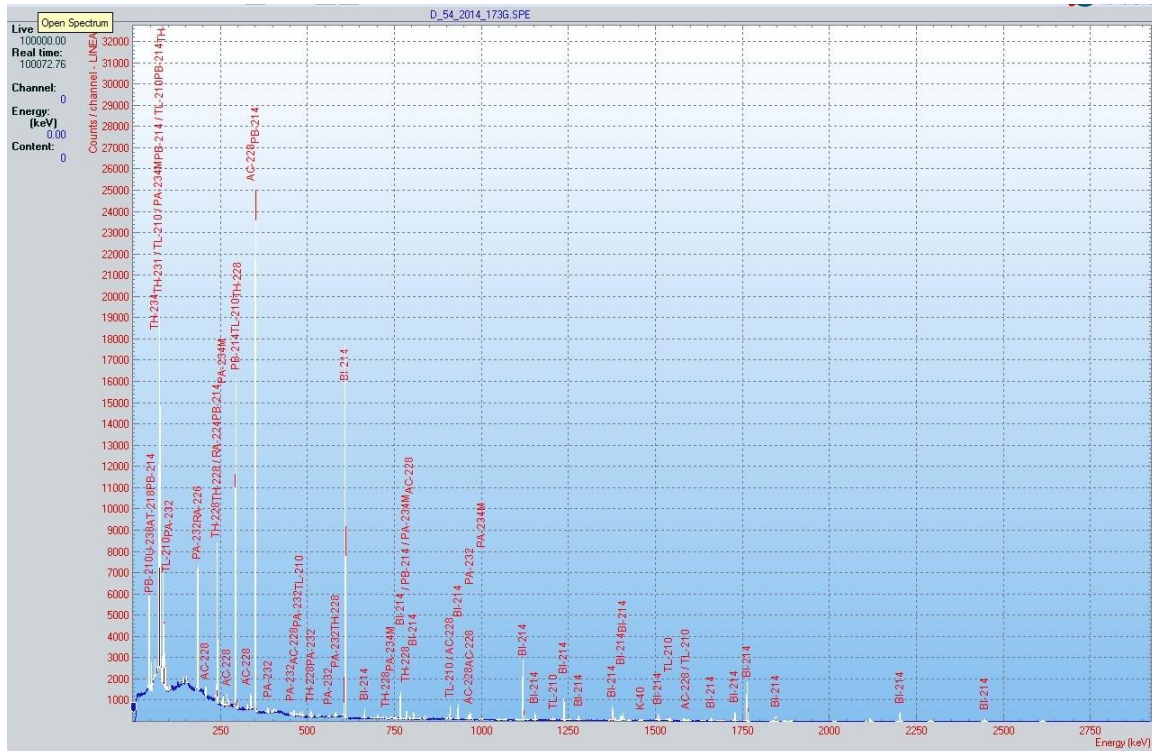


Figure 4.5 HPGe Gamma spectrum of a phosphogypsum sample

**Table 4.7 Radioactivity concentration in phosphate rock (PR) and phosphogypsum (PG) from Indian fertilizer plants**

Industry	No. of samples	Sample Type	Mean activity concentration $\pm$ standard error (Bq kg <sup>-1</sup> )					
			<sup>238</sup> U	<sup>226</sup> Ra	<sup>210</sup> Pb	<sup>228</sup> Ra	<sup>232</sup> Th	<sup>40</sup> K
A (Morocco - RP)	30	PR	1490 $\pm$ 41 (1191-1849)	1449 $\pm$ 40 (1187-1816)	1306 $\pm$ 40 (1121-1785)	19 $\pm$ 1 (7-29)	18 $\pm$ 1 (8-27)	25 $\pm$ 1 (13-45)
		PG	76 $\pm$ 7 (11-124)	695 $\pm$ 11 (419-979)	681 $\pm$ 15 (397-985)	11 $\pm$ 1 (5-20)	-	19 $\pm$ 1 ( $\leq$ 10-41)
B (South Africa - RP)	35	PR	1168 $\pm$ 40 (795-1652)	1179 $\pm$ 16 (823-1633)	1120 $\pm$ 30 (786-1612)	85 $\pm$ 3 (36-123)	86 $\pm$ 3 (32-125)	20 $\pm$ 1 (12-58)
		PG	12 $\pm$ 1 ( $\leq$ 6-23)	636 $\pm$ 7 (421-856)	596 $\pm$ 9 (411-832)	24 $\pm$ 1 (14-36)	-	12 $\pm$ 1 (11-18)
C (Jordan - RP)	20	PR	632 $\pm$ 13 (125-1047)	623 $\pm$ 5 (181-943)	654 $\pm$ 15 (135-1020)	30 $\pm$ 1 (3-113)	30 $\pm$ 1 (2-116)	23 $\pm$ 1 (11-47)
		PG	29 $\pm$ 2 (12-38)	363 $\pm$ 4 (137-847)	341 $\pm$ 10 (112-894)	17 $\pm$ 1 (5-33)	-	18 $\pm$ 1 ( $\leq$ 10-43)
D (Jordan - RP)	15	PR	763 $\pm$ 12 (236-924)	757 $\pm$ 9 (251-986)	719 $\pm$ 25 (243-972)	15 $\pm$ 1 (4-30)	16 $\pm$ 1 (4-33)	18 $\pm$ 1 (14-38)
		PG	13 $\pm$ 1 ( $\leq$ 6-21)	382 $\pm$ 4 (92-624)	390 $\pm$ 12 (105-652)	13 $\pm$ 1 (4-26)	-	12 $\pm$ 1 ( $\leq$ 10-21)
E (Indian origin ore)	15	PR	53 $\pm$ 4 (32-63)	51 $\pm$ 2 (29-67)	52 $\pm$ 2 (31-64)	7 $\pm$ 1 (3-14)	7 $\pm$ 1 (2-15)	46 $\pm$ 3 (21-64)
		PG	10 $\pm$ 1 ( $\leq$ 6-18)	35 $\pm$ 1 (17-43)	37 $\pm$ 2 (20-42)	5 $\pm$ 1 (2-8)	-	21 $\pm$ 2 ( $\leq$ 10-36)
F (Indian origin ore)	10	PR	85 $\pm$ 6 (54-147)	90 $\pm$ 5 (61-151)	95 $\pm$ 5 (59-154)	23 $\pm$ 1 (4-31)	22 $\pm$ 1 (3-30)	392 $\pm$ 5 (324-462)
		PG	11 $\pm$ 1 (7-16)	56 $\pm$ 3 (35-67)	58 $\pm$ 3 (38-72)	9 $\pm$ 1 (5-13)	-	20.5 $\pm$ 6 (178-241)

**Table 4.8 Activity concentration in phosphogypsum from different countries**

Location	Activity concentration (Bq kg <sup>-1</sup> )					References
	<sup>238</sup> U	<sup>226</sup> Ra	<sup>210</sup> Pb	<sup>232</sup> Th	<sup>228</sup> Ra	
USA-Florida	29-330	270-1203	343-11050	-	-	[91]
Brazil	<2-61	24-700	66-1135	19-138	29-273	[92]
South Africa	64-73	45-48	76-132	205-284	-	[93]
Morocco	-	1420	-	4	-	[94]
Egypt	134	411	-	19	-	[95]
Spain	318-650	580-670	600-640	18-34	9.5-11.8	[96]
Australia	10-24	280-350	320-440	4-7	-	[93]

#### 4.4.2 Fly ash

Coal, like most earth materials, contains <sup>238</sup>U, the parent element of the uranium decay series, which supports several radioactive decay products including radon. Coal fly ash is a byproduct of coal burning at electric utility plants. It is called "fly" ash because it is transported from the combustion chamber by exhaust gases. Large quantities of fly ash are expelled from coal-fired thermal power plants and these may contain enhanced levels of radionuclides along with other toxic elements. Increased interest in measuring radionuclides and radon concentration in fly ash, cement and other components of building products is due to the health hazards and environmental pollution.

Fly Ash bricks are made of fly ash, lime, gypsum and sand. These can be extensively used in all building constructional activities similar to that of common burnt clay bricks. The fly ash bricks are comparatively lighter in weight and stronger than common clay bricks. 15

samples of fly ash brick from a manufacturing unit were collected and analysed for natural radioactivity. The results of the analysis is shown in table 4.9. The result indicates that the activity of  $^{226}\text{Ra}$  and  $^{232}\text{Th}$  is little higher than clay brick. Fig. 4.6 shows the HPGe gamma spectrum of a fly ash brick sample.

**Table 4.9 Descriptive Statistics of Natural Radioactivity in Fly ash brick samples**

Parameter	Activity (Bq kg <sup>-1</sup> )		
	$^{226}\text{Ra}$	$^{232}\text{Th}$	$^{40}\text{K}$
Mean	98.8	114.4	364.6
Standard Error	8.8	5.5	21.0
Median	95.8	123.2	355.8
Standard Deviation	31.6	19.9	75.6
Sample Variance	996.4	397.2	5715.4
Range	138.5	69.9	333.8
Minimum	56.9	58.6	156.0
Maximum	195.4	128.5	489.8

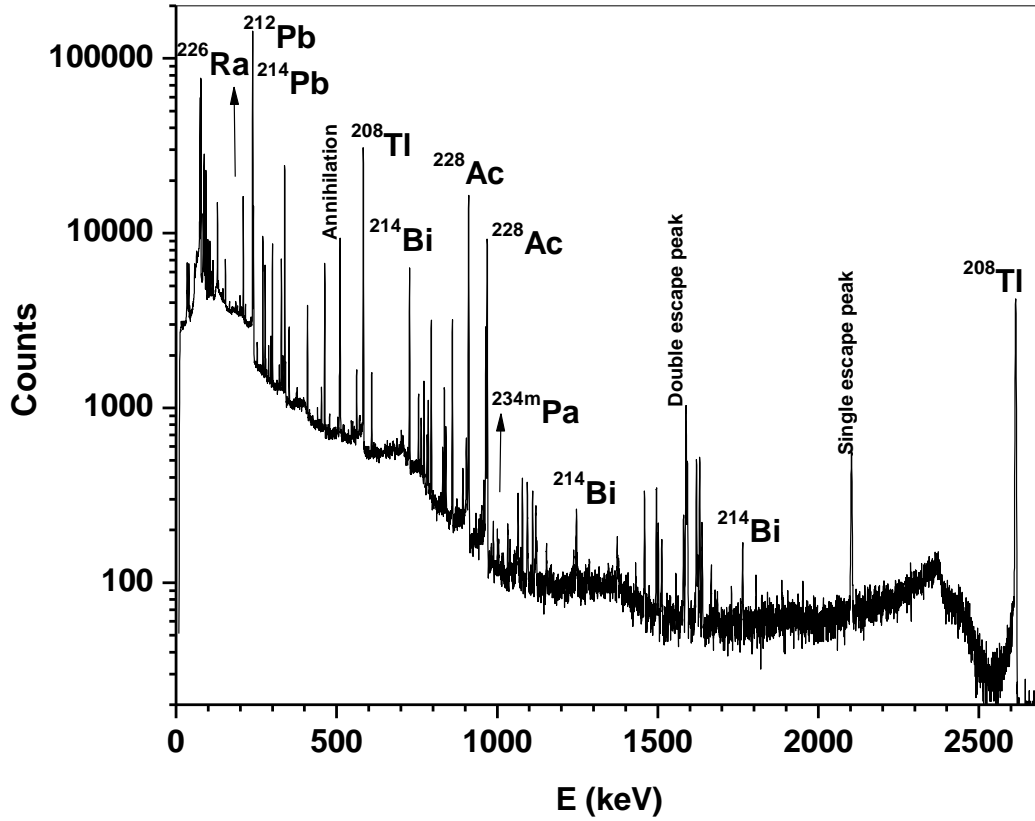


Figure 4.6 HPGe (p-type, 50 %) Gamma Spectrum of a Fly ash brick sample

---

## Chapter 5 Computation of indoor gamma dose using Monte Carlo technique

---

### 5.1 Introduction

Monte Carlo techniques are extensively used in computer calculations of radiation transport in matter. Such methods are employed to determine absorbed dose and dose equivalent distributions from both external and internal radiation sources and in shielding work. Monte Carlo techniques are used to obtain detailed computer simulations of how ionizing radiation is transported through matter. When a charged particle, photon, or neutron traverses an object, it interacts with the constituent atoms and nuclei. It gets scattered or absorbed, deposits energy, and produces secondary particles in the medium. These processes occur statistically in nature. That is, no one can say, for example, exactly how far a given 100 keV neutron will travel in soft tissue before it experiences a collision. However one can predict the distribution of flight distance ( $x$ ) that a large number of 100 keV neutrons would show before having their first collision, such a distribution can be measured directly under conditions of a narrow beam or good geometry and is found to be given by  $e^{-\mu x}$ , where  $\mu$  ( $\text{cm}^{-1}$ ) is known as macroscopic cross section of the interaction. Similarly, if the probability of each of the processes involved in the photon transport is known then by random sampling the motion of a certain particle in the matter can be followed step by step. When the particle is lost by say leakage or absorption, a new particle can be followed. Thus when a sufficiently large number of particles trajectories are obtained in this way, any desired result may be easily obtained [97].

## 5.2 History of Monte Carlo Technique

The Monte Carlo is a numerical method of solving mathematical problems by the simulation of random variables. The generally accepted birth date of the Monte Carlo method is 1949, when an article entitled “The Monte Carlo method” by Metropolis and Ulam appeared. The American mathematicians John von Neumann and Stanislaw Ulam are considered its main originators. As the name “Monte Carlo”, it is derived from that city in the Principality of Monaco famous for its casinos. The point is that one of the simplest mechanical devices for generating random numbers is the roulette wheel. As a universal numerical technique, the Monte Carlo method could only have emerged with the appearance of computers. One advantageous feature of the Monte Carlo method is the simple structure of the computation algorithm. A second feature of the method is that, as a rule, the error calculation is proportional to  $\sqrt{D/N}$ , where D is some constant, and N is the number of trials. Hence it is clear that to decrease the error by a factor of 10, it is necessary to increase N by a factor of 100. It is important to note that the method enables simulation of any process whose development is influenced by random numbers. For many mathematical problems involving no chance, the model enables us to artificially construct a probabilistic model, making possible the solution of the problems [98].

## 5.3 Monte Carlo vs. Deterministic Method

Deterministic transport methods solve a transport equation for the average particle behavior throughout the phase space of the problem. For example, the discrete ordinates method will divide phase space into many small boxes for particles to travel within. As the volumes of the boxes are decreased, these particles will take a differential amount of time to move a differential distance in space. In the limit this approaches the integro-differential transport

equation, which has derivatives in space and time. The Monte Carlo method obtains an answer by simulating individual particles and tallying certain aspects of their behavior such as the number of  ${}^6\text{Li}$  neutron capture reactions,  ${}^6\text{Li} (n, t) {}^4\text{He}$ . The average behavior of particles in a physical system is then inferred from the average behavior of the simulated particles using the central limit theorem. The tallied aspects of the simulated particles' behavior are then the obtained answer. This method transports particles in space and time so it is sometimes said this solves the integral transport equation, which does not have time or space derivatives.

#### 5.4 Random Variable and Random number

A random variable, denoted by  $X(w)$ , is a set function. It attaches a real number  $x$  to an outcome  $w$ . A random variable thus maps the abstract outcomes to the numbers on the real line. It stamps each outcome, so to say, with a real number. We call a sequence of numbers random, if it is generated by a random physical process. Physical processes such as radioactive decay, thermal noise in electronic devices, cosmic radiation arrival times etc., give rise to what we shall call a sequence of truly random numbers. [99]. For the mathematical simulation of any statistical phenomenon, where only the probability of occurrence of certain process is known, random numbers are used. A random number "R" is a number uniformly distributed between 0 and 1 such that probability  $p(R)$  of finding any particular value of  $R$  is independent of the value of  $R$ ; that is

$$p(R) = 1, \quad 0 \leq R \leq 1 \quad (5.1)$$

and probability of selecting a number from a certain gap is equal to the gap width. i.e.

$$p(R) dR = dR \quad (5.2)$$

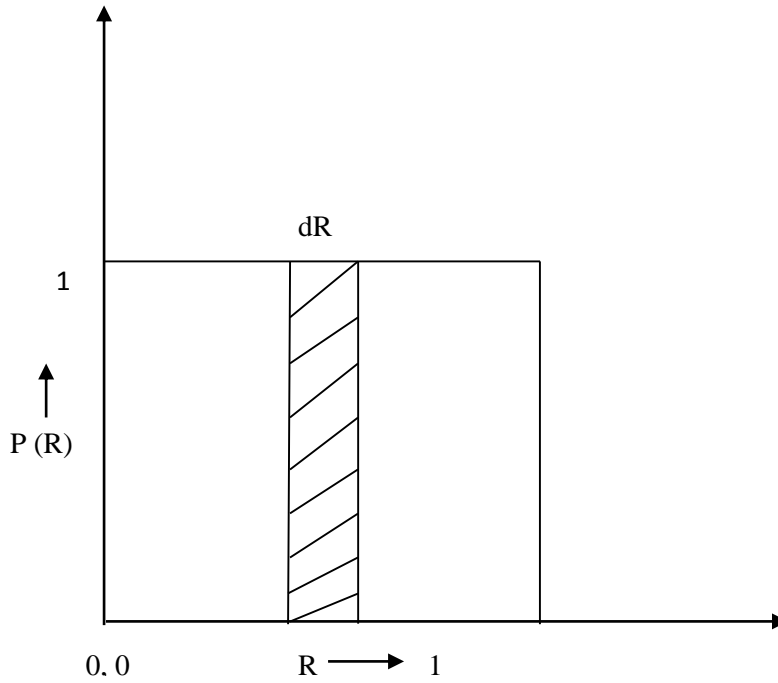
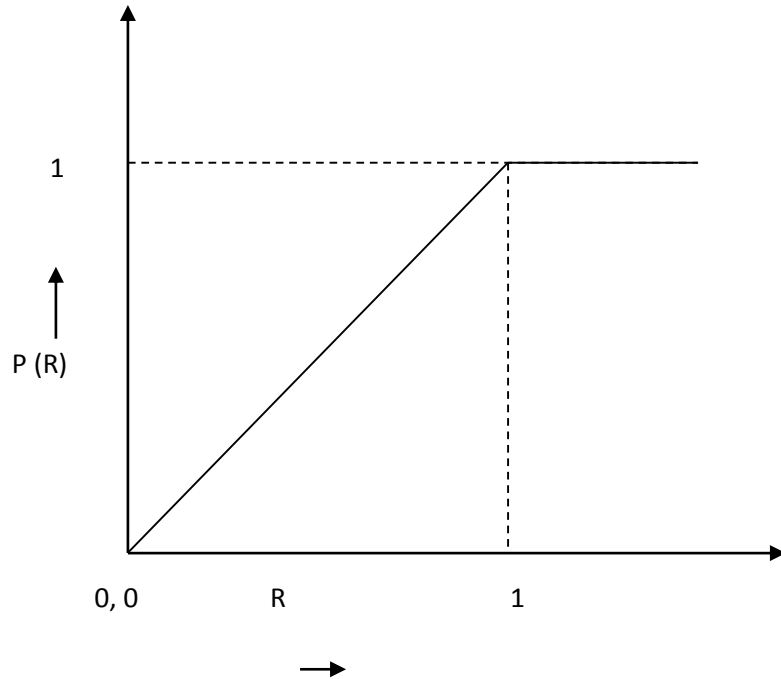


**Figure 5.1 Probability density function of random numbers**

The cumulative distribution function  $p(R)$  is given by

$$p(R) = \int_0^R p(R) dR = R, \text{ with } p(R) = 0, R < 0 \quad (5.3)$$

$$p(R) = R, 0 \leq R \leq 1 \text{ and } p(R) = 1, R > 1 \quad (5.4)$$



→  
**Figure 5.2 Cumulative distribution function**

#### 5.4.1 Discrete Random Variable

A random variable  $X(w)$  is called discrete if it can assume any of a set of discrete values  $x_1, x_2, \dots, x_n$ . [98]

$$X(w) \sim \left( \begin{matrix} x_1, x_2, \dots, x_n \\ p_1, p_2, \dots, p_n \end{matrix} \right) \quad (5.5)$$

Where  $x_1, x_2, \dots, x_n$  are the possible values of  $X(w)$ , and  $p_1, p_2, \dots, p_n$  are the corresponding probabilities. To be precise, the probability that the random variable  $X(w)$  will be equal to  $x_i$ . Equation 5.5 is called the distribution of the random variable  $X(w)$ .

The value of  $x_1, x_2, \dots, x_n$  can be arbitrary. However, the probabilities  $p_1, p_2, \dots, p_n$  must satisfy two conditions:

- i. All  $p_i$  are positive:

$$p_i > 0 \quad (5.6)$$

- ii. The sum of all the  $p_i$  equal to 1:

$$p_1 + p_2 + \dots + p_n = 1 \quad (5.7)$$

Suppose that a homogeneous medium consists of nuclei of three different types A, B, and C and probabilities of collision of a particle say neutron with them are 0.2, 0.3, and 0.5 respectively. It is clear that, if a large number of  $N$  of random numbers are produced then approximately

0.2  $N$  will fall on the interval  $0.0 < R \leq 0.2$

0.3  $N$  will fall on the interval  $0.2 < R \leq 0.5$

0.5  $N$  will fall on the interval  $0.5 < R \leq 1$  [100]

This approximation will improve with the increasing  $N$ . In this way, by the use of random numbers, one can decide which of the three types of nuclei is hit in the event of collision.

Flow diagram in fig 5.2 schematizes the procedure in the above example.

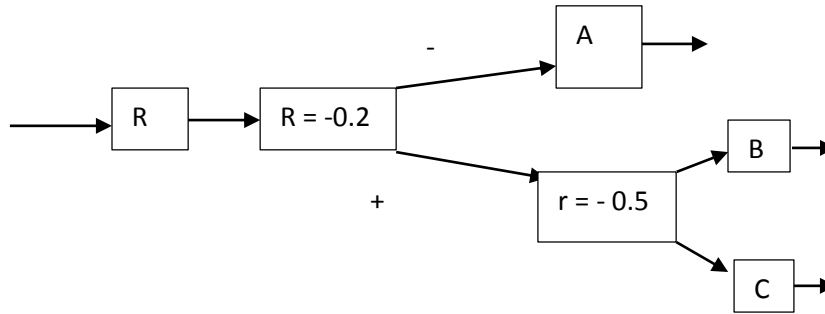


**Figure 5.3. Flow diagram of discrete random events**

### 5.4.2 Continuous Random Variable

A random variable shall be called as continuous, if it can assume any value in a certain interval  $(a, b)$ . A continuous random variable  $X(\omega)$  is defined by specifying an interval containing all its possible values, and a function  $p(x)$  that is called the probability density of the random variable  $X(\omega)$ . Let  $p(x) dx$  is the probability of  $x$  lying between  $x$  and  $x + dx$ , with  $a \leq x \leq b$  and

$$\int_a^b p(x) dx = 1 \quad (5.8)$$

Then  $p(x)$  is called the probability density function and

$$P(x) = \int_a^x p(x) dx \quad (5.9)$$

is called the probability distribution function, which is the cumulative probabilities between  $a$  and  $x$  with

$p(x)$  (at  $x = a$ ) = 0 and

$p(x)$  (at  $x = b$ ) = 1

i.e. the cumulative probabilities varies between 0 and 1 as  $x$  varies between  $a$  and  $b$ .

Therefore it is possible to equate  $p(x)$  to a random number  $R$  and uniquely determine the corresponding value of  $x$ , i.e.

$$R = p(x) = \int_a^x p(x) dx \quad (5.10)$$

Determines the value of  $x$ . Moreover, it can be shown that if  $R$  is uniformly distributed on  $0 \leq R \leq 1$ , then  $x$  falls between  $x$  and  $x + dx$  with frequency  $p(x) dx$ . From equation 5.10 we get  $dR = p(x) dx$  or  $dR/dx = p(x)$ .

Now the number of random numbers selected from interval  $dR$  are proportional to  $dR$ , therefore number of random numbers selected per unit  $x$  are proportional to  $dR/dx$  and hence  $p(x)$ . This shows that the variable is selected with probability  $p(x)$ .

### 5.5 Random Sampling technique

Monte Carlo methods are probabilistic in nature. A proper understanding of them, therefore, requires some acquaintance with probability theory. In all Monte Carlo calculations it is necessary to draw samples from specified probability distributions. Random sampling techniques are used for this purpose. Therefore, the single most important, and most distinctive feature of Monte Carlo technique is the central role of random sampling methods.

### 5.5.1 Inversion technique

This method of sampling from a given distribution is based on the following:

If  $x$  is a continuous random variable with probability density function (pdf)  $f(x)$  is normalized distribution

$$\int f(x) dx = 1 \quad (5.11)$$

Need a relation  $x = \Phi(R)$  connecting  $x$  and  $R$ .

$$f(x) = p(R) dR$$

$$\int_0^x f(x) dx = \int_0^R p(R) dR \quad (5.12)$$

$$F(x) = R$$

$$x = F^{-1}(R) = \Phi(R) \quad (5.13)$$

This method is efficient, if it is easy to find analytically the inverse of cdf of  $x$ .

**e.g. 1:**

$$f(x) = ae^{-ax} \quad 0 \leq x \quad (5.14)$$

$$\int_0^R p(R) dR = \int_0^x ae^{-ax} dx \quad (5.15)$$

$$R = 1 - e^{-ax} \quad (5.16)$$

$$x = -\frac{1}{a} \log R \quad (5.17)$$

This method is used for sampling free flight distance for neutrons / photons.

**e.g.2:**

Sampling angle for isotropic distribution.

For isotropic distribution, number per unit solid angle is constant.

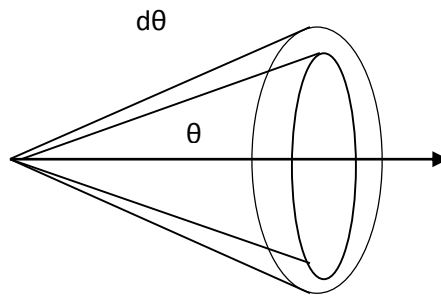


**Figure 5.4 Random sampling - Inversion method for sampling angle from isotropic distribution**

$$p(\Omega) = \frac{d\Omega}{4\pi} \quad (5.18)$$

$$= \frac{2\pi \sin\theta d\theta}{4\pi} \quad (5.19)$$

$$= \frac{1}{2} \sin\theta d\theta = p(\theta)d\theta \quad (5.20)$$

Using

$$\int_0^\theta p(\theta)d\theta = \int_0^R p(R)dR \quad (5.21)$$

$$\int_0^{\theta} \frac{1}{2} \sin \theta \, d\theta = R \quad (5.22)$$

$$\cos \theta = 2R - 1 \Rightarrow \theta = \cos^{-1}(2R - 1) \quad (5.23)$$

Isotropic distribution means  $\cos \theta$  is uniformly distributed between -1 to +1.

### 5.5.2 Rejection technique

One of the most widely used technique for generating samples from a given distribution was first introduced by Von Neumann. The technique is known as rejection method or acceptance sampling method. This method is attractive as rather complicated distributions can be sampled by performing quite simple calculations. It consists of drawing a random sample from an appropriate pdf and subjecting it to a test of some sort to determine, whether or not it will be accepted for use. Despite of this waste, rejection technique often results in simpler formulae, therefore, less average cost per accepted sample, than the inversion method.

$x$  ( $a$ ,  $b$ ) has the pdf  $f(x)$  which is normalized

$$\int_a^b f(x) dx = 1 \quad (5.24)$$

$M$  is the upper bound of  $f(x)$  for  $a \leq x \leq b$ .

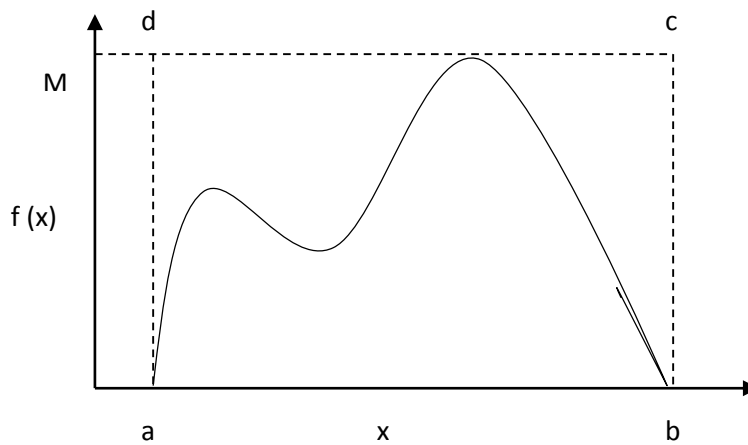


**Figure 5.5 Random sampling using rejection method**

Rejection method used to sample  $x$  involve following steps.

- i) Sample value  $x$  uniformly between  $(a, b)$  using the relation  $x = a + (b-a) R_1$   
 $R_1$  is a random number from  $u(0, 1)$
- ii) Select another random number  $R_2$
- iii) If  $R_2 \leq f(x) / M$  accept the value of  $x$  sampled in (i), else go back to step (i).

Method involves selecting a point  $[a + (b - a) R_1, MR_2]$  uniformly distributed in rectangle  $abcd$ . Step (iii) ensures acceptance of only those points that lie below the pdf curve.

Efficiency ( $E$ ) of the method = Area below pdf curve / area of rectangle  $abcd$

$$E = 1 / M (b - a)$$

To increase  $E$ ,  $M$  should be as low as possible.

Average number  $N$  of pair of random numbers needed per accepted value of  $x$ .

$$N = \sum_{n=1}^{\infty} n (1 - E)^{n-1} E \quad (5.25)$$

$$= -E \frac{d}{dE} \sum_{n=1}^{\infty} (1 - E)^n \quad (5.26)$$

$$= -E \frac{d}{dE} \left[ \frac{1 - E}{1 - (1 - E)} \right] \quad (5.27)$$

$$= \frac{1}{E} \quad (5.28)$$

### 5.6 Monte Carlo N-Particle Transport Code System (MCNP)

Among others, the MCNP code was used for the modeling of indoor dose. The MCNP Code (version 3.1) [101], developed and maintained by Los Alamos National Laboratory, is the internationally recognized code for analyzing the transport of neutrons and photons. The code deals with transport of neutrons, gamma rays, and coupled transport, i.e., transport of secondary gamma rays resulting from neutron interactions.

MCNP is a general-purpose, continuous-energy, generalized-geometry, time-dependent, coupled neutron/photon/electron Monte Carlo transport code. It can be used in several transport modes: neutron only, photon only, electron only, combined neutron/photon transport where the photons are produced by neutron interactions, neutron/photon/electron, photon/electron, or electron/photon. The neutron energy regime is from  $10^{-11}$  MeV to 20 MeV, and the photon and electron energy regimes are from 1 keV to 1000 MeV. The capability to calculate  $k_{\text{eff}}$  eigenvalues for fissile systems is also a standard feature. The

user creates an input file that is subsequently read by MCNP. The input file should contain information about the problem in areas such as:

- the geometry specification,
- the description of materials and selection of cross-section evaluations,
- the location and characteristics of the neutron, photon, or electron source,
- the type of answers or tallies desired, and
- any variance reduction techniques used to improve efficiency.

### **5.7 Estimation of Monte Carlo errors**

In Monte Carlo simulation studies, the tallies such as particle Fluence and energy Fluence are normalized to be per starting particles. For a well-behaved tally,  $R$  will be proportional to  $1/(\sqrt{N})$ , where  $N$  is the number of histories. For poorly behaved tally,  $R$  may increase as the number of histories increases. The  $\sigma$  is used to define the confidence intervals about the estimated mean allowing one to make statement about what true result is. As per Central Limit Theory as  $N$  approaches to infinity there is a 68% of chance that the true result lies in the range  $x(1 \pm \sigma)$  and a 95% chance of range  $x(1 \pm 2\sigma)$ . The confident intervals statements refer only to the precision of the Monte Carlo calculations itself and not to the accuracy of the results compared to the physical value.

For all tallies except the point detector tally, the  $\sigma$  should be less than 0.10 to produce reliable confidence intervals and for point detector tallies it should be less than 0.05. If an important but unlikely particle path, in phase space has not been sampled in a problem, the Monte Carlo results will not correct expected values and hence stated confidence interval

may not be correct. While the setting problem, it is must that one should not exclude any regions of phase space and should sample all regions of the problem adequately. Despite one's best effort, an important path may not be sampled often enough, causing confidence intervals statement to be in correct. To inform the user about this behavior, MCNP calculates a Figure Of Merit (FOM) for one tally bin of each tally as a function of the number of histories and print its values in Tally Fluctuation Chart (TFC). The FOM is defined as

$$FOM = \frac{1}{\sigma^2 T} \quad (5.29)$$

Where, T is the computer time required to complete the simulation.

The more efficient a Monte Carlo calculation is the larger the FOM value. For a well-behaved tally, the FOM value should be fairly constant. A sharp decrease in the FOM indicates that a seldom-sampled particle path has significantly affected the tally and the relative error estimate.

The estimated relative error  $r$  is inversely proportional to  $\sqrt{N}$ , where  $N$  is the number of particles in the histories. For a MCNP run, the computer time  $T$  consumed is proportional to  $N$ . Thus

$$r = \frac{C}{\sqrt{N}} \quad (5.30)$$

Where,  $C$  is a positive constant.

The  $r$  can be reduced in two ways. One is by increasing computer consumption and another is by decreasing the  $C$  value. The constant  $C$  value depends on the tally choice and or sampling choices. The first approach is limited due to the limitation in the computation

speed of the present computers. For second one, to decrease the C value, MCNP has special variance reduction technique. In the case of tally choice, the Fluence in a cell is estimated either by collision estimate or by track time estimate. The collision is obtained by tally  $1/\Sigma t$  where  $\Sigma t$  macroscopic total cross section at each collision in the cell and the track length estimate is obtained by tallying the distance, the particle moves inside the cell. As  $\Sigma t$  gets very smaller, very few particles have the collision but give enormous tallies when they do, a high variance situation. In contrast, the track length estimates gets a tally from every particle that enters the cell. For this reason MCNP has track length tallies as standard tallies, whereas collision tallies are standard.

### **5.8 Validation of MCNP for indoor dose computation**

Use of MCNP for calculating the specific air kerma rate ( $\text{nGy h}^{-1}$  per  $\text{Bq kg}^{-1}$ ) was verified by modeling the standard room model adopted in Europe and studied by many authors. This room has the dimension of  $5 \text{ m} \times 4 \text{ m} \times 2.8 \text{ m}$  with all the structures are made up of concrete of thickness 20 cm and density  $2.35 \text{ g cm}^{-3}$ . Table 5.1 shows the room model parameters used for computation of specific air kerma rate and the obtained result. It was found out that the calculated result is in good agreement with the reported values; hence MCNP is one of the user friendly codes for solving this kind of problems. Therefore MCNP code was used to model the India specific standard room models, which includes a typical living and a bed room.

**Table 5.1 Parameters used for calculation and the obtained specific air kerma rate - (Concrete structures)**

<b>Dimension of the room</b>	<b>4 m x 5 m x 2.8 m</b>		
Thickness and Density of the structures	Walls, Floor and Ceiling made up of Concrete Thickness = 20 cm density = 2.35 (2.35 g cm <sup>-3</sup> )		
Concrete structures	<b>Specific Air Kerma Rate(nGyh<sup>-1</sup>/Bqkg<sup>-1</sup>)</b>		
	<sup>226</sup> Ra	<sup>232</sup> Th	<sup>40</sup> K
This Work	<b>0.82</b>	<b>1.07</b>	<b>0.083</b>
RP-112 [46]	<b>0.92</b>	<b>1.1</b>	<b>0.08</b>

### 5.9 Indoor dose computation of Indian room models

MCNP code was used to compute the indoor gamma dose in typical room models of India. The geometry of the living room is 4.8 m x 3 m x 3m whereas the bed room is 3m x 3m x 3m. The walls are made of clay bricks, fly ash bricks, and phosphogypsum wall panels. Floor is made up of vitrified tiles. Brick walls are covered with cement plaster. Fig. 5.6 shows the room model adopted in this work. In the Monte Carlo calculation, photons from <sup>238</sup>U, and <sup>232</sup>Th decay series and <sup>40</sup>K gamma emissions were considered shown in Table 3.4 Prominent Gamma energies (keV) and emission probabilities. Both of the radioactive series are assumed to be in secular radioactive equilibrium. The details of photon source term used in the calculation are shown in tables. In the calculation, photons are assumed to be uniformly distributed in the room compartments such as walls, floor, tiles, and ceiling. The room was filled with dry air having density  $1.205 \times 10^{-3}$  g cm<sup>-3</sup>. Photon Fluence spectrum was initially scored which was subsequently converted to air kerma using the mass-energy absorption coefficient of air [102] and [103]. Up to 10<sup>7</sup> photon histories were



gravities are considered, viz.  $1.6 \text{ g cm}^{-3}$  and  $1.87 \text{ g cm}^{-3}$ . The details of the chemical composition of the clay brick used in the computation is shown in table 5.2. Cement plaster is a mixture of sand and cement in one is to four ratio, having the chemical composition as shown in table 5. 3. Concrete is used in floor and ceiling has the chemical composition as shown in table 5.4. The floor of the room is made up of vitrified tiles having the chemical composition as shown in table 5.5. Chemical composition of Indoor air assumed in the modelling is shown in table 5.6. Specific air kerma rate ( $\text{nGy h}^{-1}$  per  $\text{Bq kg}^{-1}$ ) was computed at the center of the room as well as at 1 m height from the floor as shown in table 5.7. Contribution of individual building materials on the Specific air kerma rate ( $\text{nGy h}^{-1}$  per  $\text{Bq kg}^{-1}$ ) at 1 m height due to  $^{226}\text{Ra}$ ,  $^{232}\text{Th}$ , and  $^{40}\text{K}$  is shown in fig. 5.7. About 50 % dose contributed by the brick in the wall, and 36 % is from cement plasters in the wall and ceiling. The contribution of floor tile and concrete (in both ceiling and floor) was found to be 10 % and 2.5 % respectively, as shown in fig 5.8 pie chart. It was found out that the specific air kerma rate at the center was higher than at 1 m from floor by about 5 %.

**Table 5.2 Chemical composition of clay brick**  
[104]

S. No.	Element	Fraction of Composition
1.	H	0.0024
2.	O	0.4535
3.	Al	0.0788
4.	Ca	0.0475
5.	Mn	0.0017
6.	Fe	0.1796

**Table 5.3 Chemical composition of mortar [105] and [106]**

<b>S. No.</b>	<b>Element</b>	<b>Fraction of Composition</b>
1	Si	0.3405
3	Al	0.0174
4	Fe	0.00435
5	O	0.4894

**Table 5.4 Chemical composition of ordinary concrete [107]**

<b>S. No.</b>	<b>Element</b>	<b>Fraction of Composition</b>
1	H	0.0100
2	C	0.0010
3	O	0.5291
4	Na	0.0160
5	Mg	0.0338
6	Si	0.3370
7	K	0.0130
8	Ca	0.0440
9	Mg	0.0140

**Table 5.5 Chemical composition of Floor tiles [108]**

<b>S. No.</b>	<b>Element</b>	<b>Fraction of Composition</b>
1	O	0.4800
2	Si	0.3600
3	Al	0.0830
4	Fe	0.0043
5	Ca	0.0067
6	Mg	0.0073
7	Na	0.0212

**Table 5.6 Chemical composition of dry air**  
[107]

S. No.	Element	Fraction of Composition
1	C	0.0001
2	N	0.7552
3	O	0.2317
4	Ar	0.0128

**Table 5.7 Parameters used for calculation and the obtained specific air kerma rate - (Clay brick Walls ( $\rho = 1.6 \text{ g cm}^{-3}$ ) – bed room)**

Parameters	Dimension					
Dimension of the model room	3 m $\times$ 3 m $\times$ 3m					
Thickness and density of the structures	Clay Brick walls: 23 cm, 1.6 g cm <sup>-3</sup>					
	Plaster (Cement + Sand): 3 cm, 1.6 g cm <sup>-3</sup>					
	Concrete Floor and Ceiling: 15 cm, 2.35 g cm <sup>-3</sup>					
	Floor Vitrified tile: 0.85 cm, 1.9 g cm <sup>-3</sup>					
	<b>Specific Air Kerma Rate nGy h<sup>-1</sup> per Bq kg<sup>-1</sup></b>					
Structure in the building causing irradiation	<sup>226</sup> Ra		<sup>232</sup> Th		<sup>40</sup> K	
	Center	1 m	Center	1 m	Center	1 m
Brick walls	0.3229	0.3061	0.4211	0.4033	0.0334	0.0320
Plasters	0.0755	0.0743	0.0973	0.0922	0.0072	0.0070
Concrete floor and ceiling	0.2131	0.2294	0.2820	0.3052	0.0222	0.0240
Floor tiles	0.0212	0.0332	0.0271	0.0424	0.0020	0.0031
<b>Total</b>	0.6327	0.6431	0.8275	0.8432	0.0647	0.0662

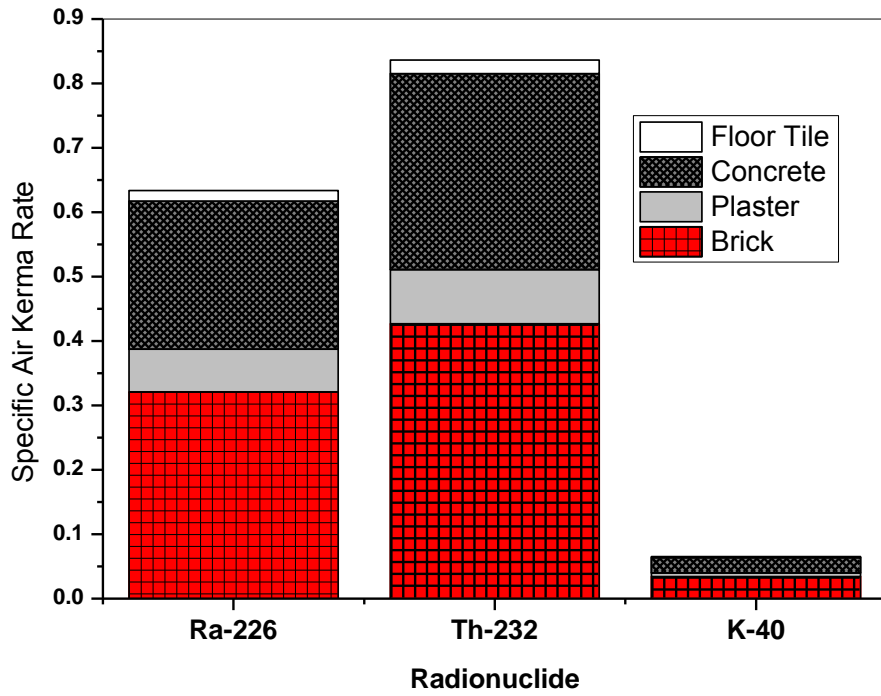


**Figure 5.7 Contribution of individual building materials on the total specific air kerma rate**

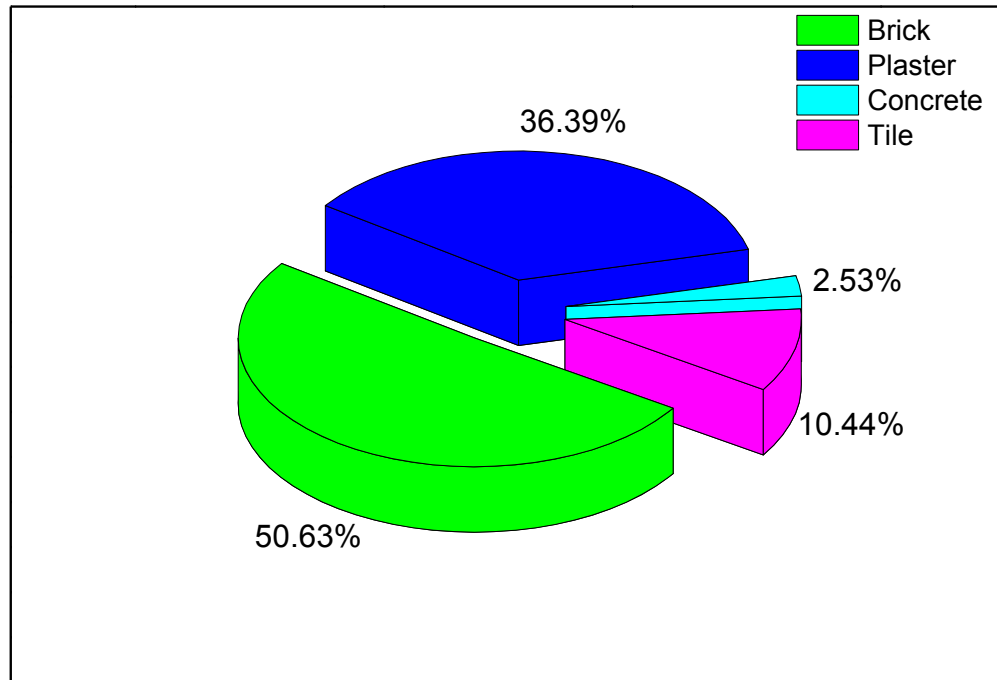


**Figure 5.8 Pie chart of individual building materials contribution to the total air kerma rate**

Sensitivity analysis was carried out to understand the effect of different room models and building material combinations on the indoor gamma dose rate.

Firstly the density of the clay brick was changed to  $1.87 \text{ gcm}^{-3}$  from  $1.6 \text{ gcm}^{-3}$  and carried out the computation. It was observed that there is no significant variation in the specific air kerma rate as can be seen in the table 5.8. The contribution of clay brick only has increased slightly, as shown in fig. 5.9. There is a reduction in the contribution from wall plasters and floor tiles, which may be attributed to the fractional attenuation in the outer plaster's air kerma rate by the brick wall with increased density. As far as concrete in the floor and ceiling are concerned there is no much impact due to the brick wall as can be seen the fig. 5.9.

Effect of clay brick wall thickness on the air kerma rate in the room was also studied by varying it to 30 cm, and 40 cm. Table 5.8 and 5.9 show the observed specific air kerma rates due to the building materials with clay brick walls of thickness 30 cm and 40 cm respectively. It was found out that there is increase in the air kerma rate due to the brick wall with respect to the increase in its thickness. The attenuation of dose rate from the concrete, plasters and floor tile has resulted in the reduction of air kerma rate in the room due to the increased wall thickness, as shown in fig. 5.10.

**Table 5.8 Parameters used for calculation and the obtained specific air kerma rate - (Clay brick Walls ( $\rho = 1.87 \text{ g cm}^{-3}$ ) – bed room)**

Parameters	Dimension					
Dimension of the model room	3 m × 3 m × 3m					
Thickness and density of the structures	Clay Brick walls: 23 cm, 1.87 g cm <sup>-3</sup> Plaster (Cement + Sand): 3 cm, 1.6 g cm <sup>-3</sup> Concrete Floor and Ceiling: 15 cm, 2.35 g cm <sup>-3</sup> Floor Vitrified tile: 0.85 cm, 1.9 g cm <sup>-3</sup>					
Structure in the building causing irradiation	<b>Specific dose rate nGy h<sup>-1</sup> per Bq kg<sup>-1</sup></b>					
	<b><sup>226</sup>Ra</b>		<b><sup>232</sup>Th</b>		<b><sup>40</sup>K</b>	
	<b>Center</b>	<b>1 m</b>	<b>Center</b>	<b>1 m</b>	<b>Center</b>	<b>1 m</b>
Brick walls	0.3400	0.3210	0.4450	0.4270	0.0360	0.0340
Plasters	0.0693	0.0663	0.0890	0.0843	0.0066	0.0058
Concrete floor and ceiling	0.2120	0.2300	0.2810	0.3040	0.0221	0.0239
Floor tiles	0.0106	0.0165	0.0135	0.0211	0.0010	0.0015
<b>Total</b>	0.6319	0.6338	0.8285	0.8364	0.0657	0.0652

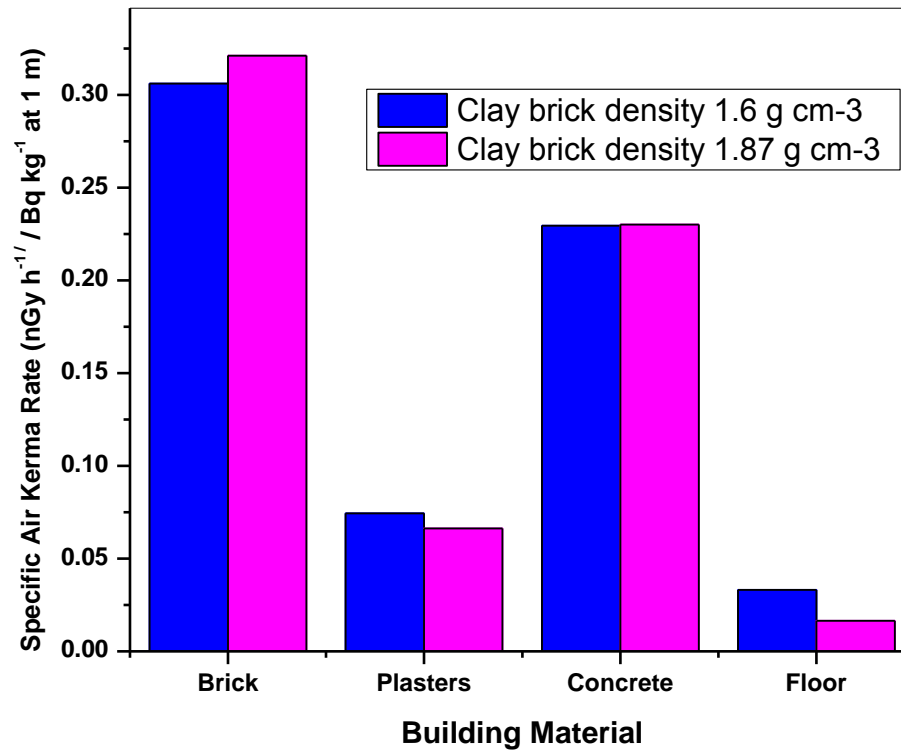


Figure 5.9 Effect of clay brick density on the specific air kerma rate

**Table 5.9 Indoor Gamma dose computation using Monte Carlo Method \_  
Clay Brick (3m x 3m x 3m, 1.87 g cm<sup>-3</sup>, 30 cm wall thickness)**

Parameters	Dimension					
Dimension of the model room	<b>3 m × 3 m × 3m</b>					
Thickness and density of the structures	Clay Brick walls 30 cm, 1.87 g cm <sup>-3</sup>					
	Plaster (Cement + Sand): 3 cm, 1.6 g cm <sup>-3</sup>					
	Concrete Floor and Ceiling: 15 cm, 2.35 g cm <sup>-3</sup>					
	Floor Vitrified tile: 0.85 cm, 1.9 g cm <sup>-3</sup>					
	<b>Specific dose rate nGy h<sup>-1</sup> per Bq kg<sup>-1</sup></b>					
Structure in the building causing irradiation	<b><sup>226</sup>Ra</b>		<b><sup>232</sup>Th</b>		<b><sup>40</sup>K</b>	
	<b>Center</b>	<b>1 m</b>	<b>Center</b>	<b>1 m</b>	<b>Center</b>	<b>1 m</b>
Brick walls	0.3480	0.3330	0.4660	0.4480	0.0367	0.0352
Plasters	0.0640	0.0614	0.0821	0.0778	0.0060	0.0059
Concrete floor and ceiling	0.1960	0.2120	0.2610	0.2820	0.0205	0.0222
Floor Tiles	0.0098	0.0150	0.0120	0.0196	0.0009	0.0014
<b>Total</b>	0.6178	0.6214	0.8211	0.8274	0.0641	0.0647

**Table 5.10 Indoor Gamma dose computation using Monte Carlo Method \_  
Clay Brick (3m x 3m x 3m, 1.87 g cm<sup>-3</sup>, 40 cm wall thickness)**

Parameters	Dimension					
Dimension of the model room	3 m × 3 m × 3m					
Thickness and density of the structures	Clay Brick walls 40 cm, 1.87 g cm <sup>-3</sup>					
	Plaster (Cement + Sand): 3 cm, 1.6 g cm <sup>-3</sup>					
	Concrete Floor and Ceiling: 15 cm, 2.35 g cm <sup>-3</sup>					
	Floor Vitrified tile: 0.85 cm, 1.9 g cm <sup>-3</sup>					
	<b>Specific dose rate nGy h<sup>-1</sup> per Bq kg<sup>-1</sup></b>					
Structure in the building causing irradiation	<sup>226</sup> Ra		<sup>232</sup> Th		<sup>40</sup> K	
	<b>Center</b>	<b>1 m</b>	<b>Center</b>	<b>1 m</b>	<b>Center</b>	<b>1 m</b>
Brick walls	0.3510	0.3360	0.4720	0.4520	0.0375	0.0360
Plasters	0.0611	0.0541	0.0755	0.0719	0.0055	0.0058
Concrete floor and ceiling	0.1780	0.1930	0.2350	0.2540	0.0185	0.0201
Floor Tiles	0.0088	0.0138	0.0114	0.0177	0.0008	0.0013
<b>Total</b>	0.5989	0.5969	0.7939	0.7956	0.0623	0.0632

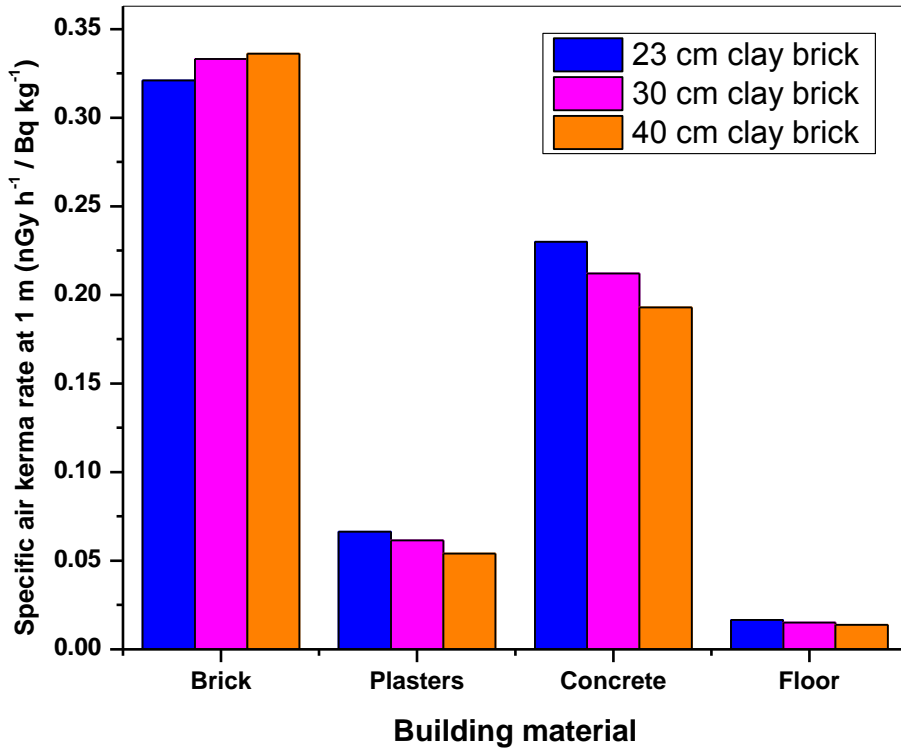


**Figure 5.10 Effect of brick wall thickness on the specific air kerma rate**

Specific air kerma rate in the typical Indian living room models with dimensions 4.8 m x 3 m x 3 m and 6 m x 3 m x 3 m were computed. All other building materials combinations were the same as above i.e. wall made up of clay brick (density = 1.87 g cm<sup>-3</sup>, thickness = 23 cm), cement plaster (density = 1.6 g cm<sup>-3</sup>, thickness = 3 cm), vitrified tile floor (density = 1.9 g cm<sup>-3</sup>, 0.85 cm) and concrete in the floor and ceiling (density = 2.35 g cm<sup>-3</sup>, 15 cm). Tables 5.10 and table 5.11 show the computed air kerma rate for the room models 4.8 m x 3 m x 3 m and 6 m x 3 m x 3 m respectively. Comparison of air kerma rate in 3 m x 3 m x 3 m bed room model, 4.8 m x 3 m x 3 m and 6 m x 3 m x 6 m living room models showed

that there is a fractional increase in air kerma rate with increased room dimension, as shown in fig. 5.11.

**Table 5.11 Parameters used for calculation and the obtained specific air kerma rate - (Clay brick Walls – Living Room)**

Parameters	Dimension					
Dimension of the model room	<b>4.8 m × 3 m × 3m</b>					
Thickness and density of the structures	Clay Brick walls: 23 cm, 1.87 g cm <sup>-3</sup>					
	Plaster (Cement + Sand): 3 cm, 1.6 g cm <sup>-3</sup>					
	Concrete Floor and Ceiling: 15 cm, 2.35 g cm <sup>-3</sup>					
	Floor Vitrified tile: 0.85 cm, 1.9 g cm <sup>-3</sup>					
	<b>Specific Air Kerma Rate nGy h<sup>-1</sup> per Bq kg<sup>-1</sup></b>					
Structure in the building causing irradiation	<sup>226</sup> Ra		<sup>232</sup> Th		<sup>40</sup> K	
	Center	1 m	Center	1 m	Center	1 m
Brick walls	0.3190	0.3070	0.4220	0.4060	0.0336	0.0322
Plasters	0.0710	0.0672	0.0913	0.0859	0.0068	0.0080
Concrete floor and ceiling	0.2550	0.2690	0.3400	0.3580	0.0267	0.0282
Floor tiles	0.0134	0.0198	0.0172	0.0254	0.0012	0.0019
<b>Total</b>	0.6584	0.6630	0.8705	0.8753	0.0683	0.0702

**Table 5.12 Indoor Gamma dose computation using Monte Carlo Method \_  
Clay Brick (6m x 3m x 3m, 1.87 g cm<sup>-3</sup>)**

Parameters	Dimension					
Dimension of the model room	6 m × 3 m × 3m					
Thickness and density of the structures	Clay Brick 23 cm, 1.87 g cm <sup>-3</sup>					
	Plaster (Cement + Sand): 3 cm, 1.6 g cm <sup>-3</sup>					
	Concrete Floor and Ceiling: 15 cm, 2.35 g cm <sup>-3</sup>					
	Floor Vitrified tile: 0.85 cm, 1.9 g cm <sup>-3</sup>					
	<b>Specific dose rate nGy h<sup>-1</sup> per Bq kg<sup>-1</sup></b>					
Structure in the building causing irradiation	<sup>226</sup> Ra		<sup>232</sup> Th		<sup>40</sup> K	
	<b>Center</b>	<b>1 m</b>	<b>Center</b>	<b>1 m</b>	<b>Center</b>	<b>1 m</b>
Brick walls	0.3050	0.2930	0.4010	0.3890	0.0319	0.0306
Plasters	0.0717	0.0675	0.0924	0.0870	0.0068	0.0093
Concrete floor and ceiling	0.2690	0.2820	0.3580	0.3760	0.0283	0.0297
Floor Tiles	0.0146	0.0211	0.0187	0.0269	0.0014	0.0020
<b>Total</b>	0.6603	0.6636	0.8701	0.8789	0.0684	0.0716

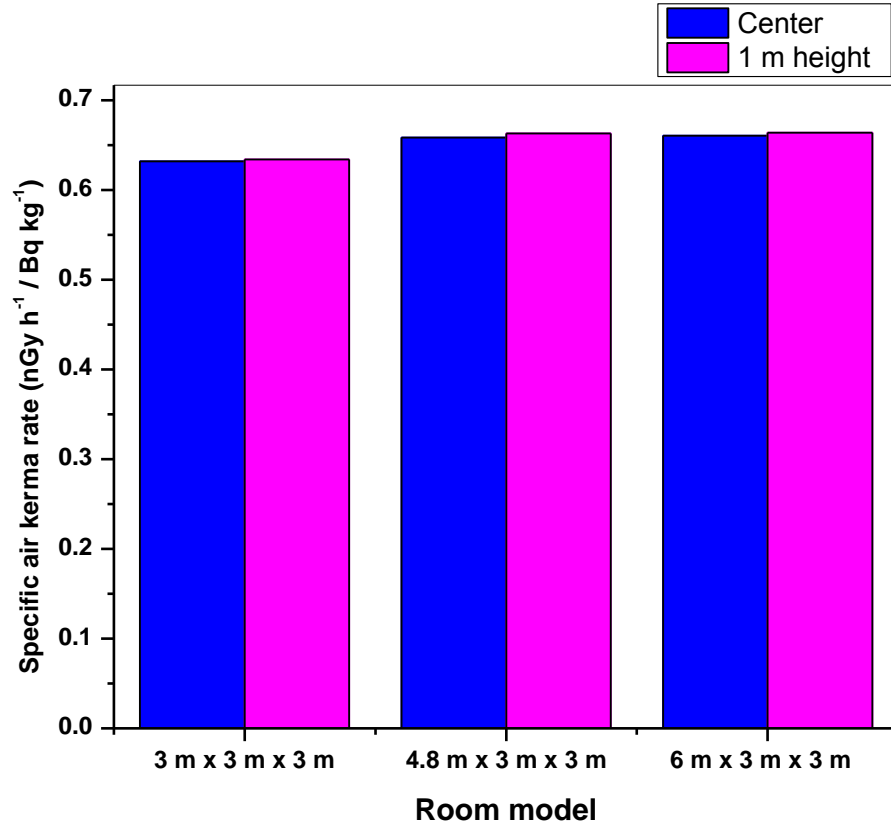


**Figure 5.11 Specific air kerma rate at 1 m and center of the room – various room models**

Instead of vitrified tile flooring, marble having density  $2.61 \text{ gcm}^{-3}$  was considered, as it is also one of the common flooring materials in India. The chemical composition of marble is shown in table 5.12. The computed specific air kerma rate for this combination is shown in table 5.13. It was observed that there is little reduction the specific air kerma rate contribution from concrete, which can be attributed to the high density and thickness of the marble as compared to vitrified tile floor covering the floor concrete. It was also observed that there is fractional increase in the total specific air kerma rate. This is also due to the increased density and thickness of the marble as compared to the vitrified tile.

**Table 5.13 Chemical composition of Marble**  
[107]

S. No.	Element	Fraction of Composition
1	H	0.009
2	C	0.1137
3	O	0.497
4	Na	0.0004
5	Mg	0.0478
6	Al	0.0042
7	Si	0.024
8	S	0.0002

**Table 5.14 Indoor Gamma dose computation using Monte Carlo Method \_  
Clay Brick (3m x 3m x 3m, 1.87 g cm<sup>-3</sup>, Marble Floor)**

Parameters	Dimension					
Dimension of the model room	3 m × 3 m × 3m					
Thickness and density of the structures	Clay Brick walls: 23 cm, 1.87 g cm <sup>-3</sup>					
	Plaster (Cement + Sand): 3 cm, 1.6 g cm <sup>-3</sup>					
	Concrete Floor and Ceiling: 15 cm, 2.35 g cm <sup>-3</sup>					
	Floor Marble: 2 cm, 2.61 g cm <sup>-3</sup>					
	<b>Specific dose rate nGy h<sup>-1</sup> per Bq kg<sup>-1</sup></b>					
Structure in the building causing irradiation	<sup>226</sup> Ra		<sup>232</sup> Th		<sup>40</sup> K	
	Center	1 m	Center	1 m	Center	1 m
Brick walls	0.3400	0.3210	0.4450	0.4270	0.0360	0.0340
Plasters	0.0693	0.0663	0.0890	0.0843	0.0066	0.0059
Concrete floor and ceiling	0.1940	0.2000	0.2600	0.2700	0.0205	0.0213
Floor Marble	0.0320	0.0490	0.0409	0.0632	0.0030	0.0046
<b>Total</b>	0.6353	0.6363	0.8349	0.8445	0.0661	0.0658

### 5.9.2 Fly Ash Brick walls

In place of clay bricks, fly ash brick wall is used because of its economic viability from thermal power plant across India. Table 5.14 shows the chemical composition of fly ash brick. The density of the fly ash brick assumed here for the calculation is  $1.87 \text{ g cm}^{-3}$  and all other combinations of the building materials were same as that of the typical bed room model as discussed above. Table 5.16 shows computed result of the specific air kerma rate. Living room with dimension  $4.8 \text{ m} \times 3 \text{ m} \times 3 \text{ m}$  was also modeled to understand the effect fly ash brick walls as compared to the clay brick walls. Table 5.17 shows the computed specific air kerma. Here also the air kerma rate at 1 m from the floor is higher than that of the bed room model ( $3 \text{ m} \times 3 \text{ m} \times 3 \text{ m}$ ). Fig.5.12 shows the comparison of specific air kerma rate at 1m height due to clay brick and fly ash bricks used in the construction of walls of the building, which indicated that there is no significant increase due to the usage of fly ash brick.

**Table 5.15 Chemical composition of fly ash brick**  
[104]

S. No.	Element	Fraction of Composition
1	C	0.0170
2	O	0.4939
3	Mg	0.0077
4	Al	0.0929
5	Si	0.2390
6	K	0.0157
7	Ca	0.0667
8	Ti	0.0033
9	Fe	0.0619

**Table 5.16 Parameters used for calculation and the obtained specific air kerma rate (Fly ash brick Walls – Bed room)**

Parameters	Dimension					
Dimension of the model room	3 m × 3 m × 3m					
Thickness and density of the structures	Fly ash Brick walls: 23 cm, 1.87 g cm <sup>-3</sup>					
	Plaster (Cement + Sand): 3 cm, 1.6 g cm <sup>-3</sup>					
	Concrete Floor and Ceiling: 15 cm, 2.35 g cm <sup>-3</sup>					
	Floor Vitrified tile: 0.85 cm, 1.9 g cm <sup>-3</sup>					
	<b>Specific Air Kerma Rate nGy h<sup>-1</sup> per Bq kg<sup>-1</sup></b>					
Structure in the building causing irradiation	<sup>226</sup> Ra		<sup>232</sup> Th		<sup>40</sup> K	
	Center	1 m	Center	1 m	Center	1 m
Fly ash Brick	0.3440	0.3270	0.4520	0.4330	0.0362	0.0340
Plasters	0.0700	0.0669	0.0898	0.0852	0.0066	0.0063
Concrete	0.2120	0.2290	0.2820	0.3050	0.0222	0.0239
Floor tiles	0.0106	0.0166	0.0135	0.0212	0.0010	0.0015
<b>Total</b>	0.6366	0.6395	0.8373	0.8444	0.0660	0.0657

**Table 5.17 Parameters used for calculation and the obtained specific air kerma rate (Fly ash brick Walls – Living Room)**

<b>Parameters</b>	<b>Dimension</b>					
Dimension of the model room	4.8 m × 3 m × 3m					
Thickness and density of the structures	Fly ash Brick walls: 23 cm, 1.87 g cm <sup>-3</sup> Plaster (Cement + Sand): 3 cm, 1.6 g cm <sup>-3</sup> Concrete Floor and Ceiling: 15 cm, 2.35 g cm <sup>-3</sup> Floor Vitrified tile: 0.85 cm, 1.9 g cm <sup>-3</sup>					
Structure in the building causing irradiation	<b>Specific Air Kerma Rate nGy h<sup>-1</sup> per Bq kg<sup>-1</sup></b>					
	<sup>226</sup> Ra		<sup>232</sup> Th		<sup>40</sup> K	
	<b>Center</b>	<b>1 m</b>	<b>Center</b>	<b>1 m</b>	<b>Center</b>	<b>1 m</b>
Fly ash Brick walls	0.3254	0.3115	0.4303	0.4123	0.0339	0.0324
Plasters	0.0717	0.0678	0.0921	0.0867	0.0068	0.0080
Concrete floor and ceiling	0.2569	0.2704	0.3415	0.3594	0.0269	0.0284
Floor tiles	0.0135	0.0199	0.0172	0.0254	0.0012	0.0019
<b>Total</b>	0.6675	0.6696	0.8811	0.8838	0.0688	0.0706

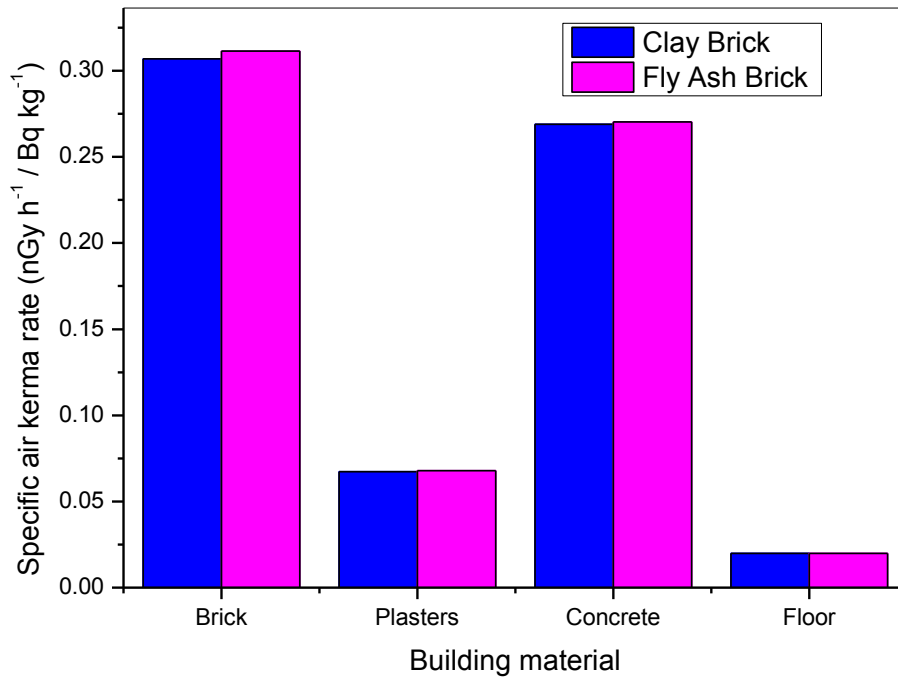


**Figure 5.12 Comparison of specific air kerma rate due to fly ash brick with clay brick in the building construction**

### 5.9.3 Phosphogypsum wall panel

Glass Fiber Reinforced Gypsum (GFRG) Panel branded as Rapid wall is a building panel product, made of calcined gypsum, plaster, reinforced with glass fibers, for Mass-scale building construction, was originally developed and used since 1990 in Australia. The panel, manufactured to a thickness of 124 mm under carefully controlled conditions to a length of 12 m and height of 3m, contains cavities that may be unfilled, partially filled or fully filled with reinforced concrete as per structural requirement. Experimental studies and research in Australia, China and India have shown that GFRG panels, suitably filled with plain reinforced concrete possesses substantial strength to act not only as load bearing elements but also as shear wall, capable of resisting lateral loads due to earthquake and wind. GFRG panel can also be used advantageously as in-fills (non-load bearing) in

combination with RCC framed columns and beams (conventional framed construction of multi-storey building) without any restriction on number of stories micro-beams and RCC screed (acting on T-beam) can be used as floor/ roof slab [109].

The same room models were adopted to model the indoor gamma dose to phosphogypsum wall panel. Table 5.18 shows the chemical composition of the phosphogypsum. Here the cavity of the panel is filled with concrete. No plaster is considered in this model. Floor also similar to the previous model made up of vitrified tile. Table 5.19 and table 5.20 show the parameters used and estimated specific air kerma rates for bed room and living room respectively made up of phosphogypsum rapid wall panel.

**Table 5.18 Chemical composition of Phosphogypsum**  
[110]

S. No.	Compound / Element	Fraction of Composition
1	CaSO <sub>4</sub> .2H <sub>2</sub> O	0.9600
2	P <sub>2</sub> O <sub>5</sub>	0.2000
3	F	0.1200
4	SiO <sub>2</sub>	0.1000
5	Al <sub>2</sub> O <sub>3</sub>	0.0020

**Table 5.19 Parameters used for calculation and the obtained specific air kerma rate (Phosphogypsum wall panel – Bed room)**

Parameters	Dimension					
Dimension of the model room	3 m × 3 m × 3m					
Thickness and density of the structures	Phosphogypsum rapid wall panel: 3 cm, 1.14 g cm <sup>-3</sup> Concrete infill : 9.4 cm, 2.35 g cm <sup>-3</sup> Floor Vitrified tile: 0.85 cm, 1.9 g cm <sup>-3</sup>					
Structure in the building causing irradiation	<b>Specific Air Kerma Rate nGy h<sup>-1</sup> per Bq kg<sup>-1</sup></b>					
	<sup>226</sup> Ra		<sup>232</sup> Th		<sup>40</sup> K	
	<b>Center</b>	<b>1 m</b>	<b>Center</b>	<b>1 m</b>	<b>Center</b>	<b>1 m</b>
Phosphogypsum	0.0722	0.0715	0.0934	0.0921	0.0070	0.0069
Concrete	0.4385	0.4254	0.5630	0.5507	0.0436	0.0425
Floor tiles	0.0103	0.0161	0.0131	0.0205	0.0009	0.0015
<b>Total</b>	0.5210	0.5130	0.6695	0.6633	0.0514	0.0508

**Table 5.20 Parameters used for calculation and the obtained specific air kerma rate (Phosphogypsum wall panel – Living room)**

Parameters	Dimension					
Dimension of the model room	4.8 m × 3 m × 3m					
Thickness and density of the structures	Phosphogypsum rapid wall panel: 3 cm, 1.14 g cm <sup>-3</sup> Concrete infill : 9.4 cm, 2.35 g cm <sup>-3</sup> Floor Vitrified tile: 0.85 cm, 1.9 g cm <sup>-3</sup>					
Structure in the building causing irradiation	<b>Specific Air Kerma Rate nGy h<sup>-1</sup> per Bq kg<sup>-1</sup></b>					
	<sup>226</sup> Ra		<sup>232</sup> Th		<sup>40</sup> K	
	<b>Center</b>	<b>1 m</b>	<b>Center</b>	<b>1 m</b>	<b>Center</b>	<b>1 m</b>
Phosphogypsum	0.0761	0.0751	0.0979	0.0960	0.0073	0.0072
Concrete	0.4460	0.4350	0.5810	0.5690	0.0447	0.0438
Floor tiles	0.0204	0.0302	0.0260	0.0385	0.0019	0.0028
<b>Total</b>	0.5425	0.5403	0.7049	0.7035	0.0539	0.0538

Table 5.21 shows the summary of the computation of specific air kerma rate in various room models. The mean specific air kerma rate at the center of the room due to  $^{226}\text{Ra}$ ,  $^{232}\text{Th}$  and  $^{40}\text{K}$  was found to be  $0.617 \text{ nGyh}^{-1}$  per  $\text{Bq kg}^{-1}$ ,  $0.810 \text{ nGyh}^{-1}$  per  $\text{Bq kg}^{-1}$  and  $0.06 \text{ nGyh}^{-1}$  per  $\text{Bq kg}^{-1}$  respectively. Whereas at 1 m height from the floor, mean specific air kerma rate due to  $^{226}\text{Ra}$ ,  $^{232}\text{Th}$  and  $^{40}\text{K}$  was found to be  $0.618 \text{ nGyh}^{-1}$  per  $\text{Bq kg}^{-1}$ ,  $0.815 \text{ nGyh}^{-1}$  per  $\text{Bq kg}^{-1}$  and  $0.0654 \text{ nGyh}^{-1}$  per  $\text{Bq kg}^{-1}$  respectively.

**Table 5.21 Summary of room models and corresponding Specific Air Kerma Rate**

S. No.	Room Models	Specific Air Kerma Rate, $\text{nGy h}^{-1}$ per $\text{Bq kg}^{-1}$					
		$^{226}\text{Ra}$		$^{232}\text{Th}$		$^{40}\text{K}$	
		Center	1 m	Center	1 m	Center	1 m
1	3m x 3m x 3m_1.6_CB	0.640	0.630	0.840	0.830	0.070	0.060
2	3m x 3m x 3m_1.87_CB1	0.634	0.632	0.836	0.828	0.065	0.059
3	3m x 3m x 3m._M_CB1	0.621	0.618	0.827	0.821	0.065	0.058
4	3m x 3m x 3m_30_CB1	0.597	0.007	0.796	0.794	0.063	0.062
5	3m x 3m x 3m_40	0.636	0.635	0.845	0.835	0.065	0.066
6	4.8m x 3m x 3m_CB1	0.660	0.658	0.880	0.871	0.070	0.068
7	6m x 3m x 3m_CB1	0.663	0.660	0.878	0.870	0.071	0.068
8	3m x 3m x 3m_FAB1	0.640	0.637	0.840	0.837	0.066	0.066
9	4.8m x 3m x 3m_FAB1	0.670	0.660	0.883	0.880	0.069	0.069
10	3m x 3m x 3m_PG	0.513	0.521	0.663	0.669	0.051	0.051
11	4.8m x 3m x 3m_PG	0.540	0.543	0.704	0.705	0.054	0.054
<b>Mean</b>		0.617	0.618	0.810	0.815	0.060	0.064

CB = Clay Brick, CB1 = Clay Brick-1, FAB = Fly Ash Brick, PG = Phosphogypsum



---

## Chapter 6 Radiological Assessment

---

### 6.1 Introduction

Certification of building materials samples for NORM has gained more attention in recent years. There is always a question regarding the permissible limit on building material natural radioactivity level. Actual level of indoor gamma dose in a room will vary depends upon the material used, thickness, density, and ventilation rate etc. It is very difficult to assess each and every building. Hence, from the measured radioactivity levels there should be some screening index, known as activity index enable to certify the materials for its suitability. Literatures of regulation of NORM in building materials has been discussed in the chapter 2. From the computed specific air kerma rate as discussed in chapter 5, India specific activity index has been derived. Comparison of the activity index between the EC-RP-112 and the new proposed from this study for various building materials was also carried out.

### 6.2 Derivation of Activity Index for gamma dose

The activity index is derived to indicate whether the annual dose due to the excess external gamma radiation in a building may exceed 1 mSv. The variation in dose rate between 1 m height and center of the room was found to be very less as shown in table 5.7. However, specific air kerma rate at 1 m height from the floor is assumed to represent the indoor gamma dose. Hence these factors are used for the derivation of activity index. The occupancy factor of 0.8 is used as per the UNSCEAR report. To convert the specific air kerma rate into effective dose,  $0.7 \text{ SvGy}^{-1}$  is the conversion factor used as per ICRP [15] and UNSCEAR. Table 6.1 shows the mean specific air kerma rate at 1 m height for  $^{226}\text{Ra}$ ,

$^{232}\text{Th}$  and  $^{40}\text{K}$ . The mean outdoor terrestrial gamma dose rate in India was found to be about  $100 \text{ nGy h}^{-1}$  [111]. This is the background dose to be subtracted while deriving the excess gamma dose indoor.

**Table 6.1 Specific air kerma rate at 1 m height computed using Monte Carlo method**

Radionuclides	Specific Air Kerma Rate, $\text{nGy h}^{-1}$ per $\text{Bq kg}^{-1}$ at 1 m
$^{226}\text{Ra}$	<b>0.62</b>
$^{232}\text{Th}$	<b>0.82</b>
$^{40}\text{K}$	<b>0.06</b>

**i. Factor for Radium**

$$0.001 \text{ Sv y}^{-1} = ((0.62 \times C_{\text{Ra}}) - 100) \times 10^{-9} \text{ Gy h}^{-1} \times 0.7 \text{ SvGy}^{-1} \times 7000 \text{ h y}^{-1}$$

This will lead to  $490.9 \text{ Bq kg}^{-1}$  of  $^{226}\text{Ra}$ .

Where  $C_{\text{Ra}}$  is the specific activity of  $^{226}\text{Ra}$

**ii. Factor for Thorium**

$$0.001 \text{ Sv y}^{-1} = ((0.82 \times C_{\text{Th}}) - 100) \times 10^{-9} \text{ Gy h}^{-1} \times 0.7 \text{ SvGy}^{-1} \times 7000 \text{ h y}^{-1}$$

This will lead to  $372 \text{ Bq kg}^{-1}$  of  $^{232}\text{Th}$ .

Where  $C_{\text{Th}}$  is the specific activity of  $^{232}\text{Th}$

**iii. Factor for Potassium**

$$0.001 \text{ Sv y}^{-1} = ((0.06 \times C_{\text{K}}) - 100) \times 10^{-9} \text{ Gy h}^{-1} \times 0.7 \text{ SvGy}^{-1} \times 7000 \text{ h y}^{-1}$$

This will lead to  $4713 \text{ Bq kg}^{-1}$  of  $^{40}\text{K}$ .

Where  $C_{\text{K}}$  is the specific activity of  $^{40}\text{K}$ .

In the final activity index, the above computed values are rounded to nearest full 100 Bq kg<sup>-1</sup> (for radium and thorium) or 1000 Bq kg<sup>-1</sup> (for potassium). The final activity index is shown in equation 6.1.

$$\frac{C_{\text{Ra}}}{500} + \frac{C_{\text{Th}}}{400} + \frac{C_{\text{K}}}{5000} \leq 1 \quad (6.1)$$

### 6.3 Activity index including radon contribution

Most of the existing regulations do not address radon emanation from building materials. At the same time, the inclusion of radon emanation test in the standards regulating radioactivity of building materials has both pros and cons, and sometimes is even desirable. In particular, RP-112 recommends considering separate limitations for radon isotopes (radon <sup>222</sup>Rn and thoron <sup>220</sup>Rn) exhaled from building materials, where previous evaluations show that building materials may be a significant source of indoor radon or thoron and restrictions put on this source are found to be an efficient and a cost-effective way to limit internal radiation exposures [112].

Numerous methods have been published in the literature to screen building materials from the radiological protection point of view. Several of them estimate effective dose indoors from gamma radiation, and some of them also account for the contribution from radon exhaled by such materials. This is the case with Austrian, Czech, Dutch and Israeli indexes, which have long been in force as national regulations.

Radon surface exhalation rate ( $j_w$ ) of the building materials is one of the important parameter required to calculate the activity concentration of radon. The following formulae have been used as suggested by Sahoo et al [113]:

$$j_w = \lambda l Q \rho f \tanh\left(\frac{d}{l}\right) \quad (6.2)$$

Where,  $j_w$  is the surface exhalation rate of the wall surface in  $\text{Bq m}^{-2} \text{h}^{-2}$ ;  $d$  is the half thickness of the wall in m;  $Q$  the specific activity of  $^{226}\text{Ra}$  of building material;  $\lambda$  the decay constant of  $^{222}\text{Rn}$  in  $\text{h}^{-1}$ ;  $f$  the radon emanation fraction;  $l$  the diffusion length of radon. The values of these parameters were taken from Amit Kumar et al [114].

Since brick is the most common wall material having high radon exhalation rate, the radon activity concentration for the clay brick was derived as shown in equation 6.20 given below:

$$C_{\text{Rn}} = \sum_i \left( \frac{j_{wi} S_i}{V (\lambda_{\text{Rn}} + \lambda_v)} \right) \quad (6.3)$$

Where  $C_{\text{Rn}}$  is the  $^{222}\text{Rn}$  activity concentration in  $\text{Bq m}^{-3}$ ;  $j_{wi}$  and  $S_i$  are the radon wall flux and surface area of wall;  $\lambda_{\text{Rn}} + \lambda_v$  effective radon removal rate;  $\lambda_v$  ventilation rate of the room in  $\text{h}^{-1}$ ;  $\lambda_{\text{Rn}}$  the radon decay constant;  $S$  and  $V$  the surface and volume of the room respectively.

$\lambda_{\text{Rn}} = 0.00755 \text{ h}^{-1}$ ;  $f = 0.1$ ;  $l = 0.5$ ,  $S/V$  = Surface to Volume ratio of the room;

$\lambda_v = 0.7 \text{ h}^{-1}$  and  $Q = 500 \text{ Bq kg}^{-1}$ , reference level for 1 mSv annual dose, as shown in eqn. 6.1.

The outdoor radon background is assumed to be  $10 \text{ Bq m}^{-3}$ . The dose criterion chosen for indoor  $^{222}\text{Rn}$  is  $3 \text{ mSv y}^{-1}$ , the lowest dose reference level in the range recommended by the ICRP for exposure to radon in dwellings [22]. It now corresponds to about  $100 \text{ Bq m}^{-3}$  indoor at home.

The value of  $\alpha$ , which accounting for the radon exhalation rate from building materials.

$$\alpha = \frac{C_{Rn}}{C_{Rn}^0} \quad (6.4)$$

Where  $C_{Rn}^0$  is the sum of radon activity concentration corresponding to the dose criterion chosen and the outdoor background of  $10 \text{ Bq m}^{-3}$ . By applying the above parameters in equation 6.1, the value of  $\alpha$  is equal to 1.85. Hence the modified index would be

$$I_{G+Rn} = (1 + 1.85) \frac{C_{Ra}}{500} + \frac{C_{Th}}{400} + \frac{C_K}{5000} \leq 4 \quad (6.5)$$

#### 6.4 Application of proposed Activity Index

Using the proposed new formula for activity index as shown in eqn.6.5, activity indices were calculated for various analysed building materials. Table 6.2 shows the computed activity index and its comparison with the  $I_{RP112}$  of the European Commission. It was found out that except phosphogypsum,  $I_{RP112}$  is more than  $I_{(G+Rn)}$ . Histogram shown in Fig. 6.1 also indicated the same. This is due to the increase in  $^{226}\text{Ra}$  activity corresponding to 1 mSv by about 65 % in the new index  $I_{(G+Rn)}$ . For  $^{232}\text{Th}$  and  $^{40}\text{K}$  the increase was found to be about 100 % and 65% respectively. However, the increase in the calculated activity index of phosphogypsum may be attributed to the inclusion of derived radon contribution (alpha value as shown in eqn. 6.4) in the formula. Also,  $^{226}\text{Ra}$  activity level was found to be high as compared to other building materials. From the analysed result, it was found out that the excess dose to be caused by these building materials, if used for construction would be very small and well within the dose criteria.

**Table 6.2 Computed Activity Index and its comparison with I<sub>RP112</sub>**

S. No.	Building Material	Mean Specific Activity (Bqkg <sup>-1</sup> )			I <sub>RP112</sub>	I <sub>(G+Rn)</sub>
		<sup>226</sup> Ra	<sup>232</sup> Th	<sup>40</sup> K		
1	Clay Brick	16	12	60	0.133	0.133
2	Fly Ash Brick	85	106	240	0.893	0.798
3	Soil	40	58	595	0.622	0.492
4	Sand	13	4	87	0.092	0.102
5	Cement	40	37	211	0.389	0.363
6	Concrete	21	16	178	0.209	0.195
7	Tile	33	62	1004	0.755	0.544
8	Phosphogypsum	500	4	18	1.693	2.864
9	Synthetic Rutile	61	195	18	1.184	0.840

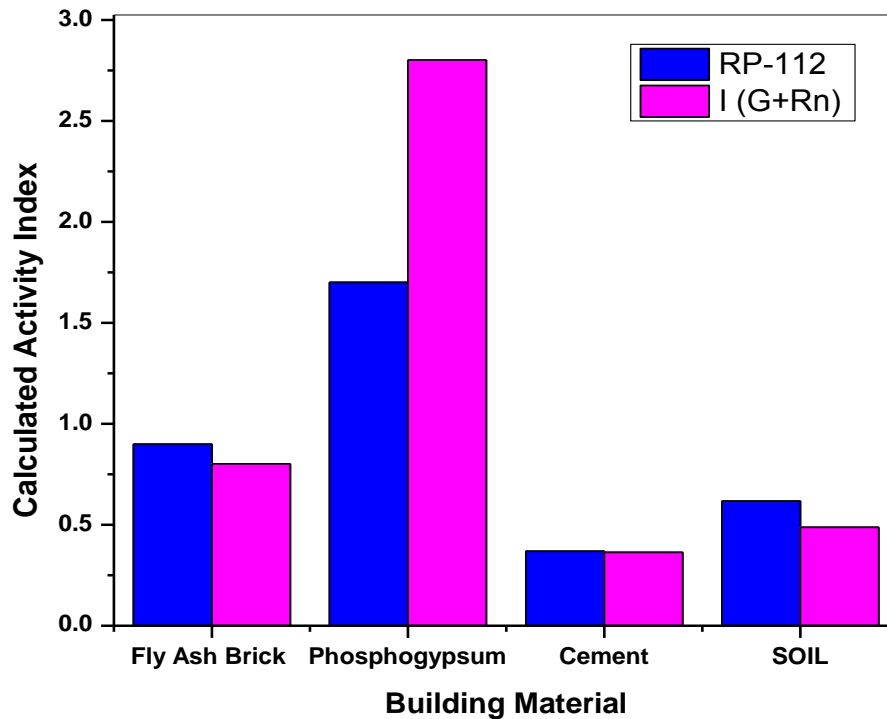


**Figure 6.1 Comparison of activity index calculated using RP-112 and the proposed I (G+Rn)**

Sensitivity analysis of effect of variation in the indoor occupancy on the indoor was also carried out. As per the new gamma activity index shown in fig 6.1, the specific activity levels of  $^{226}\text{Ra}$ ,  $^{232}\text{Th}$  and  $^{40}\text{K}$  corresponding to the 1 mSv annual dose and 80 % indoor occupancy would be  $500 \text{ Bq kg}^{-1}$ ,  $400 \text{ Bq kg}^{-1}$ ,  $5000 \text{ Bq kg}^{-1}$  respectively. For the indoor occupancies 50 %, 60 %, and 100 %, the corresponding  $^{226}\text{Ra}$  specific activity levels were estimated to be about  $688 \text{ Bq kg}^{-1}$ ,  $600 \text{ Bq kg}^{-1}$ ,  $425 \text{ Bq kg}^{-1}$  respectively. Fig. 6.2 shows the least square second order polynomial fitting of indoor occupancy and corresponding  $^{226}\text{Ra}$  specific activity for 1 mSv. It is evident that more the indoor occupancy more will be the effective dose received.

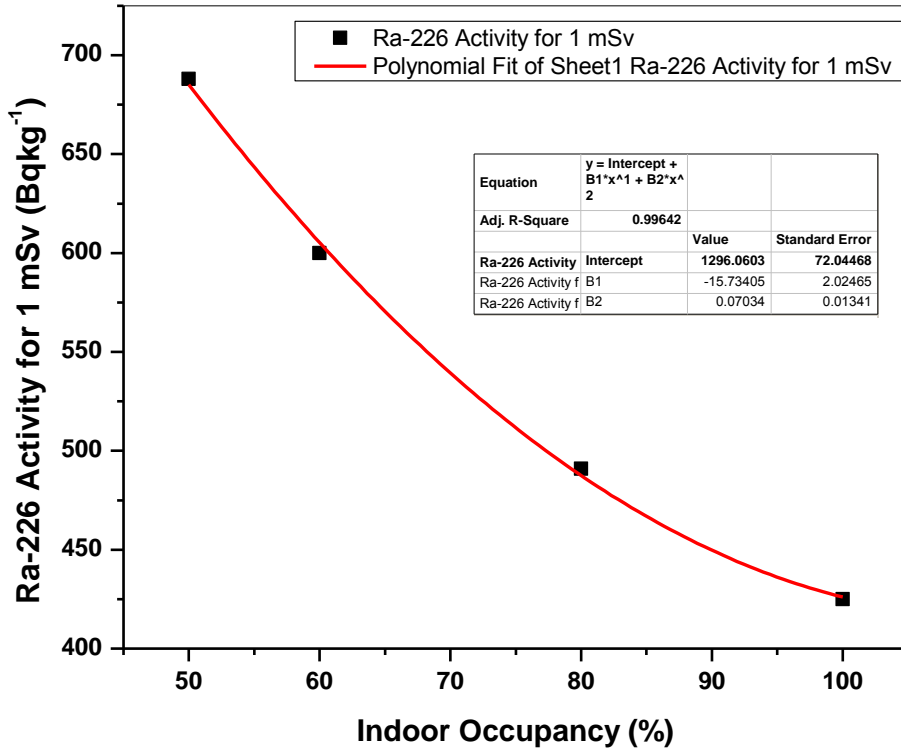


**Figure 6.2 Indoor occupancy effect on the Activity Index**

---

## Chapter 7 Conclusions

---

### 7.1 Summary and concluding remarks

Protection of the public has always been part of the radiation protection requirements. However, there has been relatively very little guidance provided specifically on the protection of the public against exposure due to natural sources of radiation in general and indoor exposure due to building materials in particular. Recent IAEA specific safety guide No. SSG-32 [51] also provided a guidance on the application of the requirements for the justification and optimization of protection by national authorities when considering control of natural sources of radiation such as radon indoors and radionuclides of natural origin in building materials. In view of the above, this thesis discusses the measurement of NORM in building materials using gamma spectrometry, calculation of indoor specific air kerma rate using Monte Carlo computation, and the derivation of the India specific regulatory screening criteria at par with the most popular European Commission recommendation, RP-112.

Measurement of natural radioactivity due to  $^{226}\text{Ra}$ ,  $^{232}\text{Th}$ , and  $^{40}\text{K}$  in various Indian building materials such as soil, sand, cement, fly ash, phosphogypsum etc. using HPGe gamma spectrometric technique. The detector has the relative efficiency of 50 % and coupled with digital signal processing electronic accessories. The spectrometry system was standardised using the IAEA certified reference materials RGU-I, RGTh-I and RGK-I for the measurement of natural radioactivity in building materials. Quality of the measurement was ensured by participating in the IAEA intercomparison of the IAEA ALMERA network, internal quality control using the background control chart and analyzing the

standard reference materials regularly.

Monte Carlo computation of indoor specific air kerma rate ( $\text{nGy h}^{-1}$  per  $\text{Bqkg}^{-1}$ ) for typical Indian room models ( $3 \text{ m} \times 3 \text{ m} \times 3 \text{ m}$ ), ( $4.8 \text{ m} \times 3 \text{ m} \times 3 \text{ m}$ ), and ( $6 \text{ m} \times 3 \text{ m} \times 3 \text{ m}$ ). MCNP Monte Carlo code was used for this computation. In order to validate the methodology, the computation was carried out for the room model of  $5 \text{ m} \times 4 \text{ m} \times 2.8 \text{ m}$  which was studied by many researchers across the world and has been in used as a regulatory tool. It was found out that the result obtained was in good agreement with the reported value. Building materials such as clay brick, fly ash brick and phosphogypsum rapid wall panel, soil sand, cement, tile, and marble were used in the modelling. Specific air kerma rate for 11 room models with different combination of building materials and room dimensions were computed.

From the radiological parameters such as the computed specific air kerma rate, radon exhalation characteristics of Indian building materials, and considering the ICRP lowest reference level on indoor radon level, a new activity index is proposed similar to that of the EC-RP112. This will help to screening the Indian building materials by simply measuring the specific activity levels of  $^{226}\text{Ra}$ ,  $^{232}\text{Th}$ , and  $^{40}\text{K}$ .

1. Natural radioactivity mainly due to  $^{226}\text{Ra}$ ,  $^{232}\text{Th}$  and  $^{40}\text{K}$  in soil samples randomly collected in Ferozepur and Faridkot district of Punjab, India.  $^{226}\text{Ra}$  activity varied from 28.6 to 51.1  $\text{Bq kg}^{-1}$  with the mean of 39.7  $\text{Bq kg}^{-1}$ . The range and mean activity of  $^{232}\text{Th}$  was 42.9 – 73.2  $\text{Bq kg}^{-1}$  and 58.2  $\text{Bq kg}^{-1}$  respectively.  $^{40}\text{K}$  activity was in the range of 470.9 – 754.9  $\text{Bq kg}^{-1}$  with the mean of 586.4  $\text{Bq kg}^{-1}$ . The mean activity index was found to be 0.62 calculated based on RP-112, whereas 0.49 using the newly developed activity index in this study. The former is based on only indoor gamma

- control, but the later covers both indoor radon and gamma dose rate.
2. Incement samples  $^{226}\text{Ra}$  activity was varying from 20.3 – 79.3 Bq kg<sup>-1</sup> with the mean of 40.3 Bq kg<sup>-1</sup>. The range and mean activity of  $^{232}\text{Th}$  was found to be 18.8 – 63.5 Bq kg<sup>-1</sup> and 36.8 Bq kg<sup>-1</sup> respectively.  $^{40}\text{K}$  activity was in the range of 160.9 – 307.2 Bq kg<sup>-1</sup> with the mean of 211.1 Bq kg<sup>-1</sup>. The calculated activity index based on the RP-112 and the proposed index  $I_{(G+Rn)}$  for the cement samples was found to be 0.37 and 0.36, respectively. Cement raw materials such as lime stone, clay, gypsum, Iron ore, Bauxite, coal were also analysed. The activity indices of RP-112 and  $I_{(G+Rn)}$  were calculated and found out that there is slight increase in the values of  $I_{(G+Rn)}$  as compared to RP-112. This may be attributed to the inclusion of radon contribution in the new proposed index,  $I_{(G+Rn)}$ .
  3. In fly ash brick samples, mean activity due to  $^{226}\text{Ra}$ ,  $^{232}\text{Th}$  and  $^{40}\text{K}$  was found to be 85.8 Bq kg<sup>-1</sup>, 106.8 Bq kg<sup>-1</sup> and 241.5 Bq kg<sup>-1</sup> respectively. The calculated activity indices were 0.9 and 0.8 respectively obtained from the RP-112 model and newly developed one.
  4. In phosphogypsum samples, the mean activity due to  $^{226}\text{Ra}$ ,  $^{232}\text{Th}$ , and  $^{40}\text{K}$  was found to be 500Bq kg<sup>-1</sup>, 4Bq kg<sup>-1</sup> and 18 Bq kg<sup>-1</sup>, respectively. The activity indices based on RP-112 and  $I_{(G+Rn)}$  were 1.7 and 2.8 respectively. Phosphogypsum rapid wall panels (PGRWAP) samples were also analysed for natural radioactivity. The mean activity due to  $^{226}\text{Ra}$ ,  $^{232}\text{Th}$ , and  $^{40}\text{K}$  was found to be 450 Bq kg<sup>-1</sup>, 12 Bq kg<sup>-1</sup> and 17Bq kg<sup>-1</sup>, respectively. The corresponding activity indices based on RP-112 and  $I_{(G+Rn)}$  were 1.6 and 2.7 respectively. As per the new criteria,  $I$  must be less than or equal to 4, so that the dose to the public will be well within the limit of 1 mSv y<sup>-1</sup>

<sup>1</sup>from gamma radiation and 3 mSv y<sup>-1</sup> from radon (lower end of the radon reference level). By applying the new criteria, it showed that the radon exposure also would be less than the ICRP lowest reference level of 3 mSv y<sup>-1</sup>.

The measured natural radioactivity levels in the studied building materials and the radiological characterization using the proposed activity index indicates that the dose to the public would be well within the acceptance criteria for controlling external as well as internal natural radiation exposure.

The new activity Index I (G+Rn) will be very useful in the certification of building materials for natural radioactivity, as a radiological screening tool.

## **7.2 Scope for future work**

There is a growing trend on natural radioactivity measurement research in India, by various academic institutes. However, there should be a well-defined protocol on the natural radioactivity measurement must be followed to ensure the harmonization of the measurement procedure. Generation of state wise database on natural radioactivity in Indian building materials including both conventional and industrial byproducts can be carried out with more systematic approach. This will lead to the generation of national database on NORM in building materials which is necessary from the regulatory point of view to assess the public exposure to natural radiation sources. Application of in-situ gamma spectrometry for the indoor natural gamma dose assessment is one of the important areas which is being carried out by very few in the world. This will avoid time consuming sample collection and processing.

---

## Bibliography

---

- [1] R. E. Faw, J. K. Shultis, Radiological Assessment Sources and Doses, Illinois: American Nuclear Society, 1999.
- [2] J. E. Martin, Physics for Radiation Protection, Wiley - VCH Verlag GmbH & Co. KGaA, 2006.
- [3] IAEA., "IAEA safety glossary : terminology used in nuclear safety and radiation," Vienna, 2007.
- [4] J. R. Cooper, K. Randle, R. S. Sokhi, Radioactive releases in the environment: Impact and Assessment, John Wiley & Sons, Ltd., 2003.
- [5] V. Valkovic, Radioactivity in the environment, Elsevier, 2000.
- [6] UNSCEAR, "Sources and effects ionising radiation. Report to the General Assembly with Annex B: Exposures from natural sources of radiation," United Nations Scientific Committee on the Effect of Atomic Radiation, New York, 2000.
- [7] IAEA, "Measurement and calculation of Radon releases from NORM residues," Austria, Vienna, 2013.
- [8] J. Sabol, P. S. Weng, Introduction to Radiation Protection Dosimetry, World Scientific, 1995.
- [9] INL, "<http://www.inl.gov/gammaray/catalogs/ge/pdf/k40.pdf>," 2014. [Online]. [Accessed 12 2014].

- [10] K. S. V. Nambi, V. K. Shukla, "A suggested guideline for exposure control from natural radioactivity in future buildings," *Bulletin of Radiation Protection*, vol. 14, no. 1 & 2, pp. 13 - 17, 1991.
- [11] IAEA, "Radiation protection and management of NORM residues in the phosphate industry," Vienna, Austria, 2013.
- [12] ICRP Publication 103, "The 2007 Recommendations of the ICRP," *Ann. ICRP*, vol. 37, no. 2 - 4, pp. 1 - 332, 2007.
- [13] IAEA, "Radiation protection and safety of radiation sources : International Basic Safety Standards - No. GSR Part 3," International Atomic Energy Agency, Austria, Vienna, 2014.
- [14] S. L. Simon, "Dosimetric considerations for environmental radiation and NORM," *Int. Congr. ser.*, vol. 1276, pp. 89-92, 2005.
- [15] ICRP, "ICRP PUBLICATION 116 Conversion Coefficients for Radiological Protection Quantities for External Radiation Exposures," *Ann. ICRP*, vol. 40, no. 2 - 5, 2010.
- [16] ICRP, "Protection of the public in situations of prolonged radiation exposure ICRP Publication 82," *Ann. ICRP*, vol. 29, no. 1-2, 2000.
- [17] IAEA, "Guidelines for radioelement mapping using gamma ray spectra data, IAEA - TECDOC - 1363," International Atomic Energy Agency, Austria, Vienna, 2003.
- [18] K. P.-H. N. Z. M. Saito, "Calculation of the effective dose and its variation from environmental gamma ray sources," *Health Phys.*, vol. 74, no. 6, pp. 698-706, 1998.

- [19] UNSCEAR, "Sources and effects of atomic Ionising Radiation, Vol.I," United Nations Scientific Committee on the Effect of Atomic Radiation, New York, 2008.
- [20] P. H. Jensen, "Are public dose limits necessary?," *Health Phys.*, vol. 79, no. 3, pp. 282 -285, 2000.
- [21] WHO, WHO handbook on indoor radon: a public health perspective, H. Z. a. F. Shannoun, Ed., Geneva: World Health Organisation, 2009.
- [22] ICRP, "ICRP statement on Radon," November 2009. [Online]. Available: [http://www.icrp.org/docs/ICRP\\_Statement\\_on\\_Radon%28November\\_2009%29.pdf](http://www.icrp.org/docs/ICRP_Statement_on_Radon%28November_2009%29.pdf). [Accessed 30 11 2014].
- [23] IAEA, "Measurement of Radionuclides in Food and the Environment - A Guide Book. Technical Report Series No. 295," International Atomic Energy Agency, Vienna, 1989.
- [24] IAEA, RPOP, "RPOP, IAEA," 2014. [Online]. Available: [https://rpop.iaea.org/RPOP/RPoP/Content/AdditionalResources/Training/1\\_TrainingMaterial/NuclearMedicine.htm](https://rpop.iaea.org/RPOP/RPoP/Content/AdditionalResources/Training/1_TrainingMaterial/NuclearMedicine.htm)). [Accessed 12 2014].
- [25] G. F. Knoll, Radiation Detection and Measurement, John Wiley & Sons, 2000.
- [26] M. J. Berger, J. H. Hubbell, S. M. Seltzer, J. Chang, J. S. Coursey, R. Sukumar, D. S. Zucker, K. Olsen, "XCOM:photon cross sections database - NIST standard reference database (XGAM)," 1998.
- [27] K. Debertin, R. G. Helmer, Gamma and X-ray Spectrometry with semiconductor detectors, North Holland, 1988.
- [28] G. Gilmore, Practical Gamma Spectrometry, John Wiley & Sons, Ltd, 2008.

- [29] IAEA, "Handbook of nuclear data for safeguards: Database extensions, August 2008," International Atomic Energy Agency, Austria, Vienna, 2008.
- [30] IAEA, "Update of X Ray and Gamma Ray Decay Data Standards for Detector - Calibration and Other Applications.," International Atomic Energy Agency, Austria, Vienna, 2007.
- [31] G. R. Gilmore, Practical Gamma-ray Spectrometry – 2nd Edition, John Wiley & Sons, 2008.
- [32] E. Stranden, "Radioactivity of building materials and gamma radiation in dwellings," *Phys. Med. Biol.*, vol. 24, no. 5, pp. 921-930, 1979.
- [33] M. Markkanen, "Radiation Dose Assessments for Materials with Elevated Natural Radioactivity. STUK-B-STO-32," Finnish Centre for Radiation and Nuclear Safety, Helsinki, Finland, 1995.
- [34] L. Koblinger, "Mathematical models of external gamma radiation and congruence of measurements," *Radiat. Prot. Dosim.*, vol. 7, no. 1-4, pp. 227-234, 1984.
- [35] M. Markkanen, "Radiation Dose Assessments for Materials with Elevated Natural Radioactivity STUK-B-STO-32," 1995.
- [36] M. F. Maduar., G. Hiromoto.,, "Evaluation of indoor gamma radiation dose in dwellings," *Radiat. Prot. Dosim.*, vol. 111, no. 2, pp. 221-228, 2004.
- [37] M. F. Maduar, M. P. Campos, B. P. Mazilli, F. L. Villaverde, "Assessment of external gamma exposure and radon levels in a dwelling constructed with phosphogypsum plates," *J. Hazard. Mater.*, vol. 190, pp. 1063-1067, 2011.

- [38] J. Al-jundi, A. Ulanovsky, G. Prohl, "Doses of external exposure in Jordan house due to gamma emitting natural radionuclides in building materials," *J. Environ. Radioact.*, vol. 100, pp. 841-846, 2009.
- [39] P. D. Jong, W. V. Dijk, "Modelling gamma radiation dose in dwellings due to building materials," *Health Phys.*, vol. 94, no. 1, pp. 33-42, 2008.
- [40] S. Risica, C. Bolzan, C. Nuccetelli, "Radioactivity in building materials: room model analysis and experimental methods," *Sci. Total Environ.*, vol. 272, pp. 119-126, 2001.
- [41] E. I. Hamilton, "The relative radioactivity of building materials," *Am. Ind. Hyg. Assoc. J.*, vol. 32, no. 6, pp. 398 - 403, 1971.
- [42] OECD - NEA, "Exposure to radiation from the natural radioactivity in building materials," Organisation for Economic Cooperation and Development, Paris, 1979.
- [43] R. Trevisi, C. Nuccetelli, S. Risica, "Screening tools to limit the use of building materials with enhanced / elevated levels of natural radioactivity: Analysis and application of index criteria," *Constr. Build. Mater.*, vol. 49, pp. 448-454, 2013.
- [44] J. Beretka, P. J. Mathew, "Natural radioactivity of Australian building materials, industrial wastes and by-products," *Health Phys.*, vol. 48, no. 1, pp. 87-95, 1985.
- [45] B. Righi, S. Luigi, "Natural radioactivity and radon exhalation in building materials used in italian Dwellings," *J. Environ. Radioact.*, vol. 88, pp. 158-170, 2006.
- [46] EC, "Radiological Protection principles concerning the natural radioactivity of the building materials, RP-112," European Commission, Luxemburg, 1999.

- [47] V. K. Shukla, S. Sadasivan, V. K. Sundaram, K. S. V. Nambi, "Assessment of gamma radiation exposure inside a newly constructed building and a proposed regulatory guideline for exposure control from natural radioactivity in future buildings," *Radiat. Prot. Dosim.*, vol. 59, no. 2, pp. 127-133, 1995.
- [48] AERB, "AERB Safety Directive No. 01/09 - Use of phosphogypsum in building and construction materials and in agriculture. Atomic Energy (Radiation Protection) Rule," Atomic Energy Regulatory Board, Mumbai, 2009.
- [49] F. Bochicchio, "The international trend about regulation of indoor radon," *Radiat. Prot. Dosim.*, vol. 146, no. 1-3, pp. 2-5, 2011.
- [50] WHO, WHO handbook on indoor radon: a public health perspective, Geneva: World Health Organisation, 2009.
- [51] IAEA, "Protection of the Public against Exposure Indoors due to Radon and Other Natural Sources of Radiation. Specific Safety Guide No. SSG - 32," International Atomic Energy Agency, Vienna, 2015.
- [52] L. Bruzzi, R. Mele, F. Padoani, "Evaluation of gamma and alpha doses due to natural radioactivity of building materials," *J. Radiol. Prot.*, vol. 12, no. 2, pp. 267-276, 1992.
- [53] S. Dziri, A. Nachab, A. Nourreddine, A. Sellam, D. Gelus, "Experimental and Simulated Effective Dose for Some Building Materials in France," *World Journal of Nuclear Science and Technology*, vol. 3, pp. 41- 45, 2013.

- [54] L. Xinwei, C. Shigang, Y. Fang, "Determination of natural radioactivity and associated radiation hazard in building materials used in Weinan, China," *Rad. Phy. Chem.*, vol. 99, pp. 62 - 67, 2014.
- [55] N. C. Silva, E. A. N. Fernandes, M. Cipriani, M. T. Taddei, "The natural radioactivity of Brazilian phosphogypsum," *J. Radioanal. Nucl. Chem.*, vol. 249, no. 1, pp. 251-255, 2001.
- [56] K. Kovler, Z. Prilutskiy, S. Antropov, N. Antropova, V. Bozhko, Z. B. Alfassi, N. Lavi, "Can scintillation detectors with low spectral resolution accurately determine radionuclides content of building materials?," *Appl. Rad. Iso.*, vol. 77, pp. 76-83, 2013.
- [57] R. Trevisi, S. Risica, M. D'Alessandro, D. Paradiso, C. Nuccetelli, "Natural radioactivity in building materials in the European Union: a database and an estimate of radiological significance," *J. Envi. Radioact.*, vol. 105, pp. 11-20, 2012.
- [58] J. Somlai, Cs. Nemeth, Z. Lendvai, R. Bodnir, "Dose contribution from school buildings containing coal slag insulation with elevated concentrations of natural radionuclides," *J. Radioanal. Nucl. Chem.*, vol. 218, no. 1, pp. 61-63, 1997.
- [59] S. Sadasivan, V. K. Shukla, S. Chinnaesakki, S. J. Sartandel, "Natural and fallout radioactivity measurement in Indian soils," *J. Radioanal. Nucl. Chem.*, vol. 256, pp. 603-607, 2003.
- [60] V. Kannan, M. P. Rajan, M. A. R. Iyengar, R. Ramesh, "Distribution of natural and anthropogenic radionuclides in soil and beach sand samples of Kalpakkam

- (India) using hyper pure germanium (HPGe) gamma ray spectrometry," *Appl. Rad. Iso.*, vol. 57, pp. 109-119, 2002.
- [61] B. Danalakshmi, S. Balasundar, K. R. Sreedevi, "Radon measurements in the residential colony of Nuclear Power Station at Kalpakkam using track detectors," *Radiat. Meas.*, vol. 43, pp. 5456-5458, 2008.
- [62] M. Sowmya, B. Senthilkumar, B. R. R. Seshan, G. Hariharan, R. Purvaja, S. Ramkumar, R. Ramesh, "Natural radioactivity and associated dose rates in soil samples from Kalpakkam, South India," *Radiat. Prot. Dosim.*, vol. 141, no. 3, pp. 239 - 247, 2010.
- [63] R. Ravisankar, K. Vanasundari, M. Suganya, Y. Raghu, A. Rajalakshmi, A. Chandrasekaran, S. Sivakumar, J. Chandramohan, P. Vijayagopal, B. Venkatraman, "Multivariate statistical analysis of radiological data of building materials used in Tiruvannamalai, Tamilnadu, India," *Applied Radiation and Iso.*, vol. 85, pp. 114-127, 2014.
- [64] G. Senthilkumar, R. Ravisankar, R. Vanasundari, I. Vijayalakshmi, P. Vijayagopal, M. T. Jose, "Assessment of radioactivity and the associated hazards in local cement types used in Tamilnadu, India," *Radiat Phys Chem*, vol. 88, pp. 45 -48, 2013.
- [65] M. P. Chougankar, K. P. Eappen, T. V. Ramachandran, P. G. Shetty, Y. S. Mayya, S. Sadasivan, V. V. Raj, "Profiles of doses to the population living in the high background radiation areas in Kerala, India," *J. Environ. Radioact.*, vol. 71, pp. 275-297, 2004.

- [66] M. U. Khandaker, P. J. Jojo, H. A. Kassim, Y. M. Amin, "Radiometric analysis of construction materials using HPGe gamma ray spectrometry," *Radiat. Prot. Dosim.*, vol. 152, no. 1-3, pp. 33 - 37, 2012.
- [67] S. Selvasekarapandian, R. Sivakumar, N. M. Manikandan, V. Meenakshisundaram, Raghunath, V. Gajendran, "Natural radionuclide distribution in soils of Gudalore, India," *Appl. Rad. Iso.*, vol. 52, pp. 299-306, 2000.
- [68] R. C. Ramola, G. S. Gussain, M. Manjari Badoni, Y. Prasad, G. Prasad, T. V. Ramachandran, "Ra-226, Th-232 and K-40 contents in soil samples from Garhwal Himalaya, India, and its radiological implications," *J. Radiol. Prot.*, vol. 28, pp. 379 - 385, 2008.
- [69] M. Yadav, M. Rawat, A. Dangwal, M. Prasad, G. S. Gusain, R. C. Ramola, "Levels and effects of natural radionuclides in soil samples of Garhwal Himalaya," *J. Radioanal. Nucl. Chem.*, vol. 302, pp. 869 - 876, 2014.
- [70] R. C. Ramola, V. M. Choubey, Ganesh Prasath, G. S. Gussain, Z. Tosheva, A. Kies, "Radionuclides analysis in the soil of Kumaun Himalaya, India, using gamma ray spectrometry," *Current Science.*, vol. 100, no. 6, pp. 906 - 914, 2011.
- [71] R. C. Ramola, "Survey of Radon and Thoron in homes of Indian Himalaya," *Radiat. Prot. Dosim.*, vol. 146, no. 1 - 3, pp. 11 - 13, 2011.
- [72] R. G. Sonkawade, K. Kant, S. Muralithar, R. Kumar, R. C. Ramola, "Natural radioactivity in common building construction and radiation shielding materials," *Atmos. Environ.*, vol. 42, pp. 2254-2259, 2008.

- [73] Viresh Kumar, T. V. Ramachandran, Rajendra Prasad, "Natural Radioactivity of Indian building Materials and by-products," *App. Rad. Iso.*, vol. 51, pp. 93 - 96, 1999.
- [74] R. Mehra, S. Kumar, R. Sonkawde, N. P. Singh, K. Badhan, "Analysis of terrestrial naturally occurring radionuclides in soil samples from some areas of Sirsa district of Haryana, India," *Environ. Earth Sci.*, vol. 59, pp. 1159-1164, 2010.
- [75] A. K. Patra, J. Sudhakar, P. M. Ravi, J. P. James, A. G. Hegde, M. L. Joshi, "Natural radioactivity distribution in geological matrices around Kaiga environment," *J. Radioanal. Nucl. Chem.*, vol. 270, no. 2, pp. 307-312, 2006.
- [76] T. V. Ramachandran, L. A. Sathish, "Nationwide Indoor Rn-222 and Rn-220 map for India: a review," *J. Environ. Radioact.*, vol. 102, pp. 975 - 986, 2011.
- [77] S. J. Dhawal, M. R. Phadatare, N. D. Thorat, G. S. Kulkarni, S. H. Pawar, "Natural radioactivity study in soil samples of South Konkan, Maharashtra, India," *Radiat. Prot. Dosim.*, vol. 157, no. 2, pp. 225-233, 2013.
- [78] S. R. Menon, B. K. Sahoo, S. Balasundar, J. J. Gaware, M. T. Jose, B. Venkatraman, Y. S. Mayya, "A comparative study between the dynamic method and passive can technique of radon exhalation measurements from samples," *AppL. Rad. Iso.*, vol. 99, pp. 172 - 178, 2015.
- [79] D. D. Jayanthi, C. G. Manian, S. Perumal, "Assessment of indoor radiation dose received by the residents of natural high background radiation areas of coastal villages of Kanyakumari district, Tamil Nadu, India," *Radiat. Phys. Chem.*, vol. 80, pp. 782-785, 2011.

- [80] K. Kant, Rashmi, S. Kuriakose, R. G. Sonkawade, R. P. Chauhan, S. K. Chakravarti, G. S. Sharma, "Radon activity and exhalation rates in indian fly ash samples," *Indian J. Pure Appl. Phys.*, vol. 48, pp. 457 - 462, 2010.
- [81] N. Karunakara, I. Yashodhara, K. Sudeep Kumara, R. M. Tripathi, S. N. Menon, S. Kadam, M. P. Chougankar, "Assessment of ambient gamma dose rate around a prospective uranium mining area of South India - A comparative study of dose by direct methods and soil radioactivity measurements," *Results in Physics*, vol. 4, pp. 20-27, 2014.
- [82] IAEA, "Quantifying uncertainty in nuclear analytical measurements," International Atomic Energy Agency, Austria, Vienna, 2004.
- [83] S. Chinnaesakki, S. V. Bara, S. J. Sartandel, R. M. Tripathi, V. D. Puranik, "Performance of HPGe gamma spectrometry system for the measurement of low level radioactivity," *J. Radioanal. Nucl. Chem.*, vol. 294, pp. 143-147, 2012.
- [84] H. Cember, T. E. Johnson, Introduction to Health Physics, McGraw- Hill, 2009.
- [85] S. V. Bara, Vishal Arora, S. Chinnaesakki, S. J. Sartandel, B. S. Bajwa, R. M. Tripathi, "Radiological assessment of natural and fallout radioactivity in the soil of Chamba and Dhramshala areas of Western Himachal Pradesh, India," *J. Radioanal. Nucl. Chem.*, vol. 291, pp. 769-776, 2012.
- [86] S. J. Sartandel, S. Chinnaesakki, S. V. Bara, N. S. Krishna, A. Vinod Kumar, R. M. Tripathi, "Assessment of natural and fallout radioactivity in soil samples of Visakhapatnam," *J. Radioanal. Nucl. Chem.*, vol. 299, no. 1, pp. 337 - 342, 2014.

- [87] S. J. Sartandel, S. V. Bara, S. Chinnaesakki, R. M. Tripathi, V. D. Puranik, "Measurement of naturally occurring radioactive materials (NORM) in beach sand minerals using HPGe based gamma-ray spectrometry," *J. Radioanal. Nucl. Chem.*, vol. 294, pp. 447 - 451, 2012.
- [88] IAEA, "Assessing the need for radiation protection measures in works involving minerals and raw materials," International Atomic Energy Agency, Austria, Vienna, 2006.
- [89] S. Chinnaesakki, S. .V. Bara, S. J. Sartandel, R. M. Tripathi, V. D. Puranik, "Radiological characterisation of synthetic rutile using gamma spectrometry," *Radiat. Prot. Dosim.*, vol. 140, no. 4, pp. 378-382, 2010.
- [90] T. V. Ramachandran, B. K. Sahoo, S. Chinnaesakki, "Assessment of natural radioactivity content of the building materials in India," in *Nuclear and Radiochemistry symposium (NUCAR-2007)*, 2007.
- [91] C. D. Hull, W. C. Burnett, "Radiochemistry of Florida Phosphogypsum," *J. Environ. Radioact.*, vol. 32, no. 3, pp. 213-238, 1996.
- [92] C. H. Saueia, B. P. Mazilli, DIT. Favaro, "Natural radioactivity in PR, phosphogypsum, and phosphate fertilizers in Brazil," *J. Radioanal. Nucl. Chem.*, vol. 264, no. 2, pp. 445-448, 2004.
- [93] IAEA , "Extent of environmental contamination of naturally occurring radioactive material (NORM) and technological options for mitigation. IAEA TECDOC No. 419," International Atomic Energy Agency, Austria, Vienna, 2003.

- [94] M. Azouazia, Y. Ouahidia, S. Fakhia, Y. Andresb, Jch. Abbeb, "Natural radioactivity in phosphates, phosphogypsum and natural waters in Morocco," *J. Environ. Radioact.*, vol. 54, pp. 231 - 242, 2001.
- [95] E. M. Hussein, "Radioactivity of phosphate ore, Super Phosphate, and Phosphogypsum in Abu-Zaabal Phosphate plant, Egypt.," *J. Health Phys.* , vol. 67, p. 280–283, 1994.
- [96] J. P. Bolivar, J. E. Martin, R. Garcia-Tenorio, J. P. Perez-Moreno, J. L. Mas, "Behaviour and fluxes of natural radionuclides in the production process of a phosphoric acid plant," *Appl. Rad. Iso.*, vol. 67, pp. 345-356, 2009.
- [97] J. E. Turner, H. A. Wright, R. N. Hamm, "A Monte Carlo Primer for Health Physicists," *Health Phys.*, vol. 48, no. 6, pp. 717 - 743, 1985.
- [98] .. M. Sobol, A Primer for the Monte Carlo Method, Florida: CRC Press LLC, 1993.
- [99] K. P. N. Murthy, Monte Carlo: basics, Indian Society for Radiation Physcs, Kalpakkam chapter, 2000.
- [100] E. D. Cashwell, and C. J. Everett, A P ractical Manual on the Monte Carlo Method, London: Pergamon Press, 1959.
- [101] J. F. Briesmeister, "MCNP – A general Monte Carlo N-particle transport code (version 3.1)," Los Alamos, United States, 1983.
- [102] J. H. Hubbell, S. M. Seltzer, "Tables of X-ray mass attenuation coefficients and mass energy-absorption coefficients 1 keV to 20 MeV for elements Z=1 to 92 and 48 additional substances of dosimetric interest," Gaithersburg, MD 20899, 1995.

- [103] ICRP, "ICRP 119, Compendium of Dose Coefficients based on ICRP Publication 60. ICRP Publication 119," *Ann. ICRP*, vol. 41, no. Supplement 1, pp. 1 - 130, 2012.
- [104] V. P. Singh, N. M. Badiger, "The gamma ray and neutron shielding factors of flyash brick materials," *J. Radiol. Prot.*, vol. 34, p. 89–101, 2014.
- [105] India Sand Pebbles, "India sand pebbles," 2014. [Online]. Available: <http://www.indiasandpebbles.com/indian-standard-sand-780450.html>. [Accessed 23 12 2014].
- [106] S. Mukherjee, S. Mandal, U. B. Adhikari, "Study on the physical and mechanical property of ordinary portland cement and fly ash paste," *International Journal of Civil and Structural Eng*, vol. 2, no. 3, pp. 734 - 736, 2012.
- [107] PNNL, "Compendium of Material Composition Data for Radiation Transport Modeling," Pacific Northwest National Laboratory, Richland, Washington 99352, 2011.
- [108] C. M. F. Vieira, S. N. Monteiro, "Evaluation of a Plastic Clay from the State of Rio de Janeiro as a Component of Porcelain Tile Body," *Revista Matéria*, vol. 12, no. 1, pp. 1 - 7, 2007.
- [109] BMTPC, "Building Materials & Technology Promotion Council," 31 May 2012. [Online]. Available: [http://www.bmtpc.org/DataFiles/CMS/file/PDF\\_Files/Annex-06\\_PAC\\_GFRG\\_Panel\\_FRBL.pdf](http://www.bmtpc.org/DataFiles/CMS/file/PDF_Files/Annex-06_PAC_GFRG_Panel_FRBL.pdf). [Accessed 25 August 2015].

- [110] A. Shakhashiro, U. Sansone, H. Wershofen, A. Bollhofer, C. K. Kim, C. S. Kim, G. Kis-Benedek, G., M. Korun, M. Moune, S. H. Lee, S. Tarjan, M. S. Al-Masri, "The new IAEA reference material:IAEA-434 technologically enhanced naturally occurring radioactive materials(TENORM) in phosphogypsum," *Appl. Radiat. Iso.*, vol. 69, pp. 231 - 236, 2011.
- [111] BARC, "<http://www.barc.gov.in/daiichi/iermon290711.pdf>," [Online]. [Accessed 17 June 2013].
- [112] K. Kovler, "Radiological constraints of using building materials and industrial by-products in construction," *Constr. Build. Mater.*, vol. 23, pp. 246-253, 2009.
- [113] B. K. Sahoo, B. K. Sapra, J. J. Gaware, S. D. Kanse, Y. S. Mayya, "A model to predict radon exhalation from walls to indoor air based on the exhalation from building material samples," *Sci. Total Environ.*, vol. 409, pp. 2635-2641, 2011.
- [114] Amit Kumar, R. P. Chauhan, M. Joshi, B. K. Sahoo,, "Modeling of indoor radon concentration from radon exhalation rates of building materials and validation through measurements," *J. Environ. Radioact.*, vol. 127, pp. 50-55, 2014.

